Advanced chemical recycling of plastic waste

Gerardo Martínez Narro

Supervisors:

Prof. Anh N. Phan

Prof. Thomas Curtis

Prof. Simon Beaumont

Prof. Ulugbek Azimov

This thesis is submitted for the degree of *Doctor of Philosophy*

School of Engineering

Newcastle University, United Kingdom

January 2024

Abstract

The increasing production of plastic waste and its related environmental impact have driven the need to research advanced chemical recycling strategies. Such methods seek to transform non-recyclable, rejected, multi-layer, and contaminated plastic waste streams into high-value chemicals, ultimately promoting a circular economy. This thesis presents a comprehensive investigation into the chemical recycling of plastic waste, encompassing multiple recycling technologies such as pyrolysis, gasification, and hydrothermal liquefaction.

The study began with an extensive critical review of existing chemical recycling technologies and their challenges, opportunities, and future development. Following, kinetic modelling of mixed plastic waste was conducted to identify the dependencies of activation energy on conversion. The derived kinetic models were then applied to the experimental data, proving to be effective at predicting thermal decomposition of single and mixed plastics. The activation energies of the studied plastics i.e., PP, PET, PS, LDPE, and HDPE, were found to be 176, 196, 215, 244, and 258 kJ mol^{-1}, respectively.

Subsequently, the study evaluated the performance of affordable catalysts derived from waste biomass for the pyrolysis of mixed plastic waste. A two-stage fixed-bed reactor setup was employed to investigate the product yield distribution, composition, and carbon nanotube (CNT) formation across different temperature ranges. The nickel- and iron-based biochar catalysts showed promising catalytic activity and CNT production with maximum H_2 yields of 4.2 and 2 wt%, and CNT yields of 34.5 and 12.4 wt%, respectively. HZSM-5 zeolite was identified as the most effective catalyst for converting heavy fractions into lighter hydrocarbons and monomer recovery, particularly at low temperatures. This was evidenced by the high gas yield of 48.4 wt% at 500 °C using zeolite compared to the low yield of the thermal run (28 wt%).

In addition, the potential of catalytic pyrolysis for converting mixed plastic waste into valuable products, such as syngas and monomers, was investigated. The optimal processing conditions for maximizing CO_2 conversion (0.389 g_{CO2} g^{-1}) while minimizing carbon deposition (4.65 wt%) were found to be a temperature of 700 °C, a CO_2 concentration of 60 mol%, and a catalyst-to-plastic ratio of 16 wt%. These conditions resulted in a syngas yield of 34.25 wt%. Additionally, the study attained a 28 wt% recovery of ethylene and propylene monomers. These results contribute to the development of efficient and sustainable processes for the conversion of

mixed plastic waste and CO_2 into valuable products, providing insights into process optimization and catalyst reusability.

Lastly, the thesis examined the technical and economic aspects of industrial-scale hydrothermal liquefaction and pyrolysis processes, as well as the outlook and impact of chemical recycling technologies.

This thesis, overall, provides a comprehensive understanding of various chemical recycling technologies and their potential applications for transforming plastic waste into high-value materials such as monomers and chemicals. The research findings contribute to the development of sustainable solutions for plastic waste management and the transition to a circular economy.

Acknowledgements

I would like to express my sincere gratitude to my supervisor, Prof. Anh Phan, whose patience, support, and insightful guidance were invaluable throughout the course of my studies. Similarly, Prof. Tom Curtis' inspiring discussions and innovative ideas, and Prof. Simon Beaumont's meticulous attention to the technical aspects of my experiments, were instrumental to my work.

Special thanks go to the Mexican National Council of Humanities, Sciences and Technologies (CONAHCYT), whose generous funding provided the foundation of my studies. I am also deeply grateful to Newcastle University, for acknowledging my efforts with the NUORS scholarship.

To my esteemed colleagues in the research group—Jirat Mankasem, Agiteh Ibrahim, Dr Long Duong, Dr Ha Phan, and Dr Ibrahim Mohammed—I extend my sincere appreciation for their collaborative spirit and valuable assistance in the lab.

My acknowledgements would not be complete without recognizing the skilled and dedicated electricians, technicians, and workshop staff, whose support was crucial in the successful execution of my project.

I owe a deep debt of gratitude to the Advanced Chemical and Materials Analysis (ACMA) unit at Newcastle University, especially to Dr Isabel Arce-Garcia, Dr Jamie Gould, Dr Alex Charlton, and Dr Karina Machado. Their expertise and assistance in conducting and interpreting EDX, SEM, XRD, and GC-MS analyses were indispensable to my research.

On a personal note, I am grateful to my family and friends. Their constant encouragement, support, and confidence in my abilities were invaluable sources of motivation and strength during this challenging journey.

Finally, my deepest gratitude is reserved for my wife, Yixuan. Her patience, understanding, and unfaltering support during these demanding years have been my anchor. This achievement would not have been possible without her.

To my parents, and my wife.

"For I found myself embarrassed by so many doubts and errors, that it seemed to me that the effort to instruct myself had no other outcome than the increasing discovery of my own ignorance."

René Descartes - Discourse on the method of rightly conducting one's reason and seeking the truth in the sciences.

Table of Contents

List of Figures

List of Tables

Chapter 1. Introduction

1.1. Background

The global increase in plastic production and consumption has resulted in a plastic waste crisis, threatening both environmental and human health. Traditional methods of waste disposal (e.g., landfilling and incineration) present significant environmental drawbacks, reinforcing the urgency of finding innovative solutions (Awasthi, Shivashankar et al. 2017). The production of plastics is heavily reliant on non-renewable resources, accounting for 27% of worldwide oil and gas consumption (Kawai and Tasaki 2016). Many plastic products exhibit short lifespans and are frequently discarded within the first year of use. Furthermore, the accumulation of non-biodegradable microplastic debris in the environment and landfill sites exacerbates this issue (Chamas, Moon et al. 2020). In 2019, the global generation of plastic waste amounted to 368 million tonnes. An overwhelming 42.6% of this waste was incinerated, 24.9% went to landfills, and a mere 32.5% was recycled (PlasticsEurope 2020). Rising costs, decreased availability of suitable landfill sites, and negative environmental and health impacts have made plastic waste a critical global environmental challenge. The plastic manufacturing industry's dependence on non-renewable resources is highlighted by the allocation of 4-6% of fossil fuels to plastic production in Europe (British Plastics Federation 2019). Plastic manufacturing and processing are predicted to account for a staggering 20% of global petroleum consumption by 2050 (World Economic Forum, Ellen MacArthur Foundation et al. 2016, Lebreton and Andrady 2019). This growing demand for petroleum resources not only exacerbates the depletion of finite fossil fuel reserves but also contributes to increased greenhouse gas emissions and environmental degradation. Investing in research and development of innovative recycling technologies will play a critical role in mitigating the environmental impact of the plastic industry.

Promoting a circular economy approach, where waste materials are processed and reintroduced to the production cycle, will help to reduce the reliance on fossil fuels and minimize the environmental impact of plastic manufacturing (Schwarz, Ligthart et al. 2021). The circular economy is an economic system aimed at eliminating waste and promoting the continual use of resources. It revolves around creating a closed-loop system where products, materials, and resources are reused, refurbished, remanufactured, and recycled, minimizing the need for new raw materials, and reducing environmental impact. This approach contrasts with the traditional linear economy, where raw materials are extracted, products are

manufactured, used, and then discarded (Grafström and Aasma 2021). One key principle of the circular economy includes designing out waste, where products are created with minimal waste and environmental impact from the outset. Another principle is to keep products and materials in use, extending their life through repair, refurbishment, and recycling (Moreno, De los Rios et al. 2016). In the circular economy, there is an emphasis on designing products with recycling in mind. This involves using materials that can be easily separated and recycled, reducing the use of toxic substances, and designing products for easy disassembly (Sumter, de Koning et al. 2020). Material recycling engineering plays a pivotal role in the circular economy by developing technologies and processes to efficiently recover and reuse materials from discarded products (Beccarello and Di Foggia 2018). Research and development in this field focus on developing advanced sorting, processing, and recycling technologies to separate and recover valuable materials from waste streams. This includes innovations in mechanical recycling, chemical recycling, and bio-based processes (Schyns and Shaver 2021, Lim, Ahn et al. 2022, Abbas-Abadi, Ureel et al. 2023). Outside of the technological aspects, the standardization of waste streams, infrastructure investment, collaborative business models, and general public awareness are crucial to achieve circularity (Burgess, Holmes et al. 2021).

Sustainability refers to the practice of utilising resources in a way that meets current needs without compromising the ability of future generations to meet their own needs. It encompasses a broad range of activities and principles that aim to preserve the environment, ensure social equity, and maintain economic viability (Alsayegh, Abdul Rahman et al. 2020). Sustainability is a complex and multidimensional concept that involves considering the long-term impacts of actions on the natural world and society, promoting responsible management of resources, and striving for a balance between development and conservation (Giovannoni and Fabietti 2013). Environmental sustainability involves practices that help preserve natural resources and reduce environmental impact, while social sustainability focuses on maintaining and improving social quality, including aspects like human rights and community development (Khan and Hou 2021, Arslan, Khan et al. 2022). Economic sustainability involves supporting economic growth and development without negatively impacting social and environmental aspects, as seen in sustainable supply chain management (Mota, Gomes et al. 2015).

Landfilling is a common method for managing plastic waste, involving several steps and considerations. Initially, plastic waste is collected from various sources and transported to landfill sites. The selection of these sites is crucial, typically focusing on areas with low

groundwater levels to minimize pollution risks and positioned far from residential areas to reduce odour and health hazards (Parvin and Tareq 2021, Adeleke, Akinlabi et al. 2022).

At the landfill site, a protective lining made of clay and synthetic materials is laid to prevent leachate, a polluted liquid, from seeping into the ground. The plastic waste is then compacted and buried in layers, each covered with soil to control odour and deter pests (Meegoda, Hettiarachchi et al. 2016). Landfills are usually equipped with systems to collect and treat leachate, and methane gas produced from waste decomposition is also captured (Show, Pal et al. 2019). Regular monitoring of groundwater and gas emissions is essential for environmental safety, and landfills require long-term maintenance even after closure.

Despite its widespread use, landfilling plastic waste poses significant challenges and environmental impacts. Landfills contribute to greenhouse gas emissions, particularly methane, and plastic waste can take centuries to decompose, releasing toxic substances in the process. The large land areas required for landfills are becoming increasingly scarce, especially near urban centres. Managing leachate is a critical challenge, as it can contaminate local water sources, leading to severe environmental and health issues (Show, Pal et al. 2019). Furthermore, landfilling does not reduce the overall amount of waste but merely stores it, offering no contribution to the circular economy's goals of recycling and reusing materials. Given these issues, there is a growing emphasis on alternative waste management methods such as recycling. Reducing plastic usage at the source and developing biodegradable plastics are also part of the efforts to lessen the environmental impact. The future of waste management lies in finding environmentally friendly alternatives that extend beyond traditional landfilling practices.

While incineration remains a prevalent method for processing plastic waste to recover energy, it poses significant environmental detriments. The process of incineration releases toxic gases, such as dioxins, polychlorinated biphenyls, mercury, furans, halogenated, and volatile organic compounds which contribute to air pollution (Shangdiar, Lin et al. 2021). Due to its significant environmental drawbacks, energy recovery via incineration is not the preferred option in the waste management hierarchy. Given these concerns, it is crucial to shift the focus of waste management towards recovering value from plastic waste in the form of monomers and chemicals, thereby minimizing further resource consumption.

Mechanical recycling is currently the most commercially utilised method to recycle plastics, with a processing capacity of over 9 Mt in Europe, while alternative recycling methods such as

chemical and solvent-based recycling reach less than 0.2 Mt (PlasticsEurope 2019, Lase, Tonini et al. 2023). The process involves an extrusion cycle that processes plastic scraps or single-polymer plastic shreds, requiring separation and cleaning procedures (e.g., sorting, washing, grinding), and adherence to the intended market's standards (Vollmer, Jenks et al. 2020). After the waste collection, the mechanical recycling steps that follow include separation and sorting (based on shape, density size, colour, and chemical composition), baling (in case the plastics were not processed where sorted), washing, size reduction by grinding, optional compounding and pelletising for ease of handling (Ragaert, Delva et al. 2017). Despite being the most environmentally friendly recycling method, it faces several challenges such as the potential reduction of the material's technical quality, thermal-mechanical degradation, the presence of legacy additives and chemicals, and inadequate technical properties of the final regranulates to meet the market's demands (Ragaert, Delva et al. 2017, Schyns and Shaver 2021). Additionally, there is also a reduction in potential market applications due to legal safety requirements such as food packaging.

Mechanical recycling occupies a crucial position in the general landscape of plastic recycling, playing a pivotal role in managing plastic waste. One of the key advantages of mechanical recycling is its suitability for certain types of plastics. It is effective for recycling common plastics such as PET, HDPE, and PP. These materials can be reprocessed through mechanical means, making this method a backbone of plastic recycling efforts for these categories. However, its effectiveness is limited for other kind of plastics that are challenging to sort or that degrade in quality upon reprocessing. Environmentally, mechanical recycling plays a crucial role. By diverting plastics from landfills, it significantly reduces waste and helps in conserving resources (Chen, Xi et al. 2011). Economically, mechanical recycling is more cost-effective than other forms of recycling in general, such as chemical recycling (Nikiema and Asiedu 2022). Its success, however, is heavily dependent on the market demand for recycled plastics, which can fluctuate based on various economic and policy factors. In the broader context of plastic recycling, mechanical recycling is complemented by other methods, including chemical recycling, to create a more comprehensive waste management system. This integration allows for handling a wider variety of plastic wastes and improving the overall efficiency of recycling programmes.

Chemical recycling of plastics focuses on the efficient recovery of materials from waste plastics (Jiang, Shi et al. 2022). The development and implementation of chemical recycling

technologies will be vital in addressing the growing challenges posed by plastic waste as sustainable waste management practices become increasingly important.

Pyrolysis of plastic waste is becoming an increasingly important method to mitigate the global plastic waste crisis. Pyrolysis is a process of thermal decomposition of materials at high temperatures (450 – 600 °C) in an inert environment that involves several stages, starting with the pre-treatment of plastic waste (e.g., sorting, cleaning and shredding), followed by the pyrolysis reaction itself, and concluding with the post-treatment of the resultant products (primarily oil, wax, gas, and char) (Martínez-Narro, Prasertcharoensuk et al. 2022). The specific output depends on the type of plastic and the pyrolysis conditions, for example, pyrolysis of polystyrene produces more aromatics compared to polyethylene, and more gaseous products are formed as processing temperature increases.

This method helps reduce the volume of plastic waste in landfills while recovering valuable resources (e.g., naphtha-range hydrocarbons and monomers), as the oil and gas products can be used to produce new plastic materials, instead of using traditional non-renewable resources such as fossil fuels. By targeting the recovery of valuable monomers and chemicals and their re-introduction to the industrial production loop (e.g., through feedstock recycling), pyrolysis has the potential to contribute to a more sustainable circular economy for plastic materials (Huang, Veksha et al. 2022).

However, the process has several challenges and limitations. Due to the high variation of plastic waste composition, the quality of the pyrolysis oils can also be variable, affecting its potential applications if they are not further refined. For example, a feedstock with higher fractions of thermally stable polyolefins, such as polyethylenes, will require a higher energy input for conversion, and may result in excessive formation of waxes and long-chain hydrocarbons.

In the broader landscape of plastic recycling, pyrolysis plays a significant role as it is particularly suited for specific applications. It is capable of processing non-recyclable plastics through traditional mechanical methods due to complex compositions (e.g., multi-layered packaging and composite materials) or contamination, that would otherwise end incinerated or in landfills (Costa, Pinto et al. 2021). A key advantage of pyrolysis over other recycling methods, such as mechanical and solvolysis, is its ability to convert mixed plastic waste. This feature is especially beneficial in managing the complexities of municipal waste streams, where plastics of different types and qualities are often mixed and are difficult to separate

(Pal, Kumar et al. 2022). Compared to incineration, it minimizes the release of harmful gases and maximizes the recovery of useful products, such as naphtha and monomers.

Pyrolysis and mechanical recycling offer contrasting methods for processing mixed plastic waste (MPW), each with its own environmental footprint. Pyrolysis significantly reduces climate change impact and life cycle energy use by approximately 50% compared to traditional energy recovery approaches (Jeswani, Krüger et al. 2021). In contrast, when evaluated against mechanical recycling, pyrolysis demonstrates a comparable performance in terms of climate change impact and energy consumption. However, pyrolysis is characterized by considerably greater impacts in various environmental aspects other than climate change and energy use, primarily due to the intensive energy demands of its process and purification stages. While pyrolysis effectively processes plastics that are challenging for mechanical recycling, this advantage is partly offset by its broader environmental impacts (Jeswani, Krüger et al. 2021). As such, pyrolysis and mechanical recycling can be viewed as complementary strategies, their suitability varying based on the specific nature of the plastic waste and the environmental goals prioritized in material recovery processes.

Depolymerization through solvolysis represents a sophisticated method characterized by its chemical approach to breaking down polymers into simpler compounds. In this process, specific solvents (e.g., glycol and methanol) are employed to cleave the long-chain molecules of plastics back into monomers or smaller oligomers. Solvolysis facilitates the reuse of plastics by converting them into high-quality raw materials suitable for creating new plastic products. Solvolysis offers a selective method for extracting monomers from polyesters and polyamides, using lower temperatures than other thermochemical methods such as pyrolysis or gasification. This method includes various processes such as hydrolysis, alcoholysis (including glycolysis and methanolysis), phosphorolysis, ammonolysis, and aminolysis. These processes specifically target and break down ether, ester, and acid amide bonds, making them suitable for polymers like polyethylene terephthalate (PET), polyurethanes (PU), polyamides (PA), polycarbonate (PC), and polylactic acid (PLA) (Vollmer, Jenks et al. 2020) . A significant advantage of solvolysis is the ability to recover monomers that can be further purified to remove additives and colorants, potentially achieving virgin-grade quality (Valerio, Muthuraj et al. 2020). This is a beneficial method for processing materials that cannot be mechanically recycled, and can be used for selective conversion and recovery of particular components in complex multi-layered materials (Huang, Pitcher et al. 2023).

This thesis is centred on the production of naphtha, light gases (hydrogen, syngas, and monomers), and carbon nanotubes rather than focusing solely on energy or fuel production, a departure from many current studies in the field (Sharuddin, Abnisa et al. 2018, Parku, Collard et al. 2020, Praveenkumar, Velusamy et al. 2022, Al-Fatesh, Al-Garadi et al. 2023). Energy recovery from fuels is a practice that resembles incineration as they both nullify the material value of plastics. Since recovering energy from plastic in the form of fuels is a one-time use, the practice is not entirely aligned with resource circularity. Furthermore, it contributes to air pollution with the release of CO_2 into the environment. Therefore, the production of new raw materials that serve as building blocks for manufacturing other chemicals is a more sustainable and environmentally friendly approach. This research opens new pathways for material recovery, specifically naphtha (a valuable raw material for the chemical manufacturing industry), monomers (mainly ethylene and propylene, which can be reintegrated to the plastic production cycle), and syngas (used to synthesize a wide array of new chemicals). Adopting this practice could potentially reduce the demand for extracting virgin materials, primarily obtained from non-renewable sources.

One of the central challenges of chemical recycling technologies is having to deal with the diverse and complex compositions of plastic waste. There are limitations in the current understanding of the thermal decomposition of various plastics and particularly mixed plastic waste (Martínez-Narro, Royston et al. 2023). Treating all plastic waste as homogeneous leads to oversimplification and inaccuracies. In this context, detailed kinetic modelling of plastic waste pyrolysis is of particular relevance. The construction of continuous pilot or industrial-scale plants requires careful design of the feeder system, as premature decomposition of the plastic feed could lead to environmental and safety risks. Consequently, conducting thermokinetic studies for a comprehensive understanding of the decomposition behaviour of plastic waste is indispensable for safe reactor design and operation.

The escalating challenges associated with plastic waste management need the adoption of effective waste management practices. The growing reliance on non-renewable resources and the environmental implications of current waste management methods, such as incineration, call for the development and implementation of alternative recycling technologies like chemical recycling. Advanced thermochemical processes hold significant potential to address the limitations of traditional recycling methods and contribute to a circular economy. By focusing on the recovery of valuable monomers and chemicals from waste plastics, chemical

recycling can reduce dependence on fossil fuels, minimize environmental pollution, and promote a more sustainable future for plastic materials. Despite the recent environmental goals such as the net zero emissions by 2050 (Bouckaert, Pales et al. 2021), most of the produced energy comes from non-renewable sources (e.g., nearly two thirds (63.3%) of electricity was produced from fossil fuels in 2019 (Ritchie, Roser et al. 2020)). As the global energy demand continues to rise, investment in research and development of these advanced recycling technologies will be crucial in mitigating the environmental impact of the plastic industry and fostering a greener, more responsible approach to plastic waste management.

The surge in recent partnerships and joint ventures leading to the establishment of new chemical recycling plants across various countries globally serves as a strong indication of the commercial viability of these projects. Table 1.1 provides a comprehensive list of recent consortiums dedicated to advancing chemical recycling technologies, detailing the involved as well as the plants that are newly established or currently under construction.

Table 1.1 Overview of recent and under-construction chemical recycling plants and associated partnerships worldwide (Bioplastics News , Neste 2021, Shell 2021).

Name	Location	Technology	Company	Consortium, partnerships, and joint-ventures in the country
Eastman	USA	Solvolysis (Methanol)	Eastman Chemical Company	• GE and Agilyx • Neste and Ravago • P&G and Eastman • SK Global Chemical and PureCycle • Shell and BlueAlp
PureCycle Technologies		Solvent-based purification	PureCycle Technologies LLC	
Agilyx		Pyrolysis	Agilyx Corporation	
Alterra Energy			Alterra Energy LLC	
Brightmark			Brightmark LLC	
New Hope Energy			New Hope Energy LLC	
Nexus Fuels			Nexus Fuels LLC	
RES Polyflow			RES Polyflow LLC	
Renewlogy	USA/India		Renewlogy LLC	N/A
Enerkem	Canada	Gasification	Enerkem Inc.	
GreenMantra		Depolymerisation	GreenMantra Technologies Ltd.	
Loop Industries			Loop Industries Inc.	
Mura Technology	UK	Hydrothermal upgrading	Mura Technology Ltd.	Neste with Mirova and Recycling Technologies
Recycling Technologies		Pyrolysis	Recycling Technologies Ltd.	
Plastic Energy	UK/Spain		Plastic Energy Ltd.	N/A
Carbios	France	Depolymerisation	Carbios SA	• Carbios and TBI • Novozymes and Carbios
Plastic Omnium		Pyrolysis	Plastic Omnium SA	
Gr3n	Switzerland	Depolymerisation	Gr3n SA	Kolon Industries and Gr3n
Ioniqa	Netherlands	Depolymerisation	Ioniqa Technologies BV	N/A
Jeplan	Japan	Solvolysis (Methanol)	Jeplan Inc.	Yokogawa and Jeplan

While the numerous benefits of chemical recycling technologies are extensively explored in this thesis, it is essential to understand that it represents just one tool in a comprehensive waste management strategy. A broader approach should involve efforts to reduce plastic production and consumption, increase mechanical recycling wherever feasible, and promote the development of biodegradable and bio-based materials.

1.2. Research gaps

This thesis addresses several research gaps and introduces novel approaches to the field of chemical recycling. Each chapter contributes to the development of more sustainable plastic waste management strategies by investigating specific research gaps and presenting solutions. The following is a list of the research gaps addressed in this thesis:

- A thorough description of the methods utilised throughout the thesis, which serve as a valuable resource for researchers aiming to understand, reproduce, and build upon the findings presented in the experimental chapters.
- Insufficient understanding of thermal decomposition kinetics of mixed plastic waste, and the complexity of applying advanced kinetic modelling methodologies, which often require expensive software.
- The comprehensive evaluation of biomass-derived catalysts incorporated with nickel, iron, and zinc, for catalytic pyrolysis of plastic waste.
- The limited understanding of the influence of CO_2 on plastic waste pyrolysis and the optimal processing conditions.
- The need for a technical and economic analysis of hydrothermal processing of plastic waste and its comparison with pyrolysis.

The need for a synthesis of the main findings and contributions of this thesis, as well as the identification of potential opportunities for future research and development in the field of chemical recycling of plastic waste.

1.3. Objectives and Scope

The main goal of this thesis is to examine the potential of advanced chemical recycling techniques for transforming plastic waste into valuable materials. The research seeks to offer an extensive understanding of the current state-of-the-art in chemical recycling technologies and the nature of mixed polymers thermal decomposition, while also investigating innovative

strategies for process optimization through the exploration of novel catalysts and CO_2 recycling.

The scope of the thesis involves the following aspects:

1. A critical review of the diverse chemical recycling technologies under investigation, including pyrolysis, hydrothermal liquefaction, and solvolysis.
2. Kinetic study of mixed plastic waste pyrolysis for the development of predictive models for complex thermal decomposition profiles.
3. Exploration and comparative analysis of various catalysts, including novel waste-derived materials, for catalytic pyrolysis of plastic waste.
4. Optimization of process parameters for the simultaneous production of valuable products (e.g., carbon nanotubes and hydrogen) and CO_2 capture during plastic waste pyrolysis.
5. Technical and economic analysis of pyrolysis and hydrothermal liquefaction of plastic waste as an emerging approach for plastic waste recycling.

General discussion and assessment of the environmental impact and potential contribution of chemical recycling technologies to the circular economy and society in general.

1.4. Thesis outline and novelty

This thesis is structured into eight chapters, each addressing a critical aspect of plastic waste recycling and its potential applications:

- **Chapter 1** presents an overview of the plastic waste issue, its environmental implications, and the necessity for alternative recycling approaches. This chapter sets the context and objectives of the thesis, delineating the scope and importance of the conducted research, identifying research gaps, and providing a statement of novelty for each chapter.
- **Chapter 2** offers a comprehensive literature review of various chemical recycling technologies currently under investigation. This chapter identifies and discusses the existing challenges and opportunities associated with these technologies and highlights areas for future development. The novel aspect lies in the systematic analysis, identification, and discussion of the latest stages of development of current technologies, the main challenges hindering their industrial implementation, opportunities for improvement, and the roadmap for their widespread adoption. In

addition, biological methods are thoroughly discussed. These are rarely covered in most chemical recycling reviews, and information on the subject is usually focused on biodegradation rather than material recovery. This comprehensive review provides a useful reference for future research and development in the fields of waste management and sustainability.

- **Chapter 3** provides a concise overview of the methodologies used in the experimental chapters of this thesis, focusing on material characterization, experimental setups, analytical techniques, and data analysis approaches. The chapter outlines the key aspects of each method, emphasizing their roles in the analysis of chemical recycling experiments.
- **Chapter 4** explores the thermal degradation kinetics of plastic waste pyrolysis, providing an in-depth analysis of the thermal decomposition of individual and mixed plastics using thermogravimetric analysis and rigorous kinetic methodologies. The chapter investigates the dependencies of activation energy on conversion and develops robust kinetic models for predicting decomposition behaviour under different heating programmes and sample compositions. The novelty lies in determining accurate multiple-step kinetic parameters for individual and mixed plastic waste samples and developing advanced kinetic models. Furthermore, a comprehensive analysis of the multi-step nature of the thermal decomposition of plastic mixtures is conducted employing state-of-the-art mathematical deconvolution techniques. This chapter offers valuable guidance to those new to the field of thermokinetic analysis, with an exhaustive and clear description of the methodologies employed for analysis. Notably, the utilization of a widely available software (i.e., Excel) enhances the accessibility of the findings to a wider audience.
- **Chapter 5** examines the catalytic pyrolysis of plastic waste, assessing the performance of various catalysts derived from waste biomass, as well as a benchmark zeolite. This chapter offers a comparative analysis of catalyst performances concerning product yield distribution, composition, and the mechanisms that drive specific product formation. The novelty of this chapter resides in employing biochar as an efficient support for metal catalysts (e.g., Ni, Fe, Zn) and comparing their performances with respect to product yield distribution, composition, and products of interest (e.g., monomers, hydrogen, carbon nanotubes). This analysis provides valuable insights for catalyst selection and optimization.

- **Chapter 6** investigates the potential of CO_2 carbon capture through catalytic pyrolysis by optimizing processing parameters, including temperature, CO_2 concentration, and catalyst-to-plastic ratio, utilizing response surface methodology. The chapter also evaluates the reusability and stability of a Ni-Al_2O_3 catalyst over multiple cycles of re-use. The novel aspect entails a thorough examination of the interactions between process parameters and their effects on response variables (e.g., product yields and CO_2 capture). Furthermore, the evaluation of catalyst reusability and stability, which is scarce in literature, provides new insights into the suitability of the Ni-Al_2O_3 catalyst for industrial applications.
- **Chapter 7** conducts a technical and economic analysis of pyrolysis and hydrothermal liquefaction (HTL) as an emerging approach for plastic waste recycling. The chapter discusses operating parameters, process flow diagrams, unit operations, processing equipment, and material and energy balances, as well as a thorough economic feasibility study for implementing HTL at an industrial scale. The novelty resides in the examination of the economic feasibility of a technology still in early development for mixed plastic waste management applications, for which such analysis has not yet been conducted. This comprehensive evaluation provides valuable insights into the viability of HTL as a potential solution for plastic waste recycling.
- **Chapter 8** concludes the thesis by summarizing the main findings and contributions of each chapter. It also identifies potential directions for future research and development in the field of advanced chemical recycling of plastic waste. The novelty lies in highlighting the most promising areas for further investigation, directing future research efforts towards addressing the global plastic waste crisis.

Chapter 2. Chemical recycling of plastic waste for sustainable polymer manufacturing: a critical review

2.1. Background

Chemical recycling has emerged as a promising approach to valorise non-recyclable, rejected, multi-layered, and contaminated plastic waste streams, such as packaging waste, aligning with the 3R's principles (reduce, reuse, and recycle). This chapter critically evaluates various chemical recycling technologies, including pyrolysis, gasification, hydrothermal, and biological methods, which hold the potential to amend the global plastic pollution crisis while recovering valuable materials. Despite the potential of these methods, substantial challenges persist, including technological limitations, elevated capital costs, feedstock variability, energy consumption, and poor regulatory frameworks. The challenges and opportunities for future development are thoroughly discussed. Continuous research and development, coupled with supportive regulatory policies that facilitate technology adoption (such as introducing plastic packaging taxes), and public awareness, are vital for advancing chemical recycling technologies and transitioning towards a circular economy. A holistic approach, integrating not only chemical recycling, but also waste reduction, reuse, and other waste management strategies, is required to resolve the plastic waste crisis, and attain a more sustainable future.

2.2. Introduction

Over the past seven decades, plastic production has increased, with a compound average growth rate of 8.6% per annum since 1950 (PlasticsEurope 2022), This increase is attributed to the versatility of plastics, which provide safety and hygiene in various applications. Packaging materials have short lifetimes and constitute more than 50% of polyolefins such as polyethylene (PE) and polypropylene (PP), followed by polyesters (PlasticsEurope 2020). As a result, they comprise up to 46% of the plastic waste stream, followed by textiles (Figure 2.1) (Tsakona and Rucevska 2020). In 2019, of the 368 million tonnes of plastic produced, only 32.5% was recycled, while 24.9% was directed to landfills and the remaining 42.6% for energy recovery (PlasticsEurope 2020). Many developing countries have inadequate regulations and recycling capabilities, and they continue to rely on landfilling for plastic waste disposal (Zhao 2018). Consequently, plastics damage the environment and contaminate water streams due to the absence of effective solid waste management.

Plastic waste generation can vary significantly depending on the level of industrialization and consumption patterns between regions. Local waste management strategies and policies can greatly influence the amount of plastic waste generated and how it is handled (Shin, Um et al. 2020). Regions with robust recycling programs and policies promoting reduction and reuse of plastics may generate less plastic waste. Events such as the COVID-19 pandemic can also cause temporary spikes in plastic waste generation due to increased use of personal protective equipment and other disposable items (Leal Filho, Salvia et al. 2022). Furthermore, the presence and scale of specific industries, such as tourism, can also influence plastic waste generation. For example, tourist areas might generate more plastic waste due to the use of disposable items for convenience and hygiene (Pandey, Dhiman et al. 2022). Therefore, the differences in plastic waste generation across regions are a result of varying economic activities, consumption patterns, waste management strategies, and external events.

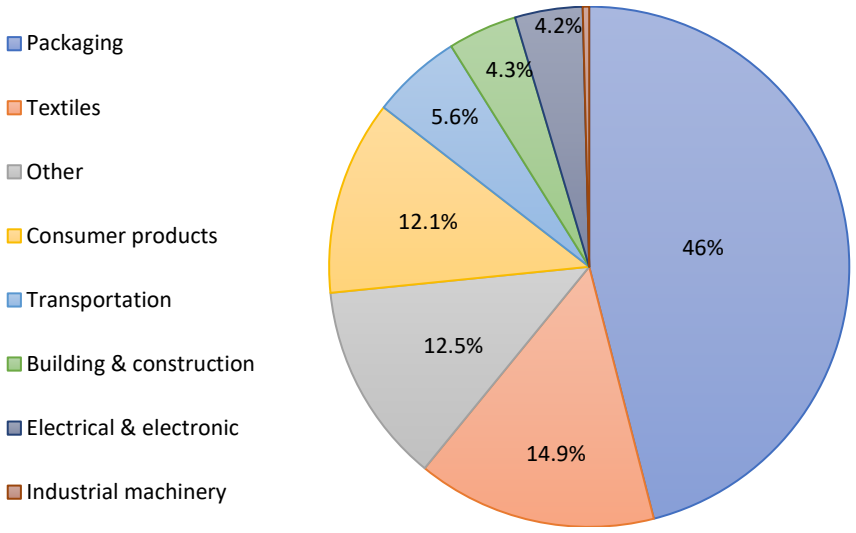

Figure 2.1. Distribution of plastic waste generation worldwide, by sector (Tsakona and Rucevska 2020).

The production rate of new plastic products differs from the generation of plastic waste due to different factors such as varying lifespans of different plastics, recycling rates and storage time. For example, single-use plastics might become waste within days of production, while more durable items like household appliances can last for years before they become waste. Some plastic products are recycled and repurposed, reducing the immediate generation of waste. Additionally, not all plastic products that are produced are immediately used or sold; some are stockpiled in warehouses or stores, awaiting sale or use.

Mechanical recycling is a crucial component in the transition towards a circular economy. The typical mechanical recycling process consists of shredding into flakes, further optical sorting

based on near-infrared technology, washing, density separation (where most polyolefins float and the rest sink), mechanical and thermal drying, and a final regranulation step by extrusion at 180–220 °C (Ragaert, Delva et al. 2017, Civancik-Uslu, Nhu et al. 2021).

However, there are several challenges associated with mechanical recycling. While this method is the most effective in terms of time, economic feasibility, and environmental impact, it is currently limited by factors such as cost, degradation of mechanical properties during the recycling process, and inconsistent quality of the recycled products (Schyns and Shaver 2021). Additionally, the reprocessing of plastics can induce degradation mechanisms that can affect the quality and usability of the recycled material. Regranulates from post-consumer flexible plastic waste are usually considered of lower quality to virgin plastics for several reasons including inefficient sorting at material recovery facilities, complex polymer compositions, and inadequate removal of impurities (Lase, Bashirgonbadi et al. 2022). For example, despite the structural similarities of polyolefins, their miscibility can become a problem during the extrusion process (Ragaert, Delva et al. 2017).

In addition to their extremely long degradation time (approximately 500 years (Ali, Elsamahy et al. 2021)), some plastics contain environmentally harmful substances such as flame retardants, phthalates, BPA, and heavy metals (e.g., Pb and Cd), which can leach from landfills, contaminate the ground, and bioaccumulate (Chen, Nath et al. 2021). Alternative technologies are needed to mitigate the environmental issues associated with plastic disposal in landfills and to recover valuable resources that support a circular economy for plastics.

In the context of non-recyclable and rejected plastic waste streams (e.g., heavily contaminated, multi-layered, multi-component materials, limited recyclability), chemical recycling represents a promising method for the recovery of valuable chemicals such as original monomers, precursors for monomer production, and other chemical substances (Soni, Singh et al. 2021). Complementary to mechanical recycling, chemical recycling contributes significantly to sustainable plastic production, with the potential to disrupt the current linear economy characterized by a “take-manufacture-consume-dispose” paradigm (Rasi, Ismail et al. 2023). Technologies such as pyrolysis or gasification offer a way to recover value (e.g., monomers and chemicals) from plastic waste that cannot be effectively managed through mechanical recycling (Kijo-Kleczkowska and Gnatowski 2022). Recovering monomers from these processes for the synthesis of novel resins is a significant contribution to sustainable plastic production. A staggering 99% of feedstock for polymer processing is

derived from fossil-fuel-based products (Nielsen, Hasselbalch et al. 2020), leaving a mere 1% originating from renewable feedstocks such as biomass (Geyer, Jambeck et al. 2017). At present, a modest 14% of end-of-life packaging plastic products are collected for recycling purposes, of which approximately 2% are effectively reintegrated into the plastic manufacturing process (World Economic Forum, Ellen MacArthur Foundation et al. 2016).

There are several routes for recovering valuable products from plastic waste through chemical recycling, utilizing temperature or a combination of temperature and solvent, with or without catalysts. Pyrolysis, a thermochemical process conducted in an inert atmosphere at temperatures ranging from >450°C to 800°C, is the most prevalent method for depolymerizing plastics (Davidson, Furlong et al. 2021). This method is versatile, capable of processing a wide range of plastic waste, including multi-layered packaging and plastics that are not recyclable by mechanical, solvolytic, and hydrothermal methods; however, the derived products are of low-quality output and typically targeted to be utilized as fuels rather than chemicals or monomers, resulting in CO_2 emissions and resource wastage (Aguado, Serrano et al. 2008, Akubo, Nahil et al. 2019, Al-Salem, Chandrasekaran et al. 2021). Additionally, pyrolysis is an energy-intensive process, requiring significant heat input to reach the reaction temperatures. This high energy demand can offset some of the environmental benefits it provides, particularly if the energy is derived from non-renewable sources. Furthermore, the upfront capital costs associated with building and operating pyrolysis facilities can be substantial, which limits the widespread adoption of this technology (Fivga and Dimitriou 2018, Djandja, Chen et al. 2022).

Recent studies have explored the conversion of plastic waste to hydrogen or synthesis gas, also known as syngas (a mixture of H_2 and CO), which can potentially be processed into precursors for polymer processing or chemicals (Younis, Gennequin et al. 2021, Shen, Zhao et al. 2022, Johar, Rylott et al. 2023). This gasification approach offers increased process flexibility in terms of feedstock use (e.g., compatible with oxygen-containing materials such as biomass) and has a positive impact on performance, rendering it a promising valorisation route (Lopez, Artetxe et al. 2018). In the context of sustainable waste management, a recent study by Chari et al. (Chari, Sebastiani et al. 2023) explored the environmental implications of gasifying nonrecyclable mixed plastic waste to generate high purity hydrogen, incorporating carbon capture and storage (CCS) to establish a low-carbon hydrogen production pathway. The process yielded a net negative climate change impact, reducing CO_2 emissions by 371 kg

per tonne of treated waste. Nonetheless, the primary drawbacks of this method are the high temperatures required for conversion (>700 °C), and the formation of tars (high molecular weight compounds that condense at 300 – 500°C), which can cause numerous processing complications, such as pipe and reactor fouling, if operating conditions are not strictly controlled (Weiland, Lundin et al. 2021).

In this review, chemical recycling technologies are systematically examined, with a focus on recent developments, advantages, and disadvantages. The challenges and future perspectives of chemical recycling of plastic waste to support sustainable polymer/plastic manufacturing are discussed in depth. Additionally, future research on chemical recycling of plastic waste, including mixed and contaminated waste, is addressed.

2.3. Chemical recycling via pyrolysis

Pyrolysis consists of a thermochemical decomposition process occurring within an inert atmosphere (e.g., N_2) with or without a catalyst, at a temperature range of 350 °C – 800°C (Kunwar, Cheng et al. 2016). This process generates various products, including gas, oil, wax, and solid residues. The distribution of these products is dependent upon multiple factors, such as process temperature, residence time, catalyst presence and properties, reactor design, plastic waste composition, and impurities (Akubo, Nahil et al. 2019). Processing temperature and residence time significantly impact product yields, with higher temperatures (>600 °C) and longer residence times favouring the production of gaseous compounds (Miskolczi, Bartha et al. 2004, Achilias, Roupakias et al. 2007). In addition, the feedstock's nature considerably affects the product composition, with polyethylene (PE) yielding more alkanes, polypropylene (PP) promoting the formation of alkenes, and polystyrene (PS) increasing the production of aromatic compounds (Williams and Williams 1999). The liquid oil and wax products derived from pyrolysis comprise a diverse array of hydrocarbons, which can be categorized into gasoline (C_4 – C_{12}), diesel (C_{12} – C_{23}), kerosene (C_{10} – C_{18}), and heavy fuel oil (C_{23} – C_{40}) (Almeida and Marques 2016). High quantities of wax may induce pipeline blockages, requiring heating during pyrolysis product transportation (Lee 2012). In the presence of an appropriate catalyst, the heavy fraction in the liquid products (waxes) can be converted into light hydrocarbons within the gasoline or diesel range (Ratnasari, Nahil et al. 2017). The use of solid catalysts, such as zeolites and silica-aluminas, can enhance the conversion of plastic waste into gas (C_1 – C_4), gasoline, and diesel ranges, at temperatures 200 – 300 °C lower than those required for thermal pyrolysis without a catalyst, consequently reducing production costs (Aguado,

Serrano et al. 2008, Miandad, Barakat et al. 2016). By appropriately manipulating process operating conditions (e.g., temperature, residence time, carrier gas) (Onwudili, Muhammad et al. 2019), catalyst type (Santos, Almeida et al. 2018), plastic-to-catalyst ratio, and reactor design (Singh and Ruj 2016), the desired product compositions and yields can be achieved.

Thermal decomposition (pyrolysis) follows a radical mechanism involving the stages of initiation, propagation or free radical transfer accompanied by β-scission, and termination (Miskolczi and Nagy 2012, Serrano, Aguado et al. 2012). The primary reaction mechanisms governing the thermal degradation of polymers include end-chain scission, random-chain scission, chain-stripping, and cross-linking, with the specific mechanism dependent upon the type of polymer being processed (Cullis and Hirschler 1981). Figure 2.2 illustrates the general steps underlying the thermal degradation reactions of prevalent polymers in mixed plastic waste (addition polymers). Thermal degradation entails the following steps: (i) initiation, involving the scission of the initial bonds in the chain to produce two radicals, which may arise at either random or end-chain positions; (ii) depropagation, characterized by the liberation of olefinic monomeric fragments from primary radicals; (iii) hydrogen chain transfer reactions, which occur as either intermolecular or intramolecular processes, leading to the formation of olefinic species and polymeric fragments, as well as the generation of secondary radicals through hydrogen abstraction between a primary radical and a polymeric fragment; (iv) β-Cleavage of secondary radicals, resulting in an end-chain olefinic group and a primary radical; (v) branch formation, occurring via interactions between two secondary radicals or a secondary and a primary radical; and (vi) termination, which unfolds either through a bimolecular mode involving the coupling of two primary radicals or by disproportionation of primary macroradicals (Stivala, Kimura et al. 1983, Clark, Alonso et al. 1999).

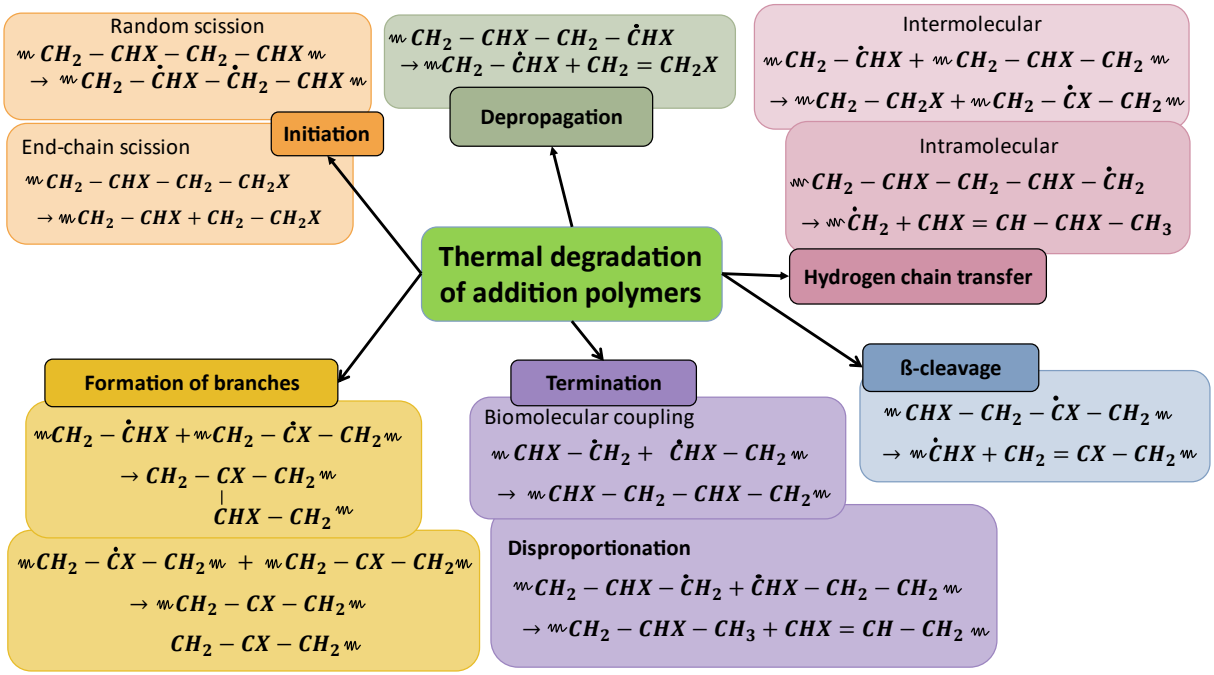

Figure 2.2. Principal reaction mechanisms for the thermal degradation of addition polymers. Adapted from (Clark, Alonso et al. 1999).

The balance of these reactions will differ as feedstock changes and depends on the molecular structure and chemical nature of each. For example, while LDPE also undergoes random chain scission like HDPE, its branched structure introduces additional complexities. The tertiary carbon atoms present at the branching points are more susceptible to radical formation, which leads to different pyrolysis pathways compared to the primary or secondary carbon atoms in HDPE. A similar behaviour can be expected for PP, as the number of tertiary carbons is higher, and it has a lower thermal stability than polyethylenes. The thermal decomposition of PET, on the other hand, is characterised for high decarboxylation reactions that results in the formation of CO and CO_2, a mechanism that is mostly absent in polyolefins.

In the case of mixed plastic waste, reaction kinetics exhibit considerable complexity, and the interactions among reactants can significantly influence the process. For example, PS undergoes decomposition first in a mixture of municipal plastic waste (including PS, polyethylene terephthalate (PET), polypropylene, low-density polyethylene (LDPE), and high-density polyethylene (HDPE) (Diaz Silvarrey and Phan 2016)), and the radicals generated from its thermal decomposition interact with the more stable polyethylene molecular chains, causing their premature decomposition (Miranda, Yang et al. 2001). In this context, activation energy may depend on conversion and vary at different heating rates, implying that the process cannot be described by a single step or first-order decomposition, but rather by a multi-step mechanism consisting of a combination of series and parallel reactions (Tuffi,

D'Abramo et al. 2018). The variation in decomposition temperature ranges for distinct plastics can be attributed to their unique thermal transitions and physical properties, which affect chain mobility and intermolecular interactions within the polymers. Furthermore, the low thermal conductivity of polymers influences heat transfer and hinders even heat distribution throughout the mixture. As a result, certain components within the mixture reach decomposition at varying temperatures (Martínez-Narro, Royston et al. 2023).

Despite the diverse thermal behaviour of plastics within mixtures, pyrolysis studies have primarily focused on individual plastics (Demirbas 2004, Diaz Silvarrey and Phan 2016) or binary mixtures (e.g., PE/PP, PE/PVC) (Sørum, Grønli et al. 2001, Hujuri, Ghoshal et al. 2008). Decomposition rates, as well as product yields and properties, depend on contaminants and interactions between intermediates derived from the reactants (Miskolczi and Nagy 2012, Almeida and Marques 2016). Consequently, conditions obtained from single plastic or binary mixture experiments may not be applicable for mixed plastics. Hence, understanding the thermochemical behaviour of plastic mixtures that resemble real waste streams is crucial. It has been reported (Bhaskar 2004) that the presence of PET in a plastic mixture containing PE, PP, and PS promotes the production of wax and solid residue. When HDPE, LDPE, PP, PVC, and PET were individually mixed with PS at equal proportions (Williams and Williams 1999), the average molecular weight of the liquid product decreased by 12-53%, with a high proportion of olefins compared to individual plastics. These effects could be attributed to the diffusion of radicals from PS decomposition at low temperatures, which destabilize polyolefins and reduce their activation energy (Miranda, Yang et al. 2001). Therefore, interactions should be considered during process design to obtain the desired products. Plastics with functional groups attached to the carbon chain decompose more easily than straight-chain hydrocarbon plastics (e.g., HDPE or LDPE) due to electron density distortion during thermal degradation (Miskolczi and Nagy 2012). As a result, the proportion of individual plastics in the mixture significantly impacts product properties. Understanding these interactions is critical for process development in chemical recycling of plastic waste, given the usual variability of input materials. This extends not only to the type of plastics involved but also to the specific grades of polymers and the additives they contain. For instance, highly branched polymers might decompose at lower temperatures due to weaker intermolecular forces as in the case of PP when compared to PE. Equally impactful are the additives within the polymers, as they may influence the overall conversion during pyrolysis (Schyns and Shaver 2021). Inert fillers might

impede heat transfer, while reactive fillers might participate in pyrolysis reactions, leading to a broader range of products. Other additives such as stabilizers, halogenated flame retardants, and antioxidants can decompose during pyrolysis, potentially forming toxic or environmentally harmful products and influencing the decomposition pathway of the main polymer. Comprehensive understanding of these aspects can aid in predicting process behaviour, refining process conditions, and managing product streams in a safe and effective manner.

Catalysts, such as zeolites (e.g., ZSM-5, HZSM-5, HBeta, natural zeolites) (Eimontas, Striūgas et al. 2021), fresh and spent fluid catalytic cracking (FCC) catalysts (Onwudili, Muhammad et al. 2019), ordered mesoporous aluminosilicates (e.g., Al-MCM-41, SBA-15) (Obalı, Sezgi et al. 2012), Al_2O_3, Ca(OH)2, Fe_2O_3, red mud (Ahmed, Batalha et al. 2022), and sulphated zirconia (Miandad, Barakat et al. 2016), are frequently employed in pyrolysis to not only minimize wax formation and operating conditions but also to enhance product selectivity. The physical and chemical properties of solid catalysts significantly influence catalytic cracking. Factors such as total surface area, pore volume, particle and pore size distribution govern the accessibility of large polymer molecules to the catalyst's internal active sites (Aguado, Serrano et al. 2007), while the acid strength and number of acid sites predominantly affect activity and selectivity during polymer degradation (Klaimy, Ciotonea et al. 2020). In zeolites, acid sites can be controlled by adjusting the plastic to catalyst ratio, or the Si/Al ratio, with higher Al content promoting increased acidity; however, lower amounts lead to more isolated Brønsted acid sites, which exhibit stronger acidity (Serrano, Aguado et al. 2012, Miskolczi, Juzsakova et al. 2019).

Zeolites, known for their characteristic microporous structure (i.e., pore sizes < 2 nm), strong acidity, and active sites, are effective catalysts for plastic waste pyrolysis (Papuga, Djurdjevic et al. 2022). These crystalline aluminosilicates possess pores ranging from 0.4 – 1.0 nm, while silica-aluminas, being amorphous aluminosilicates, contain a mesoporous (2 – 50 nm) matrix with pore sizes typically between 2–10 nm (Rouquerol, Avnir et al. 1994, Jia, Sun et al. 2013). The shape selectivity of zeolites enables high conversion rates (up to 92%) at relatively low temperatures (350 – 500 °C), enhancing gas yield and fostering the formation of light hydrocarbons and aromatics with increased market values (Aguado, Serrano et al. 2007, Almeida and Marques 2016). Generally, high microporous surface areas contribute to increased gas yields, whereas mesoporous surfaces promote a rise in liquid oil yield at the

expense of the gas fraction (Miskolczi, Juzsakova et al. 2019). Spent fluid catalytic cracking (FCC) catalysts from petroleum refining processes also yield high conversions into oil products (80 – 90%) (Lee, Noh et al. 2002, Moorthy Rajendran, Chintala et al. 2020), providing economic benefits by repurposing a residue for a different process.

The advantages of utilizing zeolite HZSM-5 in plastic waste pyrolysis include enhanced conversion efficiency, increased selectivity and cracking capability, reduced operating temperatures, regenerability and stability, as well as environmental benefits (Serra, Milato et al. 2022). Zeolites enhance plastic waste conversion during pyrolysis, elevating the production of valuable outputs such as light oils and olefin gases (e.g., ethylene and propylene) (Awayssa, Al-Yassir et al. 2014). Additionally, zeolites can decrease the energy input required for pyrolysis by generating substantial quantities of valuable products at moderate temperatures (500 – 600 °C), which in turn reduces overall energy consumption and minimises the formation of undesired byproducts like heavy waxes. However, microporous zeolites such as HZSM-5 exhibit a diffusion limitation due to small pores when reacting with long-chain bulky hydrocarbons (Corma 1997), preventing these molecules from easily accessing the internal acid sites due to steric and diffusional hindrances (Serrano, Aguado et al. 2012). The introduction of mesopores into the zeolite matrix may reduce the diffusion resistance of micropores (Zhang, Cheng et al. 2017). Recent catalytic pyrolysis research has focused on developing and applying hierarchical zeolites, which consist of bimodal microporous–mesoporous matrices with enhanced accessibility, effectively combining the advantages of both structures (Serrano, Aguado et al. 2006, Chen, Ma et al. 2012). Zhang et al. (Zhang, Cheng et al. 2018) studied the impact of external acid sites in hierarchical zeolites on selectivity towards olefins and coke deposition during pyrolysis. The findings revealed that external acid sites promote undesirable bimolecular reactions, such as alkylation, hydrogen transfer, and isomerization, due to the lack of space constraint, leading to coke deposition on the catalyst's surface. Hierarchical zeolites' internal acid sites primarily facilitate monomolecular reactions that produce low molecular weight compounds.

The catalytic cracking mechanism involves the formation of a carbenium ion, facilitating reactions such as random chain scission, β-scission, isomerization, hydrogen transfer, oligomerization, alkylation, cyclization, and aromatization (Jentoft and Gates 1997, Serra, Milato et al. 2022). The strength, density, and distribution of acid sites in the catalyst influence these mechanisms (Aguado, Serrano et al. 2007, Almeida and Marques 2016). Plastic

decomposition proceeds via an ionic mechanism, wherein the catalyst's Lewis acid sites promote hydride ion abstraction, and the Brønsted acid sites initiate hydrocarbon protonation, generating carbenium ions (Klaimy, Ciotonea et al. 2020). In the case of micropore catalysts, the initiation of the cracking reactions occurs at the catalyst's external surface or pore entrance, as the pore diameters are insufficient for large polymer molecules to enter the internal matrix. Subsequent to this initial degradation, lower molecular weight hydrocarbons can access the pores and undergo secondary reactions. The varying pore sizes account for the diverse selectivity among catalysts (Mordi, Fields et al. 1994). Table 2.1 presents experimental results from multiple pyrolysis studies employing different catalyst types. Oil and gas yields exhibit considerable differences, as they depend on various operating conditions unique to each experiment, complicating comparisons. The highest oil yield (85.5 wt%) was achieved with spent USY zeolite catalyst at 400 °C, while HZSM-5 generated the highest gas yield (93.1 wt%) at a low temperature of 360 °C. The average catalyst content relative to plastic is 23 wt%, and the average residence time of the experiments is 0.6 h.

The sustainability of a catalyst in plastic pyrolysis is not only determined by the amount of plastic it can process, but also by the efficiency of the process, the design of the catalyst, and the economic and environmental impacts of the entire life cycle of the process (Yadav, Singh et al. 2023). To determine the sustainability of a catalyst, a life cycle assessment (LCA) must be conducted, which would take into account the energy and resources used in the production of the catalyst, its operational efficiency and lifespan, and the environmental impact of its disposal.

One of the main challenges of catalytic pyrolysis is catalyst deactivation, requiring regeneration and increasing operating costs. The primary catalyst deactivation mechanisms include chemical, mechanical, or thermal processes and are categorized as follows: poisoning (active site loss due to reactant chemisorption), sintering (catalyst metal crystallite agglomeration), coke deposition/fouling (mechanical blockage), inactive compound formation (surface/catalytic phase loss), phase transformation (support thermal degradation), and particle attrition (Santamaria, Lopez et al. 2021). Owing to its practicality, the most prevalent catalyst regeneration method is air incineration. However, combustion's high exothermicity can induce overheating and local high-temperature gradients, resulting in metal sintering, coke deposition graphitization, and catalytic activity loss (Zhou, Zhao et al. 2020). After four regeneration cycles of a Nickel-alumina catalyst through combustion at 600 °C for 3 h, the H2

yield from toluene cracking decreased from 22.4% to 13% due to Ni sintering and graphitized coke (Lu, Huang et al. 2017). Even for high deactivation resistant acid catalysts like ZSM, compared to Al-MCM-41 (Aguado, Serrano et al. 2007), catalytic activity is significantly impacted. López et al. (López, de Marco et al. 2011) compared a ZSM-5 zeolite's textural properties before and after pyrolysis of municipal plastic waste (MPW) at 440 °C for 30 min, and subsequent regeneration. The micropore and BET surface areas were reduced by 99% and 29%, respectively, while the external surface area increased significantly due to coke deposition on the catalyst. After regeneration in oxygen at 550 °C, 83% and 99.7% of the lost micropore and BET surface areas were recovered, respectively. Coke deposition influences the catalytic activity of zeolites by blocking surface pores; however, regeneration processes such as calcination can restore their original activities for continued use. Aguado et al. (Aguado, Serrano et al. 2013) investigated the deactivation of a Ni-supported beta zeolite catalyst during LDPE pyrolytic volatile hydroreforming. A regeneration process involving calcination at 550 °C followed by H_2 reduction was performed, and after four deactivation-regeneration cycles, the catalyst maintained most of its activity and gasoline and light diesel selectivity. Catalyst internal porous structures play a crucial role in coke deposition and pore blockage during plastic catalytic cracking. Structures facilitating bulky molecules' unobstructed movement through the catalyst matrix are less susceptible to deactivation and activity loss. Elordi et al. (Elordi, Olazar et al. 2011) compared the deactivation of different shape selectivity zeolites (HZSM-5, HY, and Hβ) during HDPE catalytic pyrolysis in a conical spouted bed reactor. Among the tested catalysts, HZSM-5 exhibited the lowest micropore blockage and surface acidity reduction; its activity remained constant after partial deactivation. This was attributed to the unrestricted passage of coke precursors through the catalyst matrix. In addition to calcination, other methods for catalyst surface carbon deposit removal for regeneration include washing with organic solvents, supercritical fluids, plasmas, abrasion, and ultrasonication (Aguado, Serrano et al. 2013).

The large size of polymers, low thermal conductivity, and high viscosity contribute to heat and mass transfer limitations (Serrano, Aguado et al. 2012). A recently proposed approach to mitigate catalyst deactivation involves a two-stage system comprising thermal pyrolysis in the first stage, followed by catalytic reforming in the second stage (Akubo, Nahil et al. 2019, Onwudili, Muhammad et al. 2019, Wu, Kuo et al. 2019). This configuration prevents direct contact between catalysts and molten plastics (and the subsequently generated char),

allowing only shorter molecular chain volatiles to pass through the catalyst matrix. Ratnasari et al. (Ratnasari, Nahil et al. 2017) conducted two-stage catalytic pyrolysis of HDPE at 500 °C, utilizing mesoporous catalyst MCM-41 in the first stage and microporous ZSM-5 in the second stage, where the pyrolytic volatiles from the first stage thermolysis were further converted into highly aromatic gasoline-range hydrocarbons (C8 – C12). Carbon deposition on the catalysts was negligible after a single run. Metal-impregnated Y-zeolite-catalysed pyrolysis of HDPE at 600 °C in a two-stage reactor facilitated high conversion of aromatic compounds (primarily benzene, toluene, and xylene), but also considerable carbon deposition compared to the metal-free zeolite (Akubo, Nahil et al. 2019).

Some of the most substantial challenges associated with the pyrolysis method stem from the properties of the feedstock itself. The high degrees of contamination in the feed, coupled with the diversity of polymer grades and the heterogeneous nature of the mixed waste, present significant obstacles such as coking, catalyst poisoning, and corrosion. Additionally, the numerous additives (e.g., metallic pigments, calcium carbonate, talc, kaolin, glass fibres, carbon black, metal stearates, antioxidants, and other organic additives (Abbas-Abadi, Ureel et al. 2023)) contained within the feedstock further complicate the process, making it difficult to produce a valuable product suitable for feedstock recycling. The heterogeneity of plastic waste, consisting of various polymers and laminations, coupled with the lack of standardized trading and sorting practices, creates significant obstacles in recycling. Currently, the plastic waste feed lacks established standards or purity grades for classification (Burgess, Holmes et al. 2021). Regular plastic waste pyrolysis oil is unsuitable for direct use as feedstock in steam cracking units in existing refineries, owing to the abundance of impurities (Kusenberg, Eschenbacher et al. 2022). Contaminants like halogens, nitrogen, and sulphur can be extracted through hydrotreatment, a well-established but costly process due to the need for expensive hydrogen (Dabros, Stummann et al. 2018). Alternatively, methods such as filtering can be employed to improve the plastic waste feed's suitability for catalytic pyrolysis or steam cracking following thermal pyrolysis (Kusenberg, Roosen et al. 2023).

Feedstock recycling of naphtha-range pyrolysis oils in a steam cracking unit would provide the highest degree of material circularity for plastic waste (Kusenberg, Eschenbacher et al. 2022). Steam cracking produces primarily light olefins such as ethylene and propylene, from which new polymers are produced. If the pyrolysis oils were to be fed upstream in a petroleum refinery, the molecules would distribute across the multiple separation units, and some would

end up constituting fuels which are single-use and contribute to air pollution. Therefore, to maintain a high degree of material circularity, pyrolysis oils must be purified and feedstock-recycled downstream in refineries, in steam cracking units that produce monomers. As previously discussed, the numerous contaminants of pyrolysis oils make their purification extremely challenging and requires advanced hydrogen-based technologies coupled with additional separation methods such as filtration or solvent extraction (Kusenberg, Eschenbacher et al. 2021, Kusenberg, Eschenbacher et al. 2022). The extensive purification steps that are needed for pyrolysis oils to make them suitable for processing is a major cost driver that challenges their use as feedstock compared to conventional fossil fuels.

Hydrocracking is a pyrolysis process occurring in a hydrogen environment, which proceeds via C-C bond cleavage in conjunction with subsequent hydrogenation reactions of unsaturated subproducts (Weitkamp 2012). The primary advantage of employing hydrogen as a reaction medium is that, at low to moderate temperatures (i.e., 300–450 °C), the oil products are abundant in saturated hydrocarbons due to the hydrogenation of olefins, allowing direct use as fuel without additional processing, unlike those from conventional pyrolysis (Mosio-Mosiewski, Warzala et al. 2007, Munir, Irfan et al. 2018). Furthermore, hydrocracking reduces coke formation that deactivates catalysts and can remove halogens and other contaminating heteroatoms from plastic waste (Aguado, Serrano et al. 2013). Hydrocracking typically involves bifunctional solid acid catalysts to promote cracking reactions and hydrogenation (Garforth, Ali et al. 2004, Akah, Hernandez-Martinez et al. 2015). The hydrogenation effect results in a significant reduction (66-68 wt%) of solid residue compared to catalytic pyrolysis in an inert environment (Hesse and White 2004). Up to 90% conversion of PE and PS into oil (78 wt%) and gas (12 wt%) products was achieved over NiW and HY zeolite catalysts for 1 h at a temperature of 390 °C (Walendziewski and Steininger 2001). Hydride ions generated from the H_2 carrier gas inhibit coke formation and enhance selectivity towards single-ring aromatics during pyrolysis (Xue, Johnston et al. 2017). The presence of Ni in the catalyst substantially reduces the olefin content during hydrocracking of PE and PP pyrolytic oils by promoting hydrogenation reactions and, thus, inhibiting oligomerization (Escola, Aguado et al. 2012). For instance, Ni/H-Beta zeolite yields 69% of gasoline-range saturated compounds when treated with H_2 at 40 bar (Escola, Aguado et al. 2012). Fuentes-Ordóñez et al. (Fuentes-Ordóñez, Salbidegoitia et al. 2016) examined the reaction mechanism of PS hydrocracking over a bifunctional Pt/H-Beta catalyst, wherein the dominant reactions are hydrogenation-

dehydrogenation and ring-opening reactions that favour the production of paraffins, isoparaffins, and naphthenics. A schematic of the proposed reaction pathway is presented in Figure 2.3.

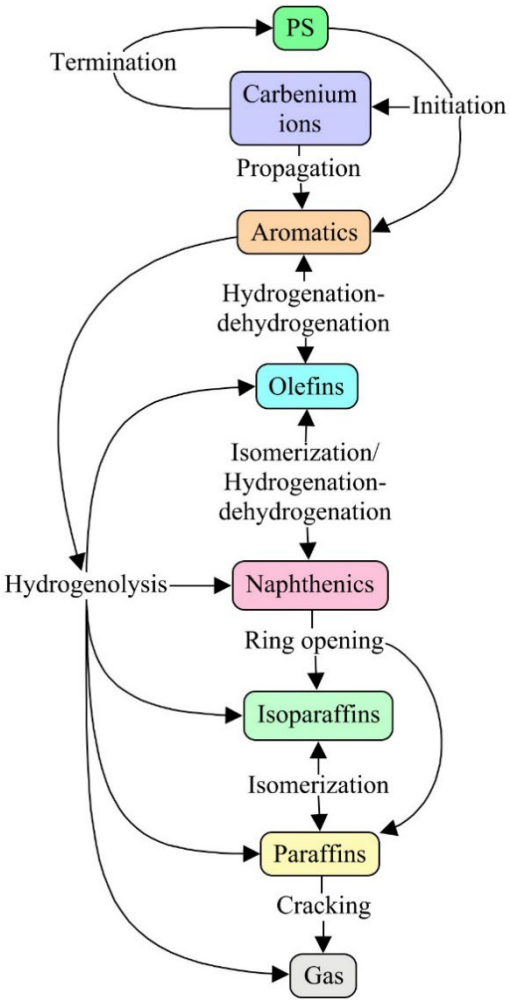

Figure 2.3. Reaction pathway of PS catalytic hydrocracking. Adapted from (Fuentes-Ordóñez, Salbidegoitia et al. 2016).

The hydrogen used in this process can come from various sources, and the sustainability and carbon footprint of the process can be significantly influenced by its source. The most commercialised hydrogen production method is steam methane reforming, and other common methods include water electrolysis, pyrolysis/gasification or biological processing of biomass (Wang, Nabavi et al. 2023). If the hydrogen is derived from fossil fuels, the process can contribute to greenhouse gas emissions. On the other hand, if the hydrogen is derived from renewable sources, the process can be considered more sustainable.

Table 2.1. Processing conditions and results of catalytic pyrolysis experiments.

Catalysts		Reactants		Process conditions			Product yields and compositions / wt%				Ref.*
Type	Surface area	Plastic to catalyst ratio	Plastics	Reactor type and stages	Residence Time / h	Temp. / °C	Oil yield	Gas yield	Oil composition	Gas composition	
Spent FCC catalyst	148 m^2g^{-1}	--	(wt%) HDPE: 19, LDPE: 43, PP: 8, PS: 15, PET: 15	Two stage, single bed reactor	0.5	500	69.5	15	--	H_2: 3, C_2: 1.5, C_3: 5.5, C_4: 4.8	a
						600	66	29.5	--	H_2: 5.2, C_2: 6.2, C_3: 8.7, C_4: 5.6	
	147 cm^2g^{-1}	30 wt%	(wt%) HDPE: 38, LDPE: 24, PP: 30, PS: 7, PVC: 1	Single stage, fluidised bed reactor	0.5	400	82.7	5.3	--	--	b
	151 m^2g^{-1}	--	Pyrolytic wax oil from municipal plastic waste	Single stage, CSTR reactor	1.8	420	78.1	8.7	C_5–C_{15}: 20 C_{15}–C_{25}: 17	--	b
Natural zeolite	--	10:1	(wt%) PE: 20, PP: 20, PS: 40, PET: 20	Single stage	1.25	450	30	38.4	--	--	c
	91.146 m^2g^{-1}	16–26:1	LDPE	Two-stage	--	450	50	39	C_5–C_{12}: 39 C_{13}–C_{20}: 50 $C_{>20}$: 11	--	d
HMCM-41	1164 m^2g^{-1}	4	LDPE, HDPE, PP	Single stage	0.5	338	--	--	Gasoline: (C_5–C_{12}): 62 Gasoil: (C_{23}-C_{40}): 19	Paraffin C_1–C_4: 9 Olefin C_2–C_4: 10	e

Table 2.1. Processing conditions and results of catalytic pyrolysis experiments (continued).

Catalysts		Reactants		Process conditions			Product yields and compositions / wt%				Ref.*
Type	Surface area	Plastic to catalyst ratio	Plastics	Reactor type and stages	Residence Time / h	Temp. / °C	Oil yield	Gas yield	Oil composition	Gas composition	
MCM-41	815 m^2g^{-1}	3:2	LDPE, HDPE, PP, PS	Single stage, fluidized bed reactor	0.33	360	5.6	87.3	Olefin: C_2–C_4: 25.5 C_5–C_8: 58.5 Paraffin: i-C_4–C_7: 5.8 C_8: 2	--	f
SiO_2-Al_2O_3	274 $cm^3\,g^{-1}$	40 wt%	HDPE	Single stage, fluidized bed reactor	--	360	2.37	85.5	Olefin: C_3–C_4: 28.5 C_5–C_7: 40 Paraffin: i-C_4–i-C_7: 10	--	g
Y-zeolite	--	16–26:1	LDPE	Two-stage	--	450	48	40	(wt%) C_5–C_{12}: 41, C_{13}–C_{20}: 50, $C_{>20}$: 9	--	d
H-ultra stabilised Y zeolite (USY)	603 m^2g^{-1}	3:2	LDPE, HDPE, PP, PS	Fluidized bed reactor	0.33	360	3.7	87.5	--	--	f

Table 2.1. Processing conditions and results of catalytic pyrolysis experiments (continued).

Catalysts		Reactants		Process conditions			Product yields and compositions / wt%				Ref.*
Type	Surface area	Plastic to catalyst ratio	Plastics	Reactor type and stages	Residence Time / h	Temp. / °C	Oil yield	Gas yield	Oil composition	Gas composition	
USY	547 cm^2g^{-1}	30 wt%	(wt%) HDPE: 38, LDPE: 24 PP: 30, PS: 7, PVC: 1	Single-stage, fluidised bed reactor	0.5	400	85.5	3.3	Olefin: C_3: 9, C_4: 18, C_5: 8.5 C_6: 8, C_7: 2.5 Paraffin: C_3: 2, i-C_4–C_8: 38	--	b
HZSM-5	412 $m^2 g^{-1}$	10:1	(wt%) PE: 40, PP: 35, PS: 18, PET: 4, PVC: 3	Single stage, semi-batch	0.5	440	57	40	Aromatics: 95.1 %	H_2: 0.8 CO_x: 5.6 C_1–C_2: 24.6 C_3–C_4: 57 C_5–C_6: 11.9	h
	397 m^2g^{-1}	3:2	LDPE, HDPE, PP, PS	Fluidized bed reactor	0.33	360	3.3	93.1	Olefin: C_2: 3, C_3: 22.5, C_4: 25, C_5: 13, C_6–C_7: 3.5 Paraffin: C_3: 3.5, i-C_4–C_7: 19.5	--	f
n-HZSM-5	430 m^2g^{-1}	4	LDPE, HDPE, PP	Single stage	0.5	462	--	--	C_5–C_{12}: 53 Aromatic: 24	Paraffin: 27.5 Olefin: 19	e

Table 2.1. Processing conditions and results of catalytic pyrolysis experiments (continued).

Catalysts		Reactants		Process conditions			Product yields and compositions / wt%				Ref.*
Type	Surface area	Plastic to catalyst ratio	Plastics	Reactor type and stages	Residence Time / h	Temp. / °C	Oil yield	Gas yield	Oil composition	Gas composition	
$CaCO_3$	--	10:8	PE, PP, PS, PET, HIPS-Br	Two-stage	--	430	66	21	--	--	i
ZSM-5 + MCM-41	ZSM-5: 266 m^2g^{-1} MCM-41: 799 m^2g^{-1}	1:2	Agricultural waste: LDPE 65 wt%, PVC 23 wt%	Two-stage	--	500	79	19	Gasoline (C_8–C_{12}): 50 High MW ($C_{>13}$): 48	C_1–C_4: 99	j
			Wastewater bottles: PET, HDPE				73.5	15	Gasoline (C_8–C_{12}): 88 High MW ($C_{>13}$): 11	C_1–C_4: 99	
			Building/construction waste: PVC, PU, PE				73	21	Gasoline (C_8–C_{12}): 69 High MW ($C_{>13}$): 30	C_1–C_4: 99	
			Household food packaging: PE, PP, PET				75	20	Gasoline (C_8–C_{12}): 90 High MW ($C_{>13}$): 8	C_1–C_4: 99	

* a= (Onwudili, Muhammad et al. 2019),b= (Lin and Yang 2007), c= (Miandad, Rehan et al. 2019),d= (Syamsiro, Saptoadi et al. 2014), e= (Aguado, Serrano et al. 2001), f= (Huang, Huang et al. 2010), g= (Lin, Yang et al. 2004), h= (Lopez-Urionabarrenechea, De Marco et al. 2012), i= (Bhaskar 2004), j= (Ratnasari, Nahil et al. 2017).

Hydrocracking is usually employed for post-processing of products obtained through pyrolysis, aiming to upgrade low-quality oils and waxes for utilization as transportation fuels. However, focusing on the use of oils as transportation fuel poses negative environmental impacts, primarily due to the elevated CO_2 emissions associated with exhaust gases from internal combustion engines. In this context, monomer recovery and feedstock recycling prove to be more environmentally beneficial, as global efforts are directed towards reducing the carbon footprint.

2.4. Chemical Recycling via hydrothermal and solvothermal processing

Hydrothermal processing enables the conversion of materials by utilising water or organic solvents as reaction media within a temperature range of 290 – 450 °C, resulting in the production of liquid, gas, and char (Wu, Zhou et al. 2014, Hongthong, Leese et al. 2020). As the confined reactor is heated, vapour pressure generated by the water or solvent reaches levels between 10 – 25 MPa. This method is particularly suitable for feedstocks with high moisture content and contamination, thus circumventing the necessity for costly sorting and energy-intensive drying processes. As water approaches its critical point, substantial alterations occur in its properties, impacting the decomposition rate, equilibrium, and primary reaction pathways (Watanabe, Hirakoso et al. 1998). The hydrothermal process is designated as hydrothermal liquefaction (HTL) when water serves as the reaction medium, or solvolysis when an organic solvent is utilized. Near its supercritical state, water exhibits non-polar solvent characteristics, enabling the dissolution of plastics while providing a medium with high heat transfer and diffusivity. Concurrently, it functions as a hydrogen donor, promoting the cracking reactions (Li and Xu 2019, Bai, Wang et al. 2020). Ionic reactions involving water molecules as reactive agents are generally enhanced in this state, as water simultaneously operates as a solvent, reactant, and catalyst with both acidic and basic properties (Pandey, Bhaskar et al. 2015, Hongthong, Leese et al. 2020).

Hydrothermal processing is a promising technique for the chemical recycling of plastic waste, enabling the recovery of monomers (e.g., terephthalic acid, caprolactam) with properties akin to their original feedstock for use in polymer processing (Darzi, Dubowski et al. 2022). A monomer is a fundamental molecular unit capable of undergoing polymerization, forming the basis for the creation of larger, complex macromolecules. This approach is particularly well-suited for condensation polymers, as they typically contain hydrolysable functional groups, such as hydroxyl, carbonyl, and amide (Fakirov 2019). Analogous to pyrolysis, the yield and

characteristics of the resultant products are dependent upon the processing temperature and the chemical composition and ratios of the feedstock (Dimitriadis 2017, Yang 2019). This method aligns well with the broader concept of chemical recycling, which is increasingly seen as a viable approach to promote the circularity of materials. Notably, the end products can be identical to the original precursors, potentially facilitating endless recycling loops and the creation of other value-added chemicals (De Hoe, Şucu et al. 2022). Table 2.2 displays the operating conditions and products generated through hydrothermal processing of plastics. The composition of gas, oil, and solid products varies significantly among different plastics and depends on the specific operating conditions employed.

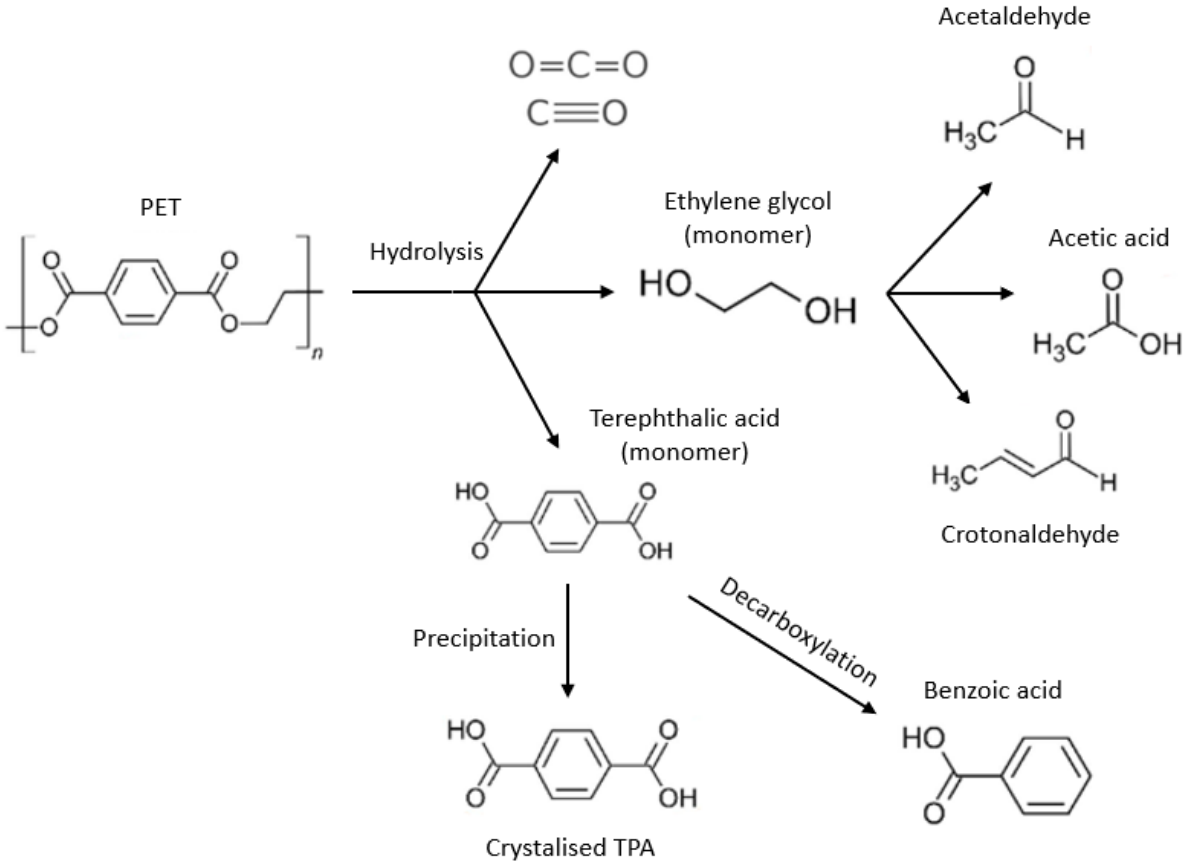

Figure 2.4. PET hydrothermal processing reaction pathway. Adapted from (Darzi, Dubowski et al. 2022).

At 400 °C and 25 MPa, polycarbonate predominantly undergoes depolymerization to its initial monomer, bisphenol A (BPA), while poly(p-phenylene oxide), styrene-butadiene, and poly(vinyl alcohol) yield a complex mixture of aromatic hydrocarbons (Pedersen and Conti 2017). HTL of PET and poly(butylene terephthalate) also yields their original monomer, terephthalic acid (TPA), as shown in Figure 2.4 (Noritake, Hori et al. 2008, Pedersen and Conti 2017). Zhao et al. (Zhao, Xia et al. 2019) conducted hydrothermal processing of e-waste

plastics, including high-impact polystyrene (HIPS), acrylonitrile butadiene styrene (ABS), polycaprolactam (PA6), and polycarbonate (PC), in subcritical water. The resulting product yields ranged from 81 – 97 wt%, comprising styrene monomers, styrene derivatives, BPA, and caprolactam (CL). Moreover, up to 89% product recovery, consisting of phenol, BPA, p-isopropenylphenol, and p-isopropylphenol, was achieved through HTL of PC under supercritical water conditions (430 °C) for a duration of 1 h (Tagaya 1999).

HTL of PC has been demonstrated as an effective method for obtaining pure phenol, which can be further utilized in the synthesis of novel resins (Ikeda, Katoh et al. 2008). The decomposition of polyurethane (PU) foam in water at 250 °C for 30 min resulted in a 90 wt% yield of toluene diamine (TDA) as the primary product (Dai, Hatano et al. 2002). Phenol and (TPA) were the main products from the HTL of poly(1,4-cyclohexylene dimethylene terephthalate) (PCT), a polymer employed in automotive and medical sectors (Xu, Xie et al. 2020). The optimal phenol yield (86.9%) was achieved at 340 °C, with a reaction time of 90 min and a water-to-plastic ratio of 10:1.

Polyolefins, including LDPE, HDPE, PP, and PS, present serious challenges for HTL processing at subcritical conditions due to the absence of functional groups capable of undergoing chemical reactions under these mild conditions (dos Passos, Glasius et al. 2020). Comprised of long chains of polymerized hydrocarbons without hydrolysable functional groups, polyolefins exhibit considerable resistance to degradation by HTL (Inderthal, Tai et al. 2021). Subcritical conditions do not provide sufficient temperature and pressure to initiate polymer chain breakdown and decomposition. The absence of functional groups in polyolefins also results in lower reactivity compared to heteroatom-containing synthetic polymers such as polyethylene terephthalate (PET), polycarbonate (PC), and polyurethane (PUR), which possess more reactive sites for hydrolysis and can thus be more readily depolymerized by HTL under subcritical conditions (Laredo, Reza et al. 2023). Therefore, supercritical conditions (i.e., temperatures exceeding 375°C and pressures surpassing 23 MPa) are essential for initiating polyolefin decomposition. The process at these conditions is usually known as supercritical water liquefaction (SWL) or gasification (SWG). At 450 °C and a reaction duration of 0.5 – 1 h, SWL of PP resulted in a 91% yield of oil comprising naphtha, jet fuel, and diesel from the (Chen, Jin et al. 2019). The SWL of HDPE at 425 °C produced linear paraffins and 1-alkenes in the oil phase, while oxygenated compounds (2-propanol, 2-butanol, 2-propanone, and 2-butanone) were produced in the aqueous phase (Moriya and Enomoto 1999). Ketone formation can be

attributed to the hydration of alkene products, which subsequently undergo oxidation into ketones in an aqueous environment. Jin et al. (Jin, Vozka et al. 2020) conducted SWL of waste PE at temperatures of 425 °C and 450 °C for durations of 2.5 h and 45 min, respectively. The process yielded 86 – 87% oil, primarily composed of hydrocarbons within gasoline and diesel ranges. By examining intermediate reaction products, the authors proposed a decomposition mechanism as follows: initially, depolymerization is instigated by free radical dissociation, cleaving C-C bonds into long-chain hydrocarbons. Subsequently, long-chain n-paraffins undergo β-scission and hydrogen abstraction, yielding α-olefins and short-chain n-paraffins, respectively. Isoparaffins form through the isomerization of short-chain n-paraffins. Additional free radicals are generated by α-olefins, which undergo conversion into naphthenes via cyclization. After one hour, naphthenes undergo dehydrogenation, first to alkylbenzenes and subsequently to polycyclic aromatics. Ultimately, olefins and paraffins transform into gas via thermal cracking (Jin, Vozka et al. 2020). A schematic representation of the reaction pathway is provided in Figure 2.5.

SWL has been demonstrated to be an effective technique for recovering valuable materials from electronic waste containing halogenated compounds, such as polychlorinated biphenyls and brominated flame retardants, achieving dehalogenation efficiencies of up to 90% (Li and Xu 2019). A maximum carbon liquefaction rate of 77.0 wt% was achieved for the SWL of high-impact polystyrene (HIPS) at 490 °C, which is approximately six times higher than that of conventional pyrolysis (Bai 2019). The content of toluene and ethylbenzene were found to be 14 wt% and 51.3 wt%, respectively. Bai et al. (Bai, Liu et al. 2019) carried out SWG on HIPS, describing the process in three stages: (i) initial thermal cracking and partial depolymerization at low temperatures (<500 °C), (ii) monomer and dimer formation at 500 – 650 °C which are subsequently cracked and gasified, (iii) residual monocyclic branched alkyl hydrocarbons undergo cracking at 650 – 800 °C, and the aromatic rings react with supercritical water, leading to significant ring-opening reactions. Concurrently, char gasification and the water-gas shift reaction become favourable at this temperature range, leading to substantial formation of H_2, CH_4, and CO_2 (Ge, Guo et al. 2013, Bai, Liu et al. 2019). SWG of individual common plastic waste (PE, PP, and PS) in the presence of ruthenium oxide catalyst primarily produced methane, up to 37 mol kg^{-1} from PE (Onwudili and Williams 2016). SWG of PP resulted in a 79.86% conversion into gas products at a temperature of 750 °C and a reaction time of 60 min (Bai, Wang et al. 2020). One benefit of HTL and SWL compared to pyrolysis is the capability of

processing various types of materials, including thermosetting polymers, thermoplastics, and composite materials, enabling the recovery of chemicals and monomers. For instance, thermoset polyesters undergo nearly complete conversion into their constituent monomers, phthalic acid and dipropylene glycol (Arturi, Sokoli et al. 2018). This process results in high yields of naphtha-range hydrocarbons, which can be then purified and fed to a steam cracking unit in a refinery to produce olefins and finally new polymers (Kusenberg, Eschenbacher et al. 2022). By ultimately creating new plastics, this approach contributes to resource conservation and provides a high degree of circularity. Instead of relying solely on traditional fossil fuels, the naphtha derived from plastic waste reduces the demand for virgin hydrocarbons, which reduces the depletion of finite natural resources and lessens the environmental impact associated with their extraction.

Accelerated decomposition reactions of phenol resins, such as PC, have been demonstrated in the presence of alkali salts and strong bases, (e.g., Na_2CO_3, NaOH, KOH, NH_4OH and $NaHCO_3$) (Tagaya 1999). Being strong bases, alkali catalysts can generate nucleophiles by abstracting a proton from the solvent in the reaction medium. These nucleophiles can then target electrophilic centres in the polymer chain, such as ester or carbonate linkages, promoting the cleavage of these bonds (Antonakou and Achilias 2013). Additionally, alkali catalysts contribute to electrophile activation by polarizing carbonyl functional groups (e.g., from ester, carbonate, and amide linkages), making them more susceptible to nucleophilic attack (Bender 1960). The catalyst donates electron density to the carbonyl oxygen, weakening the carbon-oxygen double bond and increasing the electrophilicity of the carbonyl carbon.

Tagaya et al. (Tagaya 1999) conducted HTL of PC using Na_2CO_3 (0.4 wt%) as a catalyst, achieving high yields of approximately 50 wt% at 230 °C for 24 h and 250 °C for 1 h, with phenol identified as the main product from the reaction. However, the utilization of homogeneous catalysts exhibits the drawback of their difficult separation and recovery from the reaction mixture (Ling, Tan et al. 2019). The catalyst is frequently dispersed across the liquid phase, complicating its isolation and subsequent reuse, thereby increasing costs and resource consumption. Furthermore, employing these homogeneous catalysts may introduce difficulties in downstream processing equipment.

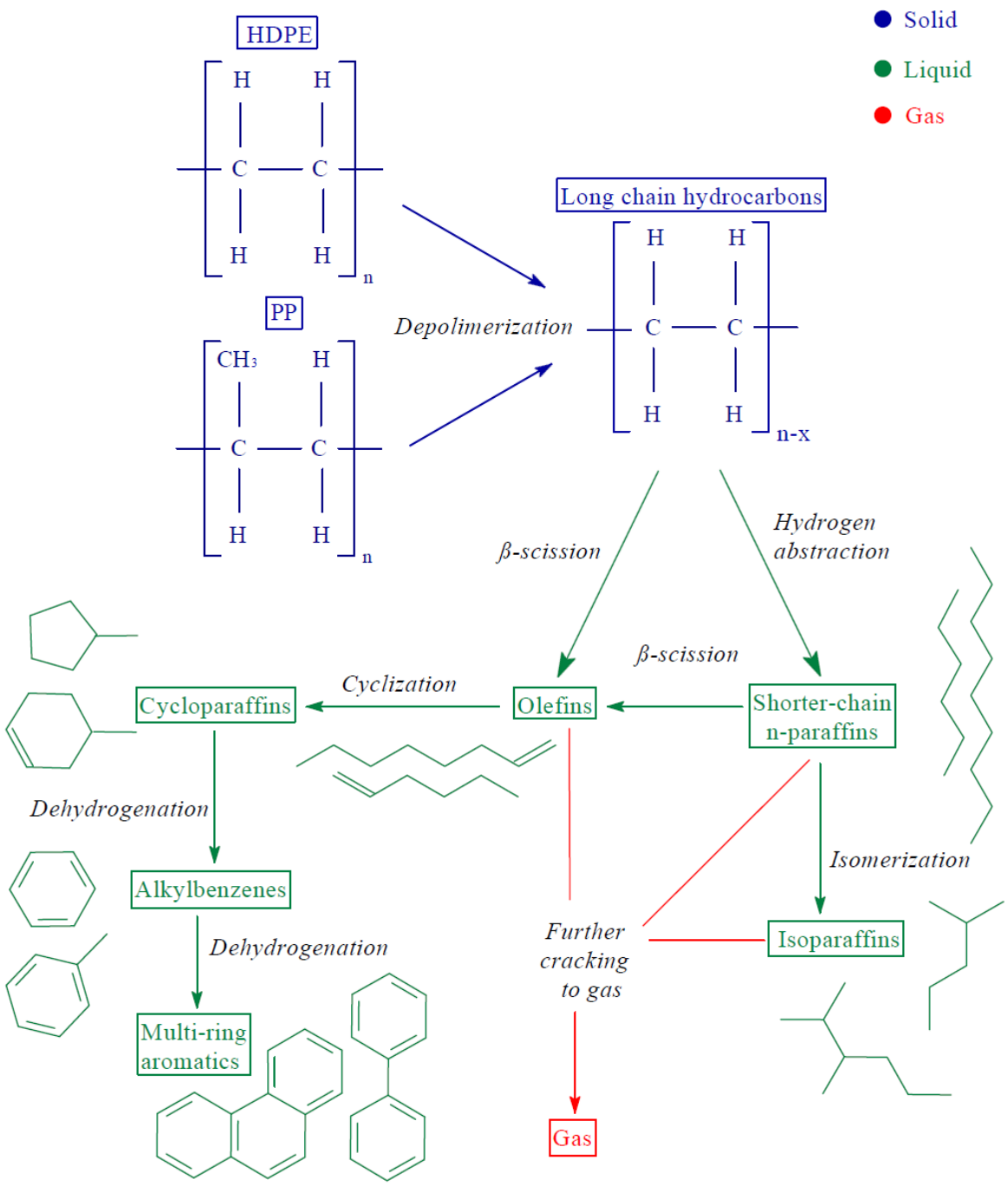

Figure 2.5. Reaction pathway of PE and PP decomposition in supercritical water. Adapted from (Chen, Jin et al. 2019, Jin, Vozka et al. 2020, Colnik, Kotnik et al. 2022).

The solubility of inorganic salts in water significantly decreases as polarity is reduced under sub- and supercritical conditions, resulting in salt precipitation that forms thermal insulating layers and potentially causes reactor blockage (Voisin, Erriguible et al. 2017). Utilizing solid catalysts, such as zeolites, can address these drawbacks, as they are easily separated from the reaction mixture (Gaide, Makareviciene et al. 2021). H-Beta zeolite has been demonstrated to enhance the conversion of waste polyamide into the monomer CL in subcritical water (Wang

2017). The catalyst increases the hydrolysis extent from 31% to over 60%, promoting the formation of linear intermediates rather than cyclic ones, thereby enhancing CL production.

Composite materials, extensively utilized in wind turbines, automotive, aeronautics, and sports industries for their exceptional properties such as low thermal expansion, high fatigue resistance, and excellent corrosion resistance in addition to mechanical properties, can have their fibres separated and recycled via HTL (Ballout, Sallem-Idrissi et al. 2022). The fibres, after being processed through HTL, are typically in a solid form, separated from the other components of the composite material (Isa, Nosbi et al. 2022). These recycled fibres can then be reused in the production of new composite materials. Thermosetting polymers, including epoxy and phenol resins, as well as thermoplastics, are frequently employed to create the polymer matrix in composite materials (Morin, Loppinet-Serani et al. 2012). However, the majority of these are currently disposed of in landfills due to their heterogeneous composition and cross-linked chains, which make them difficult to recycle using traditional mechanical recycling approaches (Job 2013). Pyrolysis can decompose the polymer matrix, but the mechanical properties (e.g., fatigue and impact resistance, tensile, flexural, compressive, and interfacial shear strength (Gao and Li 2016)) of the recovered fibres deteriorate after processing (Sokoli, Simonsen et al. 2016). HTL has been demonstrated as an effective technique for recovering monomers from carbon and glass fibre-reinforced polymer composites (CFRP and GFRP) while also preserving most of the mechanical properties (Ballout, Sallem-Idrissi et al. 2022, Protsenko and Petrov 2022). This is mainly attributed to the milder operating conditions of HTL compared to pyrolysis, which help maintain the integrity of the fibres with minimal damage (Kooduvalli, Unser et al. 2022). HTL enables the recovery of clean carbon fibres with properties akin to virgin fibres without the need for organic solvents or acids and at lower operating temperatures compared to methods like pyrolysis (Prinçaud, Aymonier et al. 2014). These fibres would otherwise accumulate in landfills or be incinerated. This efficient use of resources reduces the need for new virgin carbon fibres, thereby conserving natural resources and reducing the environmental impact associated with their production (Karuppannan Gopalraj and Kärki 2020). As much as 97 – 99% of the resin from PA6 was removed in the form of CL monomers within 15 – 30 min at subcritical temperatures (280 – 350 °C) or 10 – 15 minutes at the supercritical state (400 – 500 °C), while the mechanical properties of the fibres were preserved (Chaabani, Weiss-Hortala et al. 2017). Hydrothermal processing presents a promising alternative for chemical and material recycling to address the

challenges of composite waste management and close the loop for glass and carbon fibre-reinforced polymer composites.

Solvothermal processing employing eco-friendly organic solvents, such as glycols (ethylene glycol (EG), diethylene glycol, propylene glycol, and dipropylene glycol), has been extensively utilized for the depolymerization of polyesters through a process known as glycolysis (Xin, Zhang et al. 2021). In the presence of alcohols and water, the ester bonds undergo transesterification and hydrolysis, respectively (Grause, Matsumoto et al. 2011). The primary products recovered from PET include monomers, oligomers, bis(2-hydroxyethyl) terephthalate (BHET), TPA, glycols, dimethyl terephthalate (DMT), liquids, and gases (Raheem, Noor et al. 2019). Glycolysis is remarkably slow and unfeasible without catalysts (Bohre, Jadhao et al.). Homogeneous catalysts cannot be reused after processing, necessitating catalyst separation and product purification, ultimately generating wastewater that requires treatment (Diaz-Silvarrey, McMahon et al. 2018, Miceli, Frontera et al. 2021). Catalysts employed in PET glycolysis include metal acetates, oxides, carbonates, sulphates, titanium phosphate, zeolites, ionic liquids, and metal-organic framework catalysts (Esquer and García 2019). Meanwhile, prevalent catalysts for PU glycolysis include alkanolamines, metal hydroxides, alkoxides, acetates, and octoates. The PET glycolysis reaction initiates with glycol diffusion into the polymer matrix, leading to molecular expansion and, consequently, an enhanced diffusion rate (Fakirov 2019). Subsequently, glycol reacts with an ester bond in the polymer chain, degrading PET into lower molecular weight moieties. Glycolysis is the most widely used chemical recycling technique for recovering polyol monomers from PU and is typically conducted at around 200 °C in diethylene glycol (Zia, Bhatti et al. 2007). Hu et al. (Hu, Wang et al. 2020) carried out glycolysis of waste PET fibre using EG and zinc acetate as a catalyst, attaining an 80% yield of BHET. The PET synthesized from the recovered monomers exhibited properties comparable to those synthesized from virgin monomers.

In summary, hydrothermal processing, including HTL, SWL, and SWG has emerged as a promising technique for converting various types of plastic waste, including composites, thermosetting, and condensation polymers into valuable monomers and chemicals. However due to the lack of reactive sites in their molecular structure, this process is considerably less effective for decomposing polyolefins, which constitute the most abundant components of municipal plastic waste streams. The conditions required to obtain hydrocarbons (i.e., in the range of naphtha, diesel, or jet fuels) from polyolefins are highly stringent (i.e., >400 °C and

>25 MPa), requiring robust equipment such as specialized seals and valves capable of withstanding the temperatures and extreme pressures needed for decomposition. This renders the technology challenging to implement at an industrial scale, particularly in continuous operation. Nonetheless, hydrothermal processing has the potential to significantly contribute to sustainable waste management and resource recovery efforts from several plastic waste components. As research continues, efforts should be focused on the effective processing of polyolefins at subcritical conditions.

Table 2.2. Experimental results and conditions of hydrothermal processing of plastics.

Feedstock	Process	Operating Temperature (°C)	Reaction time (min)	Feedstock concentration (wt%)	Gas yield (wt%)	Oil yield (wt%)	Solid yield (wt%)	Main products	Ref.*
PP	SWG	500 –800	2 – 60	5 – 25	--	--	--	C_2H_x, CO_2, CO, CH_4, H_2	a
HIPS ABS PC PA6	HTL	350	60	3.2	1.0 2.0 1 .0 0.5	89 98 93 80	10 0 6 19.5	Styrene, styrene derivatives, BPA, CL.	b
PP	SWL	450	120	--	17	83	0	Naphtha, jet fuel, light diesel, diesel, lubricants	c
HIPS	SWG	350 – 550	60	2 – 10	39.6	--	--	Toluene, ethylbenzene, polycyclic aromatic hydrocarbons.	d
ABS	SWG	800	60	3	--	--	--	C_2H_x, CO_2, CO, CH_4, H_2	e
HIPS	SWL	374	5 – 60	1 – 9	--	--	--	Styrene monomers and dimers, toluene, and ethylbenzene.	f
PE	SWL	425	150	33.3	12	87	1	Aromatics, isoparaffins, n-paraffins, naphthenes, olefins.	g
HIPS ABS PC PP PA6	HTL	350	60	3.2	--	--	11 1 6 65 20	BPA, monoaromatics diphenyl-skeletons, alkanes, and CL.	h
PP PET PC PS	SWL	425	30	5.8	--	32 13 47 48	2 75 4 1.5	PP: cycloalkanes, alcohols PET: benzoic acids, long-chain fatty acids PC: bisphenol A PS: alkyl substituted benzenes	i

Table 2.2. Experimental results and conditions of hydrothermal processing of plastics (continued).

Feedstock	Process	Operating Temperature (°C)	Reaction time (min)	Feedstock concentration (wt%)	Gas yield (wt%)	Oil yield (wt%)	Solid yield (wt%)	Main products	Ref.*
PA6	HTL	330	60	--	--	84	--	CL, ε-aminocaproic acid.	j
PBT	SWL	400	15	10	--	0	50.8	PBT/PET: TPA, no oil yield.	k
PC						99.8	0	PC: phenols, BPA.	
PET						0	68.5	PLA: carboxylic acids, alcohols,	
PLA						0	0	ketones, no oil yield.	
PMA						48	0	PMA: carboxylic acids, esters.	
POM						13.7	8.1	POM: phenols, ketones.	
PPO						78.9	8.8	PPO: substituted benzenes.	
PVA						35.4	2.9	PVA: aromatics.	
SB						80.8	1.2	SB: styrene, aromatics (C_8-C_{16}).	
PE/biomass	HTL co-processing	350	15 – 60	(Plastic/biomass) 20	13	28	--	Phenolic compounds, monoaromatics, aliphatics, oxygenated compounds.	l
PP/biomass					18	30			
PET/biomass					16	32			
PA6/biomass					14	30			

* a= (Bai, Wang et al. 2020), b= (Zhao, Xia et al. 2019), c= (Chen, Jin et al. 2019), d= (Bai, Liu et al. 2019), e= (Bai, Jin et al. 2019), f= (Bai 2019), g= (Jin, Vozka et al. 2020), h= (Zhao 2018), i= (Seshasayee and Savage 2020), j= (Iwaya, Sasaki et al. 2006), k= (Pedersen and Conti 2017), l= (Hongthong, Leese et al. 2020).

2.5. Current challenges and future prospects

While each of the previously discussed chemical recycling methods present their unique advantages, it is crucial to recognize the inherent challenges associated with their large-scale implementation. The scale-up of plastic waste pyrolysis technology demands continuous reactors due to their capacity for handling increased throughput, attaining consistent product quality, and offering superior energy utilization in comparison to batch reactors. This aspect is particularly crucial in addressing the extensive volumes of plastic waste generated worldwide. Continuous reactors enable a stable flow of feedstock and products, intensifying process control and stability while reducing operational costs. However, continuous operations face multiple challenges during the scale-up of plastic pyrolysis technologies. The design of pyrolysis or gasification continuous reactors must consider the low thermal conductivity (e.g., 0.03 – 0.5 W $m^{-1}K^{-1}$ (Haynes 2016)) and glass transition temperature of the majority of polymers, and guarantee effective heat distribution to the plastic feed. Insufficient heating of the feed may impede heat and mass transfer, potentially leading to incomplete thermal degradation and the generation of low-value products (Pandey, Stormyr et al. 2020). Continuous pyrolysis reactors may experience various material-related challenges with plastic feed, such as premature degradation of the polymer, resulting in clogging or the formation of volatile compounds (Zhou, Dai et al. 2021). Given the diverse and varying composition of the plastic feedstock, preserving consistent reaction conditions, including temperature and residence time, can be challenging in continuous operations. This inconsistency might lead to fluctuations in product composition and yields, ultimately compromising process efficiency. Future research should prioritize addressing challenges associated with continuous operation in pyrolysis processes. A major area of focus involves the development of effective feedstock sorting methodologies. The implementation of chemometrics, advanced sensor technologies, and data analysis techniques, such as near-infrared (NIR) spectroscopy, Raman spectroscopy, and hyperspectral imaging, can facilitate real-time information acquisition regarding the composition of mixed plastic waste feeds, potentially reducing fluctuations in feed composition (Gosselin, Rodrigue et al. 2011, Kassouf, Maalouly et al. 2014, Zheng, Bai et al. 2018). However, overcoming challenges related to cost, calibration, and intricate data interpretation is necessary to render these techniques more accessible for widespread implementation in industrial-scale plastic waste pyrolysis. Another pivotal aspect of research involves the creation of robust and efficient catalysts for downstream processing that exhibit

resistance to deactivation (Daligaux, Richard et al. 2021). Continued research and development in these domains will substantially contribute to addressing the challenges faced by continuous pyrolysis operations.

The primary yield of pyrolysis is a low-grade mixture of oil and wax, requiring further processing and refinement to obtain value-added derivatives like naphtha, diesel, and gasoline range hydrocarbons. Such additional procedures can be costly and energy-demanding. Furthermore, feedstock contaminants (e.g., halogens, flame retardants, labels, and organic materials) exacerbate the issue. Plastic packaging waste streams generally comprise a blend of polymers and impurities, including paper, metals, organic residues, adhesives, and halogen-containing inks (Kusenberg, Roosen et al. 2022). These contaminants incorporate heteroatoms such as oxygen, nitrogen, and chlorine into the products, affecting the quality and applicability of the end products. Even after separating plastics from other solid waste components, PET and PVC are most likely to persist in the plastic mixture. PET and PVC respectively contain 33 wt% oxygen and 57 wt% chlorine. The presence of these atoms in pyrolysis oils causes numerous complications, including elevated viscosities, reduced energy content, processing equipment corrosion, and catalyst poisoning and deactivation (Kusenberg, Eschenbacher et al. 2021).

There are many studies in literature on plastic waste pyrolysis. However, many of these are focused on basic polymer systems, overlooking the complexity of commercial plastics that include layers, dyes, coatings, and various additives. Commercial polymers typically have essential additives such as antioxidants, UV stabilizers, and acid scavengers to meet their performance needs (Hahladakis, Velis et al. 2018). These additives can complicate recycling methods involving catalysts due to potential interactions with the catalyst active sites (Ellis, Rorrer et al. 2021). Recently, Jerdi et al. (Jerdy, Pham et al. 2023) studied the effect of several additives (i.e., hindered amine stabiliser, phenolic primary antioxidant, phosphite secondary antioxidant, and zinc stearate) on zeolite-catalysed plastic pyrolysis. The aminic additive was found to be the most prominent zeolite catalyst neutraliser, since the nitrogen-containing functional groups act as basic titrants to the catalyst acid sites. The phosphorus-containing additive also lowered the acidity of the catalyst, which remained low (27 % fewer acid sites) even after catalyst regeneration by calcination. The phenolic additive had a milder effect, as it does not contain inorganic species that exchange with surface sites, however, it modifies the reaction rate by competing for adsorption sites instead of deactivating them. Despite

these adverse effects, some of these additives (e.g., aminic and phenolic) can be removed from the catalyst surface by calcination. On the other hand, other additives such as zinc stearate and phosphites will accumulate permanently on the catalyst, which poses a significant challenge when considering continuous operation on industrial-scale waste processing facilities.

Integration of plastic pyrolysis products into petroleum refining facilities for feedstock recycling presents a promising strategy to capitalize on existing infrastructure. In Europe, a swift transition toward electric transportation as a substitute for fossil-fuel-powered vehicles is occurring, with projections indicating a considerable decline in refinery utilization by 2040 (Oliveira and Van Dril 2021). Given the vast scale of commercial petroleum refining operations and the implementation of economic penalties, substantial potential exists for employing plastic-derived pyrolysis oils as feedstocks in these units (e.g., steam crackers) for base chemical production, such as ethylene and propylene (Kusenberg, Eschenbacher et al. 2022). The fundamental obstacle for the widespread implementation of this method stems from the highly contaminated nature of pyrolysis oils. Consequently, to ensure compatibility with existing refining facilities, pre-treatment of plastic-derived pyrolysis oils is necessary to eliminate contaminants (e.g., halogens, oxygenates, heavy metals, and sulphur) (Castello and Rosendahl 2018). The removal of these contaminants is imperative to avoid damage to processing units and to preserve product quality. An approach for introducing pyrolysis oils to refineries involves pre-treating by hydrodeoxygenation, followed by blending with clean fossil-derived hydrocarbons such as naphtha (Venderbosch and Heeres 2011, Lindfors, Elliott et al. 2023). Nevertheless, this method presents several challenges that remain to be addressed. The elimination of halogens, particularly chlorine and bromine, can generate corrosive byproducts like hydrochloric and hydrobromic acid during hydrotreatment (Gioia and Murena 1998). These corrosive byproducts can inflict significant damage to hydrotreating equipment and may require the utilization of specialized, corrosion-resistant materials, increasing the capital expenditure costs. Heavy metals, including lead, cadmium, mercury, and iron, may be present in plastic waste, accumulate in pyrolysis oils, and cause damage to processing equipment (Kusenberg, Eschenbacher et al. 2022). These metals can induce catalyst poisoning during hydrotreatment due to metal deposition, reducing the catalyst's efficacy and increasing the frequency of catalyst replacement. The presence of nitrogen compounds in oil is also problematic, as they can hinder the hydrodechlorination process by

reacting with hydrochloric acid, forming organic salts that strongly adsorb on the catalyst surface, reducing its effectiveness (Murena and Gioia 1998). To successfully integrate pyrolysis products into petroleum refining facilities, future research must focus on enhancing pre-treatment processes for efficient contaminant removal. The establishment of feedstock standards, the implementation of quality control measures, and the utilization of advanced monitoring and analytical tools are vital for seamless integration without extensive equipment modifications. Additionally, it is essential to evaluate potential alterations required in refinery infrastructure and equipment to accommodate plastic pyrolysis oils and devise strategies for cost-effective implementation of these adaptations. This approach could pave the way for refineries to gradually transition from fossil-derived feedstock to plastic-derived oils in a sustainable way. Technological advancements will drive future prospects, enabling the capitalization of existing infrastructure for waste reduction and resource recovery.

Pyrolysis can be enhanced by integrating it with various technologies that promote the decomposition of plastic waste, such as cold plasma technology applied at low temperatures (around 250 °C) (Aminu, Nahil et al. 2020). Plasma is a distinct state of matter that comprises charged species including energetic electrons, excited molecules, and ions at non-thermal equilibrium conditions (Diaz-Silvarrey, Zhang et al. 2018). This results in an exceptionally high average electron temperature (10^4–10^5 K, 1– 10 eV) while maintaining a low bulk temperature close to room temperature. Cold plasma-assisted pyrolysis (CPAP) offers several advantages for the treatment of plastic waste. Its non-equilibrium nature allows for chemical selectivity and compatibility with catalytic processes without requiring complex electrode quenching systems, unlike thermal plasmas (Harris, Phan et al. 2018). The presence of energetic electrons creates a highly reactive environment, enabling the cleavage of C–C and C–H bonds in long-chain hydrocarbons and promoting the formation of lighter molecules (Diaz-Silvarrey, Zhang et al. 2018). This environment also enables thermodynamically unfavourable reactions to occur, potentially enhancing reaction activity and product selectivity (Zhang, Zhang et al. 2017). Future development in CPAP should focus on addressing existing challenges to increase its feasibility as a chemical recycling technology. Research should aim to reduce the high energy demand and power density (e.g., 4 kW L^{-1} (Khoja, Tahir et al. 2019)) of cold plasma generation and develop less specialized equipment to improve scalability. Robust reactor configurations that can endure continuous operation, advanced plasma generation techniques, and refined process control strategies are essential for optimizing the potential of

CPAP. Additionally, further research is required to adapt the process for diverse plastic feedstocks and impurities and to integrate it with alternative recycling methods, such as catalytic upgrading and reforming, enabling the production of high-value chemicals.

Microwave-assisted pyrolysis (MAP) has been utilized for processing various plastic wastes, including waste electrical and electronic equipment (WEEE), municipal plastic waste (MPW), polyolefins, and composites (Rosi, Bartoli et al. 2018, Moraes, Jermolovicius et al. 2020). The main advantages of MAP over conventional pyrolysis include straightforward control of reaction conditions, rapid and selective heating, and efficient energy transfer (Lopez, Artetxe et al. 2017). The selective heating mechanism facilitated by microwaves permits higher heating rates, subsequently leading to reduced reaction times and increased throughput (Goyal, Chen et al. 2022). Consequently, this results in fewer heat losses and decreased overall energy consumption, making MAP a promising option to assist pyrolysis. Despite its multiple advantages, MAP encounters several challenges that need to be addressed in future studies to realize its full potential. Achieving uniform heating of plastic waste is difficult due to the varying heterogeneous nature of the feed. Non-uniform absorption and reflection of microwave energy can reduce process efficiency, needing homogenized feedstock and even distribution of microwave energy (Ye, Zhang et al. 2021). An additional challenge involves the scale-up of the process from laboratory to industrial levels, as scaling up microwave heating systems can be complex and expensive (Duan, Yuan et al. 2023). Moreover, the interaction of microwaves with diverse plastic types and the impact of impurities in the waste feedstock need additional investigation to optimise process parameters. A crucial consideration for this process is microwave penetration. The high transparency of most plastics to microwaves renders them difficult to heat, necessitating the use of radiation absorbents, such as carbon, which can attain temperatures of approximately 1000 °C upon exposure to microwave radiation (Kumagai, Nakatani et al. 2020). Continued research is essential to understand the fundamental aspects of microwave-plastic interactions and to devise novel strategies for addressing challenges associated with scaling up and process optimization of MAP.

Waste derived carbon-based catalysts have been proposed as an economic and effective alternative for conventional catalysts (Klinghoffer, Castaldi et al. 2012, Areeprasert and Khaobang 2018, Lu, Huang et al. 2019, Li, Zhang et al. 2020). Biochar, a multifaceted carbonaceous material derived from various feedstocks and solid waste sources such as residual biomass and sewage sludge, presents a promising alternative to costly commercial

catalysts for plastic waste pyrolysis (Li, Zhang et al. 2020). The global availability, low cost, and adaptability of biochar's properties (including surface area, acidity, and pore volume) make it a desirable candidate for the chemical recycling of plastic waste, serving as a catalyst or support (Wang, Lei et al. 2020). The elevated surface area and porosity of biochar furnish a high number of active sites for catalytic reactions, thereby enhancing reaction rates and boosting the overall conversion efficiency of plastic waste pyrolysis (Xu, Yan et al. 2022). In spite of the benefits associated with employing biochar as a catalyst, the existing body of research on the utilization of raw biochar in waste plastic pyrolysis is limited. Sun et al. (Sun, Themelis et al. 2020) used carbonized sewage sludge as a catalyst for the pyrolysis of mixed MPW at 600 – 800 °C and found improved aromatic compounds selectivity. The aromatic selectivity of the biochar was attributed to Al, Fe, S and P species in the ash, which improve its surface acidity and dehydrogenation ability, while CaO and Fe species prevent formation of excessively heavy aromatics. Areeprasert & Khaobang (Areeprasert and Khaobang 2018) investigated the effects of iron oxide loaded biochar and electronic waste char on pyrolysis of a simulated e-waste plastic mixture (ABS/PC). The catalysts improved the oil yield and quality by increasing the amount of single ring aromatics. The biochar and electronic waste char showed high debromination efficiencies of 91 and 68 %, respectively. Sun et al. (Sun, Huang et al. 2018) performed pyrolysis of mixed plastics (PE, PP and PS) with biochar activated by $ZnCl_2$, KOH, and H_3PO_4, and raw biochar. Results showed an increase of selectivity towards bicyclic aromatic hydrocarbons (44 – 66%) when activated biochar was used, while alkenes were the dominant products using raw biochar (54%). A significant obstacle encountered by biochar catalysts pertains to their restricted stability, ultimately resulting in the deterioration of structural properties such as porosity and subsequent deactivation following multiple cycles of utilization. The application of biochar as catalyst in gasification processes is hindered by their susceptibility to consumption by gasifying agents such as oxygen and CO_2, requiring constant replacement (You, Ok et al. 2018). Moreover, biochar exhibits lower catalytic activity relative to alternative catalysts, such as zeolites, metal oxides, or mesoporous materials, and may require doping with metals (e.g., Ni Fe) to enhance performance (Xu, Yan et al. 2022). The characteristics of biochar exhibit substantial variability dependent upon the biomass feedstock, production parameters, and post-processing methods, which makes their control and optimization for specific catalytic applications challenging. Current research should address the prevalent stability limitations by devising innovative approaches to improve the structural properties and durability of biochars for their use as catalysts. The modification of

their composition, particularly via the incorporation of metallic ions, may serve to enhance catalytic activity, making them more competitive with other catalysts. Furthermore, refining production parameters could facilitate the precise adjustment of biochar attributes, thereby allowing customization for particular plastic waste pyrolysis applications. As a result, biochar catalysts may emerge as a sustainable and economically viable option for the chemical recycling of plastic waste. Table 2.3 displays various studies involving the pyrolysis of mixed plastics with both conventional and biochar catalysts. The results indicate favourable product quality and yields compared to non-catalytic experiments, highlighting the potential of biochar catalysts in plastic waste management.

The conversion of plastic waste into carbon materials represents a recent and promising approach in the field of chemical recycling. This process, known as controlled carbonization, involves the transformation of polymeric precursors into carbonaceous materials. The research progress in this area has led to the development of advanced carbon nanomaterials (CNMs) and polymer composites with enhanced flame retardancy (Gong, Chen et al. 2019). This approach has the potential to transform waste polymers into high value-added materials, contributing to the reutilization of waste polymers and providing an alternative to traditional waste management practices. The conversion of low-cost PET into high value-added metal-organic frameworks (MOFs) offers a new route for the large-scale production of MOFs, advancing the chemical upcycling of waste plastics (He, Hu et al. 2023).

Table 2.3. Summary of recent investigations exploring the effect of conventional and biochar catalysts on the pyrolysis of plastic mixtures.

Temperature / °C	Catalyst	Plastic mixture*	Product yield / wt%	Remarks	Reference
600	Biochar derived from sewage sludge	PE, PP, and PS	Oil: 41.3 Gas: 48.8	The selectivity of biochar was found to be high (75%) towards monocyclic aromatics, with oil containing 29.1% styrene and 12.5% xylene.	(Sun, Themelis et al. 2020)
600	Spent FCC catalyst	LD/HD-PE, PP, PS, and PET	Oil: 66 Gas: 29.5	The presence of the catalyst enhanced the production of aromatics in the oil and caused a transition towards the formation of gaseous products.	(Onwudili, Muhammad et al. 2019)
500	Biochar from gasification of poplar wood	LDPE and HDPE	Oil: 47.4 Gas: 24.6	Biochar catalyst facilitated the generation of propane, alkane, and alkene, and enabled the transfer of oxygen from HDPE to the surface of the catalyst.	(Li, Zhang et al. 2020)
500 – 600	Activated carbons	PE, PP, PS, and PET	Oil: 50.1 – 70.5 Gas: 29.3 – 49.7	Activated carbons were found to promote the creation of hydrocarbons in the jet fuel range. The catalyst's activity was greatly influenced by its acidity. Aromatization of alkanes was facilitated at higher temperatures.	(Zhang, Duan et al. 2019)
450	Acid/thermal activated natural zeolite	PS, PE, PP, and PET	Oil: 28 – 30.4 Gas: 38.4 – 39.2 Solid: 31.6 – 32.8	The use of catalysts resulted in increased production of aromatics. The heating values of the oils were in the range of 41.7–44.2 MJ kg^{-1}, which is comparable to that of conventional diesel.	(Miandad, Rehan et al. 2019)

Table 2.3. Summary of recent investigations exploring the effect of conventional and biochar catalysts on the pyrolysis of plastic mixtures (continued).

Temperature / °C	Catalyst	Plastic mixture*	Product yield / wt%	Remarks	Reference
500	$ZnCl_2$-activated biochar	PE, PP, and PS	Oil: 51.8 – 54.7 Gas: 42.5	The catalysts were found to significantly enhance the production of aromatics, with a high selectivity towards two-ring compounds (87.7%) and 1,3-diphenyl propane (37.4%).	(Sun, Huang et al. 2018)
500	KOH, H_3PO_4, and $ZnCl_2$ activated biochar	PE, PP, and PS	Oil: 42.6 – 51.8 Gas: 42.6 – 53.4	Raw biochar was found to yield a substantial amount of alkene fraction (54.9%), whereas activated biochar exhibited a higher selectivity towards aromatics.	(Sun, Huang et al. 2018)
500	MCM-41 and ZSM-5	LD/HD-PE, PP, PET, PU, PVC	Oil: 73 – 79 Gas: 15 – 21	A significant amount of oil (83.15 wt%) was produced when using an equal plastic to catalyst ratio. The resulting products had a high content of aromatics.	(Ratnasari, Nahil et al. 2017)
400 – 550	Fe-loaded biochar, Fe-loaded electronic waste char	ABS and PC	Oil: 40 – 42 Gas: 54 – 56	The use of catalysts was found to increase the production of monoaromatics. The presence of iron ions in the catalyst led to a dehalogenation effect, resulting in debromination efficiencies of 91% and 68% for Fe/BC and Fe/EWC, respectively.	(Areeprasert and Khaobang 2018)

* LDPE = Low density polyethylene, HDPE = High density polyethylene, PP = Polypropylene, PS = Polystyrene, PET = Polyethylene terephthalate, PVC = polyvinyl chloride, PU = Polyurethane, ABS = Acrylo-nitrile Butadiene Styrene, and PC = Polycarbonate.

The prevalence of PVC in plastic waste streams poses a significant challenge for chemical recycling methods. Prior to processing, PVC must be isolated due to its high chlorine content, accounting for over half of its mass, which can damage processing equipment and contaminate products. PVC comprises approximately 12% of global plastic demand and is found in most waste streams alongside polyethylene PET, PE, PP, and PS (Yu, Sun et al. 2016). Consequently, the thermal decomposition of unsorted plastics generates hydrogen chloride and unwanted chlorinated hydrocarbons resulting from the interaction of chloride from PVC and radicals (Lee 2007). Pyrolysis experiments on plastic waste mixtures containing PVC and flame retardants have been performed using carbon composite catalysts such as calcium carbonate (Bhaskar 2004) and iron oxide (Uddin, Bhaskar et al. 2002), resulting in the total elimination of chlorine and bromine from the products. Dehydrochlorination, a critical pre-treatment for chlorine removal in mixed plastics pyrolysis containing PVC, is conducted at temperatures below decomposition (approximately 300 °C) and involves an HCl separation unit (López, De Marco et al. 2011). Recent studies have reported the utilization of ionic liquids for dehydrochlorination processes, achieving near-complete chlorine removal at temperatures lower than the dehydrochlorination reaction temperature (>250 °C) (Zhao, Zhou et al. 2010, Glas, Hulsbosch et al. 2014). Oster et al. (Oster, Tedstone et al. 2020) employed phosphonium-based ionic liquids for PVC composite material dechlorination and observed a 99.8% dechlorination degree after 4 h at 160 °C, a notably low temperature for this procedure. Similar to PVC, waste electrical and electronic equipment (WEEE) plastics present recycling challenges due to the presence of harmful halogenated additives as flame retardants that require removal before processing (Sakhuja, Ghai et al. 2022). Ma et al. (Ma, Yu et al. 2017) examined the dehalogenation effects of various micro and mesoporous catalysts during brominated high-impact polystyrene (HIPS) pyrolysis. They reported a 70.47% debromination efficiency using Hβ zeolite; however, the products still contained high bromine concentrations, necessitating further upgrading. Novel techniques to generate high-quality, bromine-free oils from WEEE are required, and future research may investigate potential synergistic effects of different materials with WEEE to improve quality and halogen removal.

The predominant challenges impeding the widespread industrial implementation of hydrothermal processing for mixed plastic waste are centred around its limited efficacy in degrading primary constituents, such as polyolefins, the necessity for extreme pressures (>22 MPa), and the demand for specialized equipment. Furthermore, corrosion, induced by

elevated operating temperatures and dissolved oxygen concentrations, constitutes a substantial obstacle, as it can compromise equipment and shorten its service life (Li and Xu 2019). Investigating advanced materials and protective coatings may alleviate corrosion, albeit with a potential escalation in capital costs. Future prospects for this technology are contingent upon resolving operational issues, including deposition and blockages stemming from inorganic salt precipitation, through the development of efficient filtration or cleaning methods (Ghavami, Özdenkçi et al. 2021). The management of by-product formation (e.g., ammonia, hydrochloric acid, dissolved salts) and wastewater treatment or disposal is equally critical (Snowden-Swan, Zhu et al. 2017). Examining the potential of partially recirculating the aqueous phase, while assessing its advantages and challenges, could constitute a pivotal area of focus (Castello, Pedersen et al. 2018). Although recirculation might reduce wastewater volume and potentially decrease disposal expenses, it could concurrently elevate by-product concentrations, modify process conditions over time, and result in the accumulation of impurities and salts, ultimately impairing equipment efficiency and necessitating expensive maintenance or downtime (Kohansal, Sharma et al. 2022). A thorough assessment of the benefits and limitations of recirculating the aqueous phase must be performed before incorporating this approach into a continuous hydrothermal processing plant. To enhance the prospects for broad industrial adoption, the advancement of innovative techniques for processing polyolefins at subcritical conditions and the effective treatment of wastewater in continuous operation is of crucial importance. Such progress can increase economic feasibility and ensure compliance with environmental regulations, thereby promoting the successful implementation of hydrothermal processing technology.

2.6. Summary

Chemical recycling of plastic waste has gained attention as a potential solution to mitigate plastic pollution while recovering valuable materials. However, numerous challenges persist, including technological limitations, high capital expenditures, feedstock variability, and energy consumption. Technological advancements in processes such as pyrolysis, gasification, biological, and hydrothermal processing are imperative to enhance efficiency, scalability, and product quality. The capital-intensive nature of these technologies, along with feedstock preparation and specialized facilities, contribute to higher costs compared to mechanical recycling and landfilling. Moreover, the diverse plastic types, compositions, and contaminants in waste streams complicate chemical recycling, affecting process efficiency and end-product

quality. Energy consumption concerns arise due to substantial energy inputs, potentially negating environmental benefits if energy sources are unsustainable. For process efficiency and cost-effective operation, a fraction of the products might need to be used as an energy source for thermochemical conversion of plastics. However, this practice resembles incineration, a process that chemical recycling technologies intend to replace. In this context, integrating renewable and sustainable energy sources into the chemical recycling process is crucial to effectively reduce environmental impact and improve the carbon footprint. Unfortunately, there are limited studies addressing the potential benefits of incorporating renewable-sourced energy into chemical recycling processes.

Continuous research and development are crucial for a successful transition to a circular economy. Regulatory support, through the establishment of clear regulations and industry standards, can promote growth, commercialization, and environmental compliance. Environmental legislation should strive to reduce plastic waste and stimulate investment in recycling technologies (HM Revenue and Customs 2022). Although public awareness of the plastic waste issue has risen in recent years, further education regarding the benefits of chemical recycling and its role in addressing the problem is still necessary. This can ultimately lead to widespread public support and facilitate technology adoption.

Chapter 3. Materials and methods

This chapter provides a comprehensive overview of the methods and techniques employed in the experimental chapters of the thesis, i.e., Chapters 4 – 6. A detailed description of the pyrolysis and gasification experiments, conditions and setups are presented. Additionally, preparation and characterization of plastic waste samples, simulated plastic mixtures, and catalysts used throughout the studies are presented. Since Chapter 4 involves extensive kinetic and mathematical methodology that does not apply to others, these methods are excluded from this chapter and only the plastic characterisation is discussed. This chapter aims to facilitate a thorough and straightforward understanding of the experimental approaches that were undertaken and their implications for appropriate sample and catalyst preparation, experimental setup, and analytical procedures. By clearly outlining the methods, the research conducted in this thesis may be adequately reproduced and further developed by other researchers working in the field of chemical recycling of plastic waste.

3.1. Materials

3.1.1. Plastic waste samples

Proximate and ultimate analysis

Plastic waste samples were obtained from Byker Household Waste Recycling Centre in Newcastle upon Tyne. These selected plastics, consisting of HDPE, LDPE, PP, PS, and PET, are the principal components of plastic waste (PlasticsEurope 2020). This choice is based on their widespread use and resultant abundance in waste streams, making them representative of major plastic waste streams. These plastics vary in chemical structure, providing diverse insights into pyrolysis behaviours and product yields, which is valuable for research and development. Each type of plastic was manually isolated, thoroughly washed with soap to remove impurities, cut into 1 mm^2 squared pieces, and dried in an oven at 105 °C for 24 h. Small particle sizes were utilized for characterisation to minimize heat and mass transfer limitations during thermogravimetric analysis and differential scanning calorimetry. PVC was omitted to prevent corrosion of the processing equipment and formation of chlorinated compounds within the products.

Plastic waste typically contains a variety of additives that were originally incorporated to enhance the properties and performance of plastic products. These additives include stabilizers, such as UV absorbers and antioxidants, which help protect the plastic from

degradation due to sunlight and oxygen exposure (Pritchard 2012). Plasticizers are another common additive, especially in PVC and other flexible plastics, to increase pliability (Chaudhary, Liotta et al. 2016). Flame retardants are often found in electrical and electronic equipment materials to reduce flammability. They usually contain halogens, phosphorous, nitrogen, and metal oxides (Delva, Hubo et al. 2018). Additionally, colorants, both dyes and pigments, are used to impart desired colours and appearances to plastics (Muller 2011). The amount of additives in plastic products varies depending on the intended use and desired properties of the product. Typically, plastic products contain 20-50 wt% plasticizers, 0.1-10 wt% stabilizers, <5 wt% flame retardants, and <1 wt% each of colorants and antioxidants, relative to the weight of the plastic (Deanin 1975).

Proximate analysis, following the British standard BS-1016-3 (details found in Appendix A), was conducted to determine the moisture, ash, volatile matter, and fixed carbon content of the samples. The following equations were used:

$$Moisture\ (wt\%) = 100 \cdot \frac{ms - mf}{ms - mc} \tag{3.1}$$

$$Ash\ (wt\%) = 100 \cdot \frac{mf - mc}{ms - mc} \tag{3.2}$$

$$Volatile\ matter\ (wt\%) = 100 \cdot \frac{ms - mf}{ms - mc} - Moisture\ (wt\%) \tag{3.3}$$

$$Fixed\ carbon\ (wt\%) = 100\ (wt\%) - Volatile\ matter\ (wt\%) - Ash\ (wt\%) \tag{3.4}$$

Where mc is the crucible weight, ms is the weight of the crucible with the sample, mf is the mass of the crucible after the drying, combustion or volatilization processes. For the moisture content, around 1 g of each individual plastic sample and the simulated mixture were evenly spread on a previously weighted clean crucible and then placed inside an oven at 105 – 110 °C for 1 h. After the drying process, the crucible was left in a desiccator until it reached room temperature (20 °C) and was then weighted. For the ash content, the previously dried samples were weighted and spread over a known-weight combustion boat that was inserted in an open quartz tube (ensuring an oxidant atmosphere) inside a muffle furnace. To burn the samples, the furnace temperature was initially set and ramped to 500 °C and was maintained at this set point for 30 min, then the temperature was ramped to 815 °C and maintained for 60 min. Following, the combustion boat was removed from the furnace, placed in a desiccator until it

reached room temperature and was afterwards weighted. For volatile matter, a quartz tube was heated to 900 °C in a muffle furnace while purged with N_2 flowing at 50 ml/min to ensure an inert atmosphere. After 30 min of purging, the samples were spread on a previously weighted clean combustion boat and introduced inside the quartz tube for exactly 7 min. Following, the combustion boat was removed from the furnace and placed in a desiccator until it reached room temperature and was afterwards weighted.

The elemental analysis was conducted using a CHN628 Series Elemental Determinator following the Determination of Carbon, Hydrogen, and Nitrogen in Biomass method from LECO corporation. Details of this method can be found in the corresponding manual (Form No. 203-821-510), available from LECO corporation (LECO Corporation). The results, presented in Table 3.1, indicate that the samples consisted primarily of volatile matter (95.4 wt%), with low levels of ash (2.37 wt%) and negligible moisture (0.15 wt%). The presence of contaminants such as paint, glue, additives, and other materials raises the inorganic content of the samples, leading to an increase in ash content. The high content of volatile matter and low amount of ash and moisture makes these plastic materials suitable for a wide variety of chemical recycling methods. The experimental errors for proximate analysis results in Table 3.1 represent the standard deviation of measurements conducted in triplicate. The elemental analysis was conducted once.

Table 3.1. Proximate and elemental analyses of plastic waste samples (wt%).

Sample	Moisture	Ash	Fixed Carbon	Volatile matter	C	H	N	O[a]
PP	0.15 ± 0.04	2.18 ± 0.12	0.21 ± 0.07	97.61 ± 0.38	84.21	13.87	0.21	1.71
LDPE	0.17 ± 0.08	6.12 ± 0.29	0.60 ± 0.25	93.28 ± 2.12	83.52	14.50	0.43	1.56
PET	0.26 ± 0.13	0.70 ± 0.1	8.28 ± 1.74	91.03 ± 0.41	62.13	4.25	0.12	33.50
HDPE	0.04 ± 0.03	0.14 ± 0.06	0.22 ± 0.09	99.64 ± 0.52	85.90	13.79	0.02	0.30
PS	0.12 ± 0.07	2.43 ± 0.08	2.36 ± 1.18	95.21 ± 1.19	89.56	7.49	0.09	2.86

[a] by difference

Carbon and hydrogen are the most abundant elements in the plastic samples, while the oxygen content is minimal for all plastics, except for PET. For every pyrolysis run (Chapters 5 and 6), simulated mixtures were prepared based on the reported composition of global primary plastic waste generation (i.e., 20% HDPE, 28.5% LDPE, 27.5 PP, 9% PS, and 15% PET)

(Geyer, Jambeck et al. 2017). The plastic compositions used to develop kinetic models for thermal decomposition are described in Chapter 4.

Differential Scanning Calorimetry (DSC)

DSC is an analytical technique employed to determine the thermal transitions of polymeric materials, such as municipal plastic waste. Investigating the thermal transitions is useful for identifying polymer types since each plastic behaves in a characteristic way when subjected to a heat flow. Moreover, in a continuous industrial process in which mixed plastics are heated, it is extremely important to determine at which point the plastics will melt or become sticky. This phenomenon can cause significant complications and potentially lead to reactor or feeding system blockage. When a solid-state polymer is gradually heated, it eventually reaches a point where its chain mobility is affected, transitioning the mechanical properties from those characteristic of a brittle material to an elastic one (Lobo and Bonilla 2003). This physical change, known as the glass transition temperature (T_g), occurs over a range of temperatures (Buchwalter 2001). At this point, the specific heat capacity of the material also changes, allowing the T_g to be identified as the midpoint temperature between the beginning and end of the step change in a heat flow versus temperature plot (Byrn, Zografi et al. 2017). As the temperature continues to rise, the material reaches its melting point, the temperature at which the polymer absorbs heat to transition into the liquid phase. Subsequently, the molecules become disorganized and can move freely. This isothermal endothermic process is evident in a heat flow versus temperature plot as a drastic increase in heat flow at a constant temperature, with the melting point being the onset temperature (Holba 2017). The melting heat (T_m) can then be calculated from the area beneath the curve.

DSC tests were conducted using a TA Instruments DSC Q20. Square samples (1x1 mm^2) of each individual plastic were weighed and placed at the bottom of a standard Tzero aluminium pan, which was then covered with an aluminium lid sealed using a press. The plastic waste samples were incrementally heated from 30 to 400 °C at a heating rate of 10 °C min^{-1} under an inert N_2 atmosphere at a flow rate of 50 ml min^{-1}. All tests were performed in duplicate. The procedure involved simultaneous heating of two pans within the equipment cell. One pan contained the sample, while the other served as a reference and was filled with air. Both the sample and reference were heated at the same temperature per unit of time. Different heat flows were supplied to each pan due to the difference in specific heat capacity between the plastic waste sample and air. The differential heat flow, corresponding to the heat supplied to the plastic

waste sample, was plotted against temperature in the DSC curves. Table 3.2 presents the results of DSC analysis.

Table 3.2. DSC analysis of plastic waste (T_g = glass transition temperature, T_m = melting temperature, ΔH_m = melting heat).

Sample	T_g / °C	T_m / °C	ΔH_m / J g^{-1}
HDPE	N/D	132.05 ± 1.08	209.4 ± 13.8
LDPE	N/D	124.92 ± 3.13	151.05 ± 37.25
PP	N/D	165.19 ± 0.03	82.41 ± 5.32
PS	106.2 ± 6.23	238.51 ± 26.34	0.133 ± 0.01
PET	93.7 ± 6.345	250.68 ± 1.66	78.99 ± 37.81

3.1.2. Catalysts

Preparation

Walnut shells were selected to prepare the biochar catalyst support. Walnut shells are a multi-purpose abrasive material extensively employed in various applications including blasting, tumbling, cleaning, polishing, and filtration. Additionally, they are utilized in the cosmetic industry, non-skid surface treatments, and as fillers in various products (AZO Materials , Inc.). China and USA are the countries with the highest production of walnut shells (FAO 2023). It is important to note that using walnut shells as a catalyst could lead to several unintended consequences compared to their current use. Environmentally, increased demand may cause overharvesting, potentially harming ecosystems. Economically, it could raise walnut prices, affecting consumers and related industries. This new use might also lead to shortages and higher costs in sectors like abrasives. These factors highlight the need for a balanced approach, considering the environmental, economic, and social impacts.

The biochar, which served as both a catalyst and support for catalytic pyrolysis in Chapter 5, was produced in-house by subjecting walnut shells to pyrolysis at a temperature of 700 °C in the presence of CO_2 for 1 h. The selection of these conditions was based on their previous demonstration of generating biochars possessing high porosity and surface area characteristics (Phan 2021). After the reaction, the biochar was pulverized using a mortar and subsequently sifted to obtain a fine powder with a diameter of approximately 50 µm. Around 80 wt% of the biochar was recovered after sifting. The wet impregnation technique was used due to its straightforward implementation, minimal waste generation, and low cost (Sietsma,

Jos van Dillen et al. 2006). This procedure was based on the method developed by Xu et al. (Xu, Yan et al. 2022), however, different salt proportions with respect to biochar were used. A 100 ml solution containing either nickel nitrate hexahydrate, iron (III) nitrate nonahydrate, or zinc nitrate hexahydrate was prepared and combined with raw biochar. The proportions of nitrate and biochar were determined to achieve a 2:1 mass ratio of biochar to the resulting metal oxide (i.e., NiO, Fe_2O_3, or ZnO) after calcination. The resulting slurries were vigorously stirred for 12 h at 60 °C, then dried in an oven at 105 °C for 12 h, calcined at 600 °C in a flow of nitrogen (100 ml min^{-1}) for 4 h, and finally ground and sieved into fine particles of around 50 µm diameter. The HZSM-5 zeolite (312 SiO_2/Al_2O_3 molar ratio, 413 m^2 g^{-1} surface area) was activated by calcination in static air at 550 °C for 4 h at a heating rate of 20 °C min^{-1}.

The Ni-Al_2O_3 catalyst used in Chapter 6 was prepared via the wet impregnation method reported by Bartholomew and Farrauto, and synthesized by Laura Diaz-Silvarrey (Bartholomew and Farrauto 1976, Diaz Silvarrey 2019). A known amount of high surface area (180 m^2g^{-1}, Alfa Aesar) Al_2O_3 support pellets was mixed with a 1 M solution of $Ni(NO_3)_2{\cdot}6H_2O$ at an alumina to nickel nitrate molar ratio of 10:1. The resulting slurry was vigorously stirred at 60 °C for 1 h, dried at 105 – 110 °C for 24 h, and calcined at 550 °C for 5 h in static air. The dried Ni-Al_2O_3 catalyst was then reduced overnight in hydrogen at 550 °C and finally ground and sieved to produce a particle size of 50 – 500 µm.

Morphology and composition of fresh catalysts

The fresh catalyst's composition and structure were analysed through SEM, EDX, TEM, and BET methods. SEM images and EDX elemental mapping were obtained in a JEOL JSM-5610LV SEM operating at low vacuum and coupled with an energy dispersive X-ray spectroscopy (EDX) module. TEM images were obtained in a Philips CM100 Transmission Electron Microscope. In Figure 3.1 (a-b), the EDX elemental mapping demonstrates that the metallic particles (highlighted in red/pink) were evenly dispersed across the biochar catalyst surface.

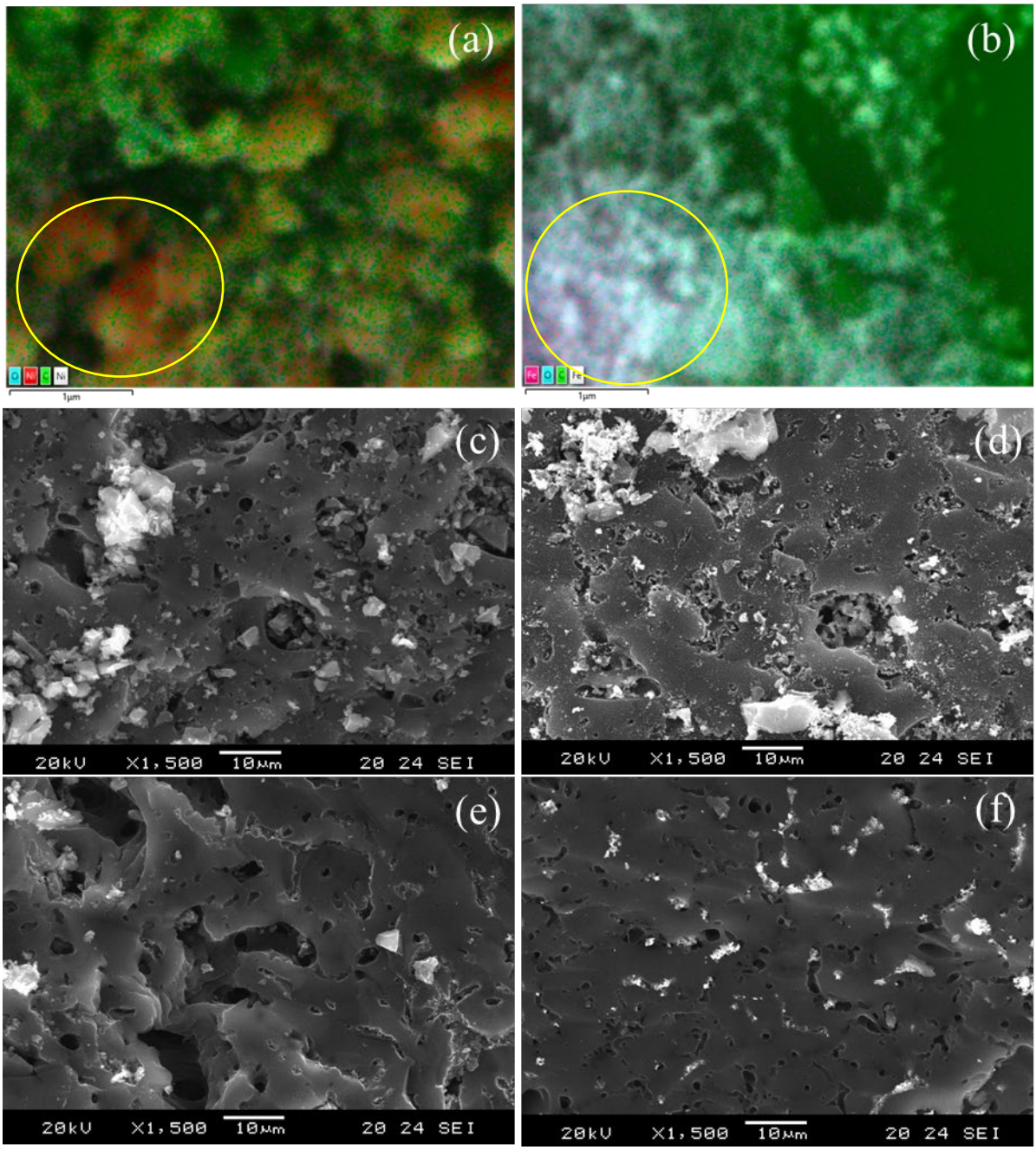

Figure 3.1. EDX mapping of nickel (a) and iron (b) doped biochars, and SEM images of raw biochar (c), nickel (d), iron (e), and zinc (f) doped biochars.

The macropore structure can be visualised in Figure 3.1 (c-f), this shape allows the bulky hydrocarbon volatiles to easily access the internal matrix of the catalyst, where reaction occurs in the surface of the mesopores and micropores (Miandad, Barakat et al. 2016). For the Ni-Al_2O_3 catalyst, EDX elemental mapping as well as SEM and TEM images are presented in Figure 3.2, in which it is shown that the Ni particles were uniformly distributed on the alumina surface forming conglomerates of <100 nm in size. TEM image analysis revealed that the average particle size was of 8.8 ± 3.6 nm with maximum and minimum sizes of 54.4 and 1.2

nm, respectively. The structural changes of biochars after being subjected to pyrolysis are illustrated and discussed in Chapter 5.

BET analysis was performed to determine the catalyst surface area by N_2 physisorption isotherms determined at 77 K using a Thermo Scientific Surfer porosimeter. The Ni-Al_2O_3 was dried overnight at 105 °C and outgassed at 150 °C for 8 h at high vacuum to remove any adsorbed materials prior to analysis. The catalyst had a total surface area of 92 m^2g^{-1}. The structural changes of this catalyst after pyrolysis, as well as reusability tests, are illustrated and discussed in Chapter 6.

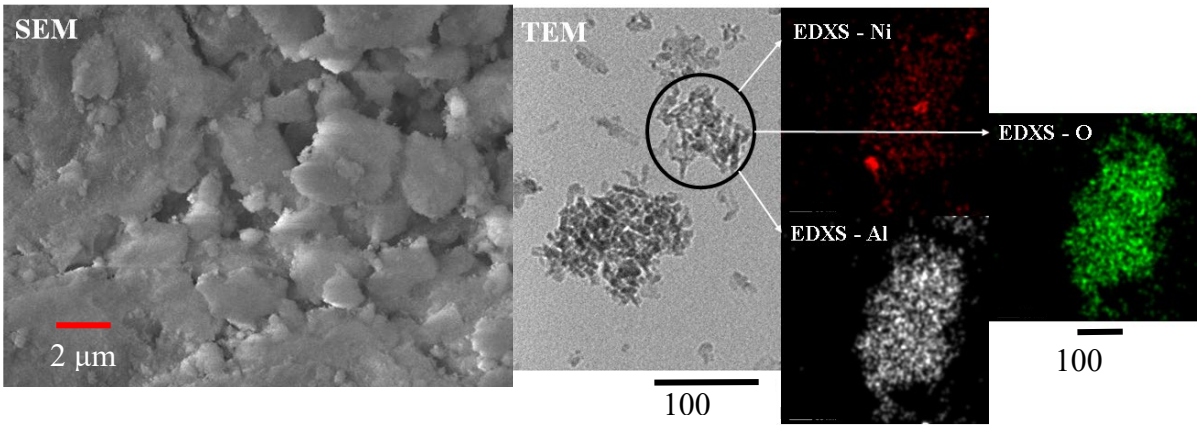

Figure 3.2. SEM image (left), TEM image (centre), and EDX (right) mapping of fresh Ni-Al_2O_3 catalyst (Diaz Silvarrey 2019).

X-Ray diffraction (XRD)

XRD analysis was performed to evaluate the crystallinity in a PANalytical X'Pert Pro MPD with Xcelerator detector using Cu Kα radiation. Figure 3.3 illustrates the XRD spectra indicating the identified phases of raw and metal-doped biochar catalysts. However, the Raw-BC sample had insufficient peaks to determine its existing phases. On the other hand, hexagonal ZnO was the only phase detected in Zn-BC, cubic nickel was the only phase of Ni-BC, and Fe-BC contained two forms of iron oxide: cubic Fe_3O_4 and FeO. Nickel oxide was not detected, and only nickel particles were present on the surface. Figure 3.4 shows the XRD spectra of fresh Ni-Al_2O_3 catalyst in which the only identified phases were cubic nickel and aluminium oxide. Nickel oxide particles were not detected due to the hydrogen reduction step, and only nickel particles remained on the surface.

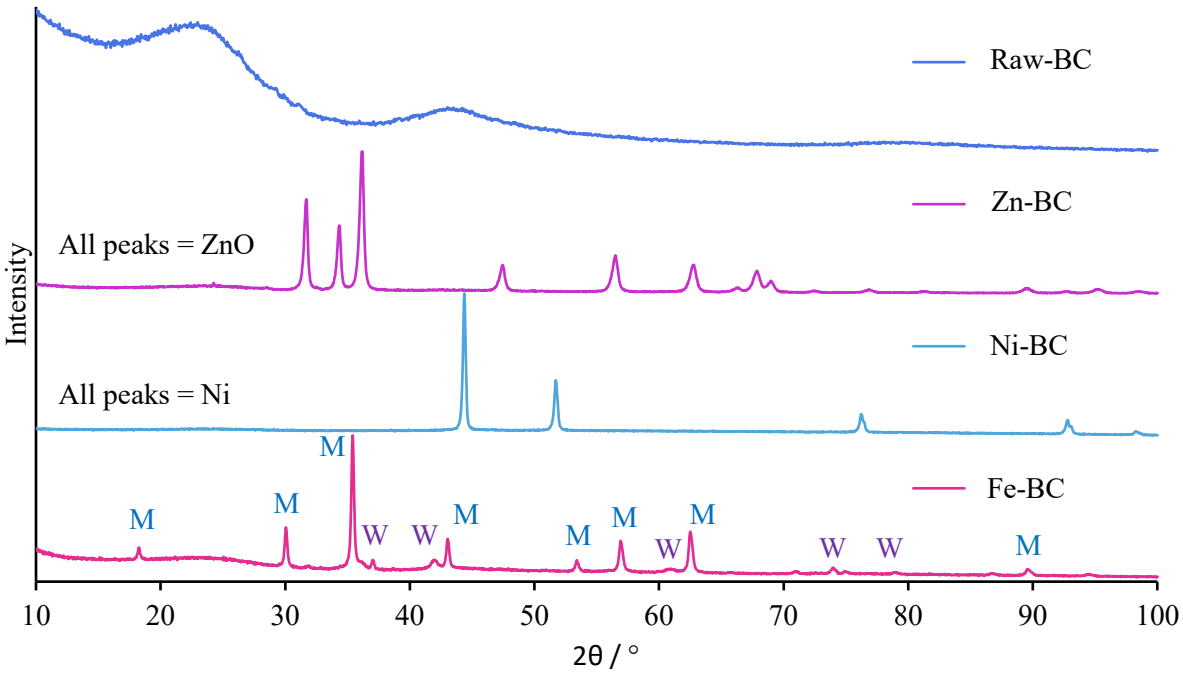

Figure 3.3. XRD spectra of biochar catalysts (M = magnetite (Fe_3O_4), W = wuestite (FeO)).

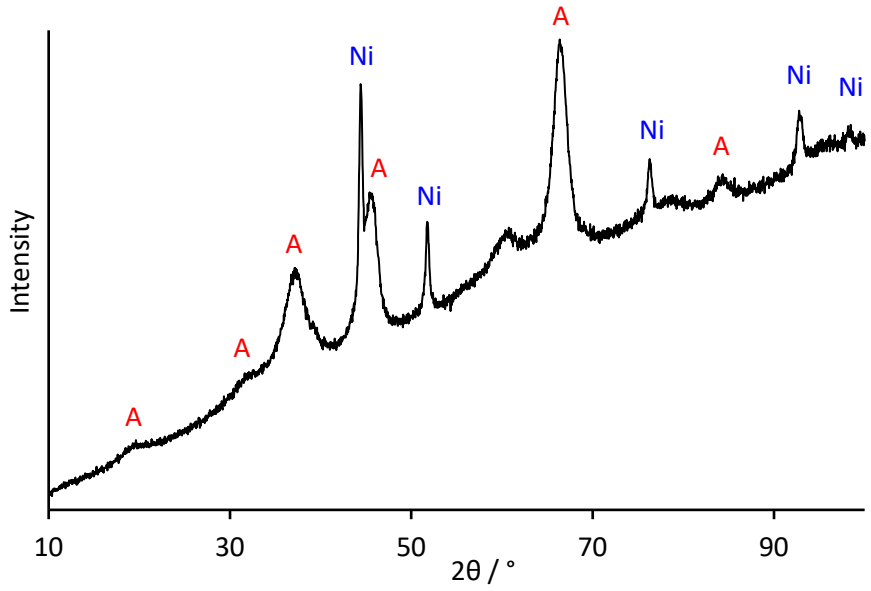

Figure 3.4. XRD spectra of Ni-Al_2O_3 catalyst (A = cubic Al_2O_3, Ni = cubic nickel).

CO_2 adsorption

The microporous structure of the biochar samples and zeolite was evaluated by CO_2 adsorption at a temperature of 0 °C by means of an Hiden Isochema Intelligent Gravimetric Analyser (IGA). The IGA is a computer-controlled ultrahigh vacuum system that automatically records isotherms while monitoring the gas admitted/emitted at each pressure point set between 0 and 100 kPa. Analytical CO_2 vapour (99.99 %) was supplied by BOC Ltd (UK). The pressure accuracy was maintained at ± 0.02 % of the pressure set point, and the pressure was controlled by three pressure transducers operating at three different ranges (0 – 0.2 kPa, 0 –

10 kPa, and 0 – 100 kPa). The sample temperature was monitored throughout the experiment, with errors of ± 0.1°C, and maintained by a cooling bath. At each adsorption step, the equilibrium value was determined to be 99.9% of the predicted value, which was calculated in real-time using the mass uptake profile. The microbalance used in the IGA had a long-term stability of ± 1 μg and a weighing resolution of 0.2 μg. To prevent disruption of the microbalance, the pressure was increased to the next set point in 60 – 100 s after achieving mass equilibrium and maintained constantly during adsorption steps. Prior to each run, approximately 50 mg of the carbon sample was degassed under vacuum (<10^{-6} Pa) at 120 °C overnight to remove any moisture until a constant weight was achieved before recording a static gas sorption/desorption isotherm. The CO_2 adsorption-desorption isotherm was analysed using the Dubinin-Radushkevich (DR) model. The DR micropore volume was obtained from the CO_2 adsorption isotherm at 0 °C within the pressure range of 0 – 100 kPa, equivalent to the relative pressure (p/p°) range of $4.6x10^{-4}$ – $2.8x10^{-2}$. Surface area and micropore volume results are summarised in Table 3.3. This analysis was conducted once; therefore, error bars are not presented. As a result of biomass undergoing thermal processing with CO_2, the raw biochar exhibits a highly porous structure with a micropore volume of 0.2 $cm^3\ g^{-1}$ and a surface area measuring 551.5 $m^2\ g^{-1}$. However, following the wet impregnation method, the overall surface area of the catalysts decreased. The most notable reduction occurred in the Ni-BC, followed by Fe-BC, while the Fe-BC structure was the least affected by the metal impregnation.

Table 3.3. Microporous structure of biochar catalysts.

Catalyst	Surface area / $m^2\ g^{-1}$	Micropore volume / $cm^3\ g^{-1}$
Raw biochar	551.4	0.2055
Ni-doped biochar	337.9	0.1259
Fe-doped biochar	473.2	0.1763
Zn-doped biochar	394.7	0.1471

Activated carbons usually present a hierarchical structure due to their wide distribution of pore sizes (Lin, Lei et al. 2023). As confirmed by the results of porosity analysis and SEM imaging, the raw biochar used as a catalyst support in Chapter 5 presents a hierarchical structure comprising micropores, mesopores, and macropores. The use of catalysts with this structure has several advantages for the pyrolysis of plastic waste, such as the potential to improve the efficiency and selectivity of the process through multiple approaches (Dong, Keil et al. 2016). One of the most notable benefits of hierarchical catalysts is the enhanced

accessibility they provide. Since the bulky nature of the plastic can lead to steric hindrances or diffusion constraints, the presence of micropores, mesopores, and macropores within a hierarchical catalyst ensures that plastic waste can readily access the catalyst's active sites (Escola, Aguado et al. 2011). Micropores contribute to the adsorption and desorption of reactants and products, while mesopores facilitate efficient mass transport and diffusion. Macropores, on the other hand, aid in preventing pore blockage and promoting bulk transport (Serrano, Aguado et al. 2012). The multilevel pore structure significantly enhances the accessibility of pyrolytic volatiles to the catalytic sites, thereby improving the overall reaction rate (Serrano, Aguado et al. 2006). Moreover, the hierarchical pore structure permits improved mass transport of reactants and products throughout the catalyst. The interconnected network of pores enables the diffusion of large molecules to the internal active sites, and the efficient removal of reaction products (Zhang, Cheng et al. 2018). This minimizes diffusional limitations and prevents pore blockage, leading to a more effective pyrolysis process. The role of support materials in determining catalyst properties cannot be overlooked, since they aid in the dissemination of active metal particles, enabling improved mass transport and providing a suitable environment for chemical reactions to occur, owing to their unique physical and chemical structure (van Deelen, Hernández Mejía et al. 2019).

3.2. Experimental

3.2.1. Reactor and condenser system setup

The reactor was constructed from stainless steel materials in the engineering workshop located at Merz Court, Newcastle University. The experimental configuration involved a two-stage fixed-bed stainless steel reactor (1.25 in diameter, and 17 in length) fitted with two heating bands (spaced 5.1 in apart) for independently controlled temperatures for the two zones. The outlet of the reactor was connected to the condensers cooled at -13 °C (measured with a thermometer) using a saturated frigorific solution of salt and ice water as illustrated in Figure 3.5. Before initiating the experiments, the reactor was purged with N_2 for 30 min to ensure the system is air-free (verified by GC analysis). Following this, the first reactor stage, holding 3 g of plastic mixture was heated at a rate of 20 °C min^{-1} and sustained at 500 °C for 40 min at a fixed N_2 carrier gas flow rate of 40 ml min^{-1}. Quartz wool and a metallic mesh support that held 0.5 g of catalyst were placed in the 2nd stage where the temperature was varied. During the thermal pyrolysis experiments, only quartz wool was in place with no catalyst. Non-condensable gases were collected at the outlet of the condenser system using

multiple Tedlar gas bags and the entirety of the gas products were collected. The mass differences in the crucible, condensers, and catalyst bed pre- and post-reaction were employed to calculate the masses of the produced char, oil, and catalyst carbon deposition, respectively. In case carbon nanotubes were detected, carbon deposition was referred to as CNT. The total mass of gaseous products was determined using gas chromatography, considering the known N_2 flow rate, collection time, and mol% of the samples. Equation 3.5 describes the mass balance:

$$M_{plastic} = M_{products} = M_{oil} + M_{gas} + M_{char} + M_{C\ deposition} \quad (3.5)$$

Where M is the mass. The product yields were then calculated by equation 3.6:

$$Y_i = 100\left(\frac{M_i}{M_{plastic}}\right) \quad (3.6)$$

Where Y is the yield (wt%), and the subscript *i* denotes the type of product (oil, gas, char, and carbon deposition. All yields reported in this thesis are referred to the initial mass of reactants (i.e., either plastic waste in Chapter 5, or the sum of reacted CO_2 and plastic in Chapter 6).

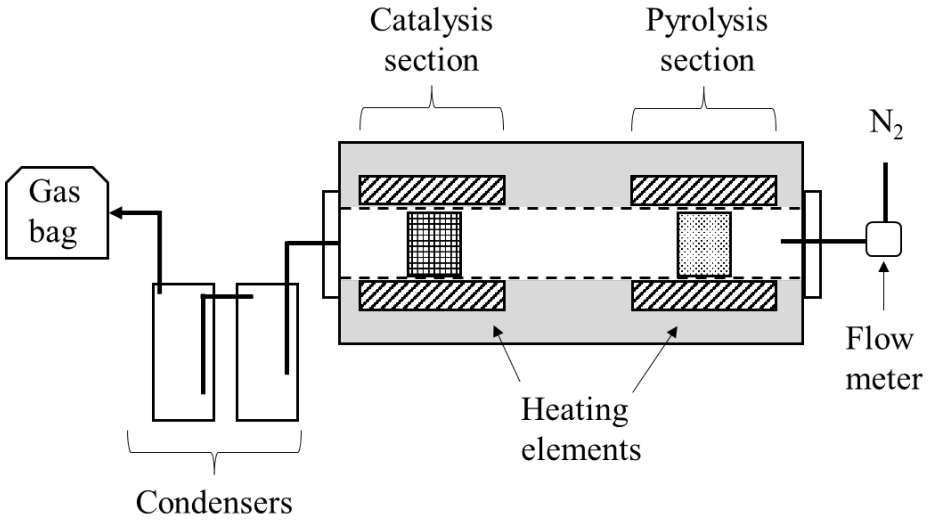

Figure 3.5. Schematic diagram of the pyrolysis-catalysis reactor and condensation system. Images of the reactor and condensers are provided in Appendix B.

3.2.2. Analysis of products

Gas analysis

Non-condensable gases were collected for a total of 50 min and analysed offline using a Varian 450 gas chromatography equipped with both TCD and FID detectors. These detectors facilitated the concurrent analysis of permanent gases (e.g., H_2, N_2, O_2, and CO), CO_2, and hydrocarbons (C1 – C4). The TCD inlet, detector, and oven temperatures were regulated at

250 °C, 175 °C, and 175 °C, respectively. Three columns were integrated into the GC, specifically a Hayesep T ultimetal, a Hayesep Q ultimetal, and a Molecular Sieve 13X. The gas specimen from the TCD detector was subsequently channelled into an Rt-Alumina BOND/MAPD column (30 m x 0.32 mm x 5 µm) connected to the FID detector, which was adjusted to 255 °C. The column was situated in an isolated oven with a programmed temperature sequence: Initially stabilized at 40 °C for 2 min, incrementally raised to 50 °C at a rate of 4 °C min^{-1}, maintained for 0.5 min, then escalated to 80 °C at 8 °C min^{-1}, and finally soared to 145 °C at 20 °C min^{-1}.

Liquid analysis

Liquid products collected from the condensers after the system cooled down were dissolved in a 1:1 mixture of ethyl acetate and n-hexane and characterised using an Agilent 5977B MSD MS Single Quadrupole Mass Analyzer, linked to an Agilent 8890 Gas Chromatography system and utilizing an HP-5MS column (30 m x 0.25 mm x 0.25 µm). The inlet and detector temperatures were fixed at 280 °C, while the oven's temperature program commenced at 60 °C for 0.5 minutes, increased to 280 °C at a rate of 6.5 °C min^{-1}, and ultimately sustained at 280 °C for 13 min. For quantitative analysis, an Agilent 7820 Gas Chromatograph was employed, featuring an identical column and heating protocol as described earlier. An internal standard (methyl stearate) and two external standards, namely C_7 – C_{40} saturated alkanes (Sigma Aldrich), and BTEX (benzene, toluene, ethylbenzene, and xylene) aromatic compounds (Sigma Aldrich), were utilized for quantification purposes.

The heating programmes employed for gas and liquid analyses were derived from prior investigations conducted on the same plastic types, utilizing the same analytical instruments, and similar experimental conditions (Diaz Silvarrey 2019).

3.2.3. Weigh hourly space velocity

A critical parameter in the design and operation of catalytic fixed-bed reactors is the weigh hourly space velocity (WHSV), which is defined as the ratio of the mass flow rate of the reactants to the catalyst in the reactor, and is typically expressed in h^{-1} (Aminu, Nahil et al. 2020) . This parameter influences the residence time of volatiles (generated upstream in the pyrolysis section) in the catalytic stage of the reactor, consequently affecting the reaction kinetics and product formation. Higher WHSV values correspond to shorter residence times, potentially leading to lower conversion rates, while lower WHSV values imply longer residence

times, which may lead to higher conversion rates but at the expense of reduced throughput. In addition, the WHSV impacts catalyst performance over time. With high WHSV values, the catalyst may experience a rapid decline in activity due to deactivation caused by coke deposition, sintering, or other factors. Lower WHSV values might slow down catalyst deactivation but may require a higher catalyst mass for a given throughput, thereby increasing the capital cost of the reactor (Zhou, Dai et al. 2021).

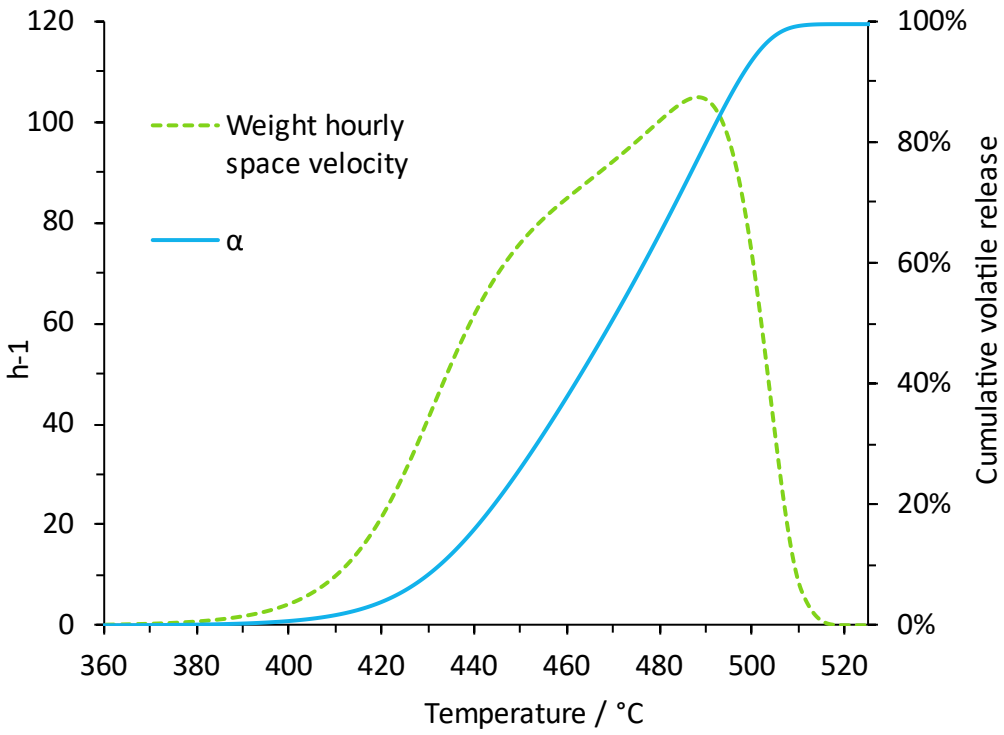

Figure 3.6. Weight hourly space velocity of the pyrolysis process (primary axis) compared to the overall volatile release (secondary axis).

Owing to the batch nature of the reactor, the release of volatile compounds is not constant, resulting in fluctuations in the WHSV. In this study, the WHSV of the system was determined using equation 3.7 by computing the rate of volatile release through the pyrolysis reaction. This was achieved by multiplying the reaction rate of the plastic mixture (details of the kinetic model development are found in Chapter 4) with the mass of volatiles present in the feedstock (i.e., the difference between the initial mass of plastic and the remaining char) over the entire reaction time, and dividing by the mass of catalyst:

$$WHSV = \frac{\frac{d\alpha}{dt}\left(m_{plastic} - m_{char}\right)}{m_{catalyst}} \tag{3.7}$$

Where dα/dt is the pyrolysis reaction rate, $m_{plastic}$, m_{char}, and $m_{catalyst}$ are the masses of initial plastic feed, char in the crucible after reaction, and catalyst, respectively. This approach

yielded a profile for WHSV as shown in Figure 3.6. The cumulative volatile release was calculated by multiplying the pyrolysis conversion by the volatile content in the plastic feed.

The reactor temperature at both stages was investigated prior to the experimental runs to confirm adequate heat transfer and stable operation. The temperature profiles are presented in Appendix C.

Chapter 4. Thermal decomposition kinetics of plastic waste

This chapter aims to determine the kinetic parameters of individual and mixed plastic waste in order to develop accurate global models for predicting pyrolysis conversion as a function of temperature, which is essential for optimal reactor design and the scaling up of pyrolysis technologies for chemical recycling. Thermogravimetric analysis was performed to investigate the dependencies of activation energy on conversion for plastic waste streams (polyolefins and polyesters), revealing significant interactions between plastic constituents (i.e., producing changes in their thermal stability), and identifying a multi-step decomposition process. Kinetic analysis was conducted using the KAS isoconversional model-free method, multivariate nonlinear regression, and kinetic deconvolution, followed by statistical validation. The deconvolution analysis increased model accuracy by isolating the individual reaction steps and their kinetics, allowing for the identification of reaction orders, pre-exponential factors, and activation energies for each step. Notably, PP and LDPE underwent decomposition through two distinct steps, while others followed a single-step process. For plastic mixtures, three dominant, partially overlapping steps were identified. The developed models were validated and utilized to predict experimental data at various heating conditions and plastic compositions, demonstrating their robustness. This study has been previously published in the journal *Chemical Thermodynamics and Thermal Analysis* under the title "Kinetic modelling of mixed plastic waste pyrolysis" (DOI: 10.1016/j.ctta.2023.100105) (Martínez-Narro, Royston et al. 2023). The chapter builds upon the work presented in the article and provides further analysis and discussion of the results, as well as a detailed exposition of the methodologies employed in the development of the models.

4.1. Background

The investigation of pyrolysis kinetics and the development of robust kinetic models are imperative for the optimization of reactor designs. Hitherto, attention has been concentrated on discerning thermochemical behaviours and product attributes of discrete plastic species, such as polyethylene (HDPE, LDPE), polypropylene (PP), polystyrene (PS), and polyethylene terephthalate (PET) (Xu, Wang et al. 2018). Research on mixtures remains limited, with the majority of models being founded on pre-arranged binary and tertiary mixtures of high-purity, uncontaminated plastic species, corresponding to the anticipated waste composition of select regions (Ceamanos, Mastral et al. 2002, Saha and Ghoshal 2007, Chowlu, Reddy et al. 2009,

Khedri and Elyasi 2016). Individual components of mixed plastic waste undergo depolymerization at distinct temperature ranges via a multitude of radical reaction mechanisms, generating pools of radicals accessible for each constituent within the mixture (Hujuri, Ghoshal et al. 2008). The diffusion of radicals across interfacial layers may stabilize or destabilize other polymers, eliciting synergistic effects in the acceleration or delay of the onset temperature for decomposition and the subsequent decomposition rate. The feedstock compositions of genuine waste streams are frequently disregarded, although additives and contaminants can significantly impact kinetic behaviours. This oversight occurs despite nonfiber plastics typically containing 7% additive by mass (Geyer, Jambeck et al. 2017). For example, it has been established that polystyrene radicals destabilize polypropylene in binary mixtures through hydrogen abstraction (Miranda, Yang et al. 2001), while biomass contaminants can cause the lignocellulosic fraction to stabilize polymers, altering the decomposition range by 20 °C (Gunasee, Carrier et al. 2016).

The kinetics of plastic pyrolysis are often oversimplified by assuming single-step decomposition or first-order reactions (Westerhout, Waanders et al. 1997, Sørum, Grønli et al. 2001, Ceamanos, Mastral et al. 2002, Blanco and Siracusa 2013). Moreover, the utilization of a diverse array of reaction conditions, materials, processing equipment, and analytical methods results in considerable variations in reported kinetic parameters and reaction models among researchers, even for identical plastic species (Encinar and González 2008). For instance, numerous authors have documented a single-step decomposition process for LDPE, with nearly indistinguishable activation energy values at differing conversion degrees (Aboulkas, El Harfi et al. 2008, Aboulkas, El harfi et al. 2010, Dubdub and Al-Yaari 2020), while others have demonstrated that decomposition occurs in multiple steps where activation energy is contingent on conversion (Saha and Ghoshal 2007, Berčič, Djinović et al. 2019, Wang, Wei et al. 2019, Budrugeac, Cucos et al. 2022). A more comprehensive understanding of mixed plastic pyrolysis kinetics is necessary to optimize operating conditions and reactor design for the successful processing of plastic waste streams.

Isoconversional methods are employed to approximate apparent kinetic parameters rather than intrinsic ones. The development of intrinsic models for mixed plastic waste pyrolysis is a complex undertaking that faces myriad challenges and cannot be accomplished exclusively through thermogravimetric data analysis (Dogu, Pelucchi et al. 2021). A pragmatic approach entails the creation of global kinetic models capable of establishing precise mathematical

relationships between temperature and the extent of conversion within specified heating rate ranges. This allows for optimal reactor design by predicting the temperature at which the feedstock decomposes. The conventional approach of determining kinetic parameters via linear regression methods is transitioning to more dependable multivariate nonlinear methods utilizing mathematical optimization techniques (Koga 2018). Recent advancements in modern isoconversional methodologies involve quantitative interpretation of activation energy dependencies on conversion, which are indicative of multi-step reaction mechanisms. The kinetic parameters of the involved steps can subsequently be evaluated through deconvolution methods that separate the overlapped rate peaks into individual ones (Vyazovkin 2018).

4.2. Materials and methods

4.2.1. Materials

Mixed plastic waste compositions were chosen based on diverse locations, including the European Union (EU) (PlasticsEurope 2019), and two municipalities in Thailand (TH) (Areeprasert, Asingsamanunt et al. 2017) and Mexico (MX) (Araiza Aguilar, Chavez Moreno et al. 2017), with the aim of developing a comprehensive model for predicting kinetic decomposition behaviour. The mixtures were made utilising the same individual plastic samples characterised and discussed in Chapter 3. The mixtures were employed for validation and assessment of model robustness. The plastic waste composition and the standards for plastic quality (e.g., additives, impurities, emulsifiers, wetting agents, inhibitors, etc.) exhibit considerable variation across different regions worldwide, making it challenging to accurately represent global composition. Additionally, the levels of contamination can differ depending on local waste management practices and industrial pollution. The types and usage patterns of plastics are influenced by regional manufacturing and consumption habits, along with local regulations, leading to variations in the prevalence of different plastic materials and their additives. The extent of weathering and degradation is also influenced by the local climate, (e.g., UV exposure and ambient temperature). For a large-scale or pilot pyrolysis facility, precise prediction, or tracing of the chemical composition of received produce would be unattainable. However, a substantial mass obtained over an extended period should exhibit a general composition approximating that presented in Table 4.1. The plastic waste samples (i.e., PET, HDPE, LDPE, PP, and PS) were cleansed, dried, and sectioned into 1 mm^2 squared pieces to minimize thermal inertia. Three simulated plastic waste mixtures were prepared in

accordance with the corresponding mass fractions of each region. Table 4.1 displays the mass proportions of the components for each mixture.

Table 4.1. Composition (wt%) of plastic utilized in the mixtures.

Region	Sample name	PET	HDPE	LDPE	PP	PS
Europe Union	EU	11.7	19.5	27.7	30.6	10.5
Thailand	TH	6.4	61.8	18.7	7.8	5.3
Mexico	MX	13	28.4	45	6.8	6.8

4.2.2. Thermogravimetric analysis

The development of kinetic models was carried out using data obtained from thermogravimetric analysis (TGA). The analyses for individual plastics and each sample mixture (EU, TH, and MX) were performed using a Perkin Elmer STA 6000 instrument. Four distinct heating rates were selected for every sample: 5, 10, 20, and 40 °C min^{-1}. The utilization of varying heating rates facilitates analysis at constant conversion, allowing for the determination of kinetic parameters via isoconversional methods. Samples were placed in a 4 mm diameter ceramic crucible, their initial weight was recorded, and subsequently, the tests were conducted within a temperature range of 30 – 700 °C, while the system was continuously purged with N_2 at a flow rate of 20 ml min^{-1}. The data for sample weight and temperature was recorded at intervals of 0.125 s.

4.2.3. Kinetic theory and model development

The kinetic parameters, or kinetic triplet (i.e., activation energy, pre-exponential factor, and reaction model), can be estimated using weight loss data acquired from TGA through the application of model-free isoconversional methods, as well as linear and nonlinear model fitting techniques. The ideal solid-state rate equation considers the variation of conversion with time or temperature, and is expressed by Equation 4.1:

$$\frac{d\alpha}{dT} = \frac{A}{\beta} exp^{\left(-\frac{E_\alpha}{RT}\right)} f(\alpha) \quad (4.1)$$

Where dα/dT is the reaction rate, α is the conversion, T the temperature (K), A the pre-exponential factor (s^{-1}), E_a the activation energy (kJ mol^{-1}), R the universal gas constant, f(α) is a function of conversion contingent upon the utilized kinetic model, and β indicates the heating rate (K s^{-1}).

Activation energy is a central concept in chemical kinetics, representing the minimum amount of energy required to initiate a chemical reaction. It acts as an energy barrier that reactants must overcome to transform into products (Mickey 1980). This concept is crucial in

understanding why certain reactions, such as thermal decomposition, require external energy inputs (e.g., heat) to proceed. According to transition state theory, reactants must reach a high-energy transition state before converting into products, and the activation energy is the difference in energy between this state and the reactants (Ptáček, Šoukal et al. 2018). It also plays an important role in determining the rate of a reaction, higher activation energies typically correspond to slower reaction rates. This relationship is mathematically expressed in Equation 4.1, which shows that a decrease in activation energy leads to an increase in the reaction rate.

The conversion is defined as shown in Equation 4.2:

$$\alpha = \frac{m_0 - m_i}{m_0 - m_f} \tag{4.2}$$

In this equation, m_o is the initial mass, m_i is mass at time i (or temperature i) and m_f the solid residue remaining after the reaction.

Isoconversional model-free methods

The fundamental principle of isoconversional methods states that, at a specific constant conversion, the reaction rate solely depends on temperature (Vyazovkin and Sbirrazzuoli 2006). These methods offer the advantage of enabling the estimation of apparent kinetic parameters without prior knowledge of the reaction model. The Kissinger-Akahira-Sunose (KAS) method (Akahira and Sunose 1971) provides a simple and effective means for determining A and E_a from TGA data if the reaction adheres to a single-step decomposition. Moreover, it is more recent and considerably more accurate than other classic integral isoconversional methods, such as the widely employed Ozawa-Flynn-Wall method (Flynn and Wall 1966, Vyazovkin 2015). Integrating Equation 4.1 yields:

$$\int_0^{\alpha} \frac{d\alpha}{f(\alpha)} = g(\alpha) = \frac{A}{\beta} \int_0^{T} exp^{\left(\frac{-E_a}{RT}\right)} dT \tag{4.3}$$

Here, g(α) represents the integral form of the reaction model. Although Equation 4.3 lacks an exact analytical solution, approximate solutions give rise to linear equations that serve as the foundation for many integral isoconversional methods, such as Equation 4.4, which is utilized for the KAS method:

$$ln\left(\frac{\beta_i}{T_{\alpha,i}^2}\right) = ln\left(\frac{RA_\alpha}{E_{a,\alpha}}\right) - ln\left(\frac{1}{f(\alpha_i)}\right) - \left(\frac{E_{a,\alpha}}{RT_{\alpha,i}}\right) \tag{4.4}$$

In this equation, T_α denotes the temperature at a given conversion for each tested heating rate. Plots of the left side of the equation ($ln(\beta_i/T_{\alpha,i}^2)$) against the reciprocal of reaction temperature ($T_{\alpha,i}^{-1}$) for each sample at every heating rate produce KAS linear plots. The temperatures utilized for the plots are those corresponding to experimental conversions in the range of 0.2 – 0.8, in intervals of 0.05. The apparent E_a is derived from the slopes of the linear regression equations, and the average E_a for each heating rate constitutes the reported value. If the reaction model is known, the apparent A can be estimated from the intercepts.

Another effective isoconversional method is the Friedman method, which is based on Equation 4.5 (Friedman 1964):

$$\ln\left[\beta_i\left(\frac{d\alpha}{dT}\right)_{\alpha,i}\right] = \ln[f(\alpha)A_\alpha] - \frac{E_\alpha}{RT_{\alpha,i}} \tag{4.5}$$

The procedure for estimating kinetic parameters from Equation 4.5 is analogous to that of KAS. This differential method is more accurate than integral methods since it does not employ any approximation. However, the integral weight loss data from TGA must be differentiated, introducing significant amounts of noise, which increases inaccuracies (Vyazovkin 2015). The integral KAS method is better suited for integral data obtained by TGA in this study. Consequently, the Friedman method is presented in this work only to enable comparison of results and assessment of calculation errors and adaptability of the analysis to this process.

Combined kinetic analysis (CKA)

The reaction mechanism of numerous solid-state thermal decomposition models can be characterized by the truncated Šesták-Berggren (TSB) empirical kinetic model function (Šesták and Berggren 1971, Burnham 2000):

$$f(\alpha) = \alpha^m(1-\alpha)^n \tag{4.6}$$

Combined kinetic analysis is a linear model fitting technique that employs the TSB model and is based on Equation 4.7 (Perez-Maqueda, Criado et al. 2006):

$$\ln\left(\frac{d\alpha}{dt}\frac{1}{\alpha^m(1-\alpha)^n}\right) = \ln cA - \frac{E_a}{RT} \tag{4.7}$$

In this equation, n represents the reaction order, m denotes the growth factor, and c is a constant relatively small in comparison to A. To perform this analysis, the conversion data requires prior differentiation ($\frac{d\alpha}{dt} = \frac{\alpha_{i+1}-\alpha_i}{t_{i+1}-t_i}$). Plots of the left side of Equation 4.7 against the reciprocal of the temperature are utilized to generate regression lines from which the

coefficient of determination (R^2) is calculated. The *m* and *n* parameters are subsequently optimized for the highest linear regression coefficient R^2. This optimisation can be readily performed in Microsoft Excel by employing the simplex linear programming algorithm within the Solver add-in. Since Equation 4.7 is in linear form, the slope of the optimised linear equation ($-E_a/R$) can be utilized to determine the activation energy (E_a) by multiplying it with the ideal gas constant. The pre-exponential factor (A) can be determined from the y-intercept of the plot ($\ln cA$), where *c* is a constant. The value of *c* can be identified using Table 4.2 below; if the values of *n* and *m* correspond to any of those in the given models, the value of *c* can be taken as the associated value provided (Vyazovkin, Burnham et al. 2011).

Table 4.2. Parameters of Equation 4.7 fitted to various reaction models (Vyazovkin, Burnham et al. 2011).

$f(\alpha)$	Parameters of equation: $c(1-\alpha)^n\alpha^m$
$(1-\alpha)^{1/2}$	$(1-\alpha)^{1/2}$
$(1-\alpha)^{2/3}$	$(1-\alpha)^{2/3}$
$(1-\alpha)$	$(1-\alpha)$
$2(1-\alpha)[-\ln(1-\alpha)]^{1/2}$	$2.079(1-\alpha)^{0.806}\alpha^{0.515}$
$3(1-\alpha)[-\ln(1-\alpha)]^{2/3}$	$3.192(1-\alpha)^{0.748}\alpha^{0.693}$
$[-\ln(1-\alpha)]^{-1}$	$0.973(1-\alpha)^{0.425}\alpha^{-1.008}$
$(3(1-\alpha)^{2/3})/(2[1-(1-\alpha)^{1/3}])$	$4.431(1-\alpha)^{0.951}\alpha^{-1.004}$

However, if no matching values of *n* and *m* are found in Table 4.2, it can be assumed that *c* is insignificant compared to A and assigned the value of 1. Consequently, the y-intercept can be taken as $\ln A$.

Nonlinear model fitting

This method surpasses linear and isoconversional methods in obtaining accurate kinetic parameters when the process occurs in multiple steps. Apparent kinetic parameters estimated by linear methods, such as KAS and CKA, are utilized as initial values for the optimization of parameters derived from Equation 4.8 (Vyazovkin, Burnham et al. 2011), which is obtained by substituting the TSB model into Equation 4.1:

$$\frac{d\alpha}{dT} = \frac{A}{\beta} exp^{\left(-\frac{E_a}{RT}\right)} \alpha^m (1-\alpha)^n \qquad (4.8)$$

For all samples at every heating rate, Equation 4.8 is numerically solved by first-order Runge-Kutta method, which introduces a dimensionless step size *h*. Initial values for temperature, (T), conversion (α), and the change in conversion with temperature (dα/dT) are required for this method (Griffiths and Higham 2010). The initial temperature (T_0) and conversion (α_0) are

taken from TGA data, with the corresponding conversion value calculated from the experimental data at this temperature using Equation 4.2. The initial dα/dT value, $(d\alpha/dT)_0$, is computed by multiplying the right side of Equation 4.8 with the step size *h*, with T_0 and α_0 as the values of T and α, respectively, and A, E_a, *n*, and *m* determined via KAS and/or CKA. The subsequent temperature value, T_1, is calculated as the initial temperature plus the step change: $T_1 = T_0 + h$. The subsequent conversion value, α_1, is computed as the initial conversion plus the initial change in conversion with temperature: $\alpha_1 = \alpha_0 + (d\alpha/dt)_0$. The successive temperature values can be calculated as $T_i = T_{(i-1)} + h$, the conversion values as $\alpha_i = \alpha_{(i-1)} + (d\alpha/dT)_{(i-1)}$, and the change in conversion with temperature values as $(d\alpha/dt)_i = h(A/\beta)\left(e^{-E_a/RT_{i-1}}\right)\alpha_{i-1}^m(1-\alpha_{i-1})^n$. Here, the subscript *i* denotes the current value, and (*i*-1) denotes the previous value of each parameter. The process continues until conversion reaches unity.

The step size in this numerical method significantly affects the model's accuracy, with smaller step sizes resulting in more accurate data (Griffiths and Higham 2010). However, in cases involving different heating rates, there are considerable differences in the number of data points recorded by TGA. Therefore, it is preferable to match the step size, which affects the temperature by a fixed increment, with the change in experimental temperature. The *h* value that yields the closest fit between experimental and calculated temperatures must be found by iterative calculation in order to obtain the same number of data points. This facilitates the creation of models with minimized squared errors between the theoretical and experimental data sets. Due to the highly endothermic nature of pyrolysis, the sample temperature does not change precisely in accordance with the TGA's programmed heating rate (Kwon, Kim et al. 2019). Consequently, the step size cannot be simply set as the heating rate.

The residual sum of squares between the experimental and calculated temperatures (RSS_T) is given as: $RSS_T = \sum_{i=1}^{n}\left(T_{exp,i} - T_{calc,i}\right)^2$. Where $T_{exp,i}$ is the experimental temperature at data point *i*, and $T_{calc,i}$ is the calculated temperature at data point *i*. This optimisation can be conducted in Excel via the generalized reduced gradient method (GRG) within the Solver add-in, which monitors the slope of the objective function as the decision variables change until an optimal point is reached (Arora 2012). The RSS value is set as the objective function to be minimized, with *h* as the only parameter to be changed, yielding the optimal step change size.

Once the optimal *h* value is determined and the experimental and theoretical data sets have the same number of data points, the RSS of the reaction rates can be calculated using Equation 4.9:

$$RSS = \sum_{i=1}^{n} \left[\left(\frac{d\alpha_i}{dT} \right)_{exp,i} - \left(\frac{d\alpha_i}{dT} \right)_{calc,i} \right]^2 = min \tag{4.9}$$

Where $(d\alpha_i/dT)_{exp,i}$ and $(d\alpha_i/dT)_{calc,i}$ are the experimental and calculated reaction rates at data points *i*, respectively. The optimisation method for RSS is analogous to that of RSS_T; however, the decision variables to change are set to the kinetic parameters E_a, A, *n*, and *m*. Integration proceeds until the minimal RSS is found. Alternatively, the analysis can be performed using the RSS of conversions instead of reaction rates.

The accuracy of this method heavily depends on the initial values of the parameters to be optimized. Therefore, the KAS and CKA results were employed to provide reliable starting points.

Kinetic Deconvolution Analysis (KDA)

Kinetic deconvolution analysis (KDA) is a method to separate partially overlapped parallel reactions from the overall kinetic data into individual partitions or steps, reflecting the net kinetic behaviour of the process (Koga 2018). Since all the components in the selected plastic waste samples can be described by the ideal solid-state rate equation, KDA can be employed as a direct method for kinetic analysis. For this method, an appropriate reaction model must be chosen, depending on the specific manner in which the reaction occurs. The conversion profile of plastics exhibits the shape of a sigmoidal curve, where the reaction begins with an acceleratory nature, starting slowly, speeding up, reaching the peak reaction rate near the middle, and finally slowing down as conversion reaches its maximum. Consequently, the TSB model was employed to represent the reaction model of plastic waste, since it is adequate for reactions with sigmoidal characteristics (Burnham 2000) and provides sufficient flexibility for the numerical iterative calculations involved in KDA and multivariate regression analysis. When more than one step is present, each has its own kinetic parameters and rate related to their extent of conversion and are represented by their specific contributions to the overall rate. Thus, Equation 4.8 becomes:

$$\beta \frac{d\alpha}{dT} = \sum_{i=1}^{n} c_i k_i(T) f_i(\alpha_i) = \sum_{i=1}^{n} c_i A_i exp^{\left(\frac{-E_{a,i}}{RT}\right)} \alpha_i^{m_i} (1-\alpha_i)^{n_i} \tag{4.10}$$

Where the subscript i represents every step, and c_i are the individual contributions of the steps, which sum to unity ($\sum_{i=1}^{n} c_i = 1$, and $\sum_{i=1}^{n} c_i \alpha_i = \alpha$).

The addition of steps using Equation 4.10 is subjected to the F-test to determine statistical significance. The test makes use of the RSS which can be readily converted to the variance (S^2) by dividing it over the degrees of freedom *f* using Equation 4.11 (Vyazovkin, Burnham et al. 2011):

$$S^2 = \frac{RSS}{f} = \frac{RSS}{N - p} \tag{4.11}$$

Where N is the number of experimental points in the iterative calculation, and p the number of kinetic parameters that were obtained from it. The experimental F value (F_{exp}) is obtained by dividing the variances of the two models:

$$F_{exp} = \frac{S_1^2}{S_2^2} \tag{4.12}$$

F_{exp} is then compared to the F critical value (F_{crit}), which can be read from F distribution tables at a chosen confidence probability, or calculated by a precise approximation equation (Opfermann 2000). If $F_{exp} > F_{crit}$, then the reduction of RSS from the model with an additional step is statistically significant, and the increased complexity of the model is then justified.

Another method that follows the same principle of separating constituent peaks from the complex reaction profile is mathematical deconvolution analysis (MDA). The method employs mathematical functions (F(t)) that have peak shapes to fit the experimental data, and the overall decomposition rate can be expressed as the sum of the individual peaks (Perejón, Sánchez-Jiménez et al. 2011, Vyazovkin, Burnham et al. 2020):

$$\frac{d\alpha}{dt} = \sum_{i=1}^{n} F_i(t) \tag{4.13}$$

Where n is the number of reaction steps. The Weibull function was used in this study due to its flexibility to accommodate asymmetrical peak shapes [56]:

$$F(t) = a_0 \left(\frac{a_3 - 1}{a_3}\right)^{\frac{1-a_3}{a_3}} \left[\frac{x - a_1}{a_2} + \left(\frac{a_3 - 1}{a_3}\right)^{\frac{1}{a_3}}\right]^{a_3 - 1} exp\left[-\left[\frac{x - a_1}{a_2} + \left(\frac{a_3 - 1}{a_3}\right)^{\frac{1}{a_3}}\right]^{a_3} + \frac{a_3 - 1}{a_3}\right] \tag{4.14}$$

Where a_0, a_1, a_2, a_3 are the amplitude, position, width, and shape parameters, respectively. After isolating the peaks, their kinetic contributions c_i were calculated as the ratios of the individual peak areas and the overall area. The deconvoluted peaks were individually

subjected to formal kinetic evaluation by nonlinear model fitting as described in the previous section.

4.3. Results and discussion

4.3.1. Thermal behaviour

Single plastics

The decomposition temperature range of plastic waste varies with the selected linear heating rate, exhibiting a clear shift toward higher temperatures at the same conversion values as the linear heating rate increases. Figure 4.1 displays the conversion and DTG plots for plastics at the selected heating rates. As only one peak is visible, it is apparent that the thermal decomposition of single plastics is dominated by a single step, implying that these plastics should exhibit a low dependence of activation energy on conversion at different heating rates. Owing to the high amount of volatile content, all plastics react almost to completion, except for PET, due to its high oxygen content and formation of complex aromatics (Holland and Hay 2002). The components of the plastic waste mixtures initiate the decomposition process in the following order: PS < PP < PET < LDPE < HDPE, with their decomposition ranges at 5 °C min^{-1} being 320 – 470, 340 – 465, 360 – 515, 380 – 530, and 410 – 535 °C, respectively.

Some researchers have reported plastics decomposing in different orders (Aboulkas, El harfi et al. 2010, Diaz Silvarrey and Phan 2016, Saad, Williams et al. 2021); these differences may be attributable to the various impurities, additives, and weak links present in the samples, particularly when treating diverse plastic waste samples and not virgin materials. However, the peak decomposition temperatures of the plastics follow a different order: PS < PET < PP < LDPE < HDPE. This difference occurs because the initial decomposition of PP takes place at a lower temperature than PET; nonetheless, it requires a higher temperature to reach its maximum decomposition rate due to greater thermal stability.

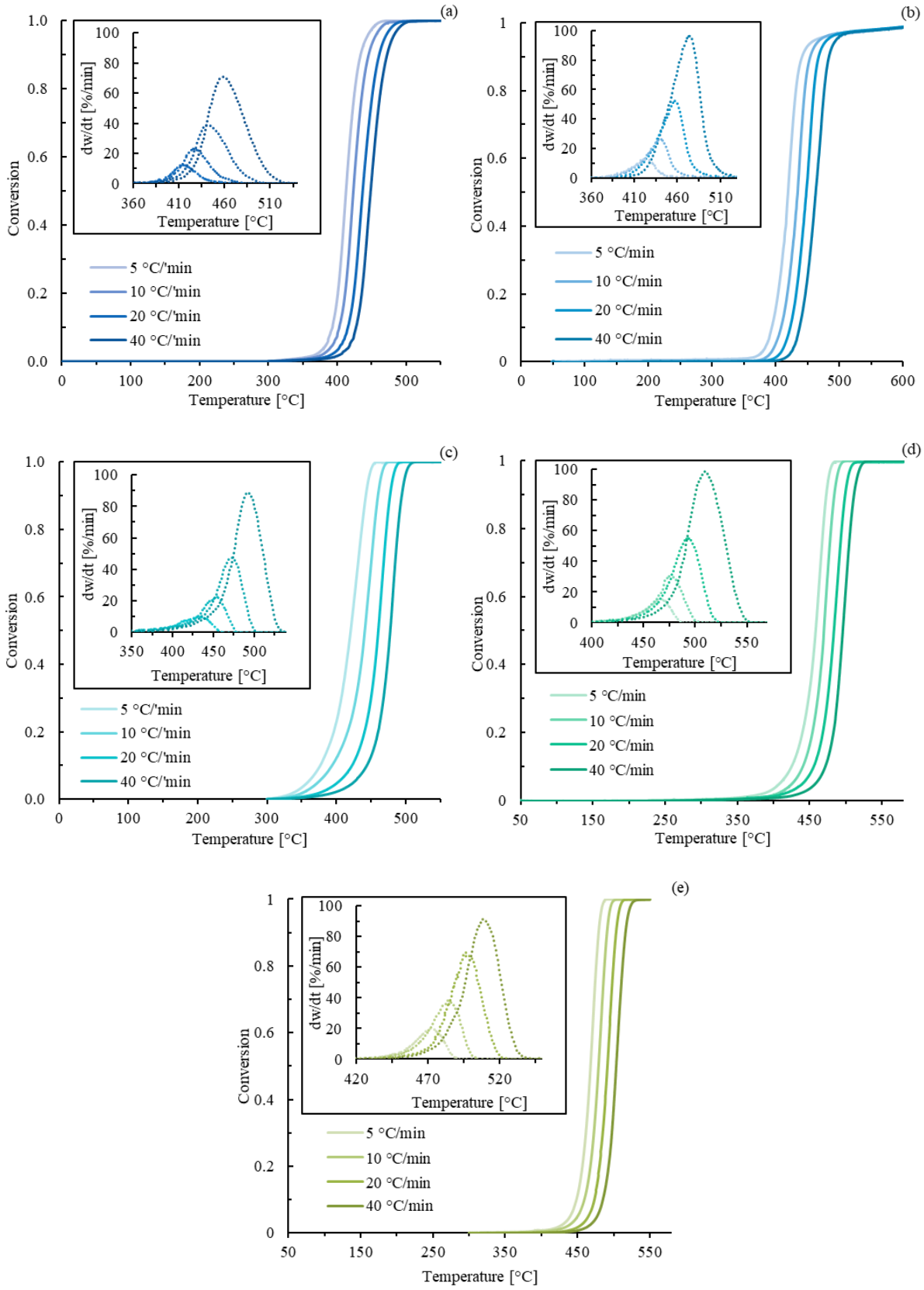

Figure 4.1. Experimental conversion and DTG curves (insets) of PS (a), PET (b), PP (c), LDPE (d), and HDPE (e) at different heating rates.

Plastic mixtures

The decomposition ranges for the mixtures at 5, 10, 20, and 40 °C min^{-1} are 350 – 480, 360 – 490, 390 – 510, and 410 – 520 °C, respectively. These variations in the decomposition temperature range might be ascribed to the thermal transition and physical properties of plastics, influencing their chain mobility and interactions. Polymers also exhibit low thermal conductivity, affecting heat transfer and slowing the distribution of heat among the mixture's components. Consequently, some components of the mixture reach decomposition at different temperatures. Figure 4.2 (a) displays the DTG curves of the EU plastic mixture at 5 °C min^{-1}. The reaction steps can be identified as peaks and inflection points or "shoulders" in the curves, with each peak and shoulder representing an individual step. Figure 4.2 (b) presents the DTG curve of the EU mixture at 40 °C min^{-1}, where identifying intermediate peaks or inflection points becomes difficult. The DTG curves of individual components are also included for visualization.

For the EU mixture at a heating rate of 5 °C min^{-1}, the first step is identified through visual inspection approximately in the range of 350 – 414 °C, primarily corresponding to the decomposition of PS, PET, and a small fraction of PP. The second step ensues in the middle of the overall reaction from 420 – 450 °C, where PP reaches its maximum conversion and reacts simultaneously with all plastics. At this juncture, PS and PET are almost entirely converted, and polyethylene structures have initiated decomposition. The reaction proceeds to the third step at around 448 °C, where both LDPE and HDPE react simultaneously in one peak alongside the remaining sub-products from the initial reactions. This last reaction step in the mixture is notably different from those of the corresponding single plastic components. When decomposed individually, LDPE and HDPE exhibit peak decomposition at 468 and 473 °C, respectively. In a mixture, the peak decompositions of LDPE and HDPE completely overlap, and in the presence of other polymeric components, the peak decomposition of these plastics occurs at 456 °C, suggesting potential interactions between components that lower the activation energy of polyethylene. At heating rates of 10 and 20 °C min^{-1}, three steps were identified for each mixture. At 40 °C min^{-1}, all mixtures exhibit a single peak, indicating that the reaction was primarily dominated by a single rate-limiting step.

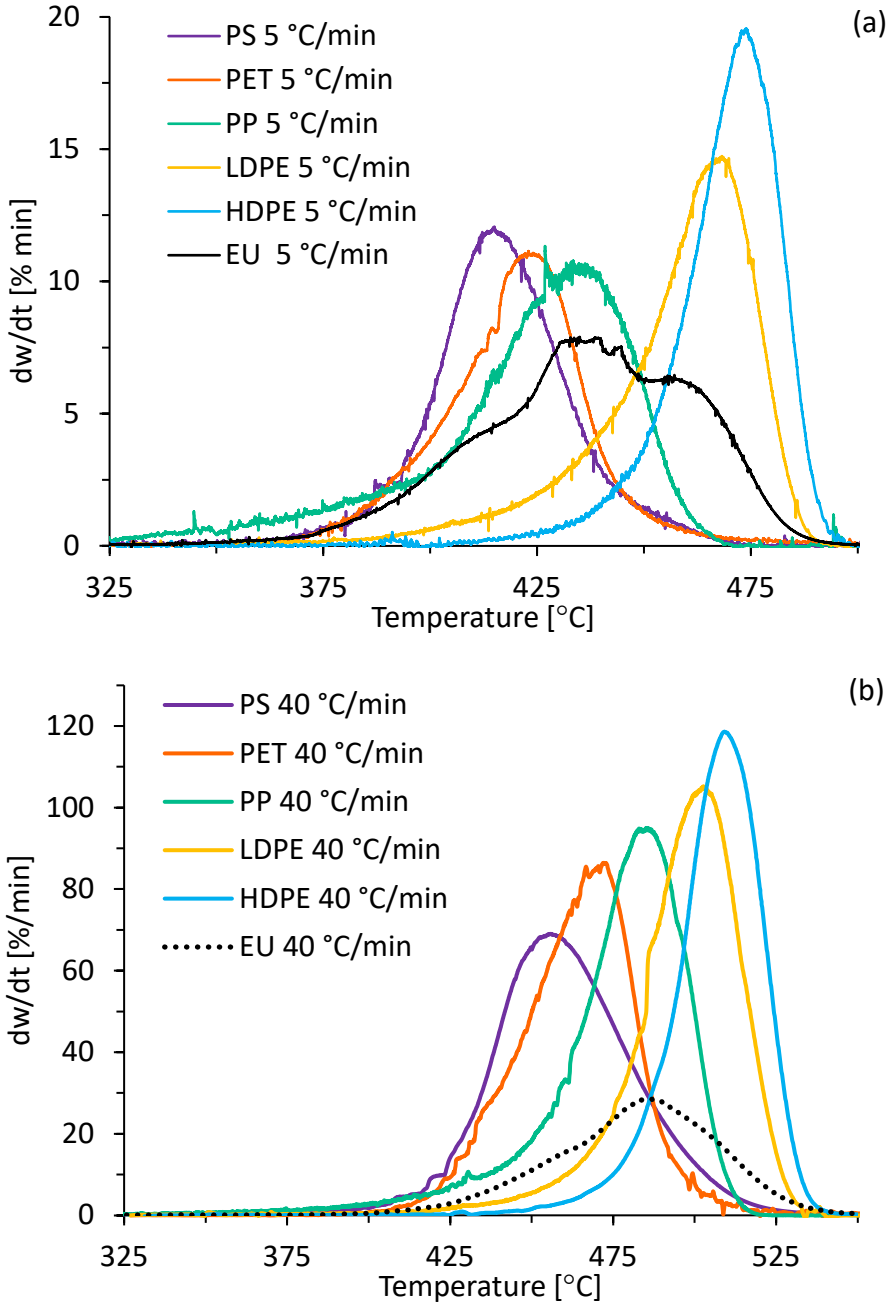

Figure 4.2. DTG curves of EU mixture and single plastics at 5 °C min^{-1} (a) and 40 °C min^{-1} (b).

At low heating rates (<20 °C min^{-1}), the DTG curves clearly indicate that the thermal decomposition of mixed plastics occurs in multiple partially overlapping steps. The gradual addition of heat provides sufficient time for components that decompose at lower temperatures (PS and PET) to complete before those that do so at higher temperatures (PP and PE). Owing to the heat diffusion constraints imposed by the characteristic low thermal conductivity of plastics, high heating rates do not allow adequate time for PS and PET to decompose entirely before PP and HD/LD-PE. As a result, as the heating rate increases (>20 °C min^{-1}), the steps for different individual plastic components overlap completely at the same temperature, and the decomposition becomes dominated by one of the steps. Consequently,

the apparent kinetic parameters calculated from the samples at heating rates higher than 20 °C min^{-1} can describe the global decomposition in a single step. However, to validate these results, they must be compared to those obtained by a multi-step model and determine whether the reduction of the error between calculated and experimental conversions by adding another step is statistically significant (Vyazovkin, Burnham et al. 2011).

The main differences between the compositions of the MX sample and the rest are the higher fraction of PET and the lower fraction of PP, which explain the two distinct steps still observed at 20 °C min^{-1}, unlike the TH samples that display only one. A high content (19.8 wt%) of PET and PS decomposing at low temperatures and a low content of PP cause the merging of the steps to occur at heating rates >20 °C min^{-1}. The first step corresponds to the decomposition of PS, PET, and a fraction of PP, and the second is assigned to the remaining PP and LD/HD-PE. The EU samples resemble the MX composition but also contain a high fraction of PP (30.6 wt%), thereby retaining three steps at 20 °C min^{-1}.

At 40 °C min^{-1}, the maximum decomposition temperatures of the EU, MX, and TH plastic mixtures are 481 °C, 493 °C, and 500 °C, respectively. The higher thermal stability of the TH mixture is attributed to its composition, as it consists primarily of polyethylenes (80.5 wt%) compared to the other samples. It is generally accepted that polyethylenes (particularly HDPE) have the highest required activation energy among common plastic waste components due to their linear molecular structure with methylene groups of stable C-C bonds (Chhabra, Bhattacharya et al. 2019). The EU and MX mixtures have a higher content of low activation energy components, such as PS and PET, which result in lower thermal stability and peak decomposition temperatures below 500 °C. A higher concentration of PS and PET substantially impacts the composition of the products, resulting in an increased presence of aromatic compounds, such as styrene, and gases like CO and CO_2, which are products of decarboxylation reactions associated with PET (Martínez-Narro, Prasertcharoensuk et al. 2022).

When considering the types of plastics that might reach an industrial-scale pyrolysis facility, it is important to recognize that not all plastics in this study are likely candidates. For instance, PET, especially in bottle form, is better suited for mechanical rather than pyrolysis recycling. Moreover, the declining use of PS suggests its reduced presence in future waste streams (Burgess, Holmes et al. 2021). Consequently, waste compositions reaching pyrolysis could be expected to be dominated by PP, LDPE, and HDPE. Such compositions would lead to greater

thermal stability in the waste streams, akin to the TH mixture, and subsequently result in a higher production of heavy waxes.

4.3.2. Isoconversional and linear model fitting results

Significant fluctuations in E_a and other kinetic parameters are observed at the beginning and end of decomposition (i.e., $0.1 > \alpha > 0.9$). The initial low E_a is attributed to the presence of weak link sites within the polymer chain, which are easily decomposed at the onset of the reaction through random chain scission as the reaction progresses toward more stable E_a values (Roussi, Vouvoudi et al. 2020). The increasing amount of carbonaceous char inhibits further polymer decomposition by the end of the reaction, resulting in higher E_a values (Dong, Gao et al. 2012, Roussi, Vouvoudi et al. 2020). To circumvent these highly variable regions, the conversion range of 0.2 – 0.8 was selected for this study. Results from KAS, Friedman, and CKA methods are summarized in Table 4.3. The KAS and Friedman isoconversional plots can be found in Appendix D. The estimated values for E_a are in good agreement with other findings in the literature for single plastics, which range from 192 – 267 kJ mol^{-1} (Aboulkas, El harfi et al. 2010, Diaz Silvarrey and Phan 2016, Xu, Wang et al. 2018). The growth factor *m* obtained via CKA was zero for all samples; however, this should be confirmed after nonlinear model fitting, with the value of zero serving only as the starting point. The apparent activation energy of the single plastics increases in the following order: PP < PET < PS < LDPE < HDPE. The EU and MX mixtures exhibit similar E_a values, while that of the TH mixture is the highest. The high content of HDPE and LDPE in the TH mixture, compared to other samples, explains the higher thermal stability observed in the DTG curves and high isoconversional activation energy. It is generally accepted that HDPE possesses the highest required activation energy among plastic polymers due to the methylene groups with stable C-C bonds, while that of LDPE is lower as branching differs (Chhabra, Bhattacharya et al. 2019).

In comparison to the KAS method, results obtained via the Friedman method exhibit greater variability in activation energy at different conversions for most samples. Only the E_a values of PP show similarity, with the rest of the individual plastics exhibiting a difference of approximately 12 kJ mol^{-1}. This difference is more pronounced for plastic mixtures, with differences of around 30 and 50 kJ mol^{-1} for MX and EU mixtures, respectively. The improved congruity of results between both methods for single plastics may be ascribed to their single-step decomposition, in contrast to mixtures. Moreover, there is considerably less noise from TGA data for individual plastic decomposition, and the differentiation error introduced with

the Friedman method is not as significant as it is for plastic mixtures. An exception can be observed for the TH mixture with a difference of only 9 kJ mol^{-1}, as it behaves similarly to individual plastics due to its high content of LDPE and HDPE.

Table 4.3. Kinetic parameters of mixtures and single plastics determined by isoconversional methods (E_a, and A) and CKA (*n*).

Sample	E_a / kJ mol^{-1}		A / s^{-1}		*n*	E_a variation / % *	
	KAS	Friedman	KAS	Friedman	*CKA*	KAS	Friedman
PS	222.77	208.37	$5.76x10^{14}$	$2.55x10^{14}$	2.84	1.3	8.6
PET	190.47	202.23	$1.07x10^{12}$	$4.10x10^{13}$	1.97	4.8	11.5
PP	175.43	176.71	$8.22x10^{10}$	$4.76x10^{11}$	1.05	16.9	29.8
LDPE	237.68	251.59	$9.32x10^{14}$	$1.42x10^{16}$	1.12	17.2	13.8
HDPE	263.82	252.27	$2.20x10^{16}$	$5.04x10^{15}$	1.08	4.5	8.7
EU mixture	223.37	272.10	$1.17\ x10^{13}$	$1.36x10^{22}$	1.09	29.4	46.1
TH mixture	267.09	276.32	$2.28x10^{14}$	$2.87x10^{18}$	0.76	11.8	18.7
MX mixture	222.17	252.05	$9.21x10^{12}$	$3.60x10^{16}$	0.92	34.9	24.9

$^{*}E_a variation = 100\left(E_{a,max} - E_{a,min}\right)/E_{a,average}$

The Friedman method is better suited for differential data, such as that of DSC. After differentiation, integral data can be smoothed to reduce noise; however, this may introduce a systematic error or shift in the data, ultimately leading to errors in the estimated kinetic parameters [41]. Consequently, only the results from the KAS integral method were employed for analyses and discussions in subsequent sections.

4.3.3. Activation energy dependencies.

Isoconversional methods are among the most employed approaches to derive kinetic parameters for thermally activated reactions. These methods enable the identification of single or multiple step reactions. If the difference between the minimum and maximum apparent E_a is less than 10 – 20% of the average, the variation is deemed insignificant, signifying that the process is adequately represented by a single step reaction with a unique kinetic triplet (Vyazovkin, Burnham et al. 2020). Conversely, if the variation is substantially high (>20 – 30%), the process is complex, necessitating the performance of a multistep kinetic analysis via multivariate nonlinear regression methods. As illustrated in Table 4.3, the low E_a variation condition is only applicable for the TH samples, whereas the EU and MX are close to 30%. The E_a dependence on conversion for each sample is presented in Figure 4.3, where the

apparent E_a values from the KAS isoconversional method are plotted against conversion. The dependence of E_a on α for single plastics is nearly negligible, ranging from 4.5 – 17.2%, corroborating that the thermal decomposition of neat plastics predominantly occurs in a single step, as initially inferred by visual inspection of their DTG curves. However, the higher variation of PP and LDPE in comparison to other individual plastics may suggest the presence of an initial decomposition step with a minor contribution to the overall kinetics, followed by the dominant step. The kinetic contribution of the steps can be ascertained by performing KDA. In contrast, the EU and MX mixtures exhibit an almost linear increase in activation energy with conversion, while the TH sample demonstrates a lower variation. This erratic behaviour in E_a vs. α applies to mixed plastics pyrolysis, particularly since the components possess different decomposition temperature ranges and the process occurs in multiple steps. The variation of E_a is less apparent for the TH mixture due to its predominantly polyethylene composition (80.5 wt%) and the highest proportion of HDPE (61.8 wt%) compared to other samples, while the other two exhibit more varied compositions. This results in greater thermal stability and, consequently, higher activation energy, while its decomposition resembles that of neat plastics, owing to the low quantities of PS, PET, and PP. However, even the TH mixture decomposes in multiple steps at low heating rates, indicating that a low dependence of E_a vs. α is not strictly indicative of an overall single step decomposition.

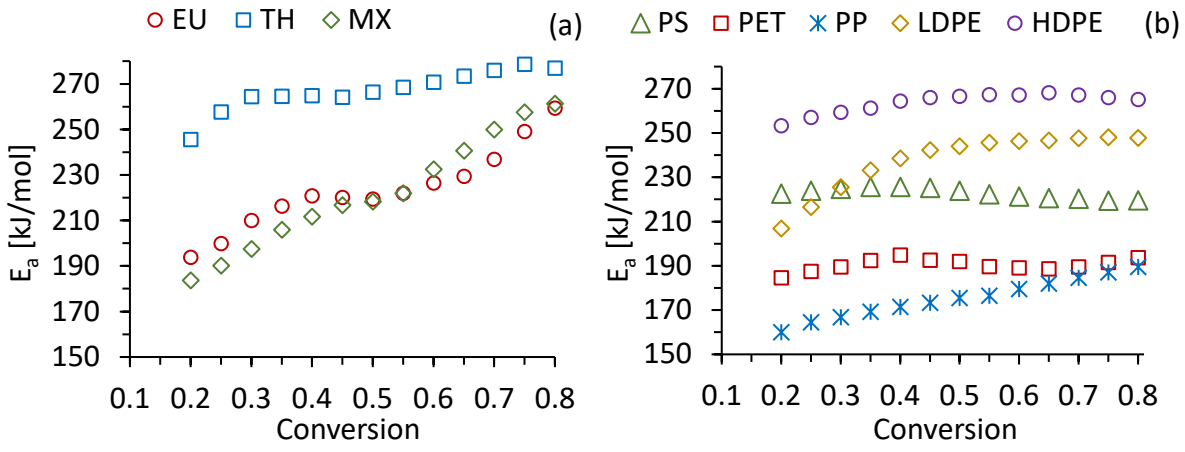

Figure 4.3. Activation energy dependence on conversion for mixtures (a) and individual plastics (b) obtained by KAS method.

4.3.4. Optimization by nonlinear model fitting

Kinetic parameters acquired solely through KAS and CKA are inadequate for predicting conversion across the decomposition temperature range (Diaz Silvarrey and Phan 2016), as demonstrated in Figure 4.4.

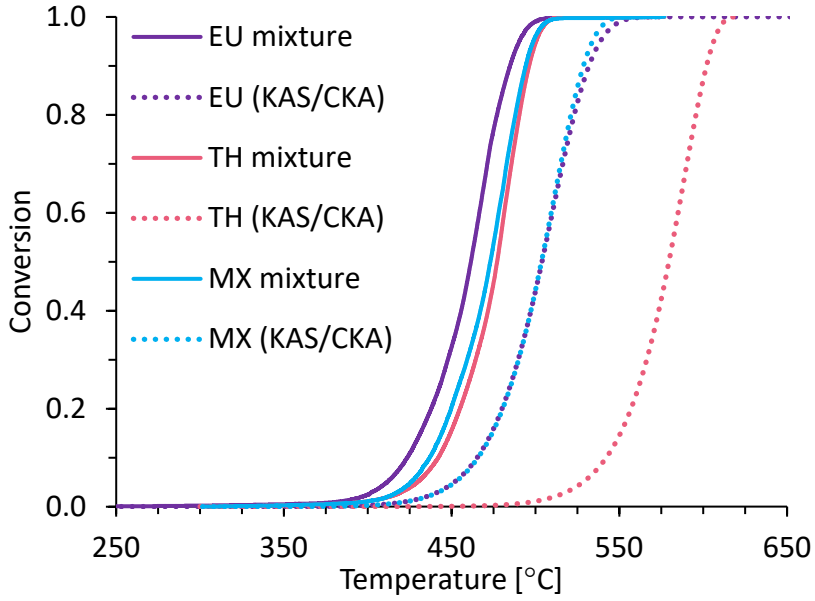

Figure 4.4. Conversion of plastic mixtures at 20 °C min^{-1} using kinetic parameters derived solely from KAS (E_a and A) and CKA (f(α)).

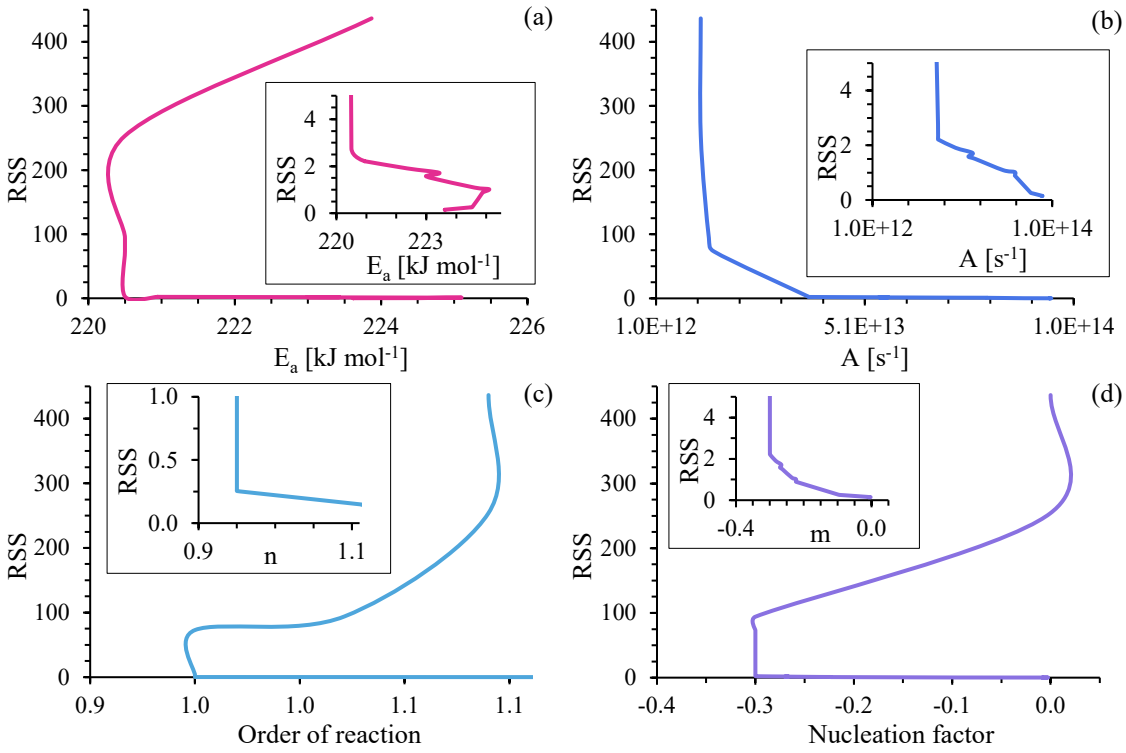

Figure 4.5. RSS values as decision variables change during multivariate nonlinear regression of EU mixture at 20 °C min^{-1}. Insets show a smaller y-axis scale.

Consequently, the kinetic parameters were further optimized to fit the experimental data via multivariate nonlinear regression. The apparent kinetic parameters derived from KAS and CKA were employed as reliable starting points for the optimization. The method produces one

kinetic triplet set per heating rate, thereby assuming that the decompositions involved occur in a single step. The procedure was applied to each sample at every heating rate, and the results were averaged to obtain global models independent of the heating rate. The minimization of the RSS objective function as the decision variables change during multivariate nonlinear regression is depicted in Figure 4.5.

The resulting theoretical conversion curves for single plastics more closely overlap with their corresponding experimental curves (Figure 4.6). Although single plastics are predominantly governed by one rate-limiting step, there are indications of smaller steps at the onset of decomposition ($\alpha < 0.2$) for PP and LDPE, while PET exhibits a distinct degradation step toward the end of the reaction ($\alpha > 0.95$) due to the formation of non-volatile conjugated aromatic rings (Holland and Hay 2002). The accuracy of these models may be further enhanced by incorporating a second set of kinetic parameters, albeit at the expense of increased complexity.

The plastic mixtures at low heating rates (i.e., <20 °C min^{-1}) display poor fits to the experimental data across the entire decomposition range due to the different steps in which they decompose, particularly since the steps exhibit varying degrees of overlap at different heating rates. After solving Equation 4.8, the first derivative of conversion concerning temperature results in a single bell-shaped curve that cannot adequately fit an experimental curve with multiple inflection points, such as those obtained for plastic mixtures at <20 °C min^{-1}. Each peak in the reaction rate curve should be described by a distinct set of kinetic parameters; however, at 40 °C min^{-1}, the individual steps are completely overlapped, and the DTG curves can be adequately fit with a single kinetic triplet. The average kinetic parameters obtained from nonlinear model fitting are presented in Table 4.4, along with the RSS to demonstrate model error variance. The estimated parameters from the kinetic analysis should yield E_a values comparable to reliable isoconversional values (Vrandečić, Erceg et al. 2010). The apparent E_a of EU, TH, and MX samples are within the ranges of 221 – 225, 265 – 268, and 220 – 223 kJ mol^{-1}, respectively, which align well with the isoconversional values derived from the KAS method.

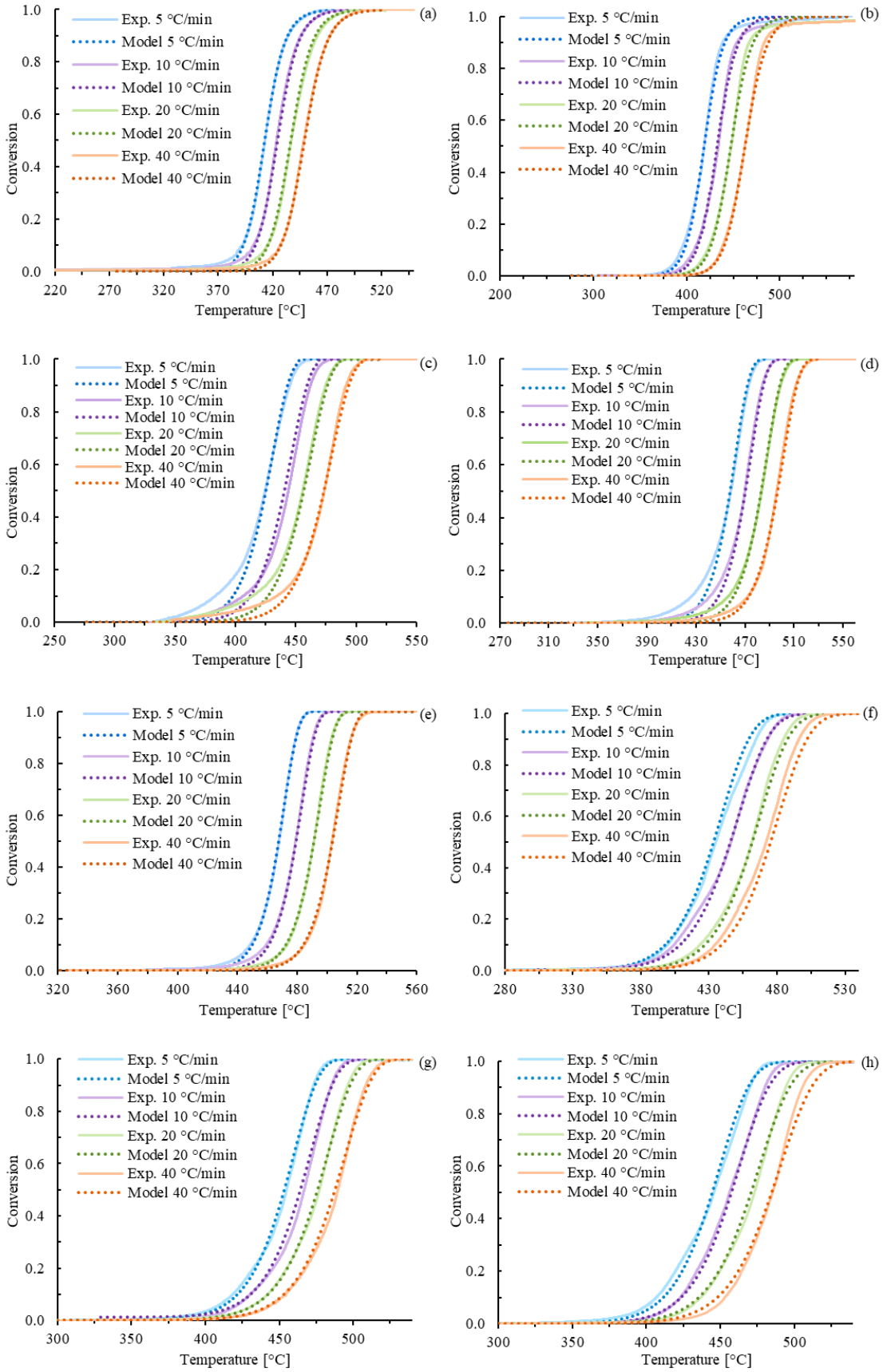

Figure 4.6. Experimental (solid lines) and theoretical (dotted) conversions of individual plastics: PS (a), PET (b), PP (c), LDPE (d), HDPE (e), and plastic mixtures: EU (f), TH (g), and MX (h) after nonlinear model fitting.

Table 4.4. Average kinetic parameters from single step nonlinear model fitting.

Sample	E / kJ mol^{-1}	A / s^{-1}	*m*	*n*	*RSS*
PS	222.7	8.4x10^{14}	0.45	1.57	5.4
PET	189.2	1.56x10^{12}	0.49	1.47	2.2
PP	175.6	5.77x10^{10}	0.30	0.83	5.3
LDPE	239.1	6.81x10^{14}	0.34	0.84	4.5
HDPE	263.9	2.87x10^{16}	0.42	0.82	3.0
EU mixture	223.8	1.04x10^{14}	-0.11	1.14	0.7
TH mixture	266.9	4.62x10^{16}	-0.13	0.96	3.0
MX mixture	222.6	5.27x10^{13}	0.01	1.1	1.6

The additivity rule was subsequently employed to predict the conversion of plastic waste mixtures using the optimized kinetic parameters of single plastics and assuming no interactions within the mixtures. Equation 4.10 was utilized for this purpose, with the weight fraction of each component represented by the c_i parameter and the *i* subscript denoting single plastic components instead of reaction steps.

The resulting conversion and rate curves do not perfectly overlap with any of the mixtures at their respective compositions and heating rates, as observed in Figure 4.7, where the reaction rates of single plastics are also displayed for comparison. This suggests that the kinetic parameters are altered when single plastics are present alongside other components in the mixture. The theoretical conversion, assuming no interactions, overestimates the decomposition temperature of the mixtures by approximately 10 °C throughout the entire reaction, indicating that interactions between components may be responsible for reducing the degradation temperature in the mixtures.

This observation is consistent with findings in the literature on synergies between plastics that decompose at low temperatures and those that decompose at high temperatures. For example, Miranda et al. (Miranda, Yang et al. 2001) investigated the kinetics of a plastic mixture (HDPE, LDPE, PP, and PS) and discovered that these interactions altered the activation energy of components in the mixture by approximately 13 kJ mol^{-1} compared to the individual plastic's thermal decomposition. This was primarily attributed to the destabilization of polyethylene by intermolecular hydrogen transfer from the degradation radicals of PS. The radicals of PS released at the onset of the reaction attack the chains of the other more stable polymers and shift their decomposition curve toward lower temperatures, while this effect results in reduced diffusion of the radicals toward other PS molecules, consequently slowing or stabilizing its decomposition (Tuffi, D'Abramo et al. 2018). Several authors have concluded

that PS is indeed the primary component responsible for the discrepancies between kinetic parameters of individual and mixed plastics, as it causes destabilization of polyolefins (Dodson and McNeill 1976, Murata and Akimoto 1979, Miranda, Yang et al. 2001).

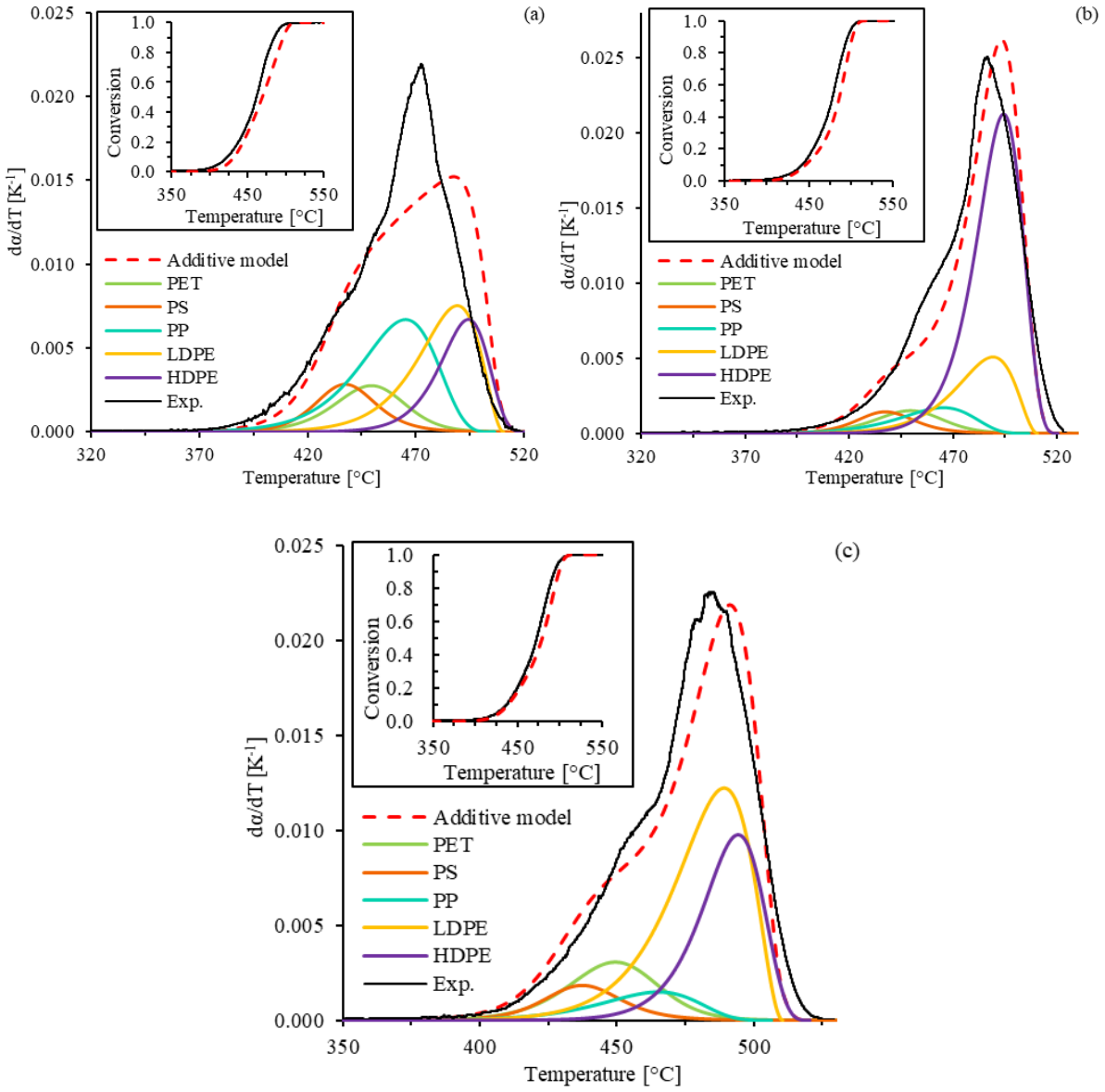

Figure 4.7. Additive model applied to EU (a), TH (b), and MX (c) compositions using kinetic parameters of individual plastics at 20 °C min^{-1}.

4.3.5. Deconvolution analysis

Deconvolution of PP and LDPE

In the analysed single plastics, PP and LDPE exhibit the highest E_a dependence on conversion, suggesting an additional decomposition step. This was corroborated after nonlinear model fitting demonstrated low fitting at the beginning of the reaction when using a single kinetic triplet, as previously illustrated in Figure 4.6. Consequently, KDA and MDA were performed

on these two plastics to investigate the kinetic contributions of each step. The initial values for this analysis were those obtained from nonlinear model fitting, except for the activation energy, which were divided into the isoconversional values at conversions of 0.2 for the first step and the average of the rest for the second. Figure 4.8 displays the conversion and DTG curves with the deconvoluted reaction steps by KDA. Results presented in Table 4.5 indicate the extent to which the isoconversional activation energy can vary when assuming single-step decomposition for materials that decompose in multiple steps.

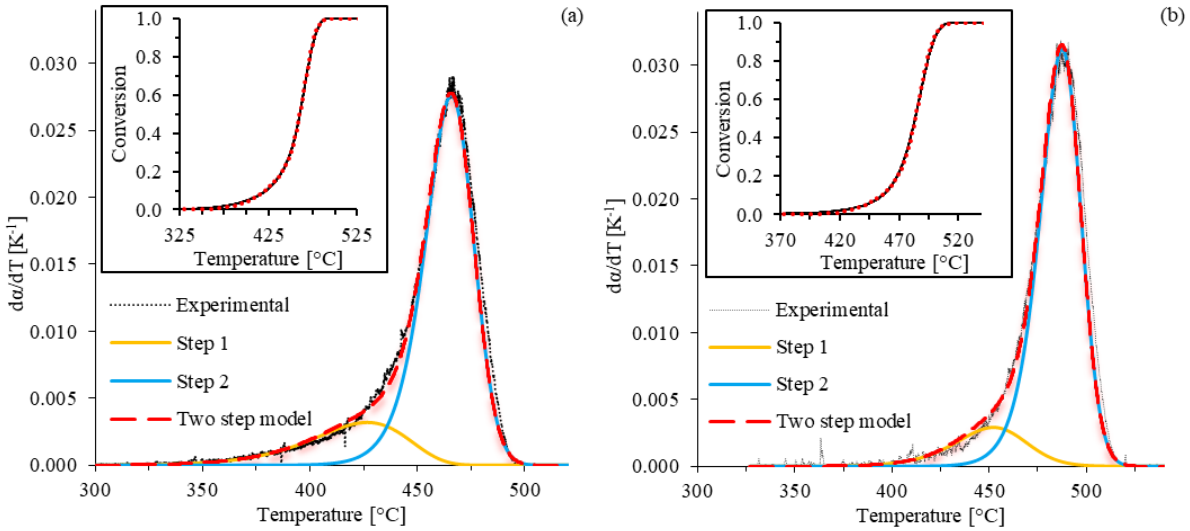

Figure 4.8. Conversion and reaction rate curves of PP (a) and LDPE (b) showing deconvoluted reaction steps at 20 °C min^{-1}.

From KAS and other isoconversional methods, E_a values are typically averaged, and these discrepancies at the beginning or end of the reaction can significantly impact the result. The initial steps of both PP and LDPE have a low contribution to the overall kinetics (15% and 9%) compared to the main reaction steps, which have E_a values approximately 26 kJ mol^{-1} higher.

Deconvolution of plastic mixtures

As plastic mixtures at low heating rates require a multistep approach, kinetic (KDA) and mathematical (MDA) deconvolution analyses were conducted to separate individual steps and obtain their kinetic triplets. During the multistep thermal degradation of solids, the overall conversion is determined by intricate mutual interactions of physical and chemical events, as well as by the continuous variation of self-generated reaction conditions (Koga 2018). An empirical approach for estimating the kinetic behaviour of each reaction step involves the use of Equation 4.10. The analysis commenced with the addition of a second term to the overall rate equation, followed by iterative calculation of variables, which now included the kinetic contribution factors (c_i). Subsequently, the reduction of RSS was subjected to the F-test to

verify statistical significance. The procedure was repeated after adding a third and fourth term to Equation 4.10. The addition of a fourth step did not yield a statistically significant reduction in RSS for any mixture. Hence, three steps were identified for each mixture, as suggested by the visual inspection of experimental DTG curves.

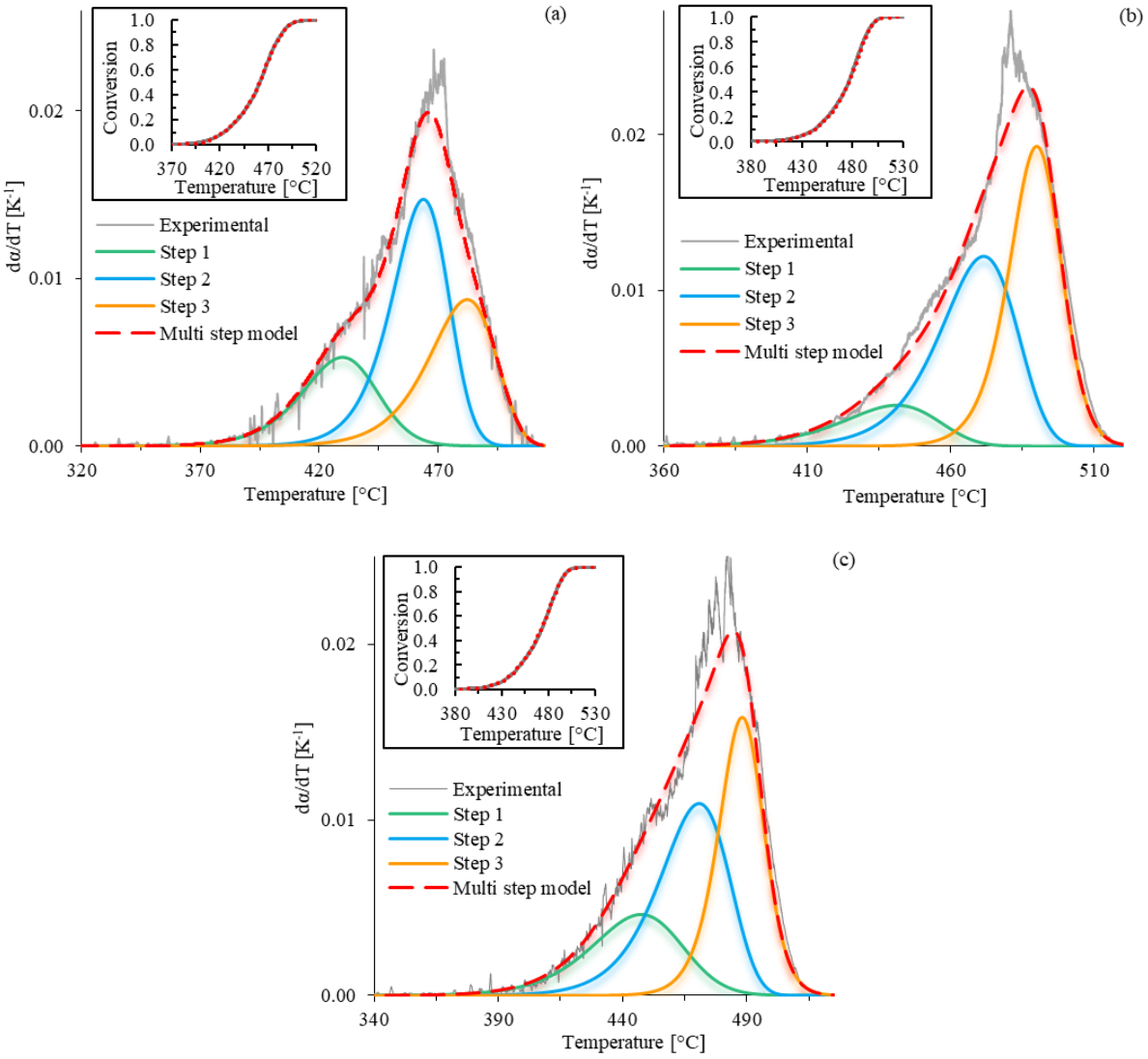

Figure 4.9. Experimental and theoretical conversion and reaction rates of EU (a), TH (b), and MX (c) mixtures showing deconvoluted reaction steps at 20 °C min^{-1}.

Table 4.5. Average results from kinetic and mathematical deconvolution analysis of single and mixed plastics.

Sample	Step	E_a / kJ mol^{-1}		A / s^{-1}		*m*		*n*		*c*		*RSS*	
		KDA	MDA	KDA	MDA	KDA	MDA	KDA	MDA	KDA	MDA	KDA	MDA
PP	1	160.1	161.8	$1.3x10^{10}$	$1.5x10^{10}$	0.10	0.17	0.95	1.14	0.15	0.20	1.2	0.8
	2	188.5	190.9	$7.8x10^{11}$	$1.2x10^{12}$	0.60	0.58	1.02	0.95	0.85	0.80		
LDPE	1	220.1	218.7	$1.7x10^{14}$	$9.7x10^{13}$	0.21	0.14	1.25	1.10	0.09	0.11	2.3	2.4
	2	244.8	248.0	$2.6x10^{15}$	$3.8x10^{15}$	0.52	0.47	1.06	0.95	0.91	0.89		
EU mixture	1	197.7	197.2	$1.4x10^{13}$	$1.2x10^{13}$	0.34	0.39	1.15	1.10	0.22	0.29	0.5	2.2
	2	224.2	223.4	$2.6x10^{14}$	$3.2x10^{14}$	0.43	0.6	1.01	0.94	0.46	0.28		
	3	245.7	247.1	$2.7x10^{15}$	$3.7x10^{15}$	0.35	0.30	1.03	1.05	0.32	0.43		
TH mixture	1	200.1	202.6	$9.1x10^{12}$	$1.0x10^{13}$	0.27	0.33	1.00	0.90	0.11	0.19	1.1	0.9
	2	219.9	217.7	$6.9x10^{13}$	$4.8x10^{13}$	0.39	0.57	0.93	0.91	0.43	0.29		
	3	247.2	249.8	$4.0x10^{15}$	$4.4x10^{15}$	0.65	0.50	1.15	1.00	0.46	0.51		
MX mixture	1	195.2	193.9	$3.1x10^{12}$	$3.3x10^{12}$	0.26	0.46	1.15	0.94	0.22	0.31	0.5	1.3
	2	218.1	216.1	$6.0x10^{13}$	$1.1x10^{14}$	0.39	0.72	1.03	0.98	0.40	0.18		
	3	245.7	246.3	$3.7x10^{15}$	$4.4x10^{15}$	0.63	0.60	1.19	1.16	0.38	0.51		

Average results from the KDA of mixtures are presented in Table 4.5. The kinetic contribution of the first step in each mixture is similar to the respective combined mass fractions of PET and PS, as these components decompose first. The second step represents all plastics decomposing simultaneously, contributing more than 40% of the reaction in each mixture. The third step exhibits the highest activation energy for every mixture, as anticipated due to the highly recalcitrant nature of LDPE and HDPE, which decompose simultaneously in this step. The experimental and theoretical reaction rates and conversions of each mixture at 20 °C min^{-1} are depicted in Figure 4.9, along with their corresponding deconvoluted reaction steps by KDA. Deconvoluted steps by MDA method can be found in Appendix E.

Figure 4.9 reveals suboptimal model fits that diverge from the experimental data. This discrepancy is likely due to the interactions among different plastic components. Additionally, the presence of additives may lead to unaccounted reaction steps in the model. Including these additional steps could enhance the model's accuracy, but it also increases complexity, potentially compromising its practical utility in real-world scenarios. This underscores the necessity of assessing the statistical significance of any extra steps before integrating them into the model. In the broader scope of chemical recycling, achieving a close alignment between experimental results and theoretical predictions is instrumental for guiding the design and operation of processes. However, enhanced accuracy does not necessarily equate to improved functionality. Although the model's reaction rate curve fits are not ideal, the conversion curve fits are sufficiently accurate for practical application in operating an industrial-scale pyrolysis reactor.

The kinetics of individual steps indicate varying values of reaction orders and growth factors among them, which contribute to the discrepancies observed when employing single-step models to predict low heating rate experimental curves. The E_a, A, and *n* values acquired from KDA and MDA are similar in most cases; however, the *m* parameter and kinetic contributions differ. This discrepancy could be attributed to the distinct methodological approaches of the methods. MDA is an empirical method based on mathematical shape analysis of overlapping peaks using statistical functions, while KDA employs the actual kinetic shape of the peaks to fit the rate equation, rendering the method more reliant on initial values. Although MDA possesses the advantage of excellent flexibility in fitting complex reaction profiles, the mathematical function could distort kinetic parameters through inaccurate kinetic curve matching and by smoothing out real reaction features (Vyazovkin, Burnham et al. 2011). If the

peaks are not adequately deconvoluted, the analysis may yield unreliable kinetic parameters when reconstructing superficial peaks (Muravyev, Pivkina et al. 2019). For practical purposes of elucidating the decomposition of plastic mixtures, both methods can aptly represent the process. Tuffi et al. (Tuffi, D'Abramo et al. 2018) examined the thermal decomposition of plastic mixtures (PS, PET, PP, and PE) at 5, 10, 15, and 20 °C min^{-1}, identifying two primary steps, with the first attributed to the simultaneous decomposition of PS and PET. The study also investigated binary mixtures, concluding that their interactions are more significant when structurally distinct components are present (e.g., PS and PE), the composition is varied (i.e., components have similar fractions in the mixture), and when components decompose in close temperature ranges.

4.3.6. Model validation

Model comparison overview

To validate the findings of this study, it is essential to first perform statistical analysis of alternative model development methods. Figure 4.10 illustrates a graded improvement between linear model fitting methods and subsequent methods for the EU mixture, tracking the rate peak more closely in stature and temperature.

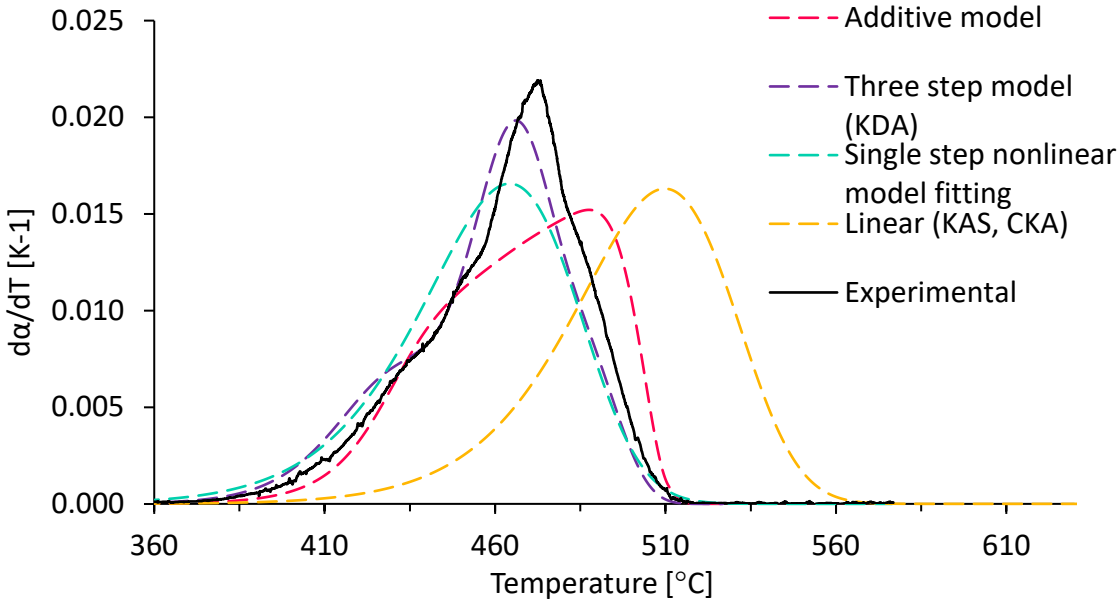

Figure 4.10. Theoretical reaction rate using kinetic parameters derived from different methods for EU mixture at 20 °C min^{-1}.

Table 4.6 displays this significant improvement statistically, with KDA models yielding the lowest RSS error variation for mixtures from each region. Three-step models permit closer

curve tracking due to the increased kinetic complexity, enabling accurate prediction of multiple inflections in the decomposition rate throughout the temperature range.

Table 4.6. RSS values of varying methods for each region at 10 °C min^{-1}.

Region	Linear	Nonlinear	Additive model	KDA	MDA
EU	3001.1	0.7	23.4	0.5	2.2
TH	57.8	3.0	12.4	1.1	0.9
MX	1142.0	1.6	10.1	0.5	1.3

The applicability of the models to mixtures with different compositions was investigated by employing the kinetic parameters of one mixture to predict the experimental curves of the other two. Figure 4.11 displays the prediction capability of the MX mixture model in comparison to the TH mixture experimental data. The TH and MX models more accurately described the conversion of other samples, while the model based on EU data resulted in higher RSS values when compared to experimental data from TH and MX mixtures. The most significant error proportion arises due to the rate curves shifting by approximately 10 – 15 °C when compared to data from other mixtures.

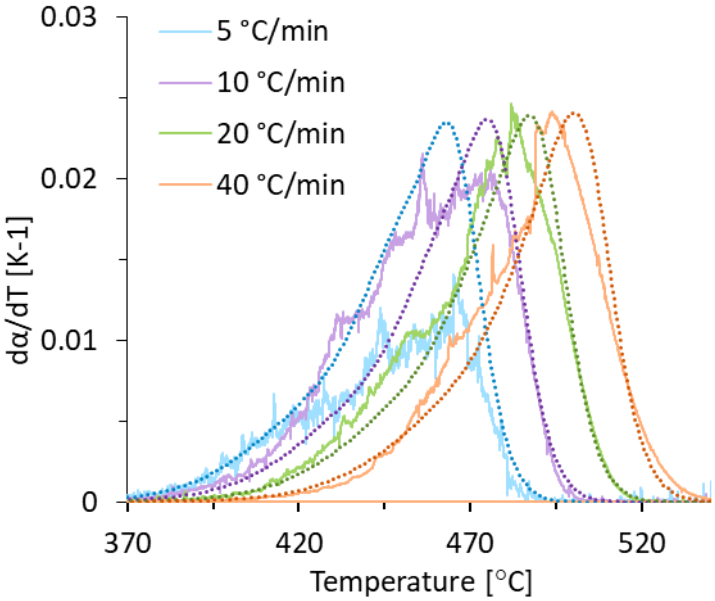

Figure 4.11. Experimental data (solid lines) of TH mixture compared to theoretical decomposition rate curves (dotted) of the multistep model based on the MX mixture. Shown at multiple heating rates.

The additive models exhibit similar shifts in decomposition temperature; however, they overestimate the decomposition temperature due to unaccounted component reactions. Kinetic parameters from the multistep model of the MX sample underestimate the

decomposition temperature of TH mixtures by approximately 11 °C. In an industrial-scale pyrolysis plant, the composition of plastic waste fed into reactors can be highly variable, with multiple contaminants and additives possibly present. Consequently, utilizing a model that slightly overestimates the pyrolysis temperature at which the reactor will operate is preferable to one that predicts a lower temperature. From an engineering standpoint, employing the additive model would ensure a safe design point for reactors.

Model prediction accuracy at various heating rates

A separate set of experiments were performed for each individual plastic sample at an alternative heating rate (i.e., 30 °C min^{-1}), which were not included in the kinetic analysis. Theoretical conversions employing the kinetic parameters obtained by single-step nonlinear model fitting (for PET, PS, and HDPE) and two-step KDA (for PP and LDPE) at 30 °C min^{-1} were subsequently compared to experimental data, and the corresponding RSS values were calculated. Figure 4.12 illustrates the experimental and predicted conversions, which exhibit a strong agreement with each other.

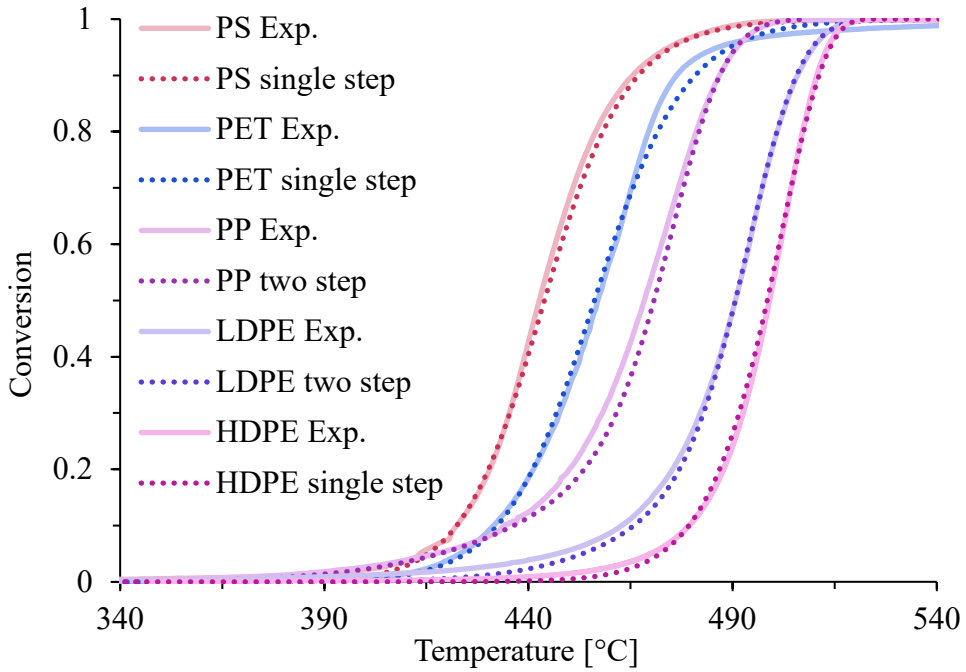

Figure 4.12. Prediction of experimental conversions of individual plastics at 30 °C min^{-1} utilizing their corresponding kinetic parameters.

The significance of kinetic models for predicting decomposition behaviour at various heating rates is crucial for their applicability in industrial settings. Thermal processes seldom have identical design energy inputs or geometry, resulting in different heating rates. Variations in curve shape at diverse heating rates stem from the reaction rates within mixtures. For

example, at slow heating rates, components with lower activation energy, such as PP or PS, may have fully co-decomposed before reaching higher temperatures where other components initiate decomposition. Consequently, slower heating rate pyrolysis may produce a distinct decomposition environment with alternative interactions and synergies between components, leading to notable inflections observed in decomposition rate curves. As a result, models generated using experimental data at higher heating rates may exhibit reduced accuracy when predicting the kinetic behaviour of more slowly heated mixtures.

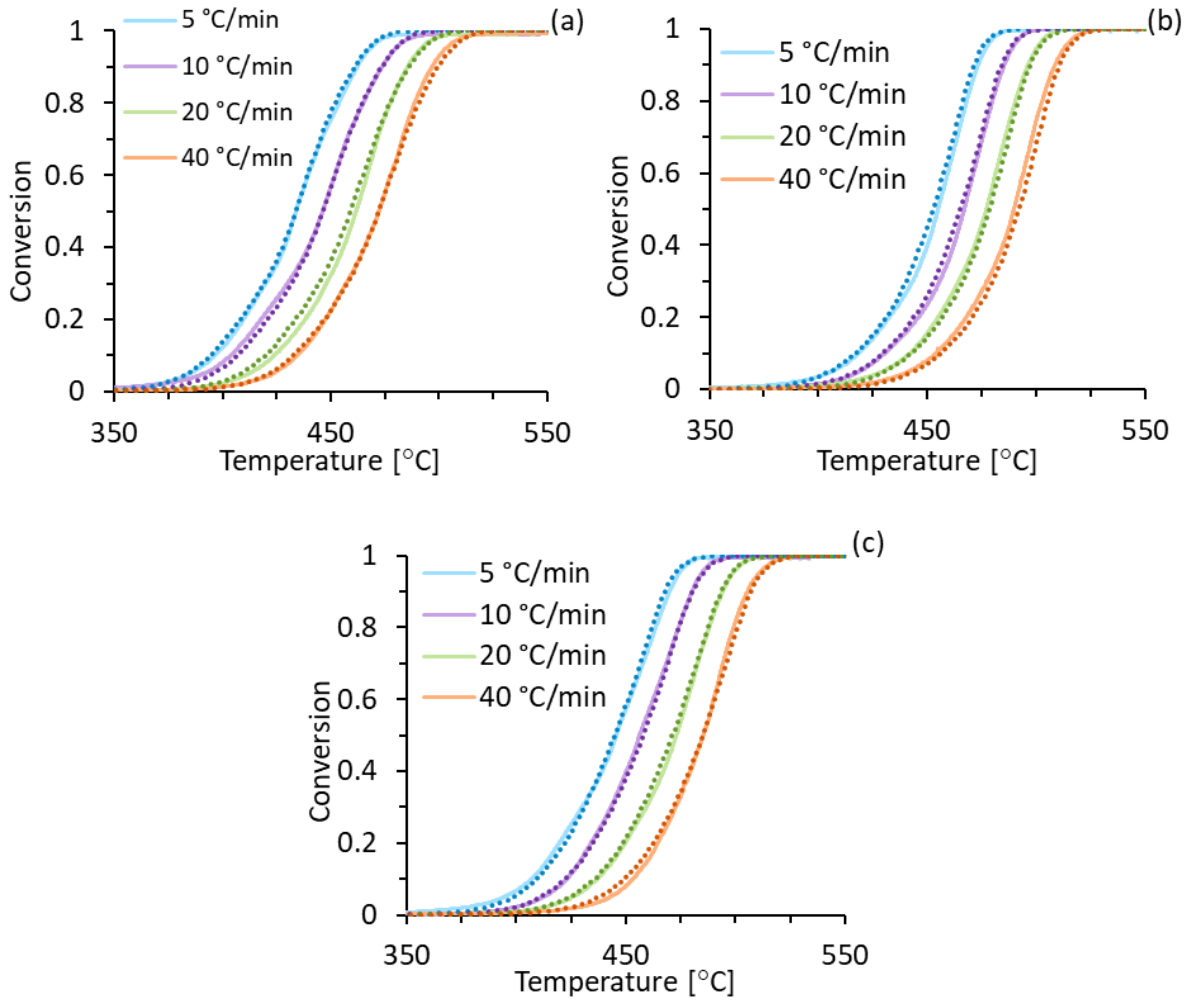

Figure 4.13. EU mixture (a), TH mixture (b), MX mixture (c) three step KDA models (dotted lines) predicting experimental conversion (solid lines) at various heating rates.

To investigate this applicability, multi-step models created using experimental data at 20 °C min^{-1} were employed to predict experimental decomposition behaviour across a range of heating rates. Figure 4.13 demonstrates that all models successfully predicted the decomposition start and end temperatures for all mixtures. This achievement can be attributed to the specification of heating rate in Equation 4.10, allowing for accurate shifts in temperature range. Inaccuracies arise in the bowing of experimental kinetics, attuned to

changing interactions at different heating rates, forming inflections in the reaction profile. Table 4.7 presents the statistical accuracy of the multi-step models at various heating rates. The increased errors at lower heating rates may be mitigated by employing more complex models with additional required deconvolution steps, although this might not be necessary due to varying input compositions and the influence of unknown additives.

Table 4.7. RSS values for KDA multistep models predicting various heating rates.

Mixture	5 °C min^{-1}	10 °C min^{-1}	20 °C min^{-1}	40 °C min^{-1}
EU	3.9	2.6	1.1	0.3
MX	12.6	3.2	0.4	0.4
TH	5.5	0.7	0.4	0.5

4.4. Summary

Thermogravimetric data of individual pure plastics (PP, PET, LDPE, HDPE, and PET) and mixed polymer samples with distinct compositions from specific origins (Europe, Thailand, and Mexico) were acquired using TGA. Pyrolysis decomposition data demonstrated that pure polymers decompose at different temperatures (PS < PP < PET < LDPE < HDPE), with activation energies ranging from 175 – 264 kJ mol^{-1}. The decomposition behaviour of most individual polymers can be closely approximated by single-step kinetic modelling employing KAS and CKA methods. However, these methods were unsuccessful in predicting the decomposition starting temperatures and reaction rate curve inflections formed by interactions between individual components in plastic mixtures. More advanced techniques were explored to determine the most suitable modelling methodology, including nonlinear, additive method, kinetic and mathematical deconvolution analysis, which varied in their degrees of accuracy. Two-step deconvolution analysis proved effective in predicting the early decomposition temperature of PP and LDPE, reducing RSS at 20 °C min^{-1}. Kinetic parameters for mixed polymer pyrolysis were developed using three-step KDA and MDA, resulting in substantially reduced statistical error when predicting experimental data. Moreover, it was demonstrated that multi-step KDA models formed from experimental data at a 20 °C min^{-1} heating rate can be applied to predict the kinetic behaviour of the same mixture across a varied temperature range. These models exhibited improved accuracy over other modelling methods throughout the entire heating range.

Chapter 5. Pyrolysis of mixed plastic waste using biochar supported catalysts

This chapter presents a comprehensive evaluation of catalysts derived from waste biomass for the pyrolysis of mixed plastic waste to generate value-added products. The study is motivated by the need to overcome the limitations present in existing plastic waste recycling approaches and aims to explore effective alternatives. A noticeable gap exists in literature regarding the performance differentiation of various metal-incorporated biochars in plastic pyrolysis. Moreover, an underexplored area is the impact of distinct catalyst bed temperatures within two-stage reactors, where initial pyrolysis and catalysis-driven processes are spatially segregated. The focus is on the catalytic pyrolysis process, a promising strategy for alleviating plastic waste issues while simultaneously enabling the extraction of valuable chemical derivatives. This chapter provides an in-depth analysis of Ni, Fe, and Zn-loaded activated carbons as catalysts, aiming to evaluate their efficacy in augmenting plastic waste recycling efficiency and their selectivity in producing hydrogen, carbon nanotubes, and monomers. Emphasis is placed on assessing the interplay of temperature variations and distinct catalysts on the yields and compositions of oil, gas, char, and carbon deposition. This inquiry, rooted in the application of waste-derived catalysts in plastic waste pyrolysis, aspires to enhance the recycling processes and underscores the viability of these catalysts as substitutes for traditional materials. Catalytic pyrolysis experiments were conducted utilizing a two-stage fixed-bed reactor, wherein the temperature was maintained at 500 °C in first stage and varied (500, 600, and 700 °C) in the 2nd stage (catalyst bed). The tested biochars were doped with nickel (Ni-BC), iron (Fe-BC), and zinc (Zn-BC) to assess the impact of metal catalysts distributed on the highly porous carbonaceous support. Furthermore, the results obtained from biochars were compared to those obtained using a commercial zeolite and non-catalytic runs. The Ni-BC and Fe-BC catalysts demonstrated superior catalytic activity compared to Zn-BC and raw biochar (Raw-BC), with Ni-BC exhibiting a higher efficacy for CNT production. The HZSM-5 catalyst exhibited the most significant reduction in oil/wax yields and increase in gas yields across all examined temperature ranges, outperforming other catalysts in converting heavy fractions into lighter counterparts and monomer recovery. These findings provide valuable insights into catalyst selection and optimization for plastic waste pyrolysis processes, with HZSM-5 emerging as the most effective catalyst, and Ni-BC and Fe-BC demonstrating promising results in terms of catalytic activity and CNT production. The comprehensive analysis of catalyst performances serves as a foundation for future research

endeavours aimed at improving plastic waste management and resource recovery through chemical recycling. Portions of the discussion presented in this chapter have been previously published in the *Journal of Environmental Chemical Engineering*, under the title "Chemical recycling of mixed plastic waste via catalytic pyrolysis" (DOI: 10.1016/j.jece.2022.108494) (Martínez-Narro, Prasertcharoensuk et al. 2022). The present chapter serves to expand upon the findings detailed in the aforementioned article.

5.1. Background

The utilization of waste-derived materials, such as biochar, as catalysts for the pyrolysis of plastic waste offers multiple advantages over conventional commercial catalysts. The employment of waste-derived materials leads to a reduction in landfill waste and provides an economically viable option, as these materials can be obtained at lower costs than other widely used catalysts (Bennett, Wilson et al. 2016). Furthermore, their application fosters innovation within the waste management sector, stimulating the exploration of new methods for repurposing waste and the development of sustainable materials (Hargreaves 2018). Johar et al. (Johar, Rylott et al. 2023) designed a biologically nickel-bound biochar catalyst for the depolymerization of polyethylene into high-value chemicals via microwave-assisted pyrolysis. This catalyst effectively enhanced the production of C_6-C_{12} aliphatics, dehydrocyclization of linear alkanes, and H_2 release as gaseous fraction. Wang et al. (Wang, Lei et al. 2021) employed nanocellulose-derived biochar as a catalyst for pyrolyzing low-density polyethylene (LDPE) into hydrogen and liquid fuels. The study revealed that at 500 °C and a biochar to LDPE ratio of >3, the plastic could be completely degraded into liquid and gas without wax formation. Moreover, the biochar catalyst proved efficient in converting real waste plastics (e.g., grocery bags and packaging trays) into valuable liquid and H_2-enriched gas products. In a separate study (Wang, Lei et al. 2020), biochars derived from agricultural waste (corn stover and Douglas fir) were utilized for the pyrolysis of waste plastics (i.e., PS, PET, PP, LDPE, and HDPE). The corn stover biochar resulted in a liquid yield of approximately 40 wt%, without wax formation, generated 60-80 vol% of H2 in the gas yield, and exhibited high activity after 20 cycles of reuse. Similarly, Park et al. (Park, Jae et al. 2019) examined the application of nickel-doped lignin-derived biochar (Ni-BC) for HDPE gasification. The Ni-BC catalyst demonstrated high H_2 yields (0.093 $mmolH_2\ g^{-1}_{plastic}$) from the gasification process, which was attributed to the high dispersion/distribution of Ni on the biochar. The study concludes that Ni supported

on char could be an economically feasible catalyst for producing hydrogen from gasification of plastics.

Nickel, iron, and zinc are more abundant and widely available than the scarcer noble metals (e.g., platinum and palladium) that are commonly used as catalysts to break down large hydrocarbon molecules, leading to lower raw material costs (Diaz 2016, Hijazi, Ala'a et al. 2019, Zhang, Starr et al. 2022). Additionally, their extraction and processing are generally less complex and expensive. The use of biochar as a support also adds to the cost-effectiveness, given that it is of low cost and derived from biomass waste.

In this study, a comprehensive investigation of the catalytic pyrolysis of plastic waste using waste-derived catalysts (metal-doped biochars) at varying catalyst bed temperatures in a two-stage fixed-bed reactor is presented. The aim is to assess the potential of these materials in enhancing the efficiency of plastic waste recycling and exploring their product selectivity. The discussion focuses on the effects of temperature and different catalysts in the oil, gas, char, and carbon deposition yields, as well as oil and gas compositions, providing valuable insights into the performance of the catalytic process.

5.2. Thermal pyrolysis

5.2.1. Product yields

The thermal pyrolysis process was carried out at temperatures of 500, 600, and 700 °C in the second stage of the reactor to establish a baseline for examining the impact of catalysts on product yields and compositions. No catalyst was added and only quartz wool was present in the catalyst bed. All yields and compositions reported in this chapter are referred to the initial plastic feed. Temperature plays a crucial role in influencing product yields, increasing temperature from 500 °C to 700 °C significantly increases the gas at the expense of oil production as shown in Figure 5.1. These results suggest that higher temperatures promote cracking reactions and carbon-carbon (C-C) bond cleavage of plastic waste volatiles, leading to higher yields of gaseous products. This can be attributed to the increased rate of chemical reactions and thermally-induced bond scissions in the plastic waste at higher temperatures (López, de Marco et al. 2011).

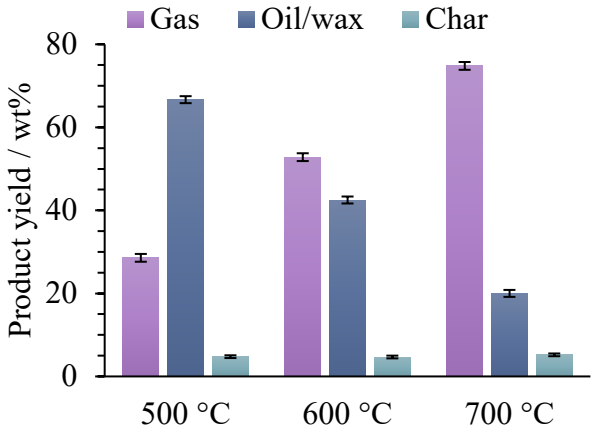

Figure 5.1. Product yields of thermal pyrolysis runs at different temperatures of the second stage.

Temperature directly affects the formation of gases during the pyrolysis of plastic waste because it influences the breakdown of chemical bonds within the plastic material, with higher temperatures leading to a higher number of broken C-C bonds and consequently lighter products (López, de Marco et al. 2011, Martínez-Narro, Royston et al. 2023). In addition, the bond dissociation energy is also affected, and the strength of chemical bonds varies among different plastic materials (Lampman 2003). As the temperature increases, more bonds within the plastic waste can be broken, leading to a greater extent of decomposition and gas formation. Since the pyrolysis section was kept at constant conditions, there is insignificant variation in the char yields (around 5 wt%). A summary of thermal pyrolysis product yields in literature and this study is presented in Table 5.1.

The variability in product yields and compositions observed in these studies in Table 5.1 can be attributed to several factors. One such factor is the type of plastic waste, which can cover a wide range of polymers, including the main components of municipal plastic waste: PS, PET, PP, PVC, LDPE, and HDPE. The chemical structure of each plastic type influences the reaction pathways, product yields, and product compositions during pyrolysis (Maqsood, Dai et al. 2021). Another contributing factor is the presence of additives and contaminants, which vary between the samples used by different researchers. Most commercial plastics contain various additives, such as fillers, plasticizers, stabilizers, and colorants. Plastic waste may also be contaminated with residual food or organic matter. These impurities can affect the pyrolysis process, leading to variations in the products among different studies (Martínez-Narro, Royston et al. 2023). For instance, food residues may introduce water, phosphorus, and nitrogen to the process, which contaminate the products. The presence of additives in plastics,

such as hindered amine light stabilizers (for protection from UV radiation), phenolic antioxidants (for prevention of oxidation and degradation), phosphites (stabilizers), and metallic stearates (used as lubricants, acid scavengers, and heat stabilizers), is particularly relevant for catalytic pyrolysis as these can interact with the catalysts used (Jerdy, Pham et al. 2023). Some additives may hinder reaction rates by deactivating or exchanging with the active sites, or permanently deposit on the catalyst surface. Competitive adsorption between additives and plastic volatiles may also occur, further impeding reactions. Pyrolysis conditions and system configuration also play a significant role in determining product yields and compositions (Alsaleh and Sattler 2014). In certain cases, an extended residence time can lead to an increase in gas production and a decrease in the yield of wax. When employing a single-stage process, the residence time within a heated zone is expected to be shorter compared to reactors consisting of two stages. When the heating rate is excessive, rapid volatilization occurs, resulting in the displacement of incompletely decomposed molecules from the heated area. Consequently, this phenomenon introduces fluctuations in the distribution of the final product. However, when conducting studies, it is common to compare them based on the temperatures utilized, disregarding variations in processing and system configurations such as these. Variations in pyrolysis conditions across different studies can account for the discrepancies in results.

The size of a pyrolysis reactor substantially impacts its heat transfer efficiency, product yield, and scalability. Smaller reactors typically ensure more efficient heat transfer and uniform temperature distribution, leading to consistent pyrolysis reactions. Conversely, larger reactors may introduce complexities in achieving uniform thermal gradients, affecting product consistency and quality. Scaling up pyrolysis from small to large reactors is not linear, as it involves complex adjustments in heat distribution and material handling. Larger reactors, while requiring greater initial investment, can offer higher throughput and long-term economic benefits (Fivga and Dimitriou 2018). However, their design must be carefully optimized to balance heat transfer, feed rate, and residence time, ensuring complete pyrolysis and desired product yields.

Table 5.1. Summary of thermal pyrolysis yields in literature and in this study.

Plastic mixture	Temperature	Gas yield	Oil yield	Char	Reference
PP, PET, PS, LDPE, HDPE	500	31.7	66.6	1.7	(Martínez-Narro, Prasertcharoensuk et al. 2022)
	600	35.0	61.7	3.3	
	700	38.3	60.0	1.7	
	800	51.7	46.6	1.7	
PP, PET, PS, LDPE, HDPE	500	5	86	9	(Genuino, Ruiz et al. 2023)
PP, PET, PS, HDPE, PVC	500	41.5	53	5.5	(López, de Marco et al. 2010)
PP, PVC, HDPE, ABS, PS	500	15 - 25	70 – 80	10 – 15	(Chang, Li et al. 2022)
PP, PET, PS, PE, PVC	500	34	65.2	0.8	(Adrados, de Marco et al. 2012)
PP, PET, PS, LDPE, HDPE, PVC	500	9.8	55.1	2.8	(Williams and Williams 1997)
	550	24.5	57.1	5.98	
	600	43.3	43.2	7.6	
	650	88.8	20.5	--	
	700	68.9	18.4	--	
PP, PET, PS, LDPE, HDPE	500	28.6	66.7	4.8	This study
	600	53.2	42.5	4.3	
	700	74.8	20.0	5.2	

5.2.2. Gas composition

The temporal evolution of gaseous products during thermal pyrolysis carried out at 600 °C is presented in Table 5.2 with gas samples collected at 2-minute intervals, corresponding to various reaction temperatures from 380 to 510 °C for off-line GC analysis. Figure 5.2 presents the reaction rate ($d\alpha/dT$) of the plastic mixture in accordance with the previously established kinetic models (Chapter 4) for individual plastic waste utilizing the additive model (Martínez-Narro, Royston et al. 2023). There is a temperature shift of approximately 40 °C between the results presented in Table 5.2 and Figure 5.2 which can be attributed to the transportation time of the products throughout the entire volume of the reactor and the condensing system.

This causes a delay of around 2 min between the exact moment of volatile release in the pyrolysis section, and the collection of gases at the condenser system outlet; however, a similar trend and behaviour can still be appreciated. Therefore, the gas profile discussion is based on the equivalent temperatures dictated by the reaction kinetics in Figure 5.2. The resulting gas profile (Table 5.2) indicates a minor increment in gas production within the initial 4 min of the reaction corresponding to the temperature range of 380 – 420 °C. Subsequently, the reaction rate accelerates at the range of 420 – 460 °C, resulting in an elevated concentration of all gases, excluding butane. A notable decrease in gas production was observed after a reaction temperature of 460 °C, which can be attributed to the sequential decomposition of individual plastics within the mixture. PS and PET are the first to undergo thermal decomposition (peak rate temperatures of 435, and 450 °C, respectively), followed by a transient period during which the majority of these two materials have been decomposed, while the remaining thermally stable plastics, such as polyethylenes, have only commenced decomposition. Consequently, there is a slight reduction in gas yield, which then rapidly escalates at >460 °C, as the overall decomposition approaches its peak rate (490 °C), before gradually decreasing as the reaction proceeds to completion at 510 °C.

Table 5.2. Gas composition profile (wt%) of thermal pyrolysis with the second stage maintained at 600 °C, at 2-minute intervals. Temperatures correspond to the first stage at the time of collection from the condenser outlet.

Temperature	420	460	500	510	510	510	510
CO2	0.038	0.282	0.850	0.497	0.887	0.553	0.283
H2	0.001	0.003	0.011	0.004	0.019	0.014	0.008
CO	0.000	0.147	0.455	0.275	0.548	0.310	0.155
CH4	0.003	0.062	0.361	0.299	0.687	0.453	0.246
Ethane	0.001	0.040	0.332	0.351	0.680	0.431	0.226
Ethylene	0.007	0.088	0.713	0.819	1.611	0.990	0.517
Propane	0.000	0.089	0.119	0.162	0.257	0.152	0.075
Propylene	0.009	0.191	1.293	1.186	2.194	1.467	0.847
Butane	0.002	0.027	0.000	0.403	0.208	0.000	0.035
Butene	0.004	0.115	0.843	0.337	1.127	0.959	0.570
Total	0.066	1.045	4.976	4.333	8.219	5.329	2.963

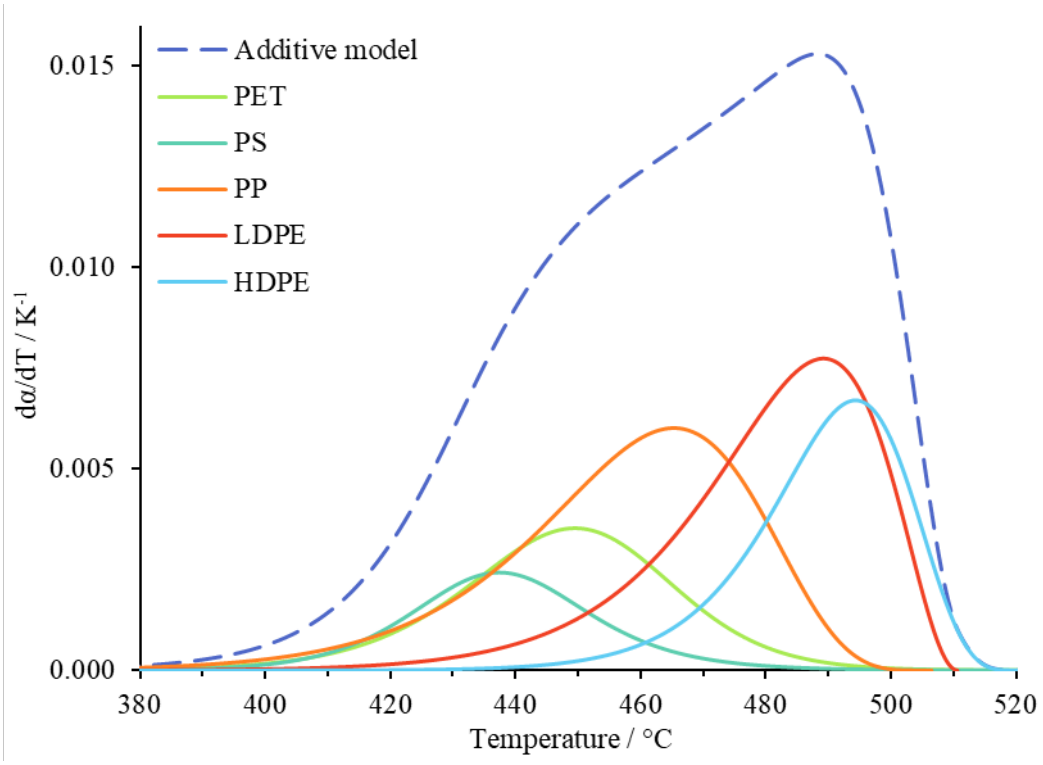

Figure 5.2. Pyrolysis reaction rate of the plastic mixture (dotted line) and individual kinetic contributions of plastic components (continuous lines) according to the additive kinetic model developed in Chapter 3 based on individual plastics.

Results in Table 5.2 indicate that the concentration of paraffins, except methane, is markedly lower than that of olefins. Unsaturated compounds such as ethylene and propylene are produced in greater amounts because most of the plastic mixture components, polypropylene and polyethylenes, undergo random chain scission reactions into their constituent olefinic monomers. In the case of plastic waste pyrolysis, the feedstock typically consists of various polymers containing a high degree of unsaturation, which favours the production of olefins over paraffins during the thermal cracking process (Dai, Zhou et al. 2022). Polyolefins, consisting of polymerized unsaturated molecules, yield unsaturated compounds upon depolymerization.

The total gas composition is shown in Figure 5.3, which primarily consists of C1 – C4 hydrocarbons (71 – 84 wt% with respect to the total gas yields), along with minor quantities (16 – 29 wt%) of H_2, CO, and CO_2. The yields of CO and CO_2 increase at higher temperatures ($\geq$600 °C), which can be attributed to PET decarboxylation reactions within the mixed plastic waste (Du, Valla et al. 2016). Furthermore, at reaction temperatures $\geq$600 °C, CO_2 interacts with plastic volatiles through hydrocarbon dry reforming reactions to produce CO and H_2 (a thorough discussion of these reactions is presented in Chapter 6). Hydrogen was detected across all experimental conditions; however, production remained relatively low compared to

other components, with a maximum yield of only 0.31 wt% at 700 °C. Elevated temperatures during pyrolysis of plastics facilitated the cleavage of C-C bonds at arbitrary positions along the polymer or hydrocarbon chain, with an average paraffinic bond energy of 83 kcal mol^{-1}, through a random chain scission mechanism (Gerö 2004, Martínez-Narro, Prasertcharoensuk et al. 2022). Consequently, as the reaction proceeded, each remaining bond exhibited an equal likelihood of rupture, thereby generating a diverse range of hydrocarbons from C_1 to C_{30+} (Martínez-Narro, Prasertcharoensuk et al. 2022). Concurrently, the cleavage of carbon-hydrogen (C-H) bonds was restricted, with an average paraffinic bond energy of 97 kcal mol^{-1} (Gerö 2004), resulting in a minimal release of H_2.

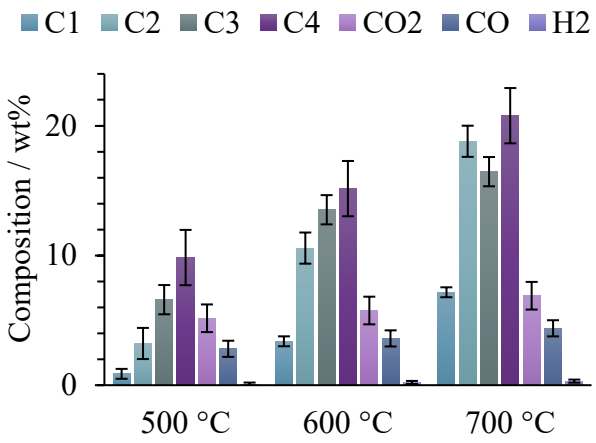

Figure 5.3. Total gas composition of thermal pyrolysis runs at different temperatures.

The yields of methane, ethane, ethylene, propane, and propylene increase significantly with temperature. This indicates that higher temperatures favour the breakdown of larger hydrocarbon molecules in the plastic waste, resulting in higher yields of these light compounds. At 500 and 600 °C, the yield of propane and propylene is higher than those of methane, ethane, and ethylene. However, as the temperature rises to 700 °C, the rate of increase of propane and propylene is less pronounced compared to those of ethane and ethylene since there is a higher conversion of heavier compounds ($\geq$C3) into lighter gaseous molecules (C1 and C2) at these conditions, as evidenced in Figures 5.1 and 5.3.

5.2.3. Oil composition

The liquid products from the thermal pyrolysis of mixed plastic waste (Figure 5.4) were found to consist of a mixture of oil and wax, with their relative proportions varying based on the processing conditions (i.e., 4.6 – 21.5 wt% with respect to the total liquid products). The yellowish and dark colours in the oils produced from the pyrolysis of plastic waste could be attributed to the presence of impurities and additives, which can influence the colour of the

resulting oil. Different types of plastics and the presence of non-plastic materials (e.g., nitrogen, and trace elements not detected in analysis techniques) can contribute to colour variations. Approximately 300 distinct compounds were identified, most of which were present in relatively low concentrations as shown in Figure 5.5.

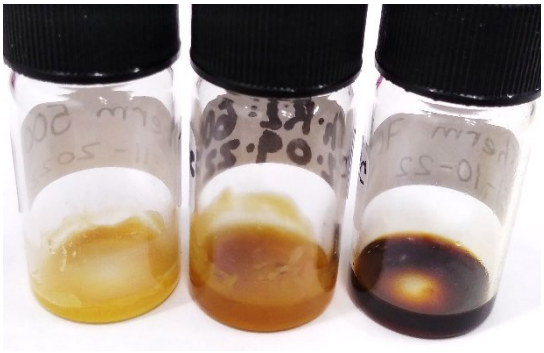

Figure 5.4. Figure 5.4. Oil/wax obtained from thermal pyrolysis runs at 500 °C (left), 600 °C (centre), and 700 °C (right).

For simplicity, hydrocarbons were categorized into three groups <C10 (light), C10-C18 (medium), and >C18(heavy (wax) hydrocarbon) fractions, respectively. The light hydrocarbon fraction, which corresponds to the carbon number range of naphtha (Boeren, van Henegouwen et al. 1985), was predominant under all examined conditions during thermal pyrolysis. As illustrated in Figure 5.6, a reduction in all fractions was observed with increasing temperature, which is attributable to the conversion of these compounds into gaseous hydrocarbons via thermal cracking reactions. The main change in the oil products with operating temperature is the marked decrease in the wax content, significantly decreased as the pyrolysis temperature increased. The wax content relative to the total oil was 21.5 wt% at 500 °C, which decreased to 14.5 wt% at 600 °C. With a subsequent increase to 700 °C, the wax fraction was further reduced to a negligible 4.6 wt%.

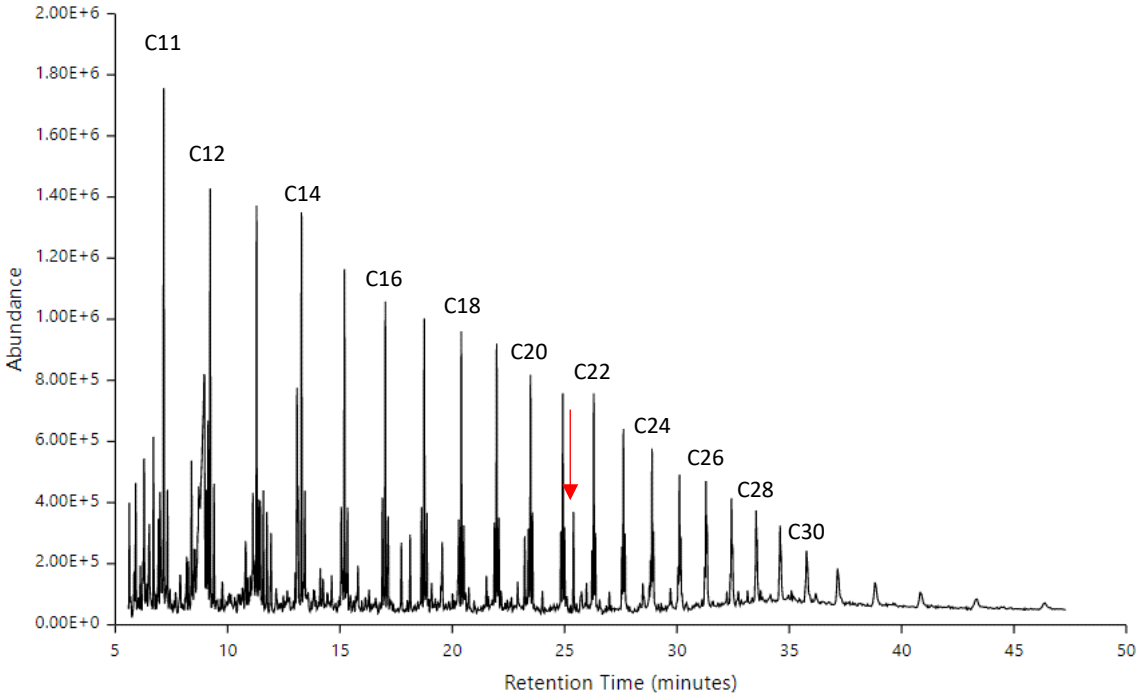

Figure 5.5. GC-MS chromatogram of liquid products from thermal pyrolysis at 600 °C. Red arrow indicates the internal standard (methyl stearate).

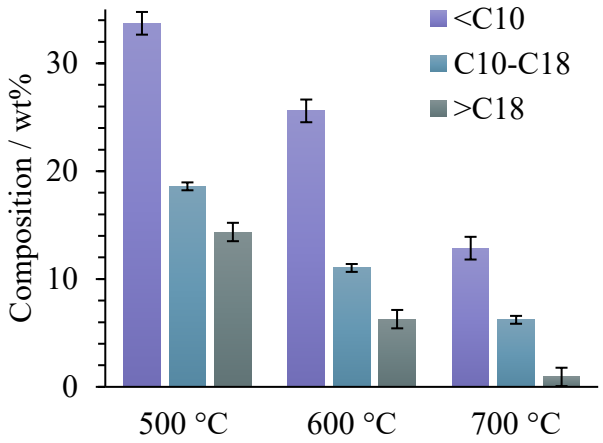

Figure 5.6. Composition of liquid products from thermal pyrolysis at different temperatures.

5.3. Raw biochar

5.3.1. Product yields

The Raw-BC exhibits moderate catalytic effects, with product yields displayed in Figure 5.7. Contrasting with thermal pyrolysis, the Raw-BC catalysed process at 500 °C yields a lower oil/wax output (60 wt% vs. 66.6 wt%) and a higher gas production (35.2 wt% vs. 28.6 wt%). For an industrial-scale pyrolysis process operating at 500 °C, the target product is primarily oil/wax. Hence, producing elevated amounts of gas at the expense of oil might not be beneficial. Upon increasing the temperature to 600 °C, the differences between both processes become negligible. At 700 °C, the gas yield from Raw-BC catalysed pyrolysis

surpasses that of the thermal trial, reaching 77.7 wt% compared to 74.8 wt%. These findings reveal that Raw-BC exerts a catalytic influence on product yields at low and high temperatures, but this effect is inconsequential at 600 °C. This implies that the moderate catalytic effect observed at 500 °C is overshadowed by the temperature effects at 600 °C, leading to equivalent product yields.

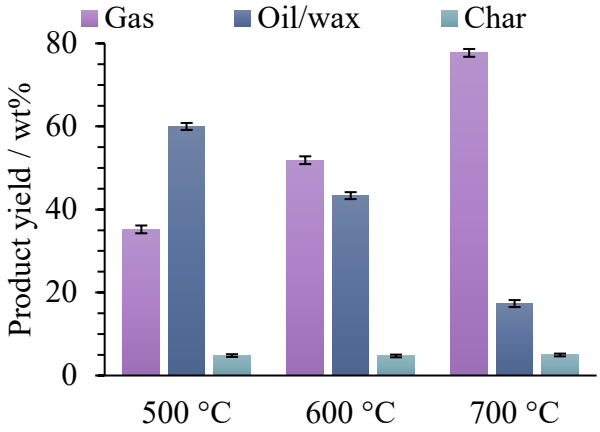

Figure 5.7. Product yields from pyrolysis-catalysis using raw biochar at different temperatures.

These results are in good agreement with those reported by Zhang et al. (Zhang, Duan et al. 2019). The authors used activated carbons and biochar as catalysts for the conversion of LDPE at 500 °C, obtaining oil yields within the range of 61.6 – 73.1 wt%, and gas yields of 24.5 – 30.0 wt%. Li et al. (Li, Zhang et al. 2020) utilised biochar derived from gasification of poplar wood chips as catalyst for the pyrolysis of mixed LDPE and HDPE (50 wt% each), and obtained oil and gas yields of 48.4 wt% and 24.6 wt%, respectively. Compared to the results obtained in this chapter, the liquid and gas yields are significantly lower, which could be explained by the varying reactor configurations and conditions used by different researchers, as discussed in section 5.2.1. Martínez-Narro et al. (Martínez-Narro, Prasertcharoensuk et al. 2022) used wood-derived biochar as catalyst for pyrolysis of mixed plastic waste (10 wt% PS, 13 wt% PET, 20 wt% HDPE, 27 wt% LDPE and 30 wt% PP) at 500 °C and varying catalyst bed temperatures (500 – 700 °C), and observed oil yields of 60 wt% at 500 °C, 47 wt% at 600 °C, and 17 wt% at 700 °C. The gas yields were 36 wt% at 500 °C, 52 wt% at 600 °C, and 82 wt% at 700 °C. The results in this study are comparable, with only minor variations within a ±5 wt% range.

5.3.2. Product composition

The influence of Raw-BC on gas composition at 500 °C, as illustrated in Figure 5.8(a), is evident in the enhanced CO_2 production, yielding 7.38 wt% compared to 5.15 wt% in the non-catalysed

process. This increase may stem from minor oxidation reactions facilitated by the biochar, as a similar marginal increment in this component is observed across all biochar-catalysed runs at low temperature (500 °C). The CO yield also exhibits a minor increase from 2.8 wt% to 3.76 wt%, while the C4 compound yield declines from 9.8 wt% to 6.7 wt%. At 600 °C, the gas composition outcomes correspond with the yield findings, revealing no substantial differences in product formation, except for CO_2, which rises from 5.7 wt% to 7.5 wt%. When the temperature increases to 700 °C, Raw-BC catalysis leads to a slight reduction in ethane and ethylene yields, from 18.8 wt% to 17.6 wt%, with a consequential increase in C4 compounds from 20.8 wt% to 22.3 wt%.

Regarding oil/wax composition (Figure 5.8(b)), all results lie within the experimental error margins; thus, no significant differences in liquid product compositions are discernible between Raw-BC catalysed pyrolysis and thermal pyrolysis across the investigated temperature range.

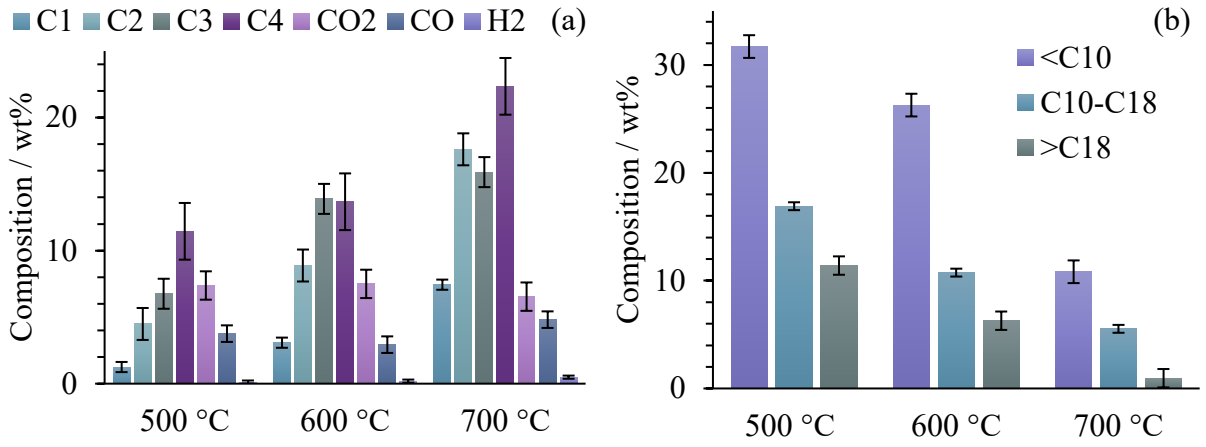

Figure 5.8. Gas (a) and oil/wax (b) composition from pyrolysis-catalysis using raw biochar at different temperatures.

5.4. Nickel-doped biochar

Nickel is considered a suitable catalyst for enhancing the cracking of plastic waste volatiles due to its excellent catalytic activity (Yoshioka, Handa et al. 2005, Liu, Zhang et al. 2017). The cleavage of C-C bonds is enhanced by the catalytic properties of nickel, which promote the decomposition of long-chain hydrocarbons and provide high selectivity for hydrogen and carbon nanotubes formation (Zhang, Nahil et al. 2017). During the transfer of plastic waste volatile hydrocarbons from the pyrolysis stage of the reactor to the catalytic stage, they encounter nickel particles dispersed on the biochar support. Nickel particles act as active sites for catalytic reactions, while the highly porous structure of biochar offers a substantial surface

area for particle deposition, fostering interaction with hydrocarbons. Nickel catalysts facilitate the cracking process by providing an active surface for the adsorption and subsequent dissociation of hydrocarbon molecules (Freel and Galwey 1968). Throughout the catalysis process, volatile hydrocarbons undergo dissociative chemisorption on the nickel surface, promoting the dissociation of hydrocarbons into adsorbed reactive species (e.g., methyl and methylene radicals) which can then participate in subsequent reactions (McKee 1962). The presence of the nickel catalyst enhances C-C bond cleavage, enabling the conversion of long-chain hydrocarbons into lighter molecules. This transformation involves the rearrangement of carbon atoms on the nickel particle surface, yielding gaseous products such as methane, ethane, ethylene, and hydrogen.

5.4.1. Product yields

The production of gaseous and oil/wax compounds (Figure 5.9) demonstrates a similar pattern in response to increasing temperatures as the thermal pyrolysis process.

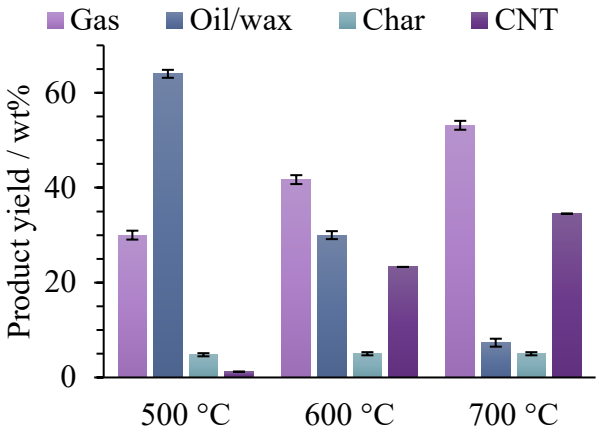

Figure 5.9. Product yields from pyrolysis-catalysis using nickel-doped biochar at different temperatures.

Nonetheless, at 600 °C, the gas yield was lower than that obtained from the thermal experiments (41.7 wt% compared to 52.8 wt%). The oil yield was also decreased (with 30 wt% in contrast to 42.5 wt% during thermal pyrolysis). This phenomenon can be attributed to the generation of carbon nanotubes (CNT) on the catalyst surface, as their formation occurs at the expense of gaseous and liquid byproducts. Figure 5.10 presents a comparison of the Ni-BC catalyst surface before and after pyrolysis at 600 °C, confirming the formation of carbon nanotubes.

The diameters of the CNTs are approximately 30 nm. As illustrated in Figure 5.9, temperatures exceeding 600 °C promote CNT formation. The nickel particles in the doped biochar serve as

catalysts for CNT growth by promoting the breakdown of hydrocarbon molecules and enabling the rearrangement of carbon atoms into a filamentous nanotube configuration (Yang, Chuang et al. 2015). Being a transition metal, nickel promotes the cleavage of C-H bonds (Bergman 2007) which can result in subsequent reactions such as functionalisation, rearrangement, or coupling reactions. The elevated formation of carbon nanotubes promoted by Ni-BC could be explained by the enhanced C-H cleavage which leads to coupling reactions in which new C-C bonds are formed and rearranged into CNTs. The CNT yield increased from a negligible 1.2 wt% to 23.3 wt% upon increasing the temperature from 500 to 600 °C and continued to rise to 34.5 wt% at 700 °C.

This indicates that the catalyst's efficiency is enhanced at elevated temperatures, resulting in a higher CNT yield. At 700 °C, CNT synthesis predominantly occurs from the liquid portion of the products, as evidenced by the high gas production of 53.2 wt% and the significantly reduced oil production of 7.3 wt%. In contrast, without a catalyst present, the oil production at 700 °C reaches up to 20 wt%.

In large-scale industrial settings, the emergence of CNTs on the surface of a catalyst during the pyrolysis reaction presents a dual-sided scenario. On one hand, this phenomenon can be beneficial or desirable, particularly when the production of CNTs is the intended objective of the process. These nanotubes are valued for their unique properties and wide range of applications in various fields (Gupta, Gupta et al. 2019). On the other hand, the formation of CNTs can be an undesirable or detrimental outcome if they are not the targeted product. In such cases, their presence may lead to complications, as they could potentially contaminate or deactivate the catalyst (Acomb, Wu et al. 2014, Zhou, Saad et al. 2020). Therefore, their formation is a critical factor that needs to be controlled and managed based on the specific goals and requirements of the industrial pyrolysis process.

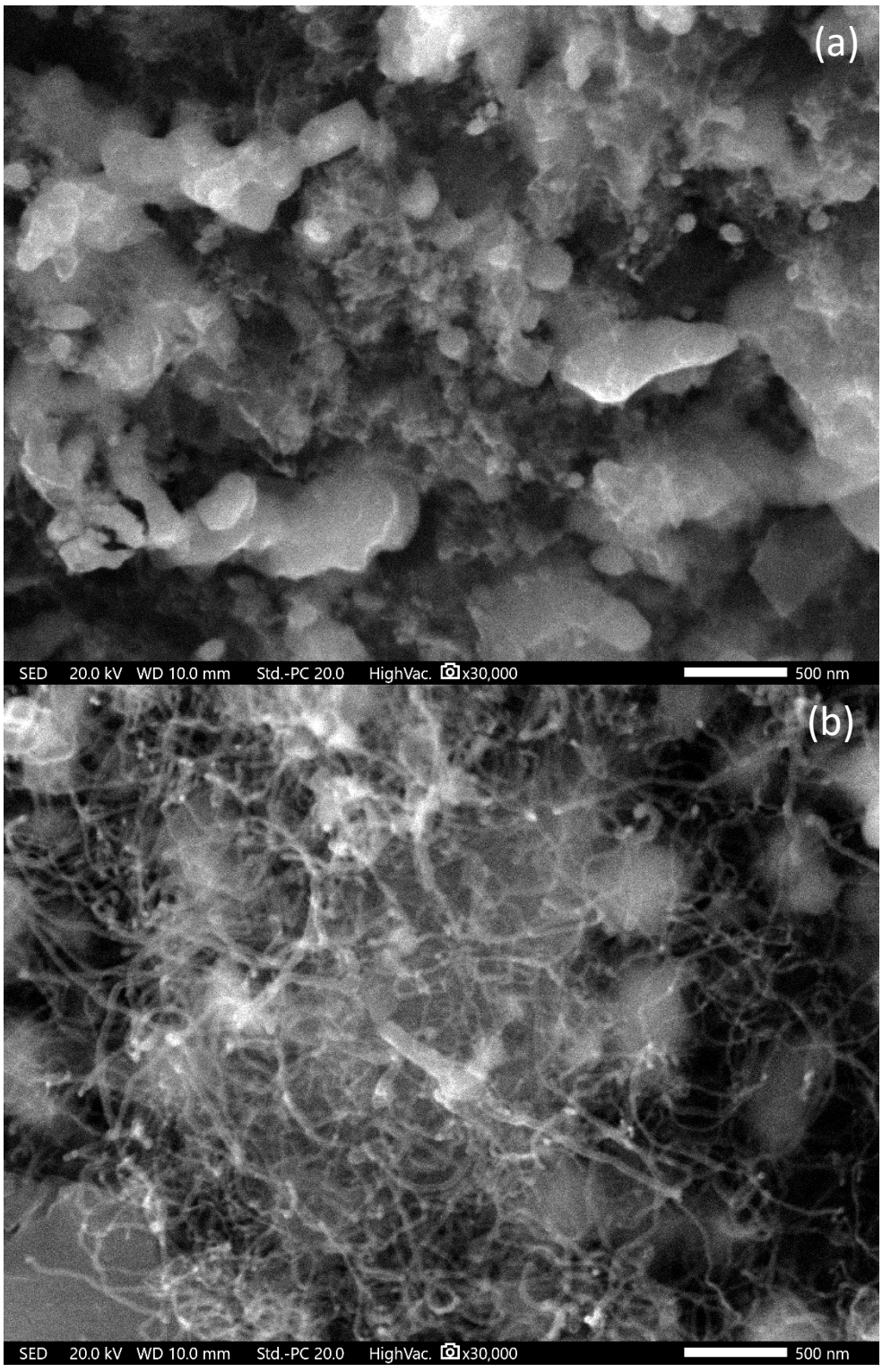

Figure 5.10. Comparison of fresh (a) and spent (b) Ni-BC showing the morphology of the synthesized carbon nanotubes.

The synthesis of CNTs for commercial applications can involve different methods. Techniques like arc discharge synthesis, laser ablation, and chemical vapour deposition (CVD), which use transition metals as catalysts (Rouf, Usman et al. 2021). The techniques for purifying carbon nanotubes differ according to their synthesis method and type. Common steps in these methods often involve filtering to eliminate larger graphite particles, employing solvents to

dissolve and remove particles from catalysts, and utilizing microfiltration along with chromatography to achieve separation based on size and to extract clusters of amorphous carbon (Brhane and Gabriel 2016). The purification process typically incorporates both chemical and physical approaches.

The separation, purification, and classification of CNTs was out of the scope of this chapter and was not conducted. However, this opens up a potential avenue for future research on the application and usefulness of CNTs derived specifically from plastic waste, a process which is currently not commercially available.

5.4.2. Product composition

The production of methane demonstrates a consistent positive correlation with temperature (depicted in Figure 5.11(a)), exhibiting a significant increase when the temperature is elevated from 600 to 700 °C, resulting in the yield more than doubling from 3.3 wt% to 7.6 wt%. The yield of C2 compounds, such as ethane and ethylene, follows a comparable trend, while maintaining consistent proportions relative to one another. Conversely, the production of C3 compounds, including propane and propylene, remains stable across the entire temperature range examined. These observations imply that the primary thermal cracking of long-chain hydrocarbons leads to an enhanced generation of lighter molecules such as methane, ethane, and ethylene compared to propane and propylene. The production of C1 and C2 compounds may also be favoured due to secondary dehydrogenation reactions facilitated by the Ni-BC catalyst in conjunction with the temperature conditions. As a result, it can be inferred that the Ni-BC catalyst exhibits high selectivity for C1 and C2 compounds over C3. A similar conclusion can be drawn for C4 compounds, which display a similar variability as C3 compounds. The marginally higher yield at 700 °C can be attributed to the increase in the overall gas yield. The yield of CO_2 exhibits minor fluctuations within the range of 3.3 wt% to 6.2 wt%. Conversely, CO production demonstrates a consistent increase, nearly doubling for each 100 °C temperature increment. Specifically, CO yield increased from 3.5 wt% to 6 wt% as temperature rose from 500 to 600 °C, and further augmented to 9 wt% at 700 °C. This behaviour can be attributed to the catalytic influence of nickel particles, which promote Boudouard and hydrocarbon reforming reactions at elevated temperatures (>600 °C) (Saad and Williams 2017). The Boudouard reaction generates CO through the combination of carbon and CO_2, while the reforming reaction transforms CO_2 and hydrocarbons into CO and H_2. These mechanisms also adduce the enhanced production of hydrogen, which markedly increases

from 0.5 wt% to 3.2 wt% upon increasing the temperature from 500 to 600 °C, and subsequently to 4.2 wt% at 700 °C. Although the hydrogen yield may appear comparatively low, the volume percentage of hydrogen in the gaseous product mixture at 600 and 700 °C constitutes 62.1 and 57.7 vol%, respectively. It is important to note that these reactions are not prominent at 500 °C, meaning that temperatures of around 600 °C or higher are required to optimise hydrogen and carbon monoxide production. The mixture of these gases, referred to as synthesis gas or syngas, is an important commercial product due to its role as a precursor for numerous industrial chemicals (e.g., alcohols, olefins, and ammonia) through advanced chemical manufacturing processes such as the Fischer-Tropsch synthesis (Pawelczyk, Wysocka et al. 2022).

As in the case of non-catalytic experiments, a consistent decrease in oil/wax yields is observed, maintaining relatively stable proportions among the three liquid hydrocarbon fractions, as illustrated in Figure 5.11(b). Nevertheless, a significant reduction in the light fraction (<C10) occurs at 700 °C. The relative proportion of light oil exhibits a minor increase from 50.3% at 500 °C to 59.5% at 600 °C, followed by a drastic decline to 38.5% at 700 °C. This indicates that at elevated temperatures (≥700 °C), the products favoured by the Ni-BC catalyst, such as CO, H_2, and CNTs, are predominantly generated at the expense of the light oil fraction.

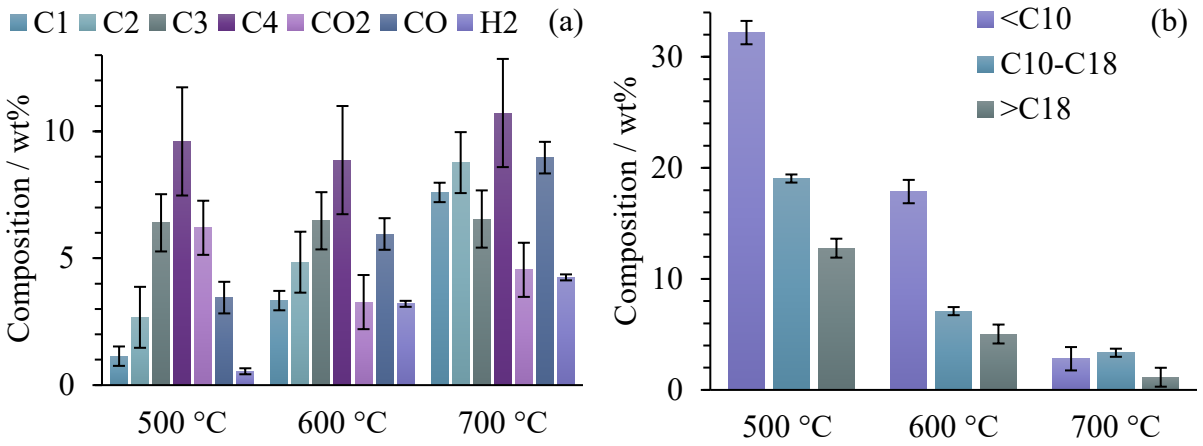

Figure 5.11. Gas (a) and oil/wax (b) composition from catalytic pyrolysis using nickel-doped biochar held at various temperatures.

5.5. Iron-doped biochar

5.5.1. Product yields

Iron-based catalysts provide the potential to improve product distribution by influencing the selectivity of pyrolysis reactions. This can result in higher yields of valuable chemicals and fuels, such as hydrogen, syngas, and carbon nanotubes (Shen, Zhao et al. 2022). The active

sites of iron catalysts promote the cleavage of carbon-carbon (C-C) and carbon-hydrogen (C-H) bonds in the complex long-chain plastic molecules, which facilitates their conversion into smaller, high-value products (He, Maurice et al. 2011). The product yields from catalytic pyrolysis using Fe-BC are presented in Figure 5.12. The yield of oil/wax is consistently reduced as the temperature increases, a behaviour extensively discussed in preceding sections. This reduction is attributed to enhanced thermal cracking, which converts liquid hydrocarbon volatiles into smaller gaseous moieties. Consequently, the gas yield demonstrates an inverse trend. When comparing the outcomes of the non-catalytic runs to those employing Fe-BC, the oil/wax yields at 500 °C are slightly lower (60 wt% vs. 66.6 wt%), while the gas yield is higher by a similar magnitude (28.6 wt% vs. 35.1 wt%). However, at 600 °C, the oil/wax yields remain practically unchanged, but the gas yield declines to 45.7 wt% in the presence of Fe-BC compared to 52.8 wt% in non-catalytic runs. Under these conditions, the CNT yield experiences a substantial increase (from 0.1 wt% at 500 °C to 7.9 wt% at 600 °C), suggesting that CNT formation at 600 °C primarily occurs at the expense of gaseous compounds. This behaviour becomes more pronounced at 700 °C, with both liquid and gas yields decreasing by approximately 6 wt% compared to non-catalytic runs.

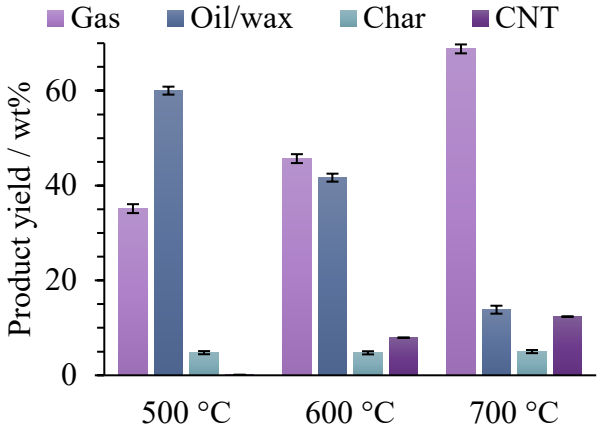

Figure 5.12. Product yields from pyrolysis-catalysis using iron-doped biochar at different temperatures.

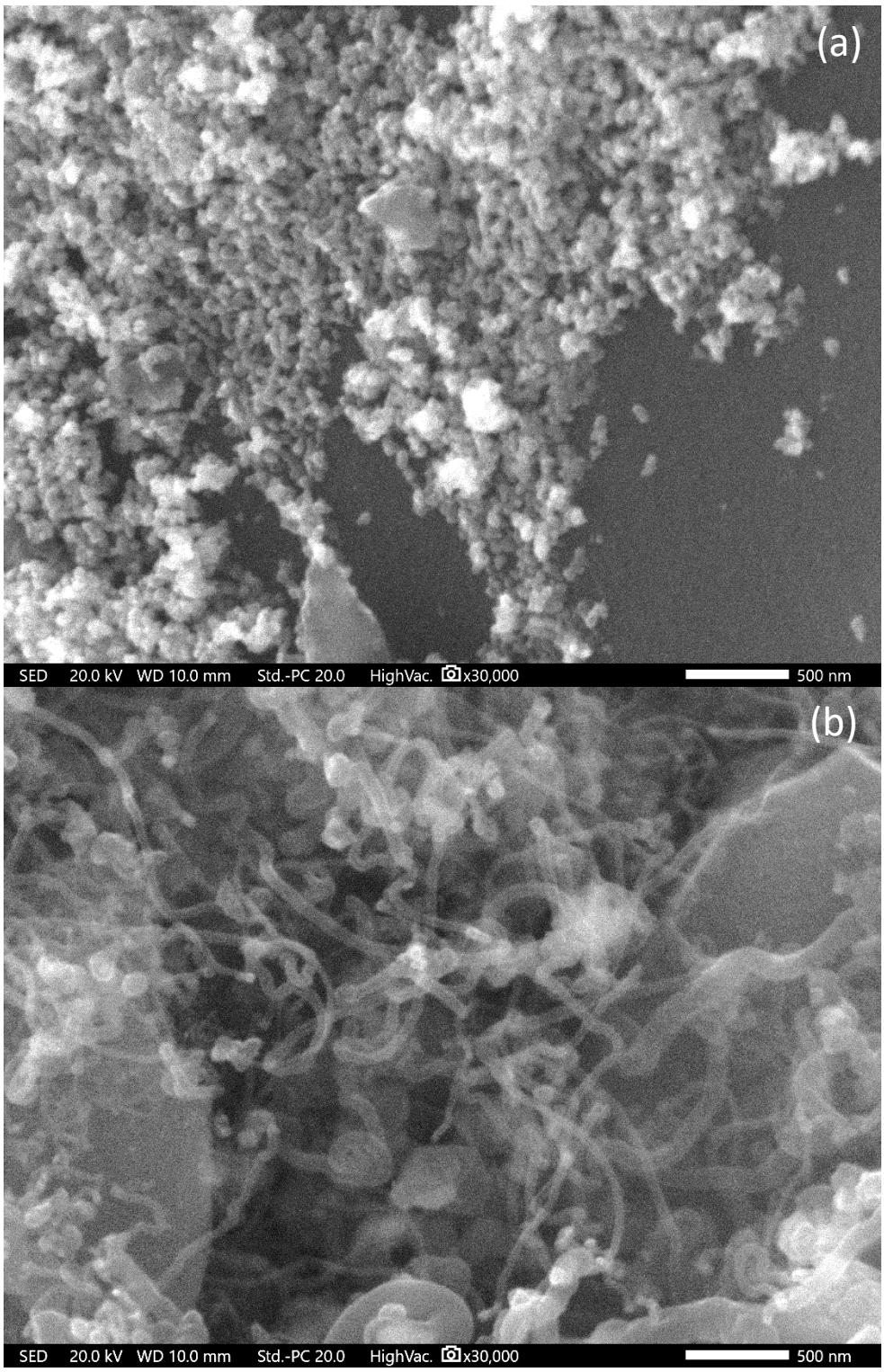

Figure 5.13. Comparison of fresh (a) and spent (b) Fe-BC, showing the morphology of the synthesized carbon nanotubes.

The lower gas yields, particularly at elevated temperatures, can be explained by the shift in product distribution towards CNTs, as more carbon is consumed from the plastic volatiles for the growth of CNTs instead of forming gaseous hydrocarbons. The yield of carbon nanotubes is negligible at 500 °C; however, as the temperature rises to 600 and 700 °C, the CNT formation increases to 7.93 wt% and 12.37 wt%, respectively. The underlying mechanism that explains

this trend can be ascribed to the catalytic role of the iron particles in the biochar, which promotes the development of filamentous carbon structures. In addition, at higher temperatures, plastic waste volatiles decompose more rapidly, providing an increased supply of carbon for the synthesis of CNTs. Figure 5.13 shows a comparison of the Fe-BC catalyst surface before and after pyrolysis, illustrating the formation of carbon nanotubes, which have a diameter of approximately 60 nm.

5.5.2. Product composition

The elevated production of CO_2 at 500 °C (illustrated in Figure 5.14(a)) may be ascribed to a minimal extent of carbon oxidation within the biochar. This is corroborated by the marginally increased yields of CO_2 (1.7 wt% on average) observed in the biochar-catalysed experiments compared to their thermal counterparts. However, with rising temperatures and considering the restricted oxygen presence in the plastic sample, the formation of CO_2 gradually shifts toward CO. The CO yield notably escalates at higher temperatures, with 3 wt% at 500 °C, 6.1 wt% at 600 °C, and 10.8 wt% at 700 °C. This occurrence can be elucidated by the catalytic influence of iron particles, which facilitate hydrocarbon reforming reactions, yielding CO and H_2. Consequently, the H_2 production is significantly augmented at elevated temperatures (0.28 wt% at 500 °C, 1.32 wt% at 600 °C, and 1.97 wt% at 700 °C). The substantial hydrogen release is directly correlated with the formation of carbon nanotubes on the catalyst surface, as the cleavage of C-H bonds is intensified by the Fe-BC catalyst and a substantial supply of carbon atoms becomes accessible for CNT synthesis.

The yields of C1-C4 gases exhibit a similar persistent positive correlation with temperature, as observed in prior experiments. As the temperature ascends from 500 to 600 °C, their relative rates of increase are analogous; however, upon further elevation to 700 °C, ethane and ethylene production surpasses that of other hydrocarbon gases. This implies that the catalytic cracking of high molecular weight hydrocarbons in the presence of Fe-BC at 700 °C is intensified, and the catalyst exhibits heightened selectivity toward C2 compounds, of which the majority (73%) is ethylene. The formation of light paraffins and olefins is favoured due to the additional hydrogenation reactions and C-H bond cleavage facilitated by the catalyst.

The high yield of the light oil fraction at 600 °C (Figure 5.14(b)) supports previous assertions that CNT formation predominantly arises from the gaseous products. Conversely, at 700 °C, a substantial decline in the light oil fraction (<C10) is detected, indicating a higher catalytic selectivity for H_2, CO, light hydrocarbon gases, and CNT formation over light oil products.

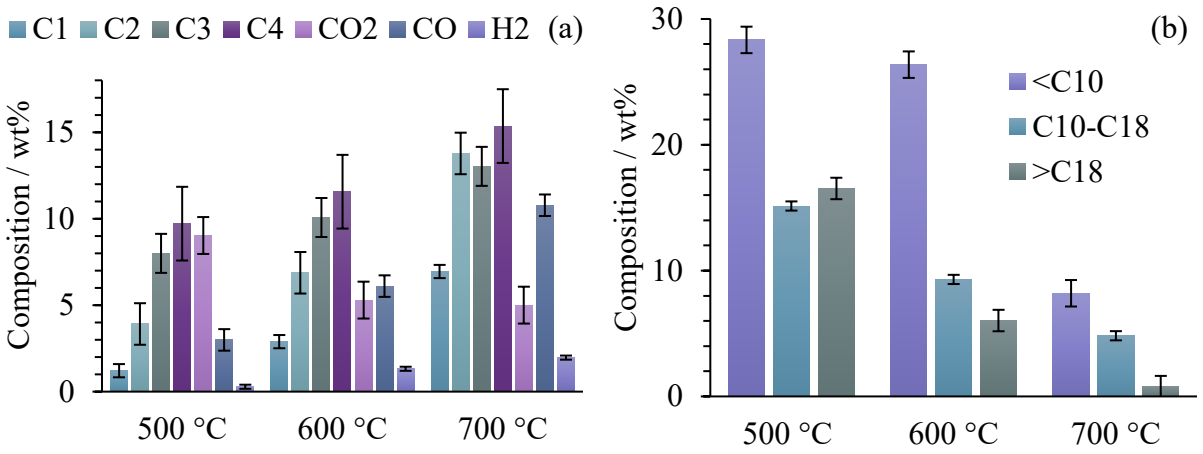

Figure 5.14. Gas (a) and oil/wax (b) composition from pyrolysis-catalysis using iron-doped biochar at different temperatures.

5.6. Zinc-doped biochar

5.6.1. Product yields

The product yields from Zn-BC catalysed pyrolysis (Figure 5.15) demonstrate a resemblance to those obtained from thermal pyrolysis. At a temperature of 500 °C, the oil/wax yield attains 63.3 wt%, while the yield for thermal pyrolysis is marginally higher at 66.6 wt%. Concurrently, the gas yield is 31.9 wt% for the catalysed process, compared to a slightly lower yield of 28.6 wt% for the thermal pyrolysis. Upon raising the temperature to 600 °C, the discrepancies in oil/wax and gas yields between the catalysed and thermal processes become statistically insignificant, suggesting minimal variations between the two methods. At 700 °C, the Zn-BC catalysed pyrolysis produces an oil/wax yield of 23.3 wt%, which is 16.65 % higher than the thermal counterpart. The corresponding Zn-BC gas yield, however, is 71.5 wt%, constituting a 4 % decrease compared to the thermal trials. Overall, the Zn-BC catalyst exhibits a subtle inclination towards gas yield at 500 °C, an inconsequential effect at 600 °C, and a slight preference for oil/wax formation over gaseous products at 700 °C. Nonetheless, the distinctions between the catalysed and thermal processes remain relatively mild, and the catalytic activity of Zn particles on biochar is significantly lower than that of previously investigated nickel and iron-based catalysts.

Carbon deposition on the catalyst surface was found to be negligible (0.3 – 0.7 wt%), and as a result, these findings were omitted from the graphical representations. This observation highlights that zinc particles do not facilitate the growth of carbon nanotubes.

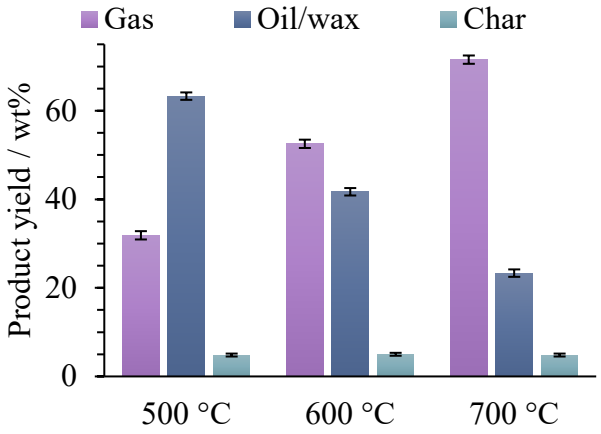

Figure 5.15. Product yields from pyrolysis-catalysis using zinc-doped biochar at different temperatures.

5.6.2. Product composition

The compositions of gas and oil/wax products from Zn-BC catalysed pyrolysis are illustrated in Figure 5.16. The most notable variation in gas compositions lies in the CO_2 yield at lower temperatures (<700 °C), where the presence of the Zn-BC catalyst leads to an increase compared to the thermal pyrolysis trials. At 500 °C, the CO_2 production for the catalysed process is 6.6 wt%, whereas the thermal process produces 5.1 wt%. This difference persists at 600 °C, with the catalysed CO_2 yield at 7.6 wt% and the thermal yield at 5.7 wt%. However, the CO_2 yields for both processes converge at 700 °C. At this elevated temperature, the H_2 generation for the catalysed process is 0.53 wt%, slightly higher than the 0.31 wt% observed in the thermal process. The remaining gas components exhibit negligible differences at corresponding temperatures in comparison to the thermal pyrolysis, as they fall within the respective experimental error margins.

As shown in Figure 5.16(b), the most pronounced difference in the oil/wax composition at 500 °C involves the medium oil fraction, which is marginally lower in the Zn-BC catalysed process compared to the thermal process (16.2 wt% vs. 18.6 wt%). This indicates that the reduction in the medium oil fraction primarily contributes to the overall decrease in liquid product yield observed in Figure 5.15, as some of this fraction is converted into gaseous products, consequently resulting in a modest increase of the gas yield. At 600 °C, no statistically significant disparities in oil/wax composition are detected between the catalysed and uncatalyzed experiments, which is consistent with the negligible differences observed in product yields at this temperature. However, upon increasing the temperature to 700 °C, the

light oil fraction exhibits a higher value (15.9 wt% vs. 12.86 wt%), accounting for the higher oil/wax yield and lower gas yield at this elevated temperature.

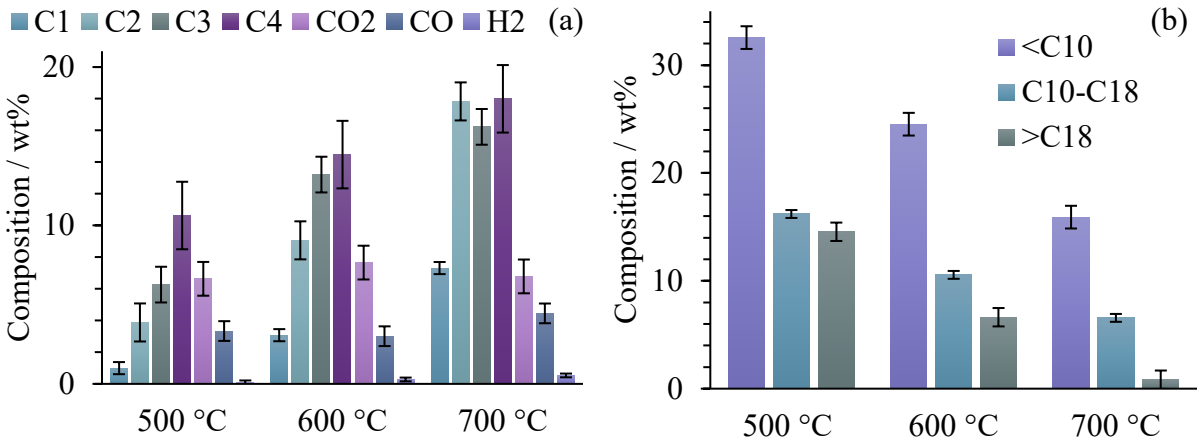

Figure 5.16. Figure 5.16. Gas (a) and oil/wax (b) composition from pyrolysis-catalysis using zinc-doped biochar at different temperatures.

5.7. Zeolite HZSM-5

5.7.1. Product yields

The use of HZSM-5 zeolite as a catalyst demonstrates a significant impact on the product yield distribution, favouring the production of lighter gaseous compounds, as shown in Figure 5.17. When comparing the catalytic process to non-catalytic pyrolysis at 500 °C, the HZSM-5 zeolite promotes a notable decrease in the oil/wax yield from 66.6 wt% to 46.7 wt%, alongside a concurrent increase in the gas yield from 28.6 wt% to 48.4 wt%. The observed outcomes demonstrate the effectiveness of the HZSM-5 zeolite in cleaving long-chain hydrocarbons present in plastic waste volatiles into lighter gaseous compounds at moderately low temperatures. This behaviour can be attributed to the distinct physicochemical characteristics of the HZSM-5 zeolite, which exhibits pronounced acidity and high shape selectivity (Feng, Zhou et al. 2022). The acidic sites of the zeolite facilitate the scission of C-C bonds within long-chain hydrocarbon molecules, whereas its well-organized pore structure promotes diffusion and enables the selective conversion of specific hydrocarbons (Trombetta, Alejandre et al. 2000, Le Minh, Alanazi et al. 2012). At 600 °C, the differences between the catalysed and non-catalysed processes become slightly less evident; however, the influence of HZSM-5 zeolite on product yields remains discernible. The oil/wax yield experiences a reduction from 42.5 wt% to 37.2 wt%, while the corresponding gas yield exhibits an increase from 52.8 wt% to 57.9 wt%. Upon further increasing the temperature to 700 °C, HZSM-5 catalysis leads to an additional decrease in oil/wax yield, reaching 16.6 wt%, and an increase in gas yield to 78 wt%.

These findings demonstrate that the HZSM-5 catalyst exerts a substantial impact on the distribution of product yields.

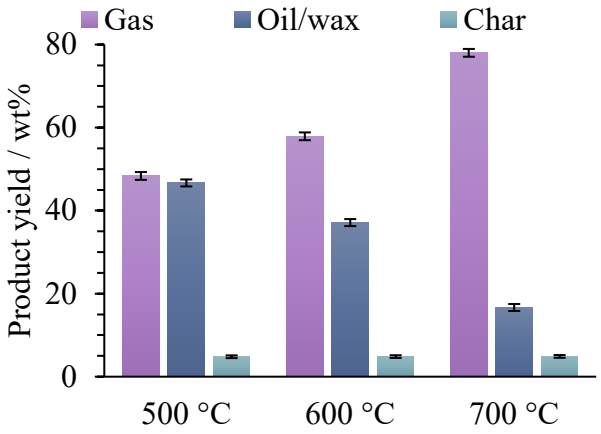

Figure 5.17. Product yields from pyrolysis-catalysis using zeolite HZSM-5 at different temperatures.

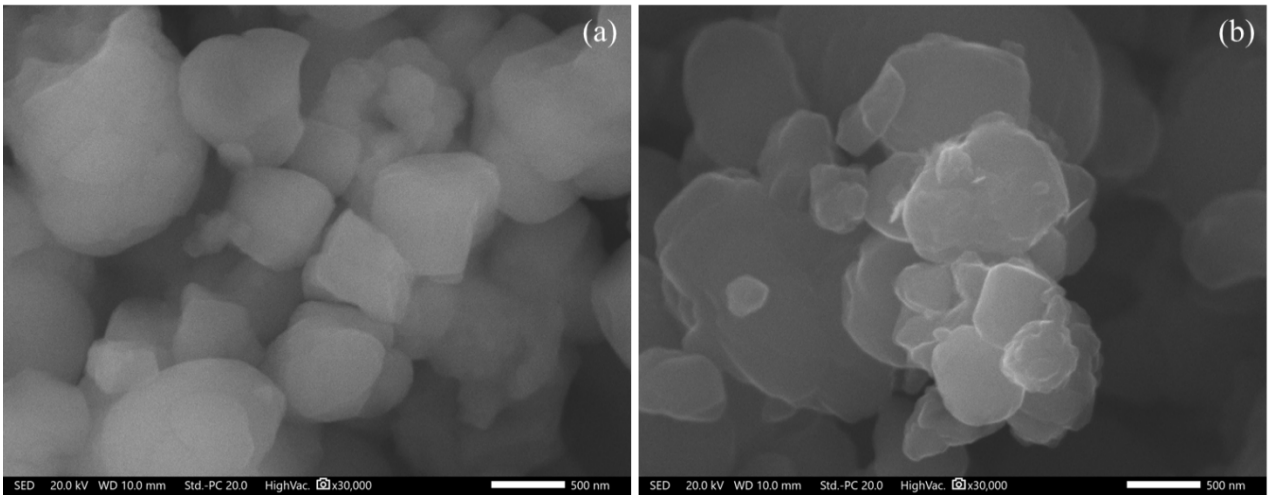

Figure 5.18. Scanning electron microscopy images of HZSM-5 zeolite before (a) and after (b) pyrolysis at 600 °C.

The observed carbon accumulation on the catalyst was minimal (<0.5 wt%), demonstrating the efficacy of the two-stage reactor design in averting catalyst deactivation due to excessive carbon deposition, which can result in pore obstruction. Figure 5.18 presents the surface morphology of HZSM-5 zeolite prior to and following the catalytic pyrolysis process at 600 °C, captured at a magnification of 30,000x. Notably, no substantial alterations to the surface characteristics are discernible.

5.7.2. Product composition

Although the differences in liquid and gaseous product yields (catalytic vs. thermal pyrolysis) are less pronounced at high temperatures (>600 °C), with differences of approximately ± 5 wt%, the product quality is significantly enhanced, favouring lighter compounds over heavier

ones. The gas product composition depicted in Figure 5.19(a) demonstrates that at 500 °C, HZSM-5 zeolite significantly enhances propane and propylene yields from 6.6 wt% to 18.4 wt% (of which 78.3% is propylene). Furthermore, C4 gas production notably increases from 9.8 wt% to 18.4 wt%, ethane and ethylene production slightly rises from 3.2 wt% to 5.1 wt%, and CO yield moderately decreases from 2.8 wt% to 1.8 wt%. These outcomes suggest that the primary product resulting from the excess conversion of volatiles into gases at low temperature is predominantly propylene, a valuable monomer in the chemical manufacturing industry. As the temperature increases to 600 °C, the only significant difference is observed in the C3 compounds, with propane and propylene production escalating from 13.5 wt% to 19.5 wt% (of which 91.2% is propylene), and the remaining products staying within the experimental error. This observation corresponds with the approximately 5.5 wt% gas yield increase at this temperature, indicating that HZSM-5 zeolite selectively converts liquid products into propane and propylene specifically. Additionally, these outcomes are consistent with findings reported in the literature, where high conversion of plastic waste volatiles into propylene has been achieved using zeolite HZSM-5 catalyst. (Arabiourrutia, Olazar et al. 2008, Ratnasari, Nahil et al. 2017, Wong, Armenise et al. 2023). At the highest temperature of 700 °C, H_2 production doubles to 0.64 wt%, CO and methane yields moderately rise from 4.4 wt% to 6.4 wt% and from 7.1 wt% to 8.3 wt%, respectively. Owing to enhanced thermal cracking, C4 compound production declines from 20.8 wt% to 15.5 wt%, while C2 compound yield increases from 18.8 wt% to 21.5 wt%. Since the C3 yield remains virtually identical to that of the non-catalysed experiments, this could indicate a shift in HZSM-5 zeolite selectivity towards ethylene.

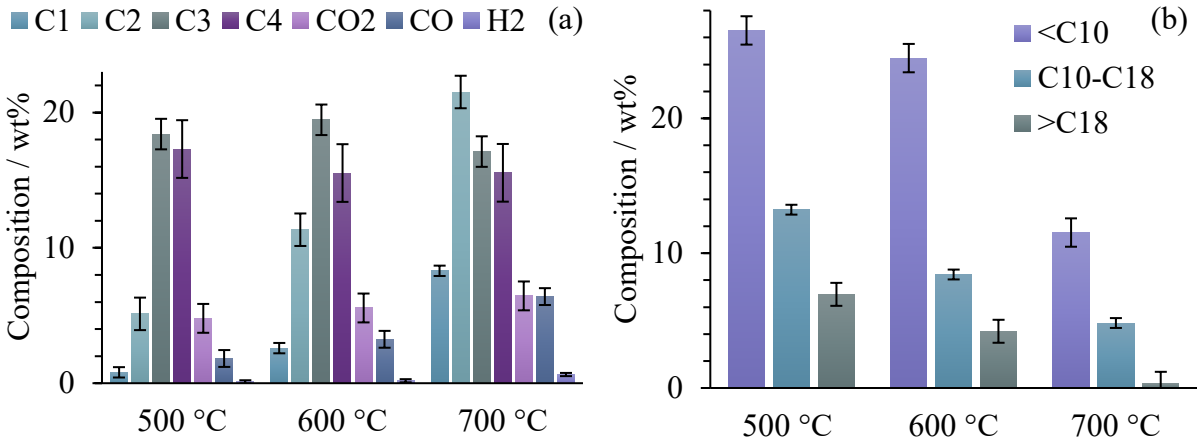

Figure 5.19. Gas (a) and oil/wax (b) composition from pyrolysis-catalysis using zeolite HZSM-5 at different temperatures.

The liquid product composition is significantly influenced by the HZSM-5 catalyst, as illustrated in Figure 5.19(b). All oil/wax fraction yields at 500 °C are lower than those observed in thermal pyrolysis. Thus, evaluating the relative content changes of each fraction in the corresponding total yield provides a more accurate understanding of the liquid product quality. At 500 °C, the light oil content in liquid products increases from 50.6% to 56.8% in the presence of HZSM-5 zeolite, while the medium fraction remains relatively constant (around 28%), and the heavy wax decreases from 21.5% to 14.9%. At 600 °C, no significant differences are observed in light oil yields, which are approximately 25 wt%. However, the medium fraction decreases from 11 wt% to 8.4 wt%, and the heavy wax decreases from 6.3 wt% to 4.2 wt%. This indicates that the relative amount of light oil in the HZSM-5 catalysed liquid products is 65.8% compared to 60.2% without a catalyst. At 700 °C, the relative amount of light oil in liquid products increases from 64.3% to 69.1%, while the medium fraction and heavy wax decrease from 31.1% to 28.9%, and 4.6% to 2.1%, respectively. The HZSM-5 catalysed pyrolysis yields a higher proportion of light oil and a lower proportion of heavy wax at all three temperatures compared to thermal pyrolysis, with the medium fraction also tending to be slightly lower in the catalysed process. The gas and liquid product compositions support the notion that HZSM-5 zeolite enhances the production of light molecules at the expense of heavier ones. This is achieved through a series of complex reactions, including cracking, cyclization, and isomerization, occurring at the zeolite's active sites (Miandad, Rehan et al. 2019). As a result, the overall yield of heavy wax is substantially reduced, demonstrating the effectiveness of HZSM-5 zeolite in cracking long-chain hydrocarbons, particularly at relatively low temperatures during plastic waste pyrolysis.

5.8. Catalyst performance comparison

Results for product yield distribution and compositions at different temperatures are summarised in Tables 5.3 – 5.5. A higher catalytic activity is observed for Ni-BC, Fe-BC, and HZSM-5 in comparison to Zn-BC and Raw biochar. The influences of Ni-BC and Fe-BC catalysts on the process display analogous patterns, with the production of H_2, CO, and CNTs (exclusively identified with Ni-BC and Fe-BC) rising as the temperature increases. Regarding product yields, the process is similar for both catalysts at 500 °C; however, as the temperature increases, the yields of gaseous and liquid products catalysed by Ni-BC progressively decrease, concomitant with an escalation in CNT production. With the notable exceptions of H_2 and CO, the yields of all other individual gaseous compounds are higher for the case of Fe-BC catalysed

pyrolysis, owing to the overall higher yield of gas. An intensified formation of CNTs is attained using the Ni-BC catalyst compared to those obtained with Fe-BC (1.2 wt% vs. 0.1 wt% at 500 °C, 23.3 wt% vs. 7.9 wt% at 600 °C, and 34.5 wt% vs. 12.4 wt%). Consequently, it can be inferred that Ni-BC is more effective at producing CNTs (and the associated increase in H_2 yields), but less effective at generating high yields of gas. This finding contrasts with other studies in the literature. For instance, Liu et al. (Liu, Aziz et al. 2013) compared the effects of iron, nickel, and cobalt on metal oxide supports as catalysts for CNT synthesis from methane at 900 °C, concluding that iron produces higher quality CNTs. This was attributed to iron's high carbon solubility, which impacts CNT nucleation and growth through various mechanisms, such as: (i) enhancing carbon supply for CNT development; (ii) generating a higher concentration force to expedite CNT formation; (iii) influencing CNT cap structure nucleation; and (iv) dictating the specific CNT variety produced (MacKenzie, Dunens et al. 2010, Liu, Aziz et al. 2013). Acomb et al. (Acomb, Wu et al. 2016) compared the effects of several metals on CNT formation from plastic waste at 800 °C, and also found iron to be more effective (i.e., higher yields) than nickel. The higher carbon solubility of iron compared to that of nickel was determined to be responsible for the higher CNT yields. Moreover, the interactions between the metal and the catalyst support were found to play a crucial role in CNT formation, with excessively strong interactions inhibiting production and weak interactions leading to metal sintering and low yields (Acomb, Wu et al. 2016). These phenomena might explain the lower CNT yields achieved using Fe-BC in this study, as the support is not a metal oxide but a carbon-based material. Since iron has a higher carbon solubility than nickel, there may be a stronger interaction between the biochar support and iron particles, thus hindering CNT formation. Nonetheless, this interaction is not excessively strong, as Fe-BC still allows some CNT formation, albeit in lower amounts than those obtained using Ni-BC. It can be concluded that nickel and iron particles exhibit an intermediate interaction with the biochar, enabling carbon nanotube formation. These results demonstrate that biochar is a suitable support for nickel and iron catalysts in facilitating plastic waste pyrolysis.

Utilizing Zn-BC and Raw-BC catalysts results in a marginal decrease in liquid product yields and a slight increase in gas yields compared to thermal pyrolysis. Although the differences in yields are near the experimental error range, these catalysts exhibit limited efficacy in converting long-chain hydrocarbons into lighter products. Similar to Ni-BC and Fe-BC, the oil/wax composition of Zn-BC and Raw-BC demonstrates a decline in the heavy wax fraction and an

increase in the light oil fraction as temperature rises; however, the changes are less pronounced than those observed for Ni-BC and Fe-BC. Overall, Raw-BC displays superior catalytic performance compared to Zn-BC, with moderately increased gas yields and reduced oil/wax yields. At 700 °C, the most significant difference is noted, as Raw-BC achieves a gas yield of 77.7 wt% while Zn-BC only reaches 71.5 wt%. This discrepancy can be attributed to the substantial reduction in surface area (from 551.4 to 394.7 $m^2 g^{-1}$) and porosity (from 0.206 to 0.147 $cm^3 g^{-1}$) of Zn-BC after the wet impregnation method, whereas Raw-BC retains its highly porous structure, providing access to internal active sites. Moreover, research has suggested that temperatures exceeding 700 °C are necessary to sufficiently activate biochar for pyrolysis or gasification processes (Gilbert, Ryu et al. 2009, Wang, Zhang et al. 2014, Zhang, Wu et al. 2015). Consequently, it can be inferred that Zn-BC was not entirely activated at the temperatures examined in this study. Although the active sites in Raw-BC exhibit much lower catalytic activity than those in Ni-BC and Fe-BC, the naturally occurring metals present in the raw biochar become increasingly active as the temperature intensifies, particularly at 800 °C (Martínez-Narro, Prasertcharoensuk et al. 2022).

Table 5.3. Product yield distribution and compositions from thermal and catalytic pyrolysis using metal-doped biochars at 500 °C.

	Product	Thermal	Ni-BC	Fe-BC	Zn-BC	Raw-BC	HZSM-5
Yields / wt%	Oil/wax	66.67	64.0	60.0	63.3	60.0	46.7
	Gas	28.6	30.0	35.1	31.9	35.2	48.4
	Char	4.76	4.8	4.8	4.8	4.8	4.8
	Carbon deposition	0	1.21	0.10	0.00	0.00	0.18
Gas composition / wt%	CO_2	5.2	6.2	9.0	6.6	7.4	4.8
	H2	0.1	0.5	0.3	0.1	0.1	0.1
	CO	2.8	3.4	3.0	3.3	3.8	1.8
	C1	0.9	1.1	1.2	1.0	1.2	0.8
	C2	3.2	2.7	3.9	3.9	4.5	5.1
	C3	6.6	6.4	8.0	6.3	6.8	18.4
	C4	9.8	9.6	9.7	10.6	11.4	17.3
Oil/wax composition / wt%	Light oil fraction(<C10)	33.7	32.2	28.3	32.6	31.7	26.5
	Medium oil fraction (C10-C18)	18.6	19.0	15.1	16.2	16.9	13.2
	Heavy oil/wax (>C18)	14.4	12.8	16.5	14.5	11.4	6.9

Table 5.4. Product yield distribution and compositions from thermal and catalytic pyrolysis using metal-doped biochars at 600 °C.

	Product	Thermal	Ni-BC	Fe-BC	Zn-BC	Raw-BC	HZSM-5
Yields / wt%	Oil/wax	42.5	30.0	41.7	41.7	43.3	37.1
	Gas	52.8	41.7	45.7	52.5	51.9	57.9
	Char	4.7	5.0	4.7	5.0	4.7	4.8
	Carbon deposition	0.0	23.30	7.93	0.77	0.1	0.15
Gas composition / wt%	CO_2	5.8	3.3	5.3	7.7	7.5	5.6
	H2	0.2	3.2	1.3	0.3	0.2	0.2
	CO	3.6	6.0	6.1	3.0	2.9	3.2
	C1	3.4	3.3	2.9	3.1	3.1	2.6
	C2	10.6	4.8	6.9	9.1	8.9	11.3
	C3	13.5	6.5	10.1	13.2	13.9	19.5
	C4	16.2	8.9	11.6	14.5	13.7	15.5
Oil/wax composition / wt%	Light oil fraction(<C10)	25.6	17.9	26.4	24.5	26.3	24.5
	Medium oil fraction (C10-C18)	11.0	7.1	9.3	10.6	10.7	8.4
	Heavy oil/wax (>C18)	6.3	5.0	6.0	6.6	6.3	4.2

Table 5.5. Product yield distribution and compositions from thermal and catalytic pyrolysis using metal-doped biochars at 700 °C.

	Product	Thermal	Ni-BC	Fe-BC	Zn-BC	Raw-BC	HZSM-5
Yields / wt%	Oil/wax	20	7.3	13.8	23.3	17.3	16.7
	Gas	74.8	53.2	68.8	71.5	77.7	78.0
	Char	5.2	5.0	5.0	4.8	5.0	4.9
	Carbon deposition	0.0	34.5	12.4	0.3	0.0	0.5
Gas composition / wt%	CO_2	6.9	4.5	5.0	6.8	6.5	6.5
	H2	0.3	4.2	2.0	0.5	0.5	0.6
	CO	4.4	9.0	10.8	4.5	4.8	6.4
	C1	7.2	7.6	6.9	7.3	7.4	8.3
	C2	18.8	8.8	13.8	17.8	17.6	21.5
	C3	16.5	6.5	13.0	16.2	15.9	17.1
	C4	20.8	10.7	15.4	18.0	22.3	15.5
Oil/wax composition / wt%	Light oil fraction(<C10)	12.9	2.8	8.2	15.9	10.8	11.5
	Medium oil fraction (C10-C18)	6.2	3.3	4.8	6.6	5.5	4.8
	Heavy oil/wax (>C18)	0.9	1.1	0.8	0.8	0.9	0.3

The HZSM-5 catalyst displays the most remarkable reduction in oil/wax yields and increase in gas yields among all the catalysts examined, with these variations being significant across all temperature ranges. Regarding oil/wax composition, HZSM-5 outperforms other catalysts in converting heavy fractions to lighter counterparts, as demonstrated by the substantial decline in the heavy wax fraction and the increase in the light oil fraction with rising temperatures. Moreover, the gas composition analysis indicates that HZSM-5 is the most appropriate catalyst for monomer recovery, with ethylene and propylene yields considerably higher than those observed with other catalysts. Ni-BC and Fe-BC also exhibited promising results, with catalytic activities comparable to that of HZSM-5 and even higher selectivities toward hydrogen, CO, and CNT production. Although all catalysts showed improved cracking at elevated temperatures, HZSM-5 proved most effective at low temperature (500 °C). This thorough comparison of catalyst performances can provide a basis for future research aimed at optimizing catalyst selection and conditions for plastic waste pyrolysis processes.

Most of the existing literature on biochars from different origins as catalysts for plastic waste pyrolysis utilise raw biochar, making it challenging to compare with the metal-doped catalysts used in this study. Moreover, it is common for researchers to conduct pyrolysis at diverse temperature ranges, which do not always match those used in this study. In their research, Sun et al. (Sun, Themelis et al. 2020) report that using carbonized sewage sludge as a catalyst in the pyrolysis of mixed municipal plastic waste at temperatures between 600 – 800 °C enhanced the selectivity for aromatic compounds. This increased selectivity was linked to the presence of aluminium, iron, sulphur, and phosphorus in the ash, enhancing the biochar's surface acidity and dehydrogenation capabilities. Additionally, the presence of calcium oxide and iron inhibited the formation of overly heavy aromatic compounds. These results, however, are not fully supported by the findings in the present chapter, as there were no significant changes in the product yields between catalysed and non-catalysed experiments using Raw-BC. In a separate study, Areeprasert and Khaobang (Areeprasert and Khaobang 2018) explored how iron oxide-loaded biochar and char from electronic waste affected the pyrolysis of a simulated plastic mixture from electronic waste (ABS/PC). They found that these catalysts boosted the yield and quality of oil, primarily by increasing the production of single ring aromatic compounds. The biochar and electronic waste char demonstrated high efficiencies in removing bromine, with rates of 91% and 68%, respectively. Further research by Sun et al. (Sun, Huang et al. 2018) involved the pyrolysis of mixed plastics (PE, PP, and PS)

using biochar activated with $ZnCl_2$, KOH, and H_3PO_4, as well as untreated biochar at 500 °C. The findings indicated a notable increase in the selectivity towards bicyclic aromatic hydrocarbons (44 – 66%) when activated biochar was utilized, in contrast to a dominance of alkenes (54%) when using raw biochar. The oil and gas product yields reported by Sun et al. using raw biochar are 59.5 wt% and 41.2 wt%, respectively. These yields are comparable to those discussed in the present chapter, with 60 wt% for oil, and 35.2 wt% for gas.

5.9. Summary

In this chapter, a comprehensive analysis of the performance of various catalysts, including Ni-BC, Fe-BC, Zn-BC, Raw biochar, and HZSM-5, for the pyrolysis of plastic waste has been conducted. The investigation primarily focused on the product yield distribution, composition, and carbon nanotube (CNT) formation. Key findings from this study are outlined below:

- The Ni-BC and Fe-BC catalysts demonstrated superior catalytic activity compared to Zn-BC and Raw biochar. Both Ni-BC and Fe-BC displayed analogous trends with increasing temperature, resulting in enhanced yields of H_2, CO, and CNTs.
- The Ni-BC catalyst proved to be more efficient in producing CNTs, yielding significantly higher amounts than those obtained using Fe-BC. However, Ni-BC exhibited a lower propensity to generate high gas yields compared to Fe-BC.
- The CNTs synthesized using Ni-BC and Fe-BC possessed diameters of approximately 30 nm and 60 nm, respectively. The results demonstrated that biochar is an appropriate support for nickel and iron catalysts, facilitating plastic waste pyrolysis.
- The Zn-BC and Raw-BC catalysts presented limited effectiveness in converting long-chain hydrocarbons into lighter products. Raw-BC outperformed Zn-BC, with moderately enhanced gas yields and diminished oil/wax yields.
- The HZSM-5 catalyst manifested the most significant reduction in oil/wax yields and increase in gas yields across all examined temperature ranges. It surpassed other catalysts in converting heavy fractions into lighter counterparts and proved to be the most suitable catalyst for monomer recovery, with markedly higher ethylene and propylene yields.

Chapter 6. Chemical recycling of plastic waste and CO_2 via catalytic pyrolysis

This chapter investigates the potential of catalytic pyrolysis for converting mixed plastic waste into valuable products, such as syngas and monomers which are essential for the chemical and polymer industries. The aim was to optimize process parameters, including temperature, CO_2 concentration, and the catalyst to plastic ratio (C:P), using response surface methodology. The interactions between these parameters and their effects on the main response variables were thoroughly examined. In addition, the reusability and stability of the Ni-Al_2O_3 catalyst was evaluated over multiple cycles to assess its suitability for industrial applications. This chapter contributes to the development of more efficient and sustainable processes for the conversion of mixed, non-recyclable plastic waste and CO_2 into valuable products by providing insights into the process optimization and catalyst reusability. The findings will support the implementation of environmentally friendly approaches to waste management and alternative production of new materials from plastic waste on an industrial scale.

6.1. Background

Catalytic pyrolysis is a promising technique for transforming waste streams into valuable commodities, such as monomers and syngas (a mixture of hydrogen and CO), which are essential precursors for the polymer and chemical manufacturing industries (Saad and Williams 2016). Syngas is a building block for the synthesis of various chemicals such as alcohols (Arora and Prasad 2016), monomers ethylene and propylene (Yahyazadeh, Dalai et al. 2021, Gholami, Gholami et al. 2022, Yu, Wang et al. 2022). Utilising CO_2 in catalytic pyrolysis of non-recyclable plastic waste for closed-loop carbon recovery addresses the global plastic waste crisis, promote sustainability and circular economy (Gao, Liang et al. 2020).

Syngas is produced from gasification of biomass/coal and hydrocarbons via steam reforming (Dascomb, Krothapalli et al. 2013, Pala, Wang et al. 2017). It can be also produced from gasification/catalytic pyrolysis plastic waste and CO_2 (Saad, Nahil et al. 2015, Saad and Williams 2016). Utilising CO_2 from industrial flue gases (containing 8 – 14 mol% of CO2 and 67 – 77 mol% of N_2) as a reactant for thermochemical processes can reduce the GHG emissions by looping CO_2 and promote the transition to a low-carbon economy (Song and Pan 2004).

Nickel-based catalysts are often used in pyrolysis to produce syngas due to their conversion efficiency, selectivity, and cost-effectiveness (Saad, Nahil et al. 2015). However, they are susceptible to deactivation over time (Er-Rbib, Bouallou et al. 2012, Abdulrasheed, Jalil et al.

2019) due to the accumulation of coke deposits on the catalyst surface and nickel sintering (Afzal, Prakash et al. 2021), which negatively impact the efficiency and longevity of the catalyst, therefore, the overall performance of the reaction. Investigating catalyst reusability not only provides insights into its performance over multiple reaction cycles/time but also aids in identifying strategies to mitigate deactivation mechanisms, develop improved catalyst formulations, regeneration techniques, or optimized reaction conditions that prolong catalyst life (Barbarias, Artetxe et al. 2019).

Catalytic pyrolysis for CO_2 capture presents a novel and unique approach compared to traditional carbon capture and storage (CCS) technologies. In terms of carbon capture efficiency, traditional CCS technologies are primarily focused on the efficient capture of CO_2 from large-scale emission sources, such as power plants and industrial facilities (Wilberforce, Olabi et al. 2021). Their efficiency is usually measured by the amount of CO_2 they can capture and store. In contrast, catalytic pyrolysis not only captures CO_2 but also utilizes it as a reactant to convert plastic waste into valuable products. Commercial CCS technologies usually achieve around 90% efficiency (Dods, Kim et al. 2021). While the pyrolysis process presented in this study may not capture CO_2 at the same scale as dedicated CCS facilities, its efficiency is enhanced by the value-added transformation of CO_2 into useful compounds, making it an attractive solution for simultaneous waste management and CO_2 utilization.

Carbon capture by catalytic pyrolysis offers a more holistic approach compared to traditional CCS technologies. Pyrolysis contributes to a circular economy by recycling plastic waste and reducing CO_2 emissions simultaneously. This dual functionality makes it a compelling option for sustainable waste management and carbon reduction, particularly in scenarios where waste plastic and CO_2 are abundant, such as industrial settings where flue gases might be available near or in-site from combustion units.

The economic viability of CCS technologies largely depends on their operational and infrastructural costs, often necessitating government subsidies or carbon pricing mechanisms to be financially feasible (Zhang, Jiang et al. 2018, Naseeb, Ramadan et al. 2022). Pyrolysis, while still in developmental stages, shows potential for economic benefits through the production of commercially valuable products from waste plastics (Fivga and Dimitriou 2018). The revenue generated from these products could potentially offset the costs of the process, making it an economically attractive option, especially if supported by favourable recycling and carbon utilization policies.

This chapter focuses on optimizing the catalytic pyrolysis process, particularly by enhancing catalyst reusability and optimizing process parameters. The novelty of this study lies mostly in the approach to using simulated flue gas compositions in the process, aiming to characterize and make predictions for future studies using real or simulated flue gases. Additionally, the conducted four-cycle reusability tests of the catalyst, which are scarce in literature, provide essential insights for future applications in industrial settings.

A critical aspect of the research is its emphasis on making the process economically viable. By optimizing various parameters such as temperature, catalyst-to-plastic ratio, and reactant concentrations, the process converts plastic to syngas in the most effective way within the experimental conditions, thereby potentially saving costs. The efficiency is further enhanced by minimizing carbon deposition on the catalyst surface, potentially leading to additional cost savings, reduced energy consumption, and improved product yields.

The closed-loop carbon recovery approach employed in this study addresses the global plastic waste crisis and promotes a circular economy. By utilizing CO_2 from industrial flue gases as a reactant, the process also aids in reducing greenhouse gas emissions, thus advancing efforts towards environmental sustainability and circularity in waste management.

6.2. Methods

The plastic samples and Ni-Al_2O_3 catalyst were prepared and characterised as outlined in Chapter 3. The experimental setup and methodology are the same as the ones used for Chapter 5, and described in Chapter 3, except for the following:

- The carrier gas flow was supplied to the first stage of the reactor at a rate of 80 ml min^{-1} and constituted a mixture of N_2 and CO_2, with varying CO_2 mole fractions (from 0 to 60 mol%) depending on the specific experimental run.
- The pyrolysis volatiles were conducted to the second stage of the reactor in which either 0.3, 0.65, or 1 g (depending on the experimental run) of Ni-Al_2O_3 catalyst was retained by quartz wool.

CO_2 becomes a reactant at certain reaction conditions within the tested range, therefore, the mass of converted CO_2 was calculated based on mass balance. A simple subtraction of the CO_2 measured at the outlet of the reactor from that of the inlet would be incorrect because the decomposition of plastic waste in the pyrolysis section generates CO_2 as well. Therefore, the amount of CO_2 generated solely by pyrolysis was measured from thermal runs in absence of

CO_2 (baseline) and considered in the mass balance around the second stage of the reactor as shown in equation 6.1:

$$M_{CO2,in} + M_{CO2,produced} - M_{CO2,converted} = M_{CO2,out} \quad (6.1)$$

Where $M_{CO2,in}$ is the mass of CO_2 in the carrier gas, $M_{CO2,produced}$ is the mass of CO_2 that is generated from the plastic waste in the first stage, $M_{CO2,converted}$ is the mass of CO_2 that is consumed in the catalytic stage of the reactor, and $M_{CO2,out}$ is the mass of CO_2 that is measured at the outlet of the system. The product yields were then calculated by equation 2:

$$Y_i = 100\left(\frac{M_i}{M_{plastic}+M_{CO2,converted}}\right) \quad (6.2)$$

Where Y is the yield (wt%), the subscript *i* denotes the type of product (oil, gas, carbon deposition, and char), and $M_{reactants}$ is the sum of the initial mass of plastic feed and converted CO_2. All yields reported in this chapter are referred to the total mass of initial reactants. This method for calculating the CO_2 conversion and the yields based on reactants was devised based on multiple studies in literature (Saad and Williams 2016, Saad and Williams 2016, Saad and Williams 2017, Saad and Williams 2017). However, these have assumed that the CO_2 produced by the plastic feed is negligible, even when PET is present in the plastic mixture, and ignored it in the calculations (i.e., $CO_{2,converted} = CO_{2,in} - CO_{2,out}$). Therefore, this chapter provides a slight increase in accuracy by taking into account the CO_2 produced by the feedstock in the calculations.

6.2.1. Design of experiments

The Box-Behnken design is an efficient approach for response surface methodology that is specifically designed to provide the maximum amount of information for the least resources (Dicholkar, Gaikar et al. 2012). This method consists of a three-level factorial design, allowing the evaluation of the main effects of the selected experimental factors (i.e, the process parameters of temperature, CO_2 inlet, and catalyst to plastic mass ratio (C:P)) on the response variables as well as their interactive effects. Understanding these interaction effects is crucial given the likelihood of interdependence between process parameters in this study. This design aids in building quadratic models that are beneficial for predicting the response at optimal levels for each variable, which helps create a reliable model for the process. The aim of this study was to investigate operating parameters, their interactions, to optimise processing conditions, and to develop a mathematical model to predict response variables. The factor levels were 500, 600, and 700 °C for temperature, 10, 21.6, and 33.3 wt% for C:P (wt% of

catalyst with respect to plastic feed), and 0, 30, and 60 mol% for CO_2 concentration with respect to N_2 (i.e., 0, 2.83, and 5.65 g h^{-1}). The selected response variables were syngas yield (i.e., the sum of CO and H_2 wt%), CO_2 conversion (g_{CO2} $g^{-1}_{plastic}$), and the product yields. Table 6.1 shows the design matrix and coded unit factors. Experimental data was analysed by the full quadratic model in equation 3:

$$Y_i = b_0 + b_1X_1 + b_2X_2 + b_3X_3 + b_{12}X_1X_2 + b_{13}X_1X_3 + b_{23}X_2X_3 + b_{11}X_1^2 + b_{22}X_2^2 + b_{33}X_3^2 \quad (6.3)$$

Where Y_i is the response variable, b_n are the effect coefficients, and the factors in coded units X_1, X_2, and X_3, are respectively the temperature, CO_2 concentration, and C:P. Significance was tested with a confidence interval of 95%.

Table 6.1. Experimental design matrix and factors in coded units.

Standard order	Run order	Temperature / °C	CO_2 concentration / mol%	Catalyst to plastic ratio	Coded factors		
					X_1	X_2	X_3
1	12	700	0	0.1	+1	-1	-1
2	2	700	60	0.1	+1	+1	-1
3	3	700	60	0.33	+1	+1	+1
4	9	700	0	0.33	+1	-1	+1
5	6	600	30	0.1	0	0	-1
6	1	600	60	0.22	0	+1	0
7	7	600	30	0.33	0	0	+1
8	13	600	0	0.22	0	-1	0
9	10	500	0	0.1	-1	-1	-1
10	4	500	60	0.1	-1	+1	-1
11	5	500	60	0.33	-1	+1	+1
12	11	500	0	0.33	-1	-1	+1
13	8*	600	30	0.22	0	0	0
14	14*	600	30	0.22	0	0	0
15	15*	600	30	0.22	0	0	0

* Centre points.

To increase the prediction capability, the obtained models were optimised and reduced by eliminating statistically insignificant terms (i.e., with a P-value higher than the significance level of 0.05). To test reproducibility, the centre point experiments (i.e., at a temperature of 600 °C, C:P of 21.6 wt%, and CO_2 concentration of 30 mol%) were conducted in triplicate, and the error was extrapolated to the rest of experimental runs.

6.3. Results and discussion

6.3.1. Thermal pyrolysis

Prior to conducting the response surface design experiments, thermal pyrolysis was performed at temperatures of 500, 600, and 700 °C without the inclusion of any catalyst or CO_2 (100% N_2 as carrier gas). These initial tests functioned as baselines, allowing the observation of changes in product yields and compositions when the process was subsequently conducted with the addition of a catalyst and CO_2. The mass of CO_2 generated from the plastic solely by pyrolysis is an important factor that must be considered in equation 6.1 to complement the mass of gaseous products. When CO_2 is added to the process, it is mixed with the CO_2 normally produced by mixed plastic waste pyrolysis and subsequently another fraction reacts with the gaseous compounds during catalysis depending on the specific conditions. As shown in Figure 6.1(b), CO_2 accounts for around 5 wt% of the plastic feed at 500 and 600 °C and slightly increases to 6.9 wt% at 700 °C. This is due to increased decarboxylation reactions at temperatures (>600 °C), and the results are consistent with other pyrolysis reports in literature (López, de Marco et al. 2011, Adrados, de Marco et al. 2012, Onwudili, Muhammad et al. 2019). Temperature significantly affects the product yields with increasing amounts of gas being generated as the temperature increases. As shown in Figure 6.1(a), the gas yield increases with temperature, at an average of 23 wt% for every 100 °C increase. During pyrolysis, the long-chain molecules from plastic waste are decomposed into various products, including gases, oil, and char. As shown in Figure 6.1(a), the yield of these largely depends on the temperature at which pyrolysis is conducted. At higher temperatures (i.e., $\geq$600 °C), the bonds in the polymers that make up the plastic break down more extensively than at lower temperatures due to enhanced thermal cracking reactions, converting larger molecules, which might otherwise condense to form oil, into light gases. Consequently, the oil yield decreases at higher temperatures because the molecules that would usually contribute to oil formation are further broken down into gases. The gas fraction (6.1(b)) is mostly comprised of C1-C4 hydrocarbons (71 – 84 wt% of the gas yield) with small amounts (16 – 29 wt% of the gas) of H_2, CO, and CO_2. The liquid products consist of a mixture of oil (in the range of C5 – C18) and wax (C18+) depending on the processing conditions, higher temperatures result in higher ratio of oil/wax.

Owing to the two-stage system setup, where pyrolysis conditions were maintained constant at 500 °C with a heating rate of 20 °C min^{-1}, the char yield was observed to be consistent across

all experiments, which is evidenced in Figure 6.1.(a). Even with the introduction of CO_2 in the first stage, no interaction was noted between the CO_2 and the plastic waste, nor was there any discernible interference with the thermal decomposition process at 500 °C. Therefore, the subsequent sections do not engage in a discussion of the produced char, as it is solely determined by the pyrolysis temperature and plastic waste composition. Both of these factors were kept constant throughout the experimental runs, leading to unvarying char yields.

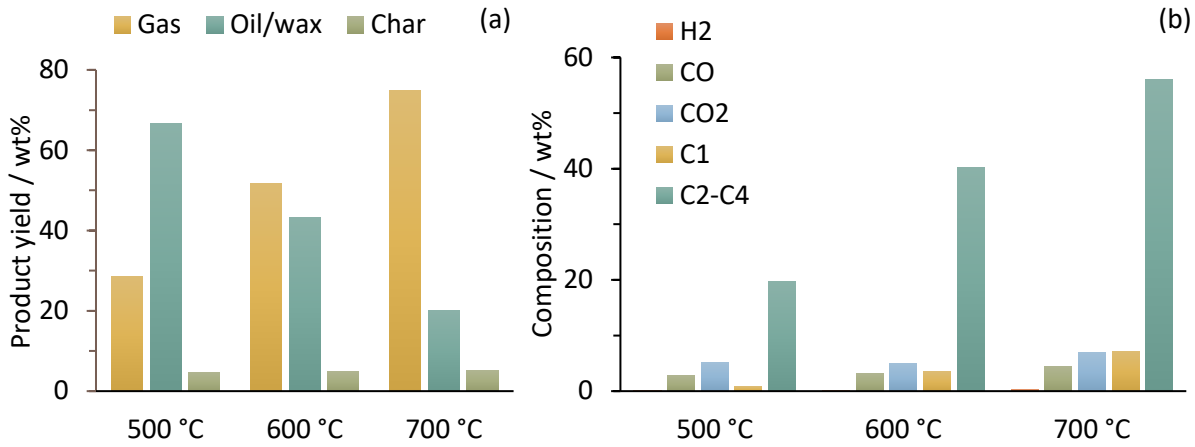

Figure 6.1. Product yields (a) and gas composition (b) of thermal pyrolysis without catalyst.

6.3.2. Model summary and analysis of variance

Following the response surface analysis, the relationships between the outputs (syngas yield, CO_2 conversion, and product yields) and the input processing parameters (temperature, CO_2 concentration at the inlet, and C:P) were fitted to the second order polynomial equations summarised in Table 6.2. Analysis of variance (ANOVA) was performed to test the accuracy of the models (Table 6.3).

To test the statistical significance of individual inputs and their interactions (X_i) on the response (output parameters, Y_i) , the p-values of the terms were compared against the predetermined significance level, evaluating the null hypothesis (i.e., that the term's coefficient is zero, indicating no correlation between the term and the response). The models were then reduced accordingly, leaving only statistically significant terms, except where the elimination of a term with a high variance inflation factor would make the model non-hierarchical. The high R^2 values confirm that most of the variance of the responses are explained by the regression models. The R^2 adjusted, a modified value that compensates for any changes in the terms, demonstrates the effectiveness of the model reduction, which in turn increased its predictive capability (R^2 predicted). In addition, the standard error (in the units of the response variables) is low in every case.

Table 6.2. Regression equations and model summary for the main response variables in uncoded units.

Response variable	Regression equation	Standard error	R^2	R^2 adjusted	R^2 predicted
Syngas yield / wt%	$Y_1 = -162.2 + 0.626X_1 - 0.87X_2 - 300.7X_3 - 0.000537X_1^2 - 0.00659X_2^2 + 444X_3^2 + 0.002547X_1X_2 + 0.2403X_1X_3$	2.83	97.9	95.6	79.3
CO_2 conversion / g_{CO2} $g^{-1}_{plastic}$	$Y_2 = 0.375 - 0.000633X_1 - 0.02059X_2 - 1.726X_3 + 0.000037X_1X_2 + 0.00295X_1X_3 + 0.00979X_2X_3$	0.036	96.8	94.7	57.6
Gas yield / wt%	$Y_3 = -440.3 + 1.49X_1 - 0.662X_2 - 102.9X_3 - 0.001057X_1^2 - 0.00426X_2^2 + 424X_3^2 + 0.001465X_1X_2 - 0.1647X_1X_3 + 0.621X_2X_3$	2.64	99.3	98.2	86.4
Oil yield / wt%	$Y_4 = 585.8 - 1.633X_1 + 0.086X_2 + 242.1X_3 + 0.001149X_1^2 + 0.00299X_2^2 - 496X_3^2 - 0.000425X_1X_2 - 0.104X_1X_3 + 0.029X_2X_3$	3.26	99.3	98.2	94.3

Table 6.3. ANOVA of regression equations.

	Deg. of freedom				Adjusted sum of squares				Adjusted mean square				F-Value				P-Value			
Source	Y_1	Y_2	Y_3	Y_4	Y_1	Y_2	Y_3	Y_4	Y_1	Y_2	Y_3	Y_4	Y_1	Y_2	Y_3	Y_4	Y_1	Y_2	Y_3	Y_4
Model	8	6	9	9	2688.3	0.35	5753.3	8559.3	336.0	0.058	639.3	951.0	42.1	46.0	91.5	89.7	0.000	0.000	0.000	0.000
Linear terms	3	3	3	3	1776.5	0.23	4480.0	7122.6	592.2	0.078	1493.4	2374.2	74.1	61.5	213.8	224.0	0.000	0.000	0.000	0.000
X_1	1	1	1	1	998.9	0.11	4397.5	6978.0	998.9	0.108	4397.5	6978.0	125.0	85.5	629.5	658.4	0.000	0.000	0.000	0.000
X_2	1	1	1	1	621.1	0.11	82.5	2.5	621.1	0.115	82.5	2.5	77.7	90.6	11.8	0.2	0.000	0.000	0.014	0.646
X_3	1	1	1	1	156.5	0.01	0.0	142.1	156.5	0.011	0.0	142.1	19.6	8.5	0.0	13.4	0.003	0.017	0.939	0.011
Squared terms	3	--	3	3	255.0	--	444.1	432.6	85.0	--	148.1	144.2	10.6	--	21.2	13.6	0.005	--	0.001	0.004
X_1^2	1	--	1	1	52.5	--	197.0	235.7	52.5	--	197.0	235.7	6.6	--	28.2	22.2	0.037	--	0.002	0.003
X_2^2	1	--	1	1	76.6	--	32.9	15.8	76.6	--	32.9	15.8	9.6	--	4.7	1.5	0.017	--	0.073	0.269
X_3^2	1	--	1	1	72.4	--	68.6	90.3	72.4	--	68.6	90.3	9.1	--	9.8	8.5	0.020	--	0.020	0.027
Binary interactions	2	3	3	3	528.1	0.12	220.1	24.9	264.0	0.039	73.4	8.3	33.0	30.4	10.5	0.8	0.000	0.000	0.008	0.545
X_1X_2	1	1	1	1	467.0	0.10	154.5	13.0	467.0	0.097	154.5	13.0	58.4	76.8	22.1	1.2	0.000	0.000	0.003	0.310
X_1X_3	1	1	1	1	61.1	0.01	28.4	11.8	61.1	0.009	28.4	11.8	7.6	7.3	4.1	1.1	0.028	0.025	0.090	0.332
X_2X_3	--	1	1	1	--	0.01	37.1	0.1	--	0.009	37.1	0.1	--	7.3	5.3	0.0	--	0.025	0.061	0.932
Error	7	9	6	6	55.9	0.01	41.9	63.6	8.0	0.001	7.0	10.6	--	--	--	--	--	--	--	--
Lack-of-Fit	5	7	4	4	51.4	0.01	38.8	57.1	10.3	0.002	9.7	14.3	4.5	48.6	6.2	4.4	0.191	0.020	0.144	0.194
Total	15	15	15	15	2744.2	0.36	5795.2	8622.9	--	--	--	--	--	--	--	--	--	--	--	--

6.3.3. Main effects and interactions of processing parameters.

Response surface analysis allows the identification and study of the effects of various input factors on the output response variables of complex processes. A graphical representation of the response surface is presented in Figure 6.2, showing the influence of temperature, CO_2 concentration, and catalyst to plastic ratio on the fitted means of the syngas yield, CO_2 conversion, gas yield, and oil yield while keeping the other factors fixed at the centre point conditions. The syngas yield in Figure 6.2(a) is strongly influenced by both temperature and CO_2 concentration, as raising the temperature from 500 to 600 °C and the concentration from 0 to 30 mol% result in a significant increase in syngas yield. As evidenced in Figure 6.2(b), the reactions between hydrocarbons and CO_2 do not occur at 500 °C. However, once the temperature reaches 600 °C, these reactions commence, transforming CO_2 to an active reactant, thus resulting in the production of syngas. Simultaneously, the concentration of CO_2 in the system plays a significant role in the yield of syngas. Once the higher temperature threshold (600 °C) has activated CO_2 as a reactant, an increase in its concentration directly affects the yield of syngas since there is now a larger supply of CO_2 available for conversion. Thus, increasing the CO_2 concentration from 0 to 30 mol% enhances the reactions between CO_2 and hydrocarbons, leading to a significantly higher syngas yield. However, beyond these points, increases in temperature and CO_2 concentration had little effect on the syngas yield. Raising the temperature to 700 °C and CO_2 concentration to 60 mol% did not result in significant changes in yield. This indicates that the optimal conditions might not be at these extreme values but somewhere between the centre point and high-end levels for these parameters. The Carbon to Plastic (C:P) ratio also significantly impacts the syngas yield, but this influence is more noticeable at the highest examined ratio. Specifically, at a C:P ratio of 33.3 wt%, the syngas yield increases notably to 30 wt%. However, the syngas yield seems to be less sensitive to changes in the C:P ratio at lower and middle-range values. Around these levels, the yield remains approximately constant at about 20 wt%, indicating that the C:P ratio's impact on syngas yield may be less significant at these ranges. CO_2 conversion (Figure 6.2(b)) follows the same trend as that of syngas yield. All the considered factors significantly affect CO_2 conversion, and therefore the production of syngas from hydrocarbons. Temperature has the largest effect, followed by CO_2 concentration at the inlet and catalyst to plastic ratio (Figure 6.2(c)). The oil yield in Figure 6.2(d) shows the opposite trends as the gas yield, increasing temperature decreased the oil yield whereas CO_2 and C:P had little effect.

This effect is explained by the fundamental principles of pyrolysis since the formation of gases occurs at the expense of liquid products.

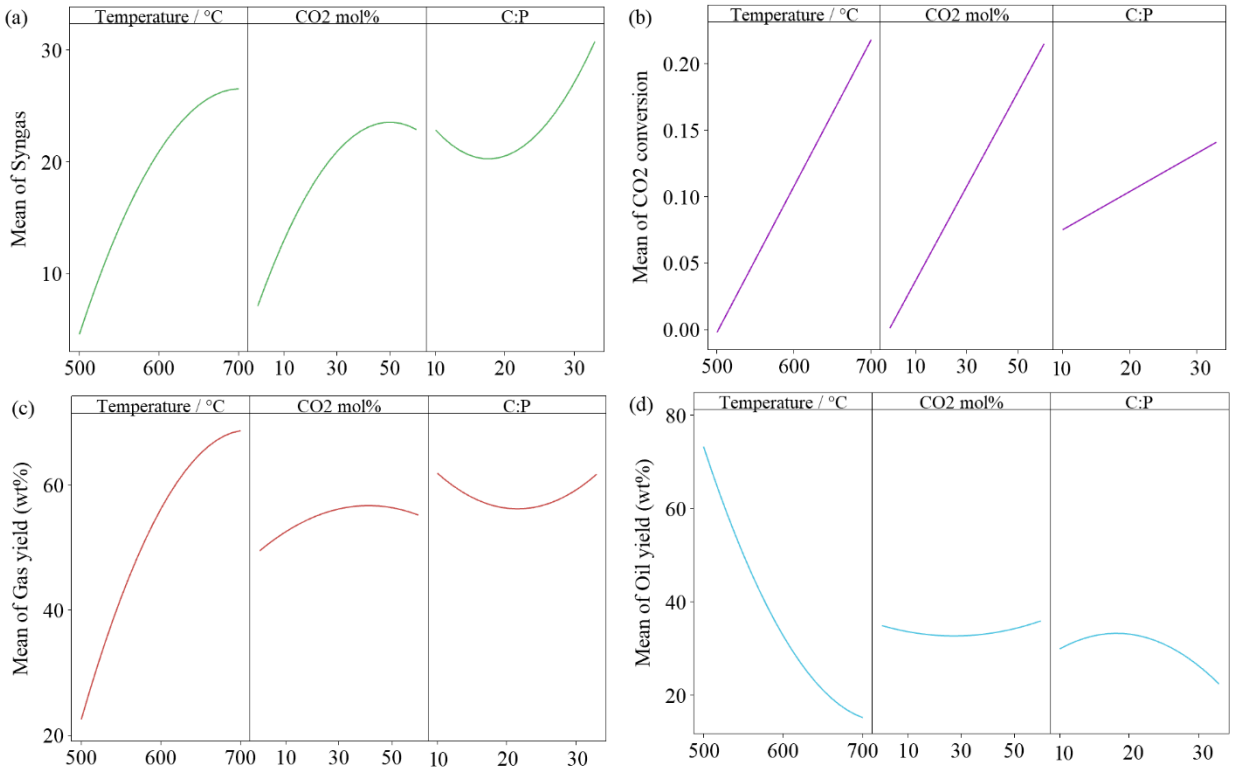

Figure 6.2. Main effects of temperature, CO_2 concentration, and catalyst to plastic ratio on the fitted means of syngas yield (a), CO_2 conversion (b), gas yield (c), and oil yield (d).

Although these results provide valuable insights into the process by examining the overall effects of processing parameters on the fitted means of response variables, a more in-depth analysis of their influence is discussed in subsequent sections including detailed oil and gas compositions, and char and carbon deposition yields.

Effect of catalyst bed temperature

Figure 6.3 shows the product yields and compositions at 500, 600 and 700 °C, compared to the low, middle, and high levels of the other factors (i.e., C:P and CO_2 concentration). The trends of gas and oil yields observed in catalytic decomposition (Figure 6.3(a)) were similar to those in thermal decomposition (6.1(a)).

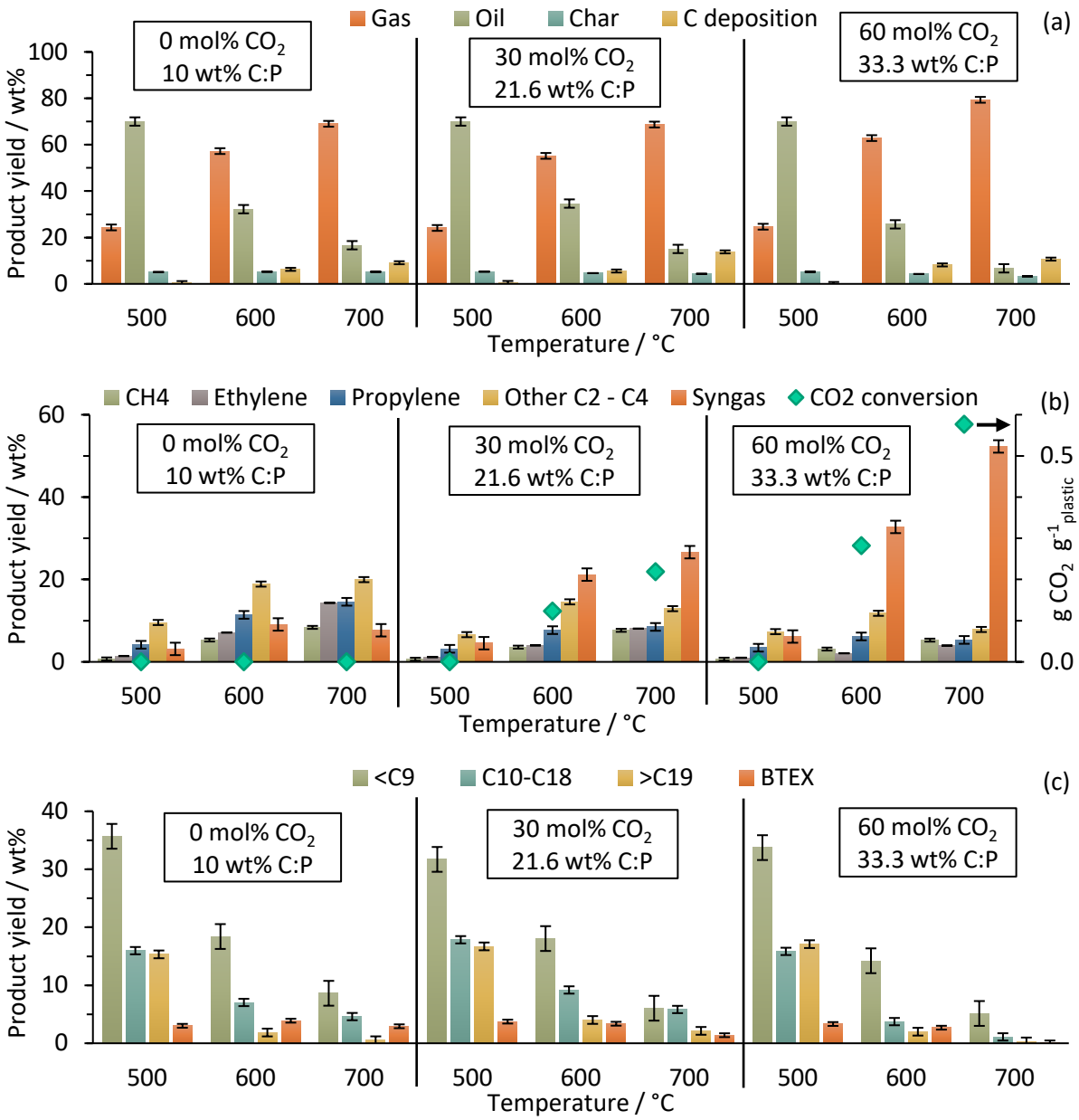

Figure 6.3. Effect of catalyst bed temperature on product yields (a), gas composition (b), and oil composition (c) at low, middle, and high factor levels.

While the increase in temperature from 500 to 600 °C doubled the gas yield, a further increase from 600 to 700 °C resulted in a more modest increase of only 26%. Carbon deposited on the catalyst surface increased with increasing operating temperature, e.g. from approximately 0.5 to 6 wt% as the temperature was raised to 600 °C, and then further increased to a range of 9 – 13.8 wt% at 700 °C. High temperatures ($\geq$600 °C) in presence of Ni-Al_2O_3 catalysts promote conversion of methane into carbon and hydrogen, resulting in increased deposits of carbon the catalyst surface (Benguerba, Dehimi et al. 2015). This phenomenon can be observed in Figure 6.4, which shows SEM images of the fresh and spent catalyst at the different tested temperatures.

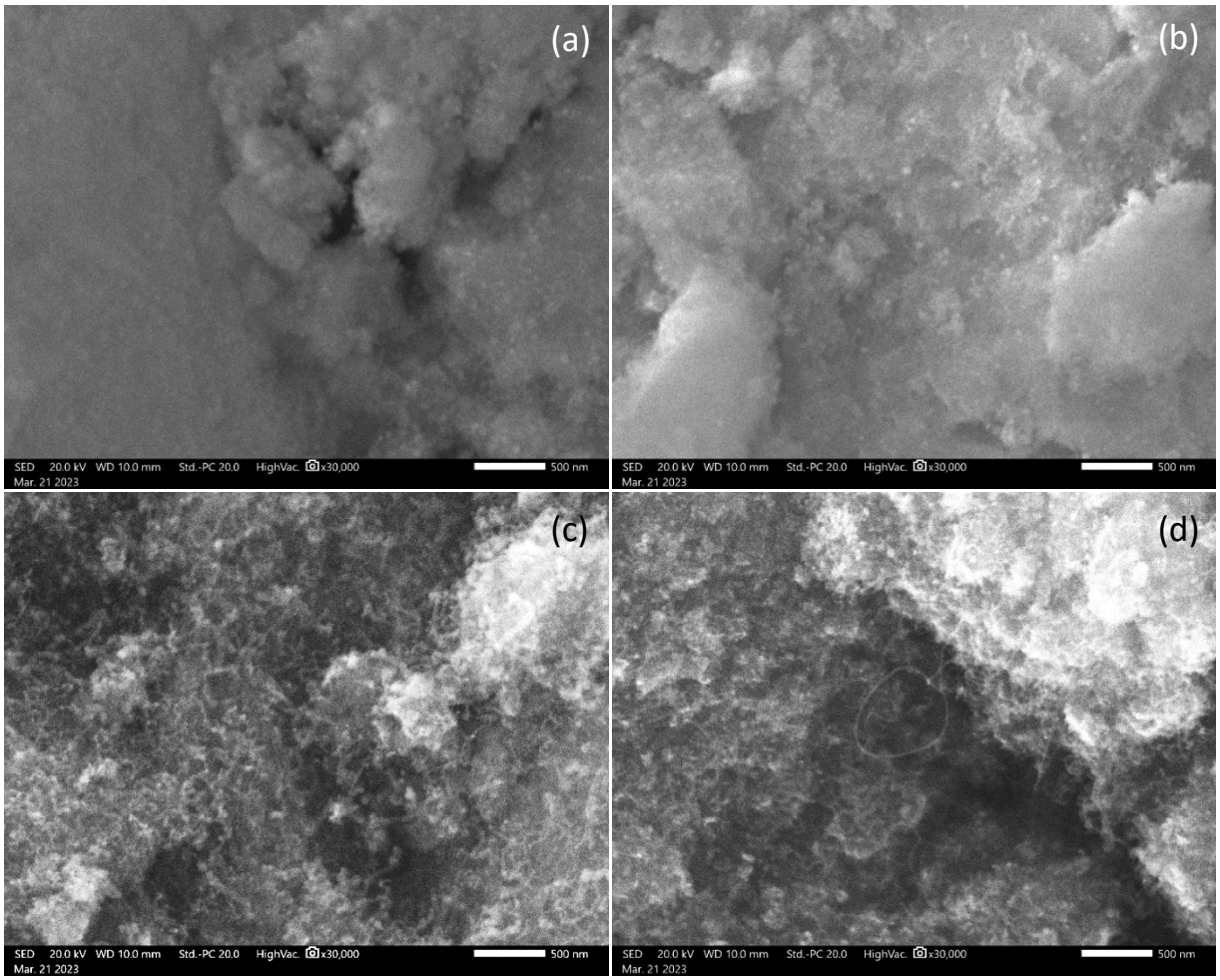

Figure 6.4. SEM images of the fresh (a) and spent catalyst at 500 °C (b), 600 °C (c), and 700 °C (d) showing the filamentous morphology of carbon deposits.

The spent catalyst at 500 °C resembles the fresh catalyst, with low carbon deposition. Conversely, at 600 °C and 700 °C a remarkable increase in carbon deposits of filamentous structure can be observed. At high temperatures (e.g., 700 °C), the enhanced catalytic activity promotes further decomposition of light gases, which results in the production of hydrogen and carbon via the methane decomposition reaction (Chesnokov and Chichkan 2009):

$$CH_4 \rightarrow C + 2H_2 \tag{6.4}$$

This mechanism explains the high amount of carbon deposits on the catalyst surface at 600 and 700 °C. The dominant CO_2 conversion reaction, which is responsible for the high syngas yields, is the hydrocarbon (dry) reforming reaction (Saad and Williams 2017):

$$C_xH_y + xCO_2 \rightarrow 2xCO + \frac{y}{2}H_2 \tag{6.5}$$

Figure 6.3(b) shows that there are no reactions between the CO_2 in the carrier gas and the pyrolytic volatiles at 500 °C, and the syngas yield remains mostly unchanged at 3 – 6 wt%. The conversion of CO_2 is only observed at temperatures ≥600 °C, e.g., doubles when the temperature is increased from 600 to 700 °C due to dry reforming of volatiles to form CO and

H_2, and the Boudouard reaction ($CO_2 + C \leftrightarrow 2CO$) at temperatures ≥600 °C. However, further increasing temperature >800°C favours the reverse Boudouard reaction (Saad and Williams 2017). In the runs with 60 mol% CO_2 and a C:P of 33.3 wt%, the liquid fraction of hydrocarbons (Figure 6.3(c)) decreased from a total of 25.7 to 6.7 wt% when increasing temperature from 600 to 700 °C to form mainly syngas and carbon deposits, since the amount of C1 – C4 gaseous hydrocarbons remains constant. This is because, as the temperature increases, the pyrolysis process favours the production of gas molecules over liquids due to increased cracking of larger hydrocarbon chains into smaller ones, shifting the product distribution from oil to gases, including syngas. At these processing conditions (60 mol% CO_2, and 33.3 wt% C:P), the most impactful change with temperature is found in the syngas yield, at 600 °C the yield is 32.8 wt% and it increases to 52.3 wt% at 700 °C. The maximum yield of ethylene and propylene monomers (14 wt% each) is achieved at 700 °C in absence of CO_2, as reaction 6.5 transforms them into syngas.

Effect of CO_2 concentration

The product yields and compositions at CO_2 concentration of 0, 30, and 60 mol% are compared to the low, middle, and high levels of temperature and C:P in Figure 6.5. At 500 °C, variations in the CO_2 concentration have a negligible impact on the product yields and oil compositions (Figure 6.5(a)). In addition, at different temperatures and C:P, the corresponding oil compositions (Figure 6.5(c))) remain the same when varying CO_2 concentrations, with the exception of the conditions 700 °C and C:P 33.3 wt% where increasing to 60 mol% minimized the medium (C10 – C18) and heavy (≥C19) fractions while the light fraction (≤C9) remained. This could be in part explained by increased activity of the catalyst at higher temperatures (700 °C) which leads to a greater cracking of hydrocarbons. The increasing concentrations of CO_2 (30 – 60 mol%) at this temperature further promoted the cleavage of C-C bonds in long-chain hydrocarbon molecules into smaller ones, resulting in a higher production of the light oil fraction (<C9). In the experiments conducted at 600 °C, when the CO2 concentration was increased from 0 to 30 mol%, there was a substantial rise in the syngas yield.

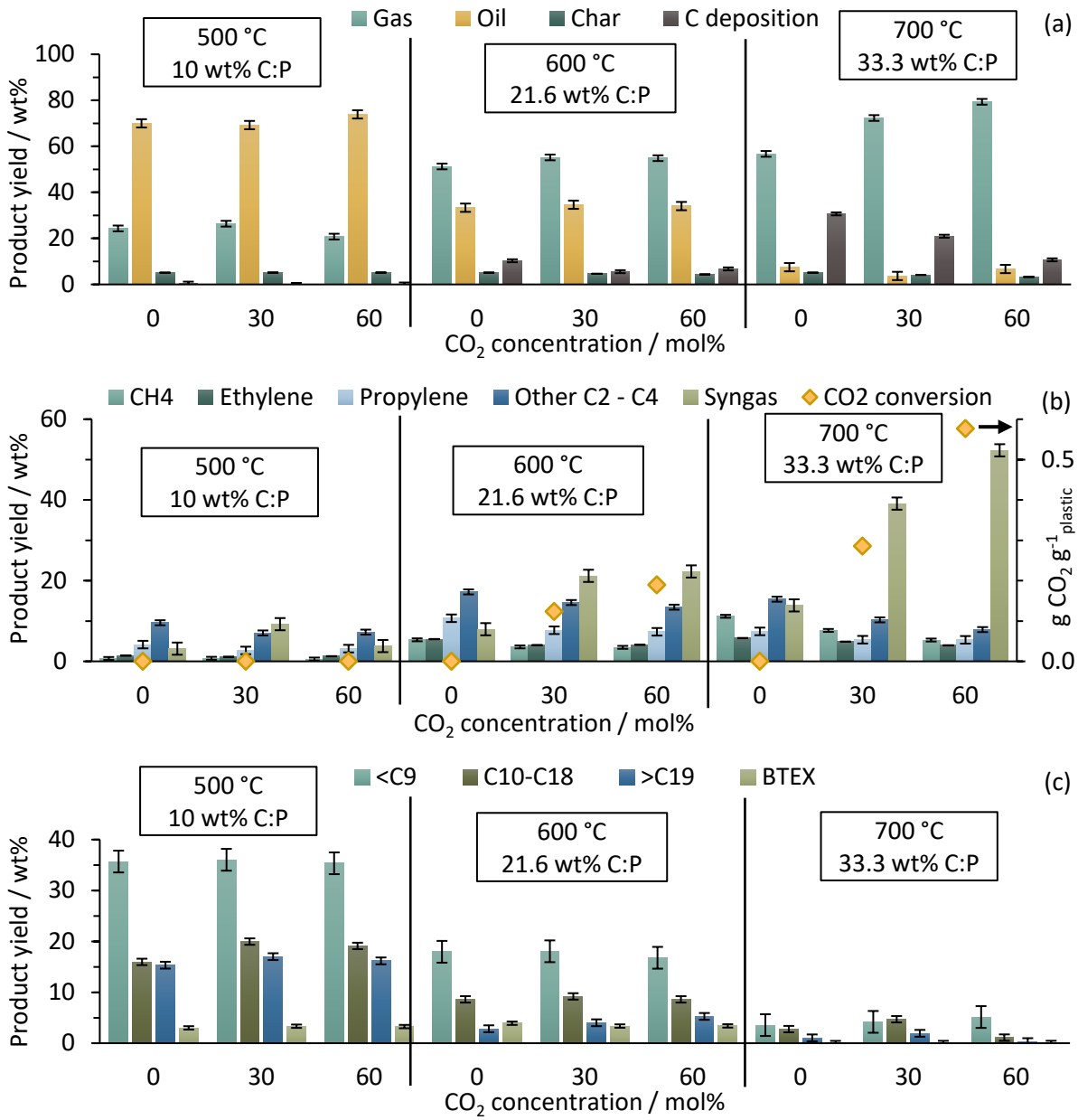

Figure 6.5. Effect of CO_2 concentration on product yields (a), gas composition (b), and oil composition (c) at low, middle, and high factor levels.

As shown in Figure 6.5(b), the syngas yield increased from 8 wt% to 21.2 wt%. Despite this increase in syngas, the total yield of all gases (including both syngas and other hydrocarbons) only increased by 3.9 wt% and the oil yield remained constant. This indicates that the increase in syngas took place mostly at the expense of other gaseous hydrocarbons. Specifically, there was an 8.8 wt%* decrease in the fraction of light hydrocarbon gases (C1–C4). There was no effect on product yields and compositions when the CO_2 concentration was further increased to 60 mol% at the same temperature and C:P. The impact of CO_2 concentration becomes significant at 700 °C and C:P 33.3 wt%, e.g., the syngas yield increased from 13.9 to 39.1 wt% and to 52.3 wt% when increasing CO_2 from 0%mol, 30 mol% to 60 mol%. At these conditions (700 °C and C:P 33.3 wt%), the highest CO_2 conversion was achieved, with a total 1.8 g of CO_2

converted into CO (i.e., 0.6 g of CO_2 per g of plastic feed). At high temperatures and C:P (e.g., 700 °C and 33.3 wt%) in the absence of CO_2, the reactions become dominated by the methane decomposition reaction ($CH_4 \rightarrow C + 2H_2$) as evidenced by the high amounts of hydrogen (4.1 wt%) and carbon deposition (30.7 wt%). The introduction of CO_2 to the system considerably reduces the amount of carbon deposition due to the reaction between carbon on the catalyst surface with CO_2 (Sengodan, Lan et al. 2018):

$$C + CO_2 \rightarrow 2CO \tag{6.6}$$

The carbon deposition was reduced from 30.7 to 20.9 wt% at a CO_2 concentration of 30 mol%, and consequently decreased to 10.7 wt% with 60 mol% CO_2. This effect highlights the advantage and importance of using CO_2 in the carrier gas to mitigate catalyst deactivation by carbon deposition while increasing the syngas yield. This effect of reduced carbon deposition agrees with a literature study by Saad et al. (Saad and Williams 2017), where the addition of 6 g h^{-1} of CO_2 to plastic waste (HDPE) pyrolysis at 800 °C decreased carbon deposition from 36.5 wt% (without CO_2) to 1.4 wt%.

In an industrial-scale pyrolysis or gasification system, several sources of CO_2 could be available for the process. One primary source is the CO_2 emitted directly from the pyrolysis process itself, as the breakdown of hydrocarbons in plastics naturally releases CO_2 when PET is present in the mixture (Martínez-Narro, Prasertcharoensuk et al. 2022). However, the CO_2 concentration would be limited to the oxygen content of a single component among various plastics. Moreover, the composition of the plastic mixture is most likely to vary, making it difficult to maintain a consistent supply. If the process involves a partial combustion step, additional CO_2 can be produced. Another option is sourcing CO_2 from industrial activities (internal or external) where CO_2 is a by-product, such as combustion processes.

In this chapter, high purity gases were utilised, however, this would not be the case when using a real CO_2 source in which the gaseous mixture will most likely contain impurities. These impurities may include sulphur compounds, nitrogen compounds, halogens, or heavy metals that may interfere with the process and equipment (Prabhansu, Karmakar et al. 2015). The corrosive nature of some of these impurities, particularly acidic compounds, can lead to equipment damage and increased maintenance costs, shortening the lifespan of vital machinery (de Oliveira, Lora et al. 2023). Flue gases usually contain water vapour as a product of combustion; therefore, these molecules may also participate in the reactions of the process. The presence of steam has been found to improve the hydrogen to carbon monoxide ratio in

the syngas produced by gasification of plastic waste (Saad and Williams 2017). The control and monitoring of impurities in the carrier gas is crucial for a large-scale industrial system involving pyrolysis of plastic waste.

Effect of catalyst to plastic ratio

Product yields and compositions at C:P of 10, 21.6, and 33.3 wt% compared to the low, middle, and high levels of temperature and CO_2 concentration are presented in Figure 6.6. The amount of catalyst has little effect on product yields and compositions at 500 °C in the absence of CO_2 in the carrier gas. At this low temperature, the reactions occurring might not be entirely dependent on the catalyst, and thermal decomposition might be the dominant process, hence the minimal effect of catalyst amount. At 600 °C and with 30 mol% of CO_2, there is a considerable reduction in the oil yield (from 34.6 to 17.9 wt%) when C:P increased from 21.6 to 33.3 wt%. The syngas yield (Figure 6.6(b)) increases from 21.2 to 31.1 wt%, and the yield of methane increases by 77% due to higher conversion of volatiles, particularly the light fraction (<C9) shown in Figure 6.6(c).

These results are consequence of the reforming of hydrocarbon volatiles in presence of CO_2, and the enhanced catalytic activity at $\geq$600 °C. The C:P ratio plays a significant role on the syngas yield and CO_2 conversion rates, particularly at a temperature of 700 °C and a CO_2 concentration of 60 mol%. For instance, even though the total gas yield remains relatively constant (between 72-79 wt%) under these conditions, the CO_2 conversion values increase notably with a higher C:P ratio (0.31, 0.44, and then 0.58 g_{CO2} g^{-1}plastic at C:P ratios of 10, 21.6, and 33.3 wt%, respectively). As the C:P ratio increases, there is more catalyst available for the reactions, leading to a higher conversion of CO_2 and hence a higher syngas yield. This leads to different overall mass of products. The syngas yield experiences a substantial increase from a range of 32-36 wt% to 52.3 wt% when the C:P ratio is increased from either 10 or 21.6 to 33.3 wt%. The total gas yield remains relatively stable under these conditions because the increase in CO_2 conversion is balanced by a decrease in the production of other gaseous products.

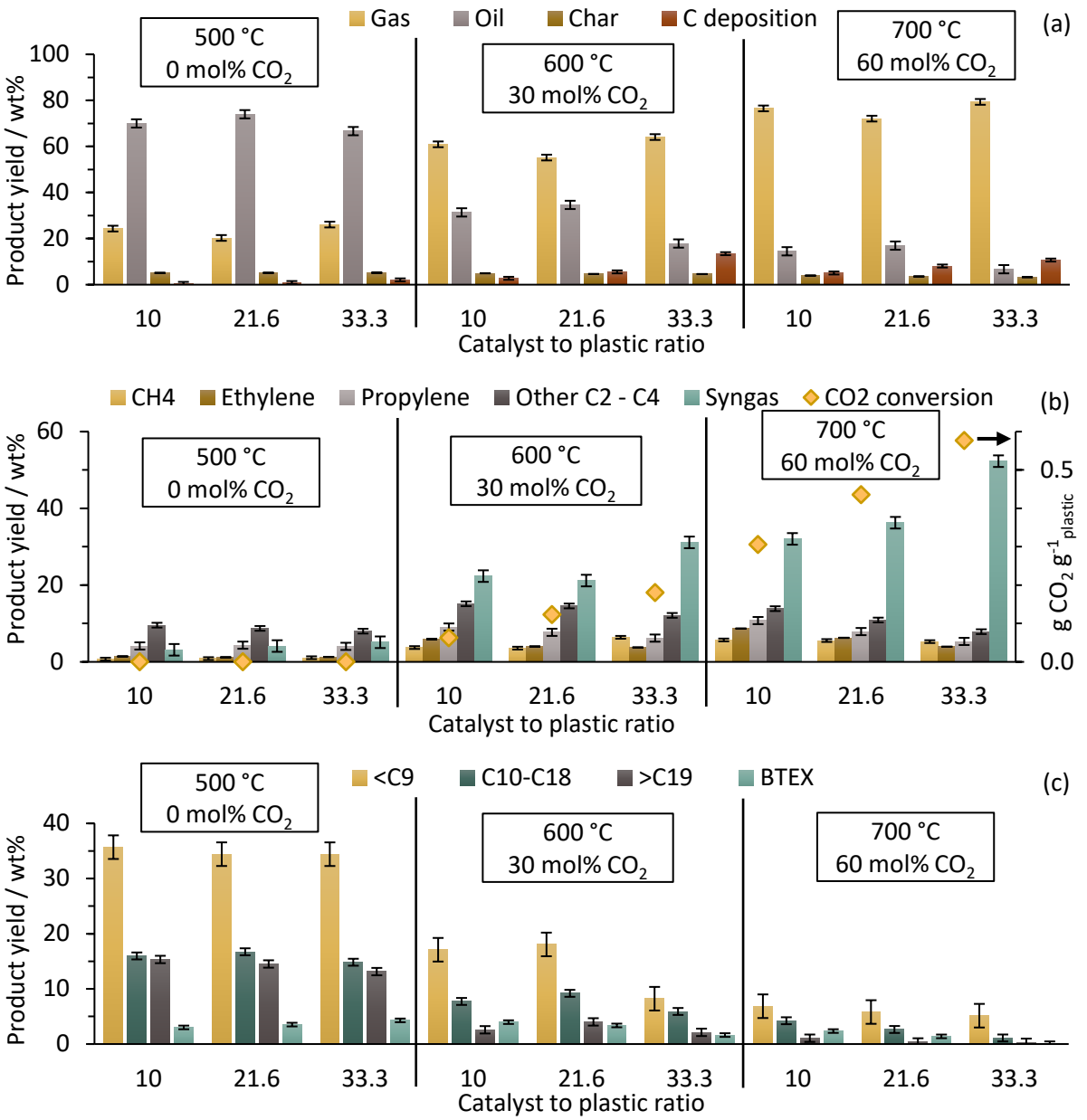

Figure 6.6. Effect of catalyst to plastic ratio on product yields (a), and gas composition (b) at low, middle, and high factor levels.

Regarding the product composition, the syngas production is most affected when the C:P ratio is raised from 21.6 to 33.3 wt%. In contrast, the impact is moderate when the increase is from 0.1 to 0.22. Moreover, the oil yield sees its most prominent reduction between the medium and high levels of the C:P ratio, dropping from 17 to 6.7 wt%. The C:P ratio is also the most influential parameter on carbon deposition, following a similar trend as the syngas yield and CO_2 conversion. Therefore, optimising this parameter to find a proper balance between the amount of catalyst in the process and the concentration of CO_2, which can consume it, is important to minimize the catalyst carbon deposition.

Interactions between processing parameters.

The interaction effects between the processing parameters at their different levels and the main response variables is presented in Figure 6.7.

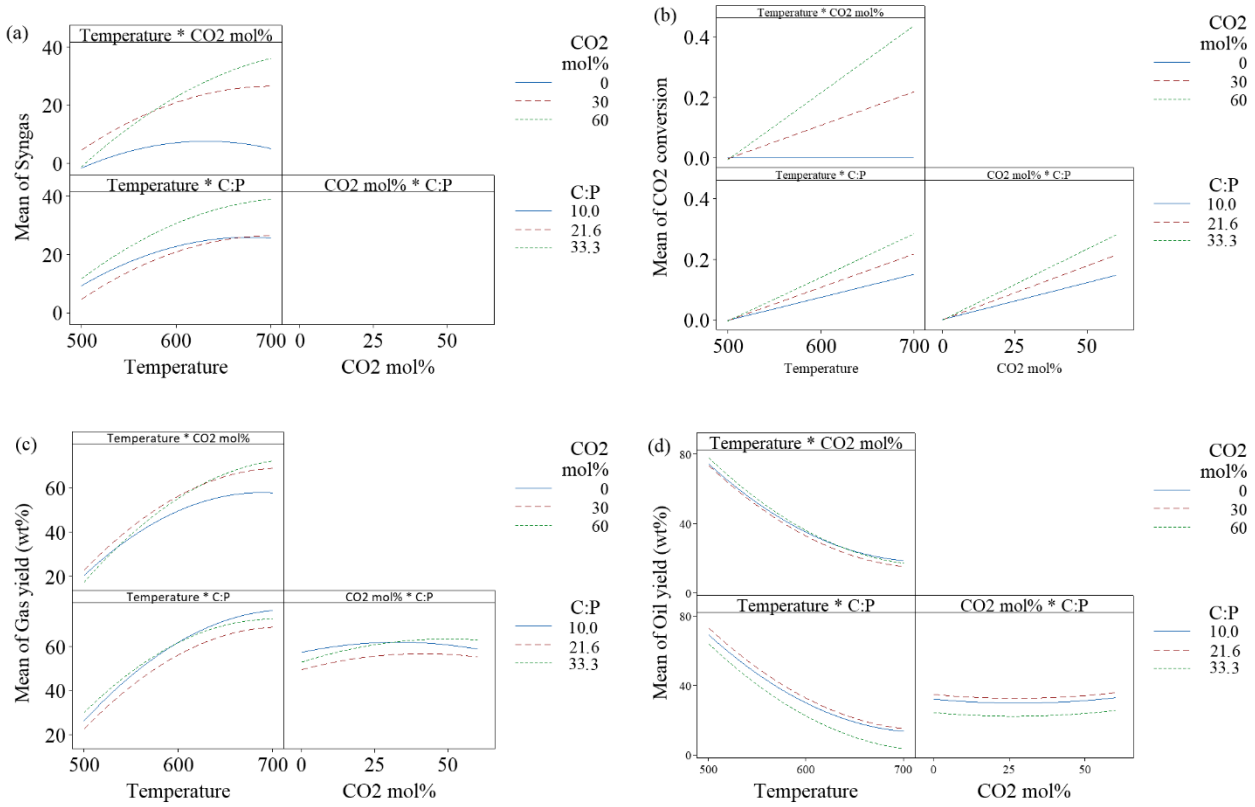

Figure 6.7. Interactions between different factor levels and the fitted means of syngas yield (a), CO_2 conversion (b), gas yield (c), and oil yield (d).

The syngas yield (Figure 6.7(a)) exhibits only minor variations at 500 °C due to the absence of strong CO_2 conversion reactions. At 700 °C when the C:P is raised from 10 to 21.6 wt%, the syngas yield was not affected, but it increased up to 37 wt% at a C:P of 33.3 wt%. The CO_2 conversion (Figure 6.7(b)) displays linear trends without any interactions between the levels of the factors. A minor interaction between temperature and C:P is observed for the gas yield in Figure 6.7(c), as the catalyst promotes hydrogen formation and carbon deposition, resulting in a slight reduction in the formation of gaseous products. No interactions are observed between temperature and CO_2 concentration, and the effect of CO_2 addition is evident. Additionally, no significant interactions are observed for oil yield in Figure 6.7(d). In general, there are few interactions and the ones observed have only a moderate impact on the process.

6.3.4. Optimisation

The most desired outcome of the process is a maximum CO_2 conversion rate which would result in the highest syngas yield; however, carbon deposition with its associated potential catalyst deactivation should also be kept at a minimum. Additionally, process conditions that favour the production of valuable precursors for the polymer industry (i.e., monomers ethylene and propylene) can be investigated and optimised. Response optimisation analysis was performed by calculating the individual (d) and composite (D) desirabilities, for which the lower, target, and upper values were selected based on the experimental data (i.e., the minimum and maximum carbon deposition and CO_2 conversion found throughout the experiments). Figure 6.8 shows that the optimal processing conditions to maximise CO_2 conversion and minimise carbon deposition are operating at a temperature of 700 °C, with a CO_2 concentration of 60 mol%, and a C:P of 16.04 wt%, which result in a CO_2 conversion of 0.389 g_{CO2} $g^{-1}_{plastic}$ and a carbon deposition of 4.645 wt%. The syngas yield for these conditions is of 34.25 wt%.

The same method was applied to determine optimal conditions for maximum monomer recovery. Operating at a temperature of 700 °C and a moderate C:P of 10 wt% in absence of CO_2 yield a total 28 wt% of ethylene and propylene monomers. It is important to carefully control the process parameters to achieve maximum monomer recovery, since deviating from the optimal conditions would directly affect their production. Increasing the amount of catalyst in the process converts ethylene and propylene into hydrogen and carbon, lowering the temperature results in lower yields, and adding CO_2 converts them into syngas.

The potential utilisation of industrial flue gases was explored by simulating its composition at a CO_2 concentration of 15 mol% and 75 mol% N_2. The model prediction for this value at the optimal conditions of 700 °C and 16.04 wt% C:P resulted in a syngas yield of 15.4 wt%, a CO_2 conversion of 0.08 g_{CO2} $g^{-1}_{plastic}$, and a carbon deposition of 13.2 wt%. These results may not be accurate due to the presence of oxygen in flue gases (2 – 5 mol%) (Song and Pan 2004), which can produce more CO and reduce the carbon deposition. Future studies may be focused on using real or simulated flue gases in this process to adequately characterize the process and make accurate predictions.

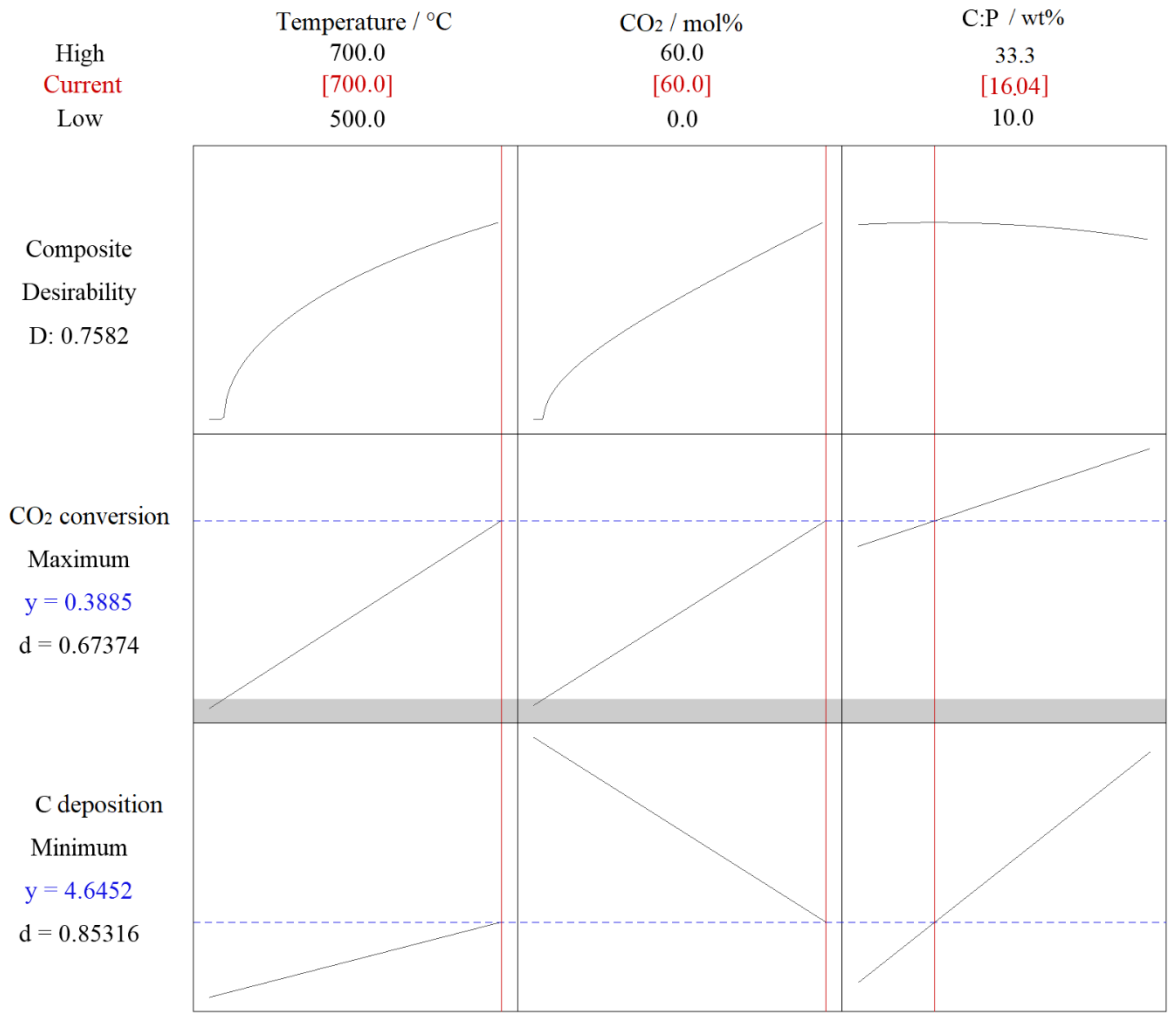

Figure 6.8. Response optimisation results for maximum CO_2 conversion (g_{CO2} $g^{-1}_{plastic}$) and minimum carbon deposition (wt%).

6.3.5. Catalyst reusability

Catalyst stability minimizes the need for frequent catalyst replacement, which is often expensive and time-consuming (Liu, Xing et al. 2023). A four-cycle reusability test was conducted to study the catalyst's performance and stability over multiple cycles of use at the centre point conditions. Over the four cycles, the gas yield was reduced from 55.2 to 49.81 wt% while the oil yield increased from 34.6 to 42 wt%, and the carbon deposition on the catalyst surface decreased from 5.55 to 2.97 wt%, as shown in Figure 6.9(a). These results suggest that catalyst performance is moderately affected by successive cycles, as evidenced by a decline in gaseous products. While it appears that carbon deposition declines with each cycle, this only pertains to the additional carbon introduced with each run, while the overall mass continues to accumulate. Figure 6.9(b)shows the gas compositions throughout the four cycles.

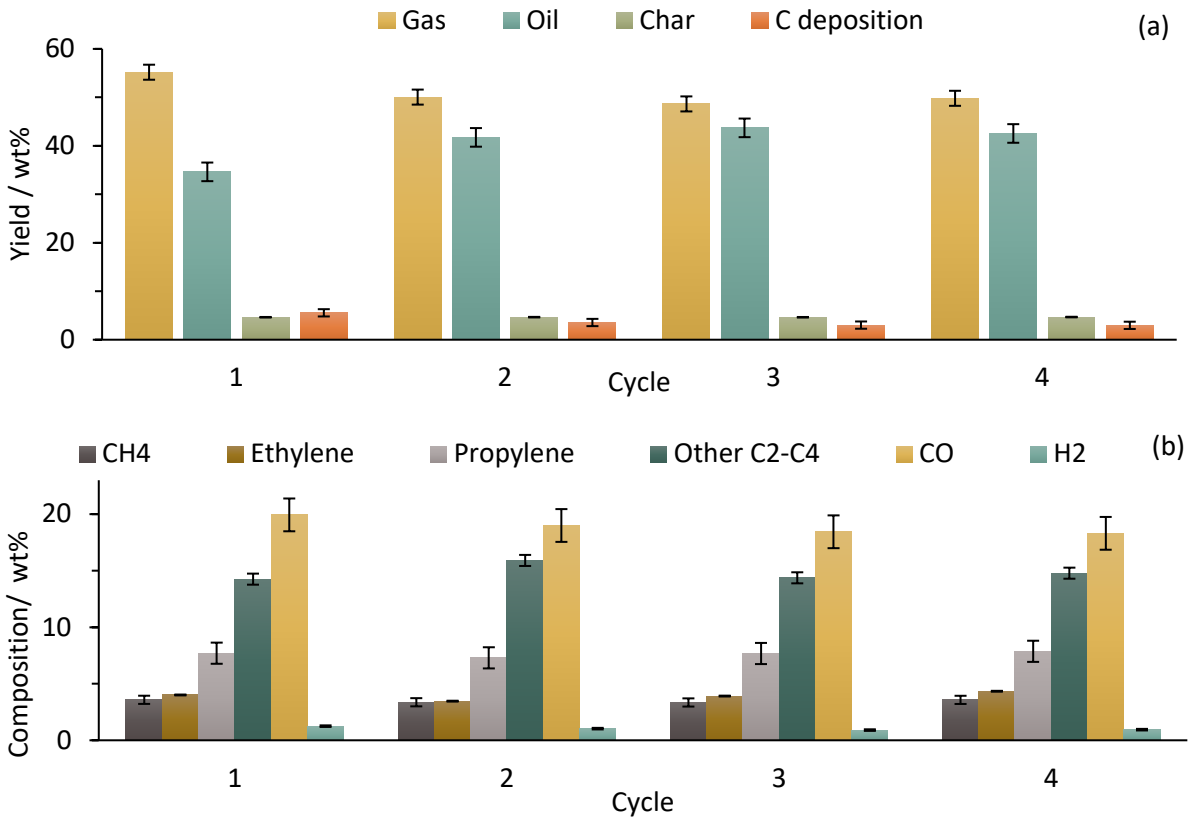

Figure 6.9. Product yields (a) and gas composition (b) of four consecutive runs at the centre point conditions reusing the same catalyst.

The errors for these experiments are the same extrapolated values of the previous experiments. There is only a minor reduction in the yields of hydrogen (from 1.25 wt% to 0.94 wt%) and CO (from 19.9 wt% to 18.3 wt%), which indicates that the catalyst has a suitable stability and retains most of its activity over four cycles. The yields of C1 – C4 gases remains relatively constant within the ranges of 3.35 – 3.58 wt% for methane, 3.46 – 4.34 wt% for ethylene, and 7.29 – 7.87 wt% for propylene. There are some changes in the catalytic performance over the four cycles, however, these are moderate and do not affect the products significantly. Nevertheless, this test is limited to the selected process conditions and number of cycles, therefore, additional runs and testing at different factor levels must be considered in future studies to fully understand the reusability of the catalyst.

The performance of the Ni-$Al2O_3$ catalyst across multiple cycles was analysed both from the product yield perspective and through SEM images. The SEM image of the fresh catalyst (Figure 6.10(a)) shows a smooth, homogeneous surface, characteristic of a new catalyst. After four cycles of reuse (Figure 6.10(b)), filamentous carbon deposits are clearly visible on the catalyst surface. This confirms the earlier observations of increasing carbon deposition as the cycles proceed.

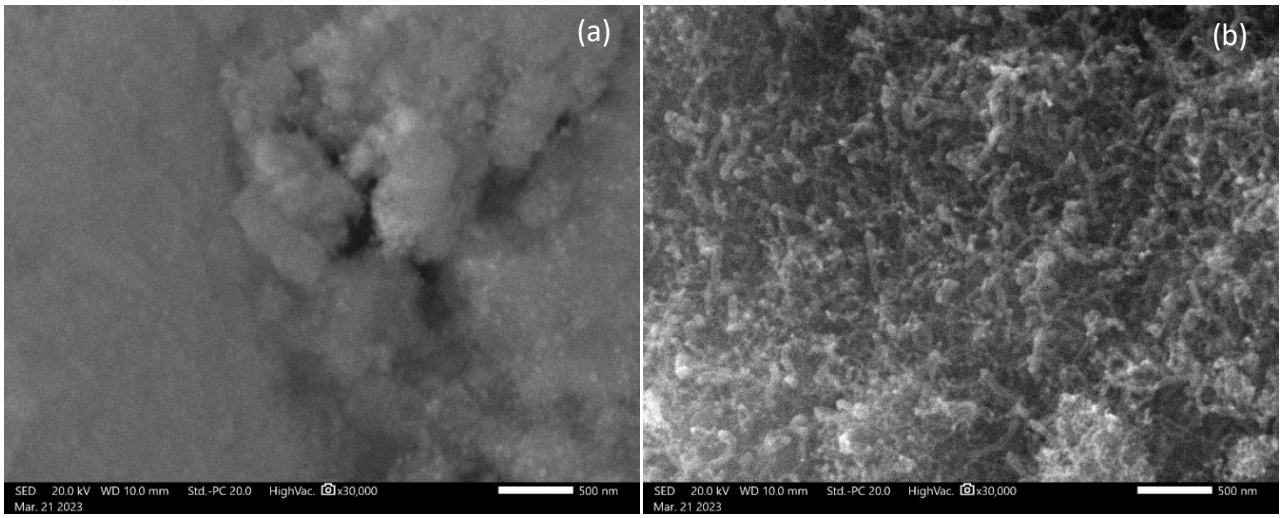

Figure 6.10. SEM images of fresh (a) and spent (b) catalyst showing morphology of the filamentous carbon deposits after four consecutive cycles of reuse.

The formation of these carbon structures could be the primary cause for the observed decrease in gas yield and the slight increase in oil yield over the four cycles. This is because the deposited carbon could obstruct and displace the Ni active sites of the catalyst, inhibiting its activity and efficiency (Li, Chen et al. 2020). The SEM images provide direct evidence of the catalyst's degradation after repeated use, which highlight the importance of developing catalysts resistant to coking or techniques for reducing carbon deposition during the catalytic pyrolysis.

6.4. Summary

In this study, the catalytic pyrolysis of mixed plastic waste for the simultaneous production of valuable products and CO_2 capture using a Ni-Al_2O_3 catalyst was investigated. The results revealed the following findings:

1. The highest syngas yield (52.3 wt%) and CO_2 conversion (0.58 g_{CO2} $g^{-1}_{plastic}$) were obtained at a temperature of 700 °C, 60 mol% of CO_2, and C:P 33.3 wt%. However, these conditions also lead to high carbon deposition of 10.7 wt%.
2. The conditions for maximizing CO_2 conversion while minimizing carbon deposition were at 700 °C, a CO_2 concentration of 60 mol%, and a C:P of 16.04 wt%. The syngas yield was 34.25 wt%, a CO_2 conversion of 0.389 g_{CO2} $g^{-1}_{plastic}$ and a carbon deposition of 4.65 wt%.
3. Maximum monomer recovery (28 wt% of ethylene and propylene) was achieved at a temperature of 700 °C and a low C:P of 10 wt% in the absence of CO_2. This finding

highlights the importance of carefully controlling process parameters to optimize monomer production.

4. The Ni-Al_2O_3 catalyst demonstrated moderate changes in performance over four cycles of use, indicating that it possesses suitable stability and retains most of its activity. However, the apparent stability could be due to the low number of tested cycles, therefore, further investigation is required to assess the long-term stability of the catalyst under various conditions and beyond the four cycles tested in this study.

This research has demonstrated the potential of catalytic pyrolysis for the conversion of mixed plastic waste into valuable products while capturing and converting CO_2. The findings contribute to the development of sustainable and efficient solutions for plastic waste management and greenhouse gas mitigation, advancing efforts towards achieving circularity.

Chapter 7. Technical and economic analysis of hydrothermal liquefaction and pyrolysis of plastic waste

The primary aim of this section is to evaluate the feasibility of the hydrothermal liquefaction (HTL) process for mixed plastic waste at an industrial level, identify the impediments limiting its widespread application, provide valuable insights and recommendations for its scale-up, and draw comparisons with the pyrolysis process. To accomplish this, an exhaustive literature review encompassing the topic of plastic waste HTL, its restrictions, and former research on mixed plastic waste recycling was performed (as outlined in Chapter 2). A process model was developed with the aid of ASPEN Plus simulation software, enabling the analysis of HTL process performance, product yields, material and energy balance, and computation of processing and equipment expenditure. Subsequent to this, an economic analysis involving capital and operational expenditure, process profitability, economic viability, and sensitivity analyses was conducted. This facilitated the recognition of key factors influencing the economic performance and feasibility of the process.

HTL experiments were initially performed during the first months of 2020, however, the laboratory equipment available at the time had a maximum temperature limit of 350 °C and was unsuitable for operation at supercritical conditions. Therefore, from the mixed plastic waste samples, only PET achieved decomposition, while HDPE, LDPE, PP, and PS remained chemically unchanged and only melted. An image of one of the failed experiments is shown in Appendix F. During the COVID-19 pandemic, the study moved to a paper-based techno-economic analysis of HTL at supercritical conditions and its comparison to pyrolysis.

A fraction of the theoretical aspects of this chapter, primarily regarding the fundamentals of the HTL process, has been previously published in the book *Liquid Biofuels: Fundamentals, Characterization, and Applications*, specifically in Chapter 5 – Co-liquefaction of biomass to biofuels (DOI: 10.1002/9781119793038.ch5) (Martínez-Narro and Phan 2021).

7.1. Hydrothermal liquefaction

7.1.1. Background

HTL has recently emerged as a promising technique for addressing the issue of mixed plastic waste. This thermochemical process proposes a method for converting plastic waste into valuable end-products including chemicals and monomers. Nevertheless, present limitations

in the HTL process include the inability to decompose polyolefins under subcritical conditions, the demand for exceedingly high pressures and robust equipment, and challenges associated with scaling up the process for industrial applications. A technical and economic analysis (TEA) of the HTL process is crucial for comprehending the process feasibility, identifying potential improvements, and evaluating the overall viability of this chemical recycling method. Through the implementation of a TEA, this chapter seeks to contribute to the current knowledge of chemical recycling by addressing prevailing limitations, offering insights into process optimization, and evaluating the prospective profitability of HTL within the context of mixed plastic waste management.

Scope and limitations

This chapter will concentrate on polyolefins, the predominant constituents of plastic waste streams. The production of liquid products via the HTL process is the main focus, rather than gases, which are typically associated with supercritical water gasification. Given that this study will not involve experimental work, numerous assumptions regarding feedstock compositions and impurities, interactions among feed components, and product yields and compositions are made. Furthermore, assumptions related to the economic analysis are also requisite, including tax, inflation, and discount rates, plant capacity, and key processing equipment. The HTL product compositions are based on literature outcomes, and the study will depend on existing data and information from external investigations. Despite these constraints, the results of this research will provide valuable insights into the technical and economic aspects of the HTL process for mixed plastic waste recycling.

Although this chapter predominantly focuses on assessing the technical and economic feasibility of HTL, a TEA of pyrolysis is also undertaken to facilitate comparative analysis between the two processes. The economic advantages of pyrolysis are demonstrated employing experimental yields and product compositions presented in Chapter 5. Furthermore, the key distinctions, challenges, and merits associated with both processes are explored and discussed.

7.1.2. Methods

The process simulation software ASPEN Plus was utilised to generate the process flow diagram, and material and energy balances. The heat exchanger was designed and modelled

employing ASPEN Exchanger Design and Rating (EDR), and the cost of utilities was evaluated by ASPEN Process Economic Analyzer (APEA) based on the material and energy balances.

Plastic waste feedstock

The main components of plastic waste streams are polyolefins (i.e., HDPE, LDPE, PP, and PS) and polyesters (PET and PU). As discussed in Chapter 2, polyesters can be readily depolymerised by HTL at subcritical conditions due to the presence of hydrolysable functional groups in their polymeric chain. Therefore, as polyolefins represent the main challenge for HTL and constitute the majority of plastic waste streams, these plastics were selected as feedstock for this study. Due to the lack of complete physical property sets for polymers in ASPEN Plus (e.g., incomplete enthalpies of formation), n-heptacontane ($C_{70}H_{142}$) was utilised as a model compound for the plastic feed since it is a long-chain linear hydrocarbon. The average elemental composition of polyolefins (presented in Chapter 3, Table 3.1) is 85.8 wt% carbon and 12.4 wt% hydrogen, which is in good agreement with that of n-heptacontane (85.5 wt% C and 14.5 wt% H).

HTL process description

Process flow diagram

The hydrothermal liquefaction process is designed to efficiently convert waste plastics into valuable hydrocarbon products under supercritical water conditions. This thermochemical method takes advantage of the unique properties of water at supercritical conditions, which lead to the solubilization of plastics. The HTL process, depicted in Figure 7.1, begins with the waste plastics being ground to a particle size of approximately 5x5 mm, which ensures effective mixing and interaction with the supercritical water.

The ground plastics are subsequently mixed with pre-heated water to form a slurry with a composition of 20 wt% plastics and 80 wt% water. This slurry is then heated and fed to the HTL reactor, which operates at a temperature of 450 °C and a pressure of 25 MPa. Upon completion of the reaction in the HTL reactor, the product stream is depressurized to 1 atm and cooled down to 20 °C using a heat exchanger. Following this cooling step, the non-condensable gases are separated from the product mixture in a flash tank. The ash and solid residues generated during the process are separated from the product stream using membrane filters. Although the ash content seems to be low at 2.3 wt%, a plant operating at a feed rate of 400 t d^{-1} would produce 9.2 t d^{-1} of ash, which is a substantial amount that needs

to be separated by a system of filters and subsequently disposed of via landfill. The remaining liquid products are then directed to a decanter, where the oil products are separated from the aqueous phase, which is recirculated back into the system.

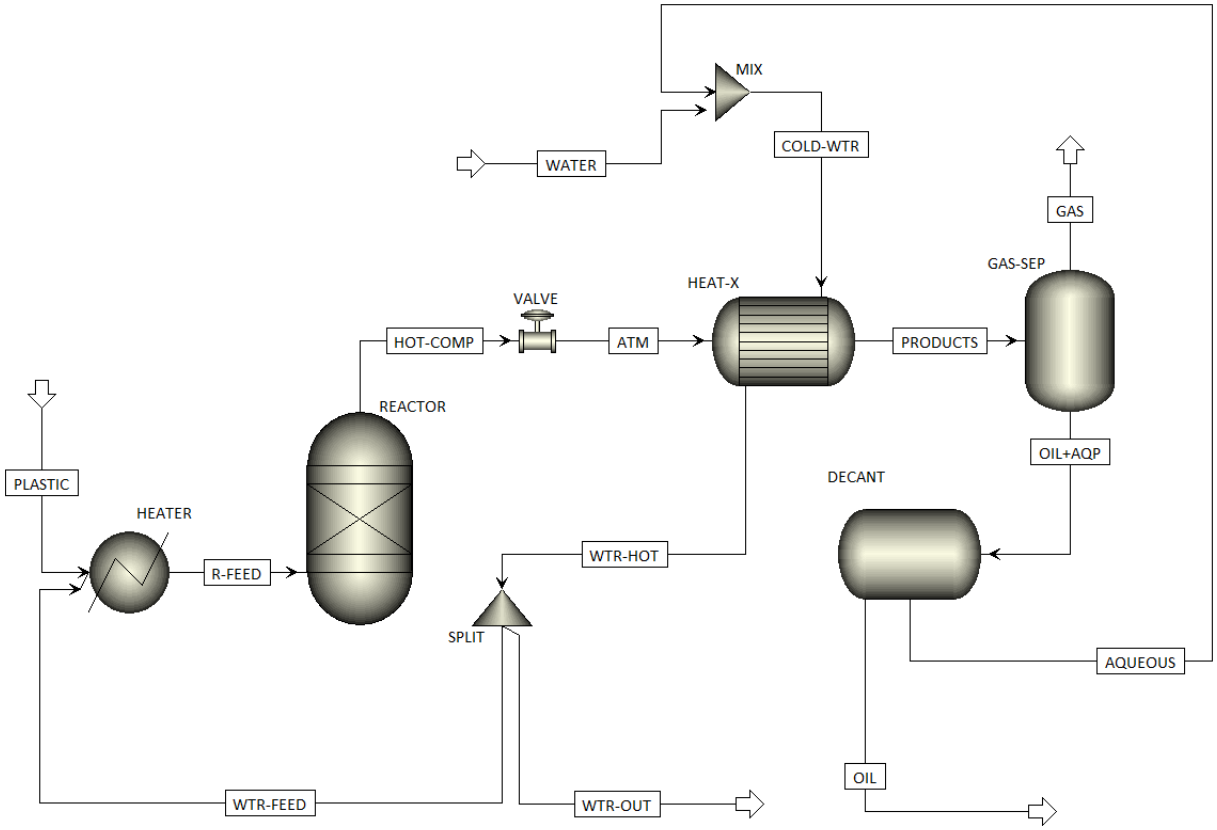

Figure 7.1. HTL process flow diagram.

Input parameters and assumptions

In order to construct a reliable model and conduct a meaningful technical and economic analysis of the HTL process, several key assumptions have been made. These assumptions, while simplifying the process simulation and analysis, provide a practical and reasonable approximation of the process and are important to the validity of the ASPEN Plus model and the overall analysis, and they are as follows:

- Adequate simulation of feed and products using model compounds. Due to the complexity of the plastic waste feed and the HTL products, it is assumed that these can be adequately simulated using model compounds in the ASPEN Plus. This assumption simplifies the process simulation and helps to get a straightforward approximation of the process performance and product yields.
- This study assumes that all carbon fed into the HTL process will be completely converted into liquid or gaseous products.

- The price of HTL liquid products resembles the price of naphtha. In the economic analysis, it is assumed that the HTL liquid products can be sold at a price similar to that of naphtha. This assumption is based on the similar composition and energy content of the HTL liquid products and naphtha, and it provides a basis for estimating the potential revenue from the HTL process.
- Minimal transfer of carbon into the aqueous phase. It is assumed that the carbon content of the plastic waste feedstock is primarily converted into the liquid and gaseous products, with minimal transfer into the aqueous phase. This assumption is supported by other studies found in literature, where negligible carbon content in the aqueous phase is reported (Chen, Jin et al. 2019, Zhao, Yuan et al. 2021).

The base scenario considered for this study is centred on an industrial-scale plant capable of processing 400 t d^{-1} of dry plastic feedstock. The HTL reactor used in this study is modelled using a yield reactor block, for which the product yields must be specified within the input parameters. The liquid products obtained from HTL were categorized into three distinct fractions: light (naphtha-range), medium (diesel-range), and heavy (wax). The model compounds representing these fractions in the simulation are n-octane, n-hexadecane, and n-octacosane respectively. For gaseous products, ethane was used as the model compound. Literature studies focusing on the HTL of polyolefins are extremely scarce, with most studies concentrating on PE and PP. Only a single study has been found to report on the HTL of PS in supercritical water. As such, the product yields and compositions used for this analysis were derived from available literature, specifically outlined in Table 7.1.

The work of Chen et al. (Chen, Jin et al. 2019) and Zhao et al. (Zhao, Yuan et al. 2021) served as a primary source for this data as their research reports oil results in terms of hydrocarbon fractions, making it compatible with the scope of this study. For the purpose of this simulation, the feed composition was assumed to consist of 50 wt% PP and 50 wt% PE. The yield of each product was subsequently calculated by multiplying the individual contributions from PP and PE by 0.5 and summing the results. The calculated yield for each product, presented in Table 7.2, was then incorporated as a specification in the reactor block of the ASPEN Plus model.

Table 7.1. Product yields and compositions of recent HTL studies conducted on polyolefins.

Plastic feed	Process conditions		Product yields / wt%				Compositions		Reference
	Temp. / °C	Pressure / MPa	Gas	Oil	Aqueous	Solid	Gas	Oil / wt% of total oil	
PP	450	23	4.5	91	--	4.5	C1-C5	Naphtha: 75 Diesel: 16 Heavy: 11	(Chen, Jin et al. 2019)
PP	450	29 – 40	4	90	4.5	1.5	C2-C4	--	(Colnik, Kotnik et al. 2022)
PP	400	25	12.4	86.4	--	1.2	--	Naphtha: 28 Diesel: 36 Heavy: 36	(Zhao, Yuan et al. 2021)
LDPE	400	25	12.8	87	--	0.2	--	Naphtha: 20 Diesel: 30 Heavy: 50	
HDPE	450	23	11	83	--	6	--	--	(Jin, Vozka et al. 2020)
PS	450	25	50	47	1	2	--	--	(Seshasayee and Savage 2020)

Table 7.2. Simulated product composition and representative model compounds.

Product	Model compound	Composition / wt%
Gas (C1 – C4)	Ethane (C2)	8.6
C5 – C12 (naphtha range oil)	N-Octane (C8)	43.4
C10 – C25 (diesel range oil)	N-Hexadecane (C16)	21
Wax (C25+ wax)	N-Octacosane (C28)	27

Operating parameters, such as temperature and pressure, were informed by the studies displayed in Table 7.1. Based on these studies, a temperature of 450 °C and a pressure of 25 MPa were selected for the simulation, as these conditions appear to yield the most favourable oil outputs.

The thermodynamic property method employed for the process unit operations in the ASPEN Plus simulation was the Peng-Robinson equation of state (PR-EOS). This method is highly suitable for modelling processes related to refinery applications due to its precision in calculating properties of hydrocarbon systems and light gases (Carlson 1996). Since PR-EOS is unsuitable for highly polar molecules, a separate fluid property package, Steam NBS, was used for the water component. The thermodynamic property tables from this method are based on the International Association for the Properties of Steam (IAPS) formulation, and are suitable for estimating properties of water at supercritical conditions (Haar 1984, Sharma, Pilkhwal et al. 2010). During a chemical process simulation, it is crucial to select the appropriate thermodynamic property methods and be aware of their potential limitations to avoid errors. While the PR-EOS can handle non-ideality, there are conditions or compounds where its accuracy might be compromised, such as in predicting critical points and the need for binary interaction coefficients for mixtures (Wu and Prausnitz 1998). These thermodynamic inaccuracies can significantly impact the TEA of a processing plant. This can result in errors in equipment sizing, increased operational costs, safety concerns, higher capital investments, and reduced profitability or feasibility of the plant.

Technical and economic analysis methodology

A comprehensive economic analysis of a project also requires several assumptions. These include the expected lifetime of the plant, plant capacity, operating hours, discount rate, tax rate, inflation rate, depreciation rate, capital charges, maintenance costs, and local taxes. The plant's expected lifetime and capacity play a significant role in determining the depreciation period, equipment sizing, and net present value calculations. Operating time directly influences the production rates, operating costs, and labour requirements. The discount rate embodies the time value of money and the opportunity cost of capital, while the tax rate has a direct bearing on the project's net income and cash flows (Harden 2014). The inflation rate can impact costs, revenues, and the real versus theoretical financial performance of the project. The depreciation rate determines the rate at which the plant's capital assets lose their value over time, which in turn affects tax calculations and cash flows (Internal Revenue Service 2022). Maintenance costs, included in operating costs, pertain to the upkeep and repair of the plant's equipment and facilities. Lastly, local taxes, levies, or fees instituted by local governments can influence the project's overall costs and cash flows. Documenting these assumptions is critical, and sensitivity analyses should be conducted to comprehend the

impact of changes in these key assumptions on the economic viability of the project. This approach allows for a robust but flexible understanding of the financial feasibility of the HTL process. The assumptions for this study are outlined in Table 7.3, and are based on typical values for chemical manufacturing plants (Sinnott 2005). Additionally, it is assumed that the source of the plastic waste is close to the waste processing facility and the transportation costs are not included in the analysis.

Table 7.3. Assumptions for the economic evaluation.

Plant location	UK
Plant life	20 years
Plant capacity	400 t d^{-1}
Operating time	8000 h a^{-1}
Discount rate	8%
Tax rate	20%
Inflation rate	2%
Plant salvage value	20% of fixed capital
Maintenance	5% of fixed capital
Operating labour	5% of fixed capital
Supervision	20% of operating labour
Plant overheads	50% of operating labour
Capital charges	10% of fixed capital
Insurance	1% of fixed capital
Local taxes	2% of fixed capital
Miscellaneous materials	10% of maintenance cost

Capital cost assessment

The estimation of purchased equipment cost and overall fixed capital cost of the HTL plant was carried out by utilising equation 7.1:

$$C_e = bS^n \tag{7.1}$$

Where C_e is the purchased equipment cost (£), b is a cost constant related to the equipment, S is the characteristic size parameter, and n is the index for the type of equipment. The values for this equation were obtained from (Sinnott 2005), and the results from the system mass balance were utilised to determine the size parameter. Since the values estimated by equation 7.1 are based on costs from the year 2004, the present cost of the equipment in 2023 was calculated by considering the historic inflation rate through the future value equation (Mankiw 2020):

$$FV = PV(1 + r)^n \tag{7.2}$$

Where FV stands for future value, PV is the known cost in a previous or present year, r is the inflation rate, and n is the difference in years. The 10-year average inflation rate of the UK (3.07 % (European Central Bank 2023)) was used for this study.

The Lang factor is a simple factorial method used in the early stages of industrial plant design to estimate the total installation cost of a project based on the cost of the major processing equipment (Bauman 1964). The method is essentially the employment of a ratio that represents the relationship between the total installed cost of a plant and the cost of its major processing equipment, as shown in equation 7.3:

$$C_T = \left(f_{L,DC}\right) \times \left(f_{L,IC}\right) \sum_{i=1}^{n} \left(C_{e,i}\right) \tag{7.3}$$

Where C_T is the overall capital cost of the plant, $f_{L,DC}$ is the sum of the direct cost Lang factors for the corresponding process category, $f_{L,DC}$ is the sum of the indirect cost Lang factors, and $C_{e,i}$ is the purchased cost of an individual equipment. The direct cost items involved in the construction of a plant include equipment installation, piping, instrumentation, utilities, storages, electrical, buildings, site development, and ancillary buildings, while the indirect costs include design and engineering, contractor's fee, and contingency (Sinnott 2005).

The reactor purchased cost was assumed to be 11,389,410 USD, as reported by Knorr et al. (Knorr, Lukas et al. 2013) in 2011 for a continuous biomass HTL plant of similar size to the one considered in this study. After converting the cost to GBP at the average exchange rate of 2011 (USD = 0.6337 GBP (Exchange Rates UK. (2011) 2023)) and after applying equation 7.2, the total purchase cost for 2023 is £ 7,217,469.

Operating cost assessment

The direct production costs associated with the process include maintenance, operating labour, supervision, plant overheads, capital charges, insurance, local taxes, miscellaneous materials, utilities, and feedstock (Sinnott 2005). These were estimated by applying distinct percentages of the fixed capital cost, maintenance cost and operating labour. Ash disposal is considered a fixed operating cost and is accounted for in the overall cost estimation through the Plant Overheads category along with other costs such as general management, and plant security.

Economic evaluation

Since the majority of polyolefin HTL products are naphtha-range hydrocarbons, as shown in Table 7.1, the price of naphtha was used to calculate the profits of the HTL process. The average monthly price of naphtha was 792.8 USD t^{-1} from 2020 – 2022 (Krungsri Research 2022). This price was converted into GBP at an exchange rate of 0.8 (May 2023) and multiplied by the annual production of oil from the HTL process to estimate the total revenue.

The operating income was adjusted to inflation:

$$OI_n = (R_n - OC_n) \times (1 + IR_n) \tag{7.4}$$

Where the subscript *n* indicates a particular year, OI is the adjusted operating income before depreciation (£ a^{-1}), R is the revenue, OC are the annual operating costs of the plant, and IR is the inflation rate.

Depreciation represents an annual tax deduction, enabling the recovery of the cost or underlying value of specific assets throughout their utilization period (Internal Revenue Service 2022). This deduction accounts for the wear and tear, decline, or obsolescence of such property over time. The depreciation expense is calculated by the straight line method shown in equation 7.5 (Kim, Ko et al. 2016):

$$DE = \left(\frac{C_T - SV}{PL}\right) \tag{7.5}$$

Where DE is the constant annual depreciation expense (£ a^{-1}), SV is the salvage value (i.e., the residual value of the plant at the end of its service life, in £), and PL is the plant life. The salvage value can be assumed to represent a fraction of the initial capital cost, with the default APEA value for the UK being 20% (Fivga and Dimitriou 2018).

The taxes (T) were estimated by applying the tax rate (TR) to the taxable income, i.e., the difference between the operating income and the depreciation expense as shown in equation 7.6, which allowed the subsequent calculation of the cash flow after taxes (CFAT) (Creese 2018):

$$T_n = (OI_n - DE_n) \times TR \tag{7.6}$$

$$CFAT_n = OI_n - T_n \tag{7.7}$$

As indicated by the subscripts in equations 7.4 – 7.7, the cash flow is presented as the value in a particular year, however, this does not adequately reflect the time value of money, i.e.,

the money earned in the earlier years of a project is more useful than that earned in later years (Glendinning 1988). Therefore, it is useful to estimate the value of a plant based on its expected future cash flows. To this end, a discounted cash flow (DCF) analysis was conducted by applying a discount rate (r) to the CFAT of each period to determine the present value (PV) of expected future cash flows as shown in equation 7.8 (Sinnott 2005):

$$PV_n = \frac{CFAT_n}{(1+r)^n} \tag{7.8}$$

The PV of each period can be utilised to create a cumulative cash flow diagram by plotting the initial capital investment and then adding the net cash flows for subsequent periods. This provides a visual representation of the project's financial performance over time and allows the identification of the pay-back time, i.e., the point at which the cumulative cash flow becomes positive, and the initial investment is paid off.

To determine if the project is profitable, the net present value (NPV) must be calculated by subtracting the fixed capital cost to the summation of discounted present values using equation 7.9 (Gallo 2014):

$$NPV = \sum_{n=1}^{n=t} \frac{PV_n}{(1+r)^n} - C_T \tag{7.9}$$

A net present value greater than zero indicates that the project is profitable, while a negative one means that the capital investment would not be paid off in the considered project's life.

7.1.3. Results and Discussion

HTL process simulation results

The PFD illustrating the main mass and energy balance results is depicted in Figure 7.2. The complete summary of the material and energy balances for each stage and stream of the HTL system is presented in Table 7.4.

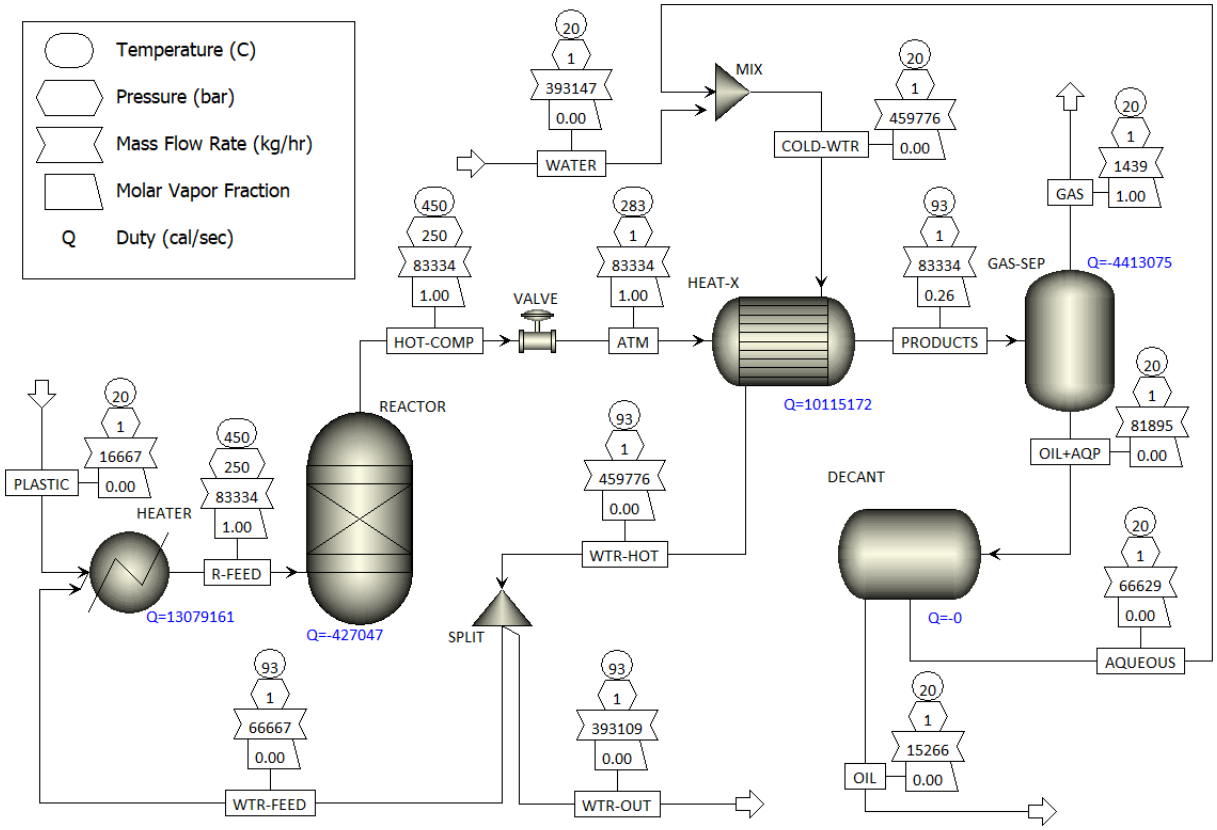

Figure 7.2. HTL process flow diagram indicating material and energy balances in each unit.

The heat energy required for the decomposition of plastic (denoted as reactor yield heat duty) was determined to be -1.786 MW, representing 3.26% of the total energy needed to elevate the plastic feed and water medium to the operational conditions. The depressurization stage, implemented via a valve at the reactor outlet, reduces the product temperature from 450 °C down to 283 °C before it proceeds through the heat exchanger. This step effectively removes 77.3% of the initially supplied energy. The heat exchanger operates with a cooling water flow rate of 393.1 m^3 h^{-1} at 20 °C, which is combined with 66.7 m^3 h^{-1} of the recirculated aqueous phase. Of this mixture, 72.1 m^3 h^{-1} is redirected back into the heater. The design and operation details of the heat exchanger are summarised in Table 7.5.

Table 7.4. HTL process stream summary.

Description	Units	PLASTIC	WTR-FEED	R-FEED	HOT-COMP	ATM	COLD-WTR	WTR-HOT	WTR-OUT	PRO-DUCTS	OIL +AQP	GAS	AQUE-OUS	OIL
From		--	SPLIT	HEATER	REAC-TOR	VALVE	MIX	HEAT-X	SPLIT	HEAT-X	GAS-SEP	GAS-SEP	DECANT	DECANT
To		HEATER	HEATER	REACTOR	VALVE	HEAT-X	HEAT-X	SPLIT	--	GAS-SEP	DECANT	--	MIX	--
Phase		Liq.	Liq.	Vap.	Vap.	Vap.	Liq.	Liq.	Liq.	Mixed	Liq.	Vap.	Liq.	Liq.
Temperature	°C	20.0	93.7	450.0	450.0	282.9	20.0	93.7	93.7	93.2	20.0	20.0	20.0	20.0
Pressure	atm	1.00	0.94	246.73	246.73	1.00	1.00	0.94	0.94	0.83	0.83	0.83	0.83	0.83
Mass Flows	kg h^{-1}	16667	66667	83334	83334	83334	453592	453592	386925	83334	81895	1439	66629	15266
WATER	kg h^{-1}	0	66667	66667	66667	66667	453592	453592	386925	66667	66648	19	66629	19
ETHANE	kg h^{-1}	0	0	0	1433	1433	0	0	0	1433	81	1353	0	81
N-C8	kg h^{-1}	0	0	0	7233	7233	0	0	0	7233	7166	67	0	7166
N-C16	kg h^{-1}	0	0	0	3500	3500	0	0	0	3500	3500	0	0	3500
N-C28	kg h^{-1}	0	0	0	4500	4500	0	0	0	4500	4500	0	0	4500
N-C70	kg h^{-1}	16667	0	16667	0	0	0	0	0	0	0	0	0	0
Mass Frac.														
WATER		0.000	1.000	0.800	0.800	0.800	1.000	1.000	1.000	0.800	0.814	0.013	1.000	0.001
ETHANE		0.000	0.000	0.000	0.017	0.017	0.000	0.000	0.000	0.017	0.001	0.940	0.000	0.005
N-C8		0.000	0.000	0.000	0.087	0.087	0.000	0.000	0.000	0.087	0.088	0.047	0.000	0.469
N-C16		0.000	0.000	0.000	0.042	0.042	0.000	0.000	0.000	0.042	0.043	0.000	0.000	0.229
N-C28		0.000	0.000	0.000	0.054	0.054	0.000	0.000	0.000	0.054	0.055	0.000	0.000	0.295
N-C70		1.000	0.000	0.200	0.000	0.000	0.000	0.000	0.000	0.000	0.000	0.000	0.000	0.000
Volume Flow	m^3 h	2.7	72.1	652.3	647.5	174600	454.2	490.4	418.3	36591	88.4	1333	66.7	21.7
Average MW		983.9	18.0	22.4	21.7	21.7	18.0	18.0	18.0	21.7	21.6	30.9	18.0	163.6
Vap. Fraction		0	0	1	1	1	0	0	0	0.39	0	1	0	0
Liq. Fraction		1	1	0	0	0	1	1	1	0.61	1	0	1	1
Solid Frac.		0	0	0	0	0	0	0	0	0	0	0	0	0
Enthalpy	kJ kg^{-1}	-1749	-15660	-10515	-10592	-10592	-15995	-15660	-15660	-12413	-13401	-2894	-15995	-2082
Entropy	kJ $kg^{-1}K^{-1}$	-7.26	-8.38	-3.96	-3.92	-2.00	-9.40	-8.38	-8.38	-6.68	-9.03	-5.72	-9.40	-7.43
Density	kg m^3	6222.3	924.9	127.8	128.7	0.5	998.8	924.9	924.9	2.3	926.2	1.1	998.8	703.2
Heat capacity	kJ $kmol^{-1}$ K^{-1}	1830.1	82.6	87.0	89.2	46.4	81.5	82.6	82.6	77.0	87.7	53.6	81.5	332.8

The main energy losses in the system are in the separation units and especially the cooling water stream, as only 14.5 % of the hot water is recirculated and the rest leaves the system.

The simulation results reveal critical information regarding the energy requirements and potential cost savings for the HTL process. In the modelled process, the heater's heat duty responsible for raising the plastic feed and pre-heated water from 93 °C to the reaction conditions of 450 °C and 25 MPa is 54.7 MW. The inclusion of a heat exchanger in the process allows for significant energy recovery, leading to a 10.18% reduction in the heater's energy input before the reactor. Without water recirculation, the process would necessitate a considerably higher energy input of 60.9 MW to elevate water from ambient temperature (20 °C) to 450 °C. The efficient utilization of energy results in substantial cost savings. Specifically, the utility cost associated with natural gas for heating is reduced from £ 9,776,286 to £ 8,781,060 with hot water recirculation. These figures underscore the critical role of a well-designed heat exchanger in the system and demonstrate the economic advantage of pre-heating the water prior to introducing it to the reactor.

Table 7.5. Heat exchanger shell and tube general results.

Overall results	
Hot stream location	Tubes
Heat duty	43.16 MW
Required exchanger area	1048.4 m^2
Actual exchanger area	1046.7 m^2
Avg. heat transfer coefficient	844.7 W m^{-2} K^{-1}
UA	885.7 kW K^{-1}
LMTD	47.6 °C
Vibration indication	NO
Shell and tube thermal results	
Mean metal temperature	69.3 °C
Bulk and wall film coefficient	4.8 kW m^2 K^{-1}
Thermal resistance	0.2 m^2K kW^{-1}

Economic analysis results

Capital and operating costs

The capital investment for the HTL plant, designed to produce 366.4 t of oil per day, is estimated at £60 million as outlined in Table 7.6. A significant portion of this investment is concentrated in the reaction section, with the heater and reactor representing 19.7% and 76.1% of the total capital cost, respectively. These components require robust materials capable of withstanding the process's high-pressure and temperature conditions, which

largely explains their substantial costs. The heat exchanger, specifically designed and optimized for this process using the specialized EDR program, has a more accurate purchase cost estimation derived from APEA, providing a superior precision compared to the standard estimation equation 7.1.

Table 7.6. Capital cost of major equipment items in GBP.

Equipment	Purchased cost		Lang factors		Installed cost / £
	In 2004	In 2023	Direct costs	Indirect costs	
Shredder	5,706	10,135	3.15	1.4	44,695
Pump	167,353	297,267	3.15	1.4	1,310,947
Heater	1,513,900	2,689,122	3.15	1.4	11,859,028
Reactor [a]	7,217,469	10,374,621	3.15	1.4	45,752,079
Heat exchanger [b]	--	201,400	3.15	1.4	888,174
Filters	3,628	6,446	3.15	1.4	28,430
Separation system	30,323	53,862	3.15	1.4	237,531
Total (C_T)					**60,120,884**

[a] Based on the HTL reactor from (Knorr, Lukas et al. 2013), cost from 2011; [b] Calculated by EDR and APEA.

Table 7.7. Plant annual operating and production costs.

Operating costs	Calculation basis	Cost / £ a^{-1}
Maintenance	5% of fixed capital	3,006,044
Operating labour	5% of fixed capital	3,006,044
Supervision	20% of operating labour	601,208
Plant overheads	50% of operating labour	1,503,022
Capital charges	10% of fixed capital	6,012,088
Insurance	1% of fixed capital	601,208
Local taxes	2% of fixed capital	1,202,416
Miscellaneous materials	10% of maintenance cost	300,604
Utilities [a]	APEA calculation	8,781,060
Feedstock [a]	194 £ t^{-1} (Recycled UK Limited 2023)	28,324,000
Operating cost		**53,337,694**
Production cost	= Operating cost / Production rate	**0.4367 £ kg^{-1}**

[a] Based on mass and energy balances.

The yearly operating expenses for the HTL plant, presented in Table 7.7, are projected to be £53,330,024. The significant portions of these costs are attributed to utilities, predominantly natural gas used for heating the reactor, and the feedstock, accounting for 16.4% and 53% of the total operating costs, respectively. A more precise approach, rather than relying on percentages of capital cost, was employed to estimate the utilities cost by incorporating the mass and energy balances from APEA. This brings the production cost to 0.4184 £ kg^{-1}. Notably, this figure is 33% lower than the naphtha selling price considered in this study, further highlighting the plant's potential profitability.

Economic viability and profitability

With a yearly oil production of 122,128 t at a naphtha price of 634.24 £ t^{-1}, the annual revenue from oil products is estimated to be £ 70,586,954, as shown in Table 7.8. Comparing the annual operating costs with the revenue, the economic viability of the plant can be assessed. An accurate assessment of profitability is achieved when the capital costs and depreciation rate of the plant are considered.

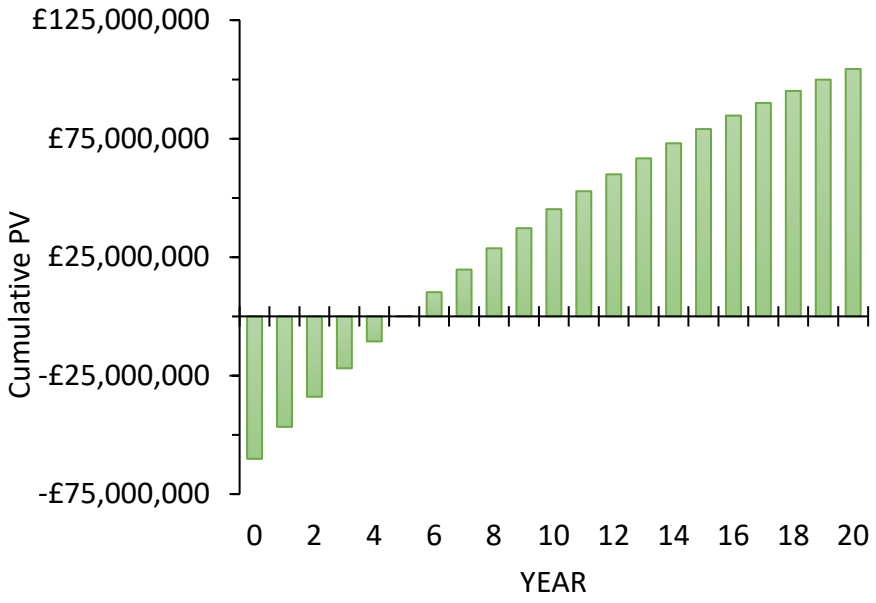

Figure 7.3. Discounted cash flow diagram of the HTL plant.

Table 7.8. Yearly product revenue.

Price of naphtha / £ t^{-1}	634.24
Yearly oil production (8000 h of operating time) / t a^{-1}	122,128
Revenue from oil products / £ a^{-1}	**70,586,954**

The discounted present values for each year of the plant's life are shown in Figure 7.3. The net present value was calculated at £ 104.5 million with an investment pay-back time of 5 years, indicating that the project is feasible and profitable.

Sensitivity analysis

The NPV, a critical indicator of project profitability, is strongly influenced by several key parameters which may fluctuate under different scenarios or specific years. Recognizing the uncertainties associated with these parameters, a sensitivity analysis was conducted to evaluate their potential impact on the economic performance of the project. Specifically, the feedstock cost, plant capacity, product selling price, and discount rate were selected for the

analysis due to their direct influence on both revenue and cost. The analysis examines the variation in these parameters and assesses the resulting changes in NPV and pay-back time, providing a more nuanced understanding of the potential economic viability of the project under varying conditions.

Effect of product selling price (revenue)

A realistic range of values for the selling price of naphtha was selected for the sensitivity analysis based on historical data. According to a report (Trading Economics), the price of naphtha reached its lowest value in the past decade at 138.4 USD t^{-1} in April 2020, and it peaked at 996 USD t-1 in March 2022. Therefore, these values were chosen as the lower and upper bounds for the selling price, providing a realistic examination of the project's potential economic performance under different market conditions.

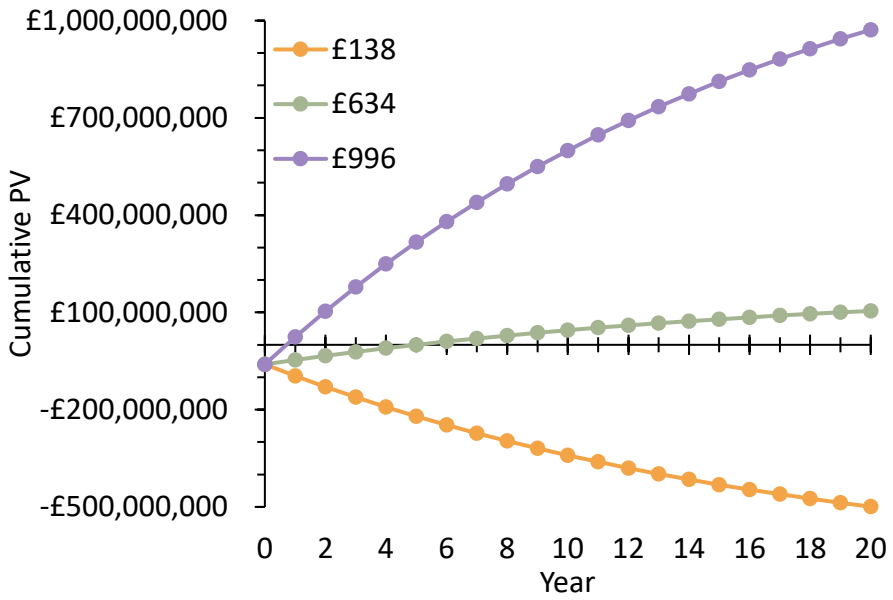

Figure 7.4. Discounted cash flow diagram for the HTL plant at different product selling prices.

The sensitivity analysis for the selling price, presented in Figure 7.4, shows a substantial impact on the project's NPV and payback period, as it influences the project's revenue, and therefore, its profitability. At the lower selling price of £138, the project is economically unfeasible with a negative NPV of about £-499 million, and the project never pays back its initial investment. This scenario suggests that the project is highly sensitive to this parameter, making it critical for the project's success to maintain a selling price above this lower limit.

At the base selling price of £634, the project is economically viable, with a positive NPV of approximately £104.4 million and a payback period of 5 years. This means the project is expected to recover its initial investment in 5 years and generate a profit thereafter.

At the higher selling price of £996, the project is highly profitable, with a remarkable increase in NPV to around £971.5 million and a significantly reduced payback period to only 8 months. The project's substantial profitability at this price level indicates the potential benefits of favourable market conditions or strategic decisions that could increase the product selling price.

The plant's high sensitivity to the selling price of naphtha implies a level of market risk as well. If the selling price were to decrease significantly due to external factors such as increased competition, market saturation, or decreased demand, the project could potentially become unviable. Thus, strategies to mitigate this risk, such as securing long-term contracts at a guaranteed price might be advisable.

Effect of discount rate

Three values for the discount rate were selected to represent a typical range for industrial projects: 4%, 8%, and 12%. The higher value of 12% represents a high-risk investment environment or higher cost of capital, while the lower rate of 4% represents a low-risk project or a period of lower interest rates. Figure 7.5 shows the discounted cash flow diagram at different discount rates.

The results show a strong dependence of the project's NPV on the discount rate, although not as impactful as the previously discussed revenue parameter. In comparison to the base case of 8%, at a higher discount rate of 12%, the NPV drops from £104.4M to £62.5M, and the payback period extends slightly from 5 to 5.7 years. Conversely, with a lower discount rate of 4%, the NPV increases substantially to £172.9M, and the project's payback period shortens to 4.46 years. These results demonstrate the importance of financial conditions for the economic viability of the project. Careful financial planning and risk management in project development are crucial for the success of a project. Obtaining favourable financing conditions that result in a lower discount rate could significantly improve the project's financial performance. In contrast, more challenging financing conditions could extend the project's payback period and reduce its profitability.

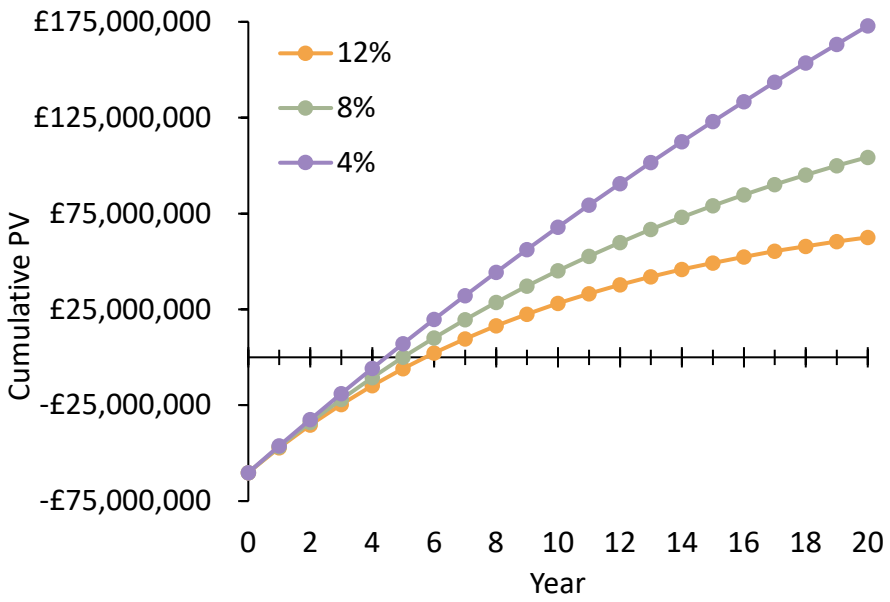

Figure 7.5. Discounted cash flow diagram for the HTL plant at different discount rates.

Effect of plant capacity

The effect of plant capacity, shown in Figure 7.6, was evaluated at a range of ±50% throughput with respect to the base case of 400 t d^{-1}. With a 50% reduction in capacity to 200 t d^{-1}, the project becomes economically unfeasible, as evidenced by a negative NPV of -£50.3M and an undefined payback period. This outcome emphasises the importance of plant uptime and operational efficiency, as reductions in production can significantly prolong or impede the project's ability to recover the initial investment.

On the other hand, increasing the plant capacity by 50% to 600 t d^{-1} leads to a substantial rise in the NPV to £617.8M and a reduction in the payback period to only one year. This denotes the scalability benefits of the project and the potential for enhanced profitability with higher production. Nonetheless, while higher plant capacities increase profitability, as demonstrated by the improved NPV and reduced payback period, they also require a corresponding increase in capital investment. The upfront costs can pose financial challenges and careful cost-benefit analyses must be conducted to determine scaling-up feasibility.

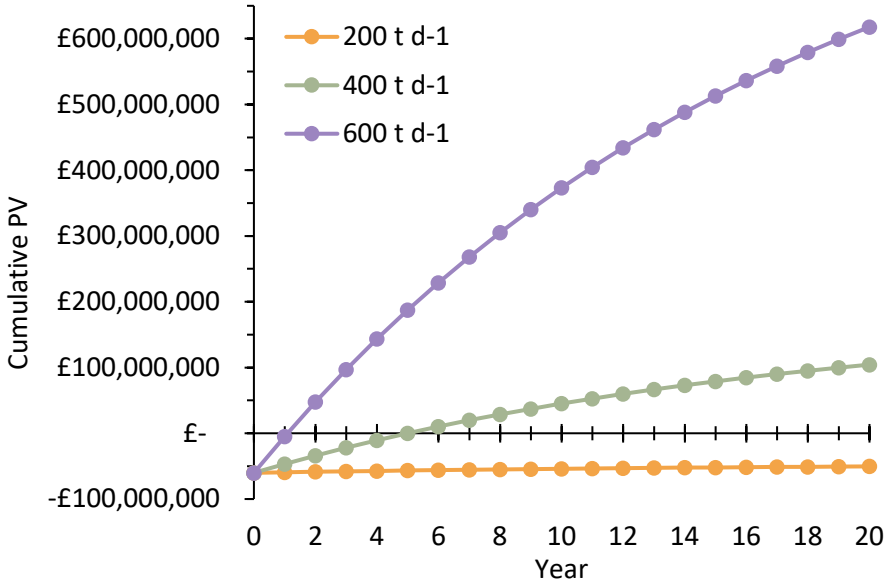

Figure 7.6. Discounted cash flow diagram for HTL plants of different capacities.

Effect of feedstock cost

The cost of feedstock is a critical factor in the economic stability of an industrial-scale chemical recycling plant, and its variability can lead to significant challenges. Fluctuating feedstock prices directly impact operating costs, which in turn can cause profit margins to vary, making it difficult for the plant to maintain financial stability. If the cost of feedstock increases significantly, and the plant is unable to pass these costs onto customers through higher product prices, profitability will inevitably decline. In terms of financial planning, the unpredictability of feedstock costs complicates budgeting efforts. Plants must anticipate potential price increases, which may necessitate keeping a larger reserve of working capital on hand to buffer against these fluctuations. This level of unpredictability can also hinder the plant's ability to make informed long-term financial decisions, such as investing in new technology or expanding operational capacity. Moreover, a volatile feedstock market requires a robust supply chain strategy (Burgess, Holmes et al. 2021). This might involve negotiating long-term contracts with suppliers to stabilize prices or diversifying the sources of feedstock to reduce risk. The pricing strategy for the products must also be flexible; it should account for the variability in feedstock costs to ensure that the plant remains competitive in the market. The current plastic feedstock costs may vary from around 170 to 260 £ t^{-1} (Victory 2021). Therefore, the sensitivity analysis, shown in Figure 7.7, was conducted within this feedstock cost range.

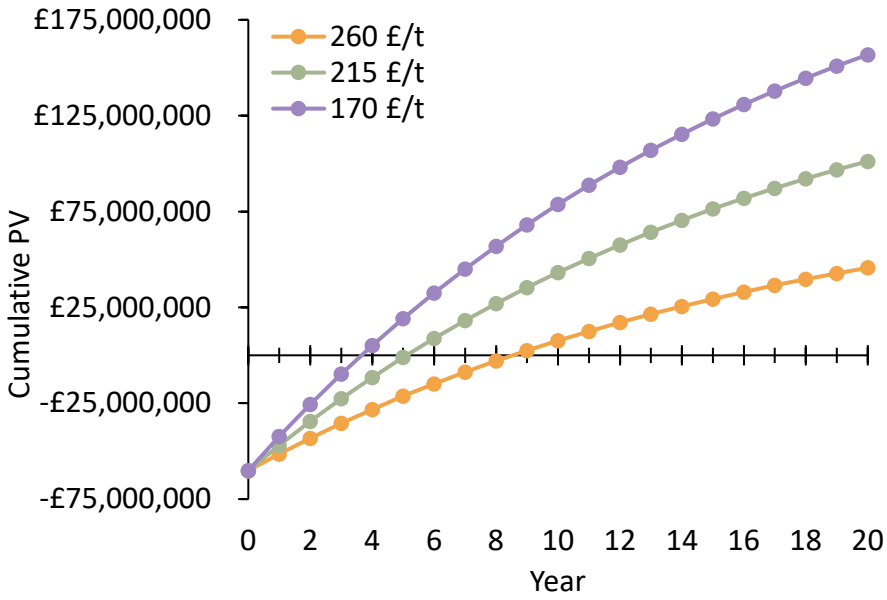

Figure 7.7. Discounted cash flow diagram for the HTL plant at different feedstock costs.

As operations commence, the impact of feedstock cost becomes increasingly apparent. At the lower cost of 170 £ t^{-1}, the plant recovers from its initial investment more quickly, moving into positive NPV after 3.6 years and showing a steady increase in NPV thereafter. In contrast, at £215/t, the plant takes longer to reach a positive NPV, only doing so in the fifth year, while at £260/t, the plant still operates at a loss by the eighth year. This demonstrates a clear correlation between feedstock cost and the time taken to achieve a return on investment. The higher the feedstock cost, the longer the payback period, and the lower the overall NPV over the analysed period. This analysis underscores the sensitivity of chemical recycling plant economics to feedstock pricing, highlighting the need for careful financial planning and the potential benefits of securing long-term, cost-effective feedstock supplies to ensure financial viability and avoid potential risks.

7.2. Technical and economic analysis of pyrolysis

7.2.1. Process description and methods

The process flow diagram, material, and energy balances were modelled employing ASPEN Plus, with the cost of utilities evaluated by APEA, as detailed in section 7.1.2. The Peng-Robinson equation of state was also utilised for modelling the pyrolysis plant.

Plastic waste feedstock

The plastic waste composition was the same used for the plastic mixtures in Chapters 5 and 6, comprising 20% HDPE, 28.5% LDPE, 27.5 PP, 9% PS, and 15% PET. The model compound n-

heptacontane ($C_{70}H_{142}$) was utilised to represent the mixture of polyolefins. Since 15 wt% of PET is present in the feed, and PET is comprised of 33.33 wt% of oxygen, 5 wt% O_2 was added to the feed to account for the oxygen content of PET and keep the element balance. The same plant capacity as that of the HTL section (7.1) was maintained (400 t d^{-1}) to enable comparisons with the economic performance of both processes.

Input parameters and process flow diagram

The plastic is fed to the pyrolysis reactor which operates at 500 °C. This temperature was chosen because it results in the highest oil yield (66.6 wt%). The heat input to the reactor is entirely provided by direct combustion of the char produced by pyrolysis and a fraction of the non-condensable gases in a separate combustion unit, as shown in Figure 7.8. Following pyrolysis, the solid char is separated in a cyclone and fed to the combustion unit. The condensing system consists of three separate units in series at different temperatures in order to separate the products by boiling point distribution. This results in heavy waxes and high-boiling-point compounds collected from the first condenser at 200 °C. The rest of the volatiles are conducted to the next condensing units at 100 °C and 10 °C to recover the middle and light fractions, respectively. The non-condensable gases are separated in the las condenser, after which a fraction of the gases is recirculated into a combustion unit to supply energy for the pyrolysis reactor. The split fraction was optimised to obtain the value which results in a temperature of 500 °C at the outlet of the pyrolysis reactor. The rest of the gas can be used in the plant as an alternative energy source for heat or power generation or purified and sold separately.

In contrast to the HTL process described in section 7.1, the product distribution (solid, liquid, and gas yields) was based on the experimental results of thermal pyrolysis from Chapter 5, as shown in Table 7.9. The composition of the gaseous products was the same as that from the thermal pyrolysis experiments, while the liquid composition was simulated utilising the same model compounds as in section 7.1 (i.e., C8 for light hydrocarbon fraction, C16 for the middle fraction, and C28 for heavy waxes) with their composition based on experimental results.

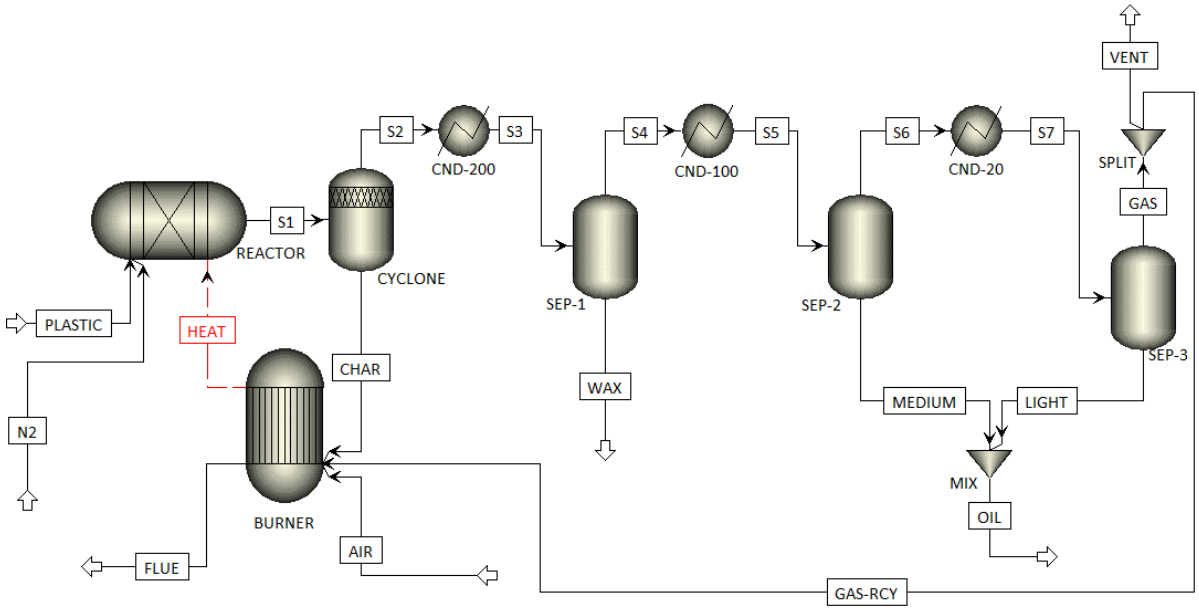

Figure 7.8. Pyrolysis process flow diagram.

Table 7.9. Experimental product yields and compositions of pyrolysis used as input for the ASPEN Plus simulation.

Product	Yield / wt%	Composition / wt% [a]	
Gas	28.6	Methane	0.87
		Ethane	0.96
		Ethylene	2.25
		Propane	1.98
		Propylene	4.60
		Butane	2.95
		Butene	6.88
		Hydrogen	0.08
		Carbon monoxide	2.80
		Carbon dioxide	5.16
Liquid	66.6	Light fraction (C8)	33.71
		Middle fraction (C16)	18.60
		Heavy fraction (C28)	14.36
Char	4.8	Carbon [b]	4.80

[a] wt% with respect to plastic before pyrolysis; [b] Char assumed to consist only of carbon.

7.2.2. TEA methodology

In conducting the TEA for the pyrolysis process, the same methodology and assumptions used in the evaluation of costs and profits from the HTL process (Section 7.1.2.4) was followed. This approach ensured consistency in the analysis, enabling a fair comparison between the two processes.

7.2.3. Results and discussion

Pyrolysis process simulation results

The main results pertaining to material and energy balance from the pyrolysis process simulation are depicted in Figure 7.9. The energy flow required for elevating the temperature of the products to the operational level of 500 °C and enabling the pyrolysis reactions was calculated to be 11.75 MW. In order to generate this requisite heat, the inputs of air and fuel gas to the combustion reactor underwent optimisation to ensure optimal efficiency while keeping the pyrolysis products at the desired 500 °C.

The optimised air intake for combustion was determined to be 23,000 kg h^{-1}. An excess supply of air could compromise the heat transfer to the pyrolysis reactor, necessitating a greater recirculation of fuel gas, leading to significant energy wastage. Simultaneously, the fraction of non-condensable gases from the process to be recirculated to the combustion reactor was also optimized. The ideal recirculation fraction was found to be 13.5 wt%, consisting of 9.9 wt% of combustible gases, 1.52 wt% CO_2, and 88.58 wt% N_2. The low requirement for recirculated gases for combustion can be attributed to the substantial energy contribution from the pyrolysis char. In the absence of char, the combustion reactor would only be able to supply 4.5 MW, causing the pyrolysis reactor temperature to fall short at 246 °C. A complete summary of the pyrolysis process stream mass balance is provided in Appendix G for further reference.

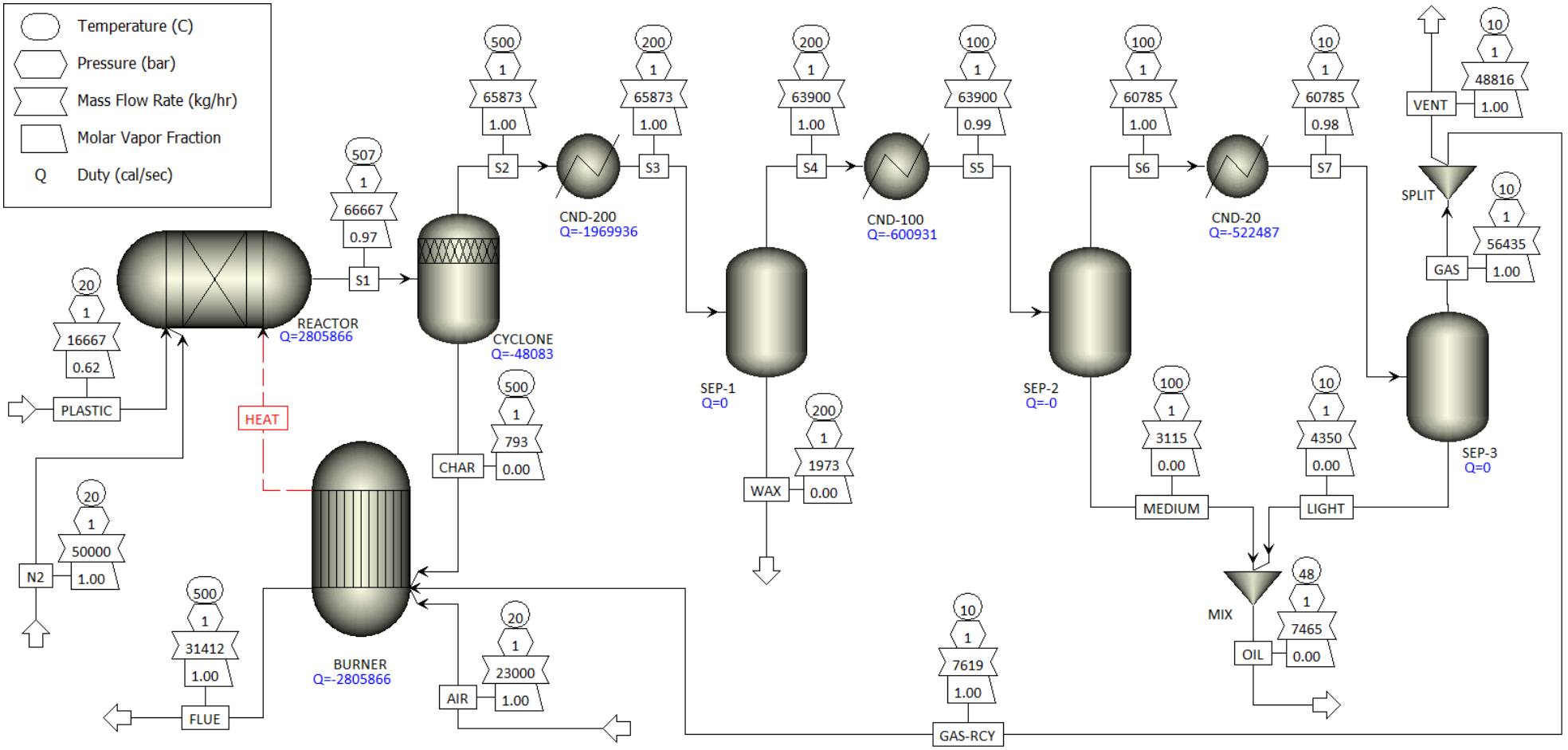

Figure 7.9. Pyrolysis process flow diagram indicating the principal material and energy balances of each unit.

Economic analysis results

The capital costs associated with the major equipment for the pyrolysis process are summarised in Table 7.10. The total capital investment for a plant with the listed equipment is £10,712,476. Analogous to the HTL process, the most significant costs are linked to the reaction section (combustion unit and pyrolysis reactor), accounting for 68.6% of the capital investment.

Table 7.10. Capital cost of major equipment items.

Equipment	Purchased cost / £		Lang factors		Installed cost / £
	In 2004	In 2023	Direct costs	Indirect costs	
Shredder	5,706	10,136	3.15	1.4	44,700
Combustion unit	449,115	797,757	3.15	1.4	3,518,108
Reactor [a]	868,500	1,542,706	3.15	1.4	3,830,085
Condensing system	129,900	230,740	3.15	1.4	1,017,563
Heat exchangers [a]	522,000	927,222	3.15	1.4	2,302,020
Total (C_T)					**10,712,476**

[a] Calculated by APEA, based on material and energy balances.

The annual operating costs for the pyrolysis plant were estimated to be £31,248,370, as shown in Table 7.11. When considering the production rate of the plant, this translates to a production cost of £0.4138 per kg of produced pyrolysis oil. This value is comparable to the production cost associated with HTL, which is £0.4184 per kg. Thus, from a cost perspective, the two processes are remarkably similar in terms of their production costs.

Table 7.11. Pyrolysis plant annual operating and production costs.

Operating costs	Calculation basis	Cost / £ a^{-1}
Maintenance	5% of fixed capital	535,624
Operating labour	5% of fixed capital	535,624
Supervision	20% of operating labour	107,125
Plant overheads	50% of operating labour	267,812
Capital charges	10% of fixed capital	1,071,248
Insurance	1% of fixed capital	107,125
Local taxes	2% of fixed capital	214,250
Miscellaneous materials	10% of maintenance cost	53,562
Utilities [a]	APEA calculation	32,000
Feedstock [a]	194 £ t^{-1} (Recycled UK Limited 2023)	28,324,000
Operating cost		**31,248,370**
Production cost	= Operating cost / Production rate	**0.4138 £ kg^{-1}**

[a] based on mass and energy balances.

When comparing the costs of utilities for the pyrolysis and HTL processes, there is a staggering difference. Pyrolysis requires significantly less expenditure on utilities, costing around £32,000

annually, compared to the £8,781,060 required for HTL. This substantial difference can be attributed to the self-sustaining nature of the pyrolysis process, which directly generates the energy required for operation. This is achieved by combusting a fraction of the process's gaseous output to provide the necessary heat energy, thereby reducing reliance on external energy sources such as natural gas. On the other hand, the HTL process presents higher energy losses, primarily due to the inherent attributes of the process and the properties of the water medium involved (e.g., high specific energy). Despite the employment of a heat exchanger to recover a fraction of the thermal energy, HTL struggles with efficient heat recovery and must depend more heavily on external heat sources, such as natural gas. This is a consequence of the challenge of effectively extracting and reusing all the heat absorbed by the supercritical water, resulting in a significant energy loss. Another notable difference between the two processes lies in the phase separation stage. In HTL, the supercritical conditions blur the distinction between the liquid and gas phases, complicating the separation of oil and water based on their typical physical properties. In consequence, the separation must be conducted in the liquid phase after depressurising and cooling the system, which increases the complexity and potentially the cost of the process due to energy losses.

The revenue generated by the pyrolysis process, presented in Table 7.12, is lower than that of the HTL process. With an annual oil production of 75,504 t (as opposed to HTL's 122,128 t), the revenue from oil products for the pyrolysis process stands at £47,887,657. This is significantly less than the revenue for the HTL process, which is £70,586,954. However, the key factor to consider in an economic analysis is the net present value. Despite the lower revenue, the NPV of the pyrolysis process is £144,278,953, which is higher than the NPV for the HTL process (£104,499,516).

Table 7.12. Yearly product revenue.

Price of naphtha / £ t^{-1}	634.24
Yearly oil production (8000 h of operating time) / t a^{-1}	75,504
Revenue from oil products / £ a^{-1}	**47,887,657**

This indicates that the pyrolysis process, despite generating less revenue, could offer a better return on investment over time. In addition, the payback time is considerably lower for pyrolysis at 1.3 years as shown in Figure 7.10. This is explained by the lower capital and operating costs associated with the pyrolysis process, as well as its self-sustaining process, which reduces the expenditure on utilities.

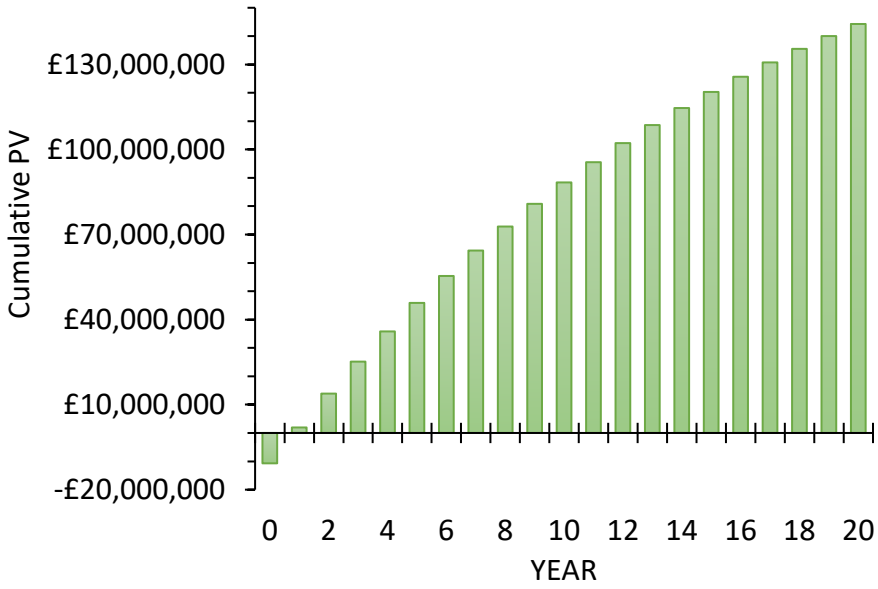

Figure 7.10. Discounted cash flow diagram of the pyrolysis plant.

7.3. Limitations of the study

This study, while rigorously conducted, presents several limitations. One significant constraint lies within the assumptions made for both the technical and economic aspects of the analysis. The composition of the plastic waste feedstock was simulated by a model compound and kept constant for both processes while assuming that the plastic waste was readily available and free from pre-treatment requirements and contaminants. In reality, however, the composition of plastic waste can vary greatly, and steps such as sorting, and cleaning may be necessary. The study also faced limitations due to a lack of literature studies and data availability for the HTL process, which could affect the accuracy of the results. The compositions of the HTL products are based on scarce literature results, which are lab-scale batch experiments that may not exactly reflect those of a scaled-up continuous process.

The ASPEN Plus simulations relied on simplified models, which may not fully capture the intricacies of these operations. In actual practice, these processes involve numerous additional considerations regarding equipment configuration, dimensions, and physical phenomena, such as heat and mass transfer limitations, which can affect the yield and composition of the products. The models also overlooked potential issues related to equipment fouling, which could impact both the productivity and profitability of these processes. Additional equipment and instrumentation may be necessary upstream for feedstock pre-treatment or downstream for product transportation, which was outside the scope of this study.

In regard to the economic evaluation method, the price of naphtha may not accurately represent the actual selling price of the pyrolysis products, as these may differ in quality compared to commercial fossil-fuel-derived naphtha. Additionally, using the net present value approach has its own limitations. The NPV method assumes a constant discount rate, which might not be the case in reality, and does not account for the risks or uncertainties associated with future cash flows. HTL is a process still in early development for plastic waste feeds, and in the absence of enough research data, an accurate estimation of discount rates becomes challenging.

The data used for simulations, as well as the estimated costs, inherently carry a degree of uncertainty, and these uncertainties were not quantified in the study, thus the results should be interpreted with caution. Addressing these limitations in future research could involve refining and expanding the process simulation models, incorporating more realistic assumptions based on actual experiments, and making a more extensive sensitivity analysis, all of which could provide a more robust foundation for decision-making.

7.4. Summary

This study presented a detailed techno-economic analysis of the HTL process and its comparison to pyrolysis. Sensitivity analyses highlighted the impact of selling price, discount rate, and plant capacity on the economic performance of the process. Notably, high variations in selling price dramatically affected the NPV and payback period, highlighting the importance of stable market conditions in the economic viability of the HTL process. Future work could involve a more detailed sensitivity analysis, considering a wider range of parameters and scenarios.

Both the HTL and pyrolysis processes hold potential for the conversion of plastic waste into valuable fuel products. However, they each present their own economic and technical challenges that must be carefully considered. While the HTL process may have a higher oil production and revenue, the pyrolysis process offers lower operating costs and a potentially higher return on investment. HTL requires a high capital investment due to the high-pressure operating conditions and suffers from significant energy losses. Pyrolysis, operating at lower pressure, has less complex and cheaper reactor design, and its energy generation is largely self-sustained, leading to lower utility costs. Despite generating less revenue, pyrolysis has a higher net present value, suggesting a better long-term return on investment. Both processes

have their advantages and challenges, and their economic performance is highly sensitive to factors like selling price, discount rate, and plant capacity.

Chapter 8. Conclusions and recommendations for future studies

Chemical recycling, in the context of sustainability, has become a vital component in the comprehensive management of plastic waste, offering a sustainable and environmentally friendly approach that complements mechanical recycling. It focuses on the efficient recovery of valuable materials from waste plastics, reducing dependence on fossil fuels and minimizing environmental pollution. This approach aligns with the principles of a circular economy, aiming to reintroduce recovered materials back into the production cycle, thereby reducing the need for new raw materials and cutting down the environmental impact. Chemical recycling faces challenges due to the complex compositions of plastic waste, but its development and implementation hold significant potential to address these limitations, contributing to a circular economy and fostering a more sustainable future for plastic materials. These technologies represent a crucial shift towards responsible resource management, balancing development with conservation, and preserving the environment for future generations.

This thesis presents a comprehensive exploration of the chemical recycling of plastic waste. Through a close examination of thermal decomposition kinetics, the influential role of catalysts in pyrolysis, the use of catalytic pyrolysis for simultaneous plastic recycling and CO_2 capture, and a thorough techno-economic analysis of the hydrothermal liquefaction and pyrolysis processes, this research presents a multi-faceted perspective on the complex issue of plastic waste management. Each chapter provides insights that collectively contribute to an overall understanding of this field, highlighting the opportunities and challenges of these thermochemical recycling methods and setting the stage for future research and application in sustainable waste management.

8.1. Conclusions from chapters 4 – 7

8.1.1. Chapter 4 - Thermal decomposition kinetics of plastic waste

- Individual plastics, including PP, PET, LDPE, HDPE, and PS, demonstrate distinct pyrolysis decomposition temperatures and activation energies, furthering the understanding of their thermal behaviours in the context of thermochemical methods for chemical recycling.

- Conventional linear kinetic methods (i.e., single-step KAS and CKA), while generally successful for individual plastics, have limitations in predicting the beginning of decomposition and the rate curve inflections of mixed plastic samples.
- Two-step deconvolution analysis, both kinetic and mathematical, is effective for predicting the early decomposition temperatures of PP and LDPE, indicating the importance of a more detailed modelling approach when dealing with complex decomposition behaviours.
- Kinetic parameters for mixed plastic pyrolysis derived from experimental data and developed using three-step kinetic and mathematical deconvolution analysis are substantially more accurate in predicting experimental data compared to single-step models.
- Kinetics of individual plastics can be successfully used in an additive model to predict the decomposition of any mixture of known composition across a varied temperature range, showing their versatility and robustness.

8.1.2. Chapter 5 - Pyrolysis of mixed plastic waste using biochar supported catalysts

- The choice of catalyst greatly influences the product yield and composition during plastic waste pyrolysis. Ni-BC, Fe-BC, and HZSM-5 outperformed Zn-BC and Raw biochar in terms of catalytic activity.
- Ni-BC and Fe-BC displayed similar trends in product yields, showing increased production of H_2, CO, and CNTs with increasing temperature. Of the two, Ni-BC was found to be the most efficient in producing CNTs, though it produced lower gas yields than Fe-BC.
- HZSM-5 is the most suitable catalyst for pyrolysis at low temperatures (500 °C).
- Both Zn-BC and Raw-BC demonstrated limited efficacy in converting long-chain hydrocarbons into lighter products. Among these two, Raw-BC had moderately enhanced gas yields and reduced oil/wax yields compared to Zn-BC.
- This study has demonstrated that biochar can be a suitable support for Ni-BC and Fe-BC in facilitating the pyrolysis of plastic waste, providing a promising route for H_2 and CNT production.

8.1.3. Chapter 6 - Chemical recycling of plastic waste and CO_2 via catalytic pyrolysis

- The highest syngas yield (52.3 wt%) and CO_2 conversion (0.58 g_{CO2} $g^{-1}_{plastic}$) were achieved at a temperature of 700 °C, with a CO_2 concentration of 60 mol%, and a catalyst to plastic ratio of 33.3 wt%. However, these conditions also led to high carbon deposition (10.7 wt%), suggesting a compromise needs to be made between maximizing syngas yield and minimizing carbon deposition.
- The optimal conditions for achieving the highest CO_2 conversion while minimizing carbon deposition were found to be a temperature of 700 °C, a CO_2 concentration of 60 mol%, and a C:P of 16.04 wt%. These conditions resulted in a CO_2 conversion of 0.389 g_{CO2} $g^{-1}_{plastic}$, a carbon deposition of 4.65 wt%, and a syngas yield of 34.25 wt%.
- The optimal conditions for maximizing monomer recovery (28 wt% of ethylene and propylene) were determined to be a temperature of 700 °C and a C:P of 10 wt% in the absence of CO_2.
- Over four reuse cycles, the Ni-Al_2O_3 catalyst showed moderate deactivation, with gas yields moderately decreasing and oil yields increasing. Carbon deposition on the catalyst surface also decreased with each cycle, suggesting some degree of regeneration by reaction with CO_2.

8.1.4. Chapter 7 - Technical and economic analysis of hydrothermal liquefaction and pyrolysis of plastic waste

- Both the HTL and pyrolysis processes exhibit potential for converting plastic waste into valuable fuel products, but present distinct economic and technical attributes. The HTL process yields higher oil production and revenue but requires substantial capital investment due to its high-pressure operating conditions and suffers from significant energy losses. On the other hand, the pyrolysis process, although generating less revenue, operates at lower pressure, has less complex and cheaper reactor design, and its energy generation is largely self-sustaining. This leads to lower utility costs, shorter payback periods, and higher NPV, suggesting a potentially superior long-term return on investment.
- A crucial difference between the two processes is their energy consumption. Pyrolysis requires significantly lower utility costs, thanks to its self-sustaining nature, in which a fraction of the process's gaseous output is combusted to provide the necessary heat

energy, reducing reliance on external energy sources. This contrasts with the HTL process, which suffers from higher energy losses.

- The economic performance of both processes is highly sensitive to factors such as selling price, discount rate, and plant capacity. Fluctuations in selling price dramatically affect NPV and payback periods, emphasizing the significance of stable market conditions for the economic viability of these processes.
- Since the selling price of HTL and pyrolysis products is critical for the feasibility of industrial-scale plants, there is great potential for chemical recycling to thrive under the auspices of a supportive governmental regulatory framework. If governments were to enact policies that ensure a stable selling price, it would substantially mitigate risks associated with price fluctuations, thereby encouraging the initiation of more chemical recycling projects. Such strategic measures would guarantee the economic feasibility of these ventures, promoting both the growth and sustainability of the chemical recycling industry.

8.2. Recommendations for future work

8.2.1. Chapter 4

- Future studies on kinetics could investigate the interactions between different types of plastics during decomposition, particularly in situations where structurally distinct components are present (e.g., PS and PE), and the composition is varied.
- The effects of impurities (e.g., additives, dyes, plasticiser), as well as different plastic grades, could be explored to have a clear understanding of how these components affect decomposition kinetics and model predictions.
- Investigating the kinetics of plastics in presence of CO_2 at varying N_2:CO_2 mol% ratios would prove useful to confirm if CO_2 influences the thermal decomposition of plastics.

8.2.2. Chapter 5

- Given the promising results obtained with Ni-BC and Fe-BC catalysts, further research could be directed towards optimizing them to achieve higher gas yields. Different catalyst preparation methods or varying the metal loadings on the biochars could be explored to study their impact on product yields and composition.

- While Ni-BC, Fe-BC, Zn-BC, Raw-BC, and HZSM-5 were evaluated in this study, other potential catalysts could be explored. Different metal-based or zeolite catalysts could be tested to determine if they offer improved performance.
- Future work could focus on catalyst reusability tests, assessing their performance over multiple cycles of use to evaluate their long-term stability and the feasibility of catalyst regeneration.
- As pyrolysis involves a complex interplay of temperature, catalyst to plastic ratio, and feedstock composition, a more comprehensive study could be conducted to optimize these parameters to achieve maximum product yield and selectivity.
- Conducting pilot-scale studies in continuous operation would provide insights into the potential viability of using these catalysts for plastic waste pyrolysis at a larger scale than laboratory studies.

8.2.3. Chapter 6

- Test the process with real or simulated industrial flue gases to better characterize the process and improve its relevance to real-world applications.
- Continue to optimize the process conditions to maximize syngas and monomer yields while minimizing carbon deposition by testing a wider range of temperatures, CO_2 concentrations, and C:P ratios.
- Evaluate the long-term stability and reusability of the Ni-Al2O3 catalyst over more cycles and investigate other catalyst materials that may offer better performance.
- Investigate the scalability and economic viability of this approach, which would be critical for its potential adoption in industrial applications.
- Consider the full lifecycle analysis of the process to account for the environmental impact of catalyst production and disposal, as well as the potential benefits of CO_2 capture and plastic waste reduction.
- Explore separation, purification, and upgrading technologies for the produced syngas and monomers in order to produce high-quality materials.

8.2.4. Chapter 7

- Lab- and pilot-scale studies could be carried out to validate the ASPEN Plus simulations and their assumptions. This can help identify the actual bottlenecks in both processes, which are not currently considered in the simulation models.

- Opportunities for energy recovery and heat integration within both processes could be explored to reduce the overall operating costs.
- To better understand the financial risks associated with both processes, a risk assessment could be performed considering uncertainties in key factors such as selling price of products, capital costs, operating costs, and potential technical issues that could arise during the operation of the plant.
- A more detailed sensitivity analysis could be performed, considering a wider range of parameters and scenarios to better assess the robustness of the economic viability of both processes.
- An environmental impact assessment could be conducted to evaluate the environmental footprint and potential emissions of both processes. This can provide additional insights on the sustainability of the processes and their impact on climate change.

References

Abbas-Abadi, M. S., Y. Ureel, A. Eschenbacher, F. H. Vermeire, R. J. Varghese, J. Oenema, G. D. Stefanidis and K. M. Van Geem (2023). "Challenges and opportunities of light olefin production via thermal and catalytic pyrolysis of end-of-life polyolefins: Towards full recyclability." Progress in Energy and Combustion Science **96**: 101046.

Abdulrasheed, A., A. A. Jalil, Y. Gambo, M. Ibrahim, H. U. Hambali and M. Y. Shahul Hamid (2019). "A review on catalyst development for dry reforming of methane to syngas: Recent advances." Renewable and Sustainable Energy Reviews **108**: 175-193.

Aboulkas, A., K. El Harfi and A. El Bouadili (2008). "Pyrolysis of olive residue/low density polyethylene mixture: Part I Thermogravimetric kinetics." Journal of Fuel Chemistry and Technology **36**(6): 672-678.

Aboulkas, A., K. El harfi and A. El Bouadili (2010). "Thermal degradation behaviors of polyethylene and polypropylene. Part I: Pyrolysis kinetics and mechanisms." Energy Conversion and Management **51**(7): 1363-1369.

Achilias, D. S., C. Roupakias, P. Megalokonomos, A. A. Lappas and E. V. Antonakou (2007). "Chemical recycling of plastic wastes made from polyethylene (LDPE and HDPE) and polypropylene (PP)." Journal of Hazardous Materials **149**(3): 536-542.

Acomb, J. C., C. Wu and P. T. Williams (2014). "Control of steam input to the pyrolysis-gasification of waste plastics for improved production of hydrogen or carbon nanotubes." Applied Catalysis B: Environmental **147**: 571-584.

Acomb, J. C., C. F. Wu and P. T. Williams (2016). "The use of different metal catalysts for the simultaneous production of carbon nanotubes and hydrogen from pyrolysis of plastic feedstocks." Applied Catalysis B-Environmental **180**: 497-510.

Adeleke, O., S. A. Akinlabi, T.-C. Jen and I. Dunmade (2022). "Environmental impact assessment of the current, emerging, and alternative waste management systems using life cycle assessment tools: a case study of Johannesburg, South Africa." Environmental Science and Pollution Research **29**(5): 7366-7381.

Adrados, A., I. de Marco, B. M. Caballero, A. Lopez-Urionabarrenechea, M. F. Laresgoiti and A. Torres (2012). "Pyrolysis of plastic packaging waste: A comparison of plastic residuals from material recovery facilities with simulated plastic waste." Waste Management **32**(5): 826-832.

Adrados, A., I. de Marco, B. M. Caballero, A. López, M. F. Laresgoiti and A. Torres (2012). "Pyrolysis of plastic packaging waste: A comparison of plastic residuals from material recovery facilities with simulated plastic waste." Waste Management **32**(5): 826-832.

Afzal, S., A. Prakash, P. Littlewood, H. Choudhury, Z. Khan Ghouri, S. Mansour, D. Wang, T. Marks, E. Weitz and P. Stair (2021). "Catalyst deactivation by carbon deposition: The remarkable case of nickel confined by atomic layer deposition." ChemCatChem **13**(13): 2988-3000.

Aguado, J., D. Serrano, J. Sotelo, R. Van Grieken and J. Escola (2001). "Influence of the operating variables on the catalytic conversion of a polyolefin mixture over HMCM-41 and nanosized HZSM-5." Industrial & engineering chemistry research **40**(24): 5696-5704.

Aguado, J., D. P. Serrano and J. M. Escola (2008). "Fuels from Waste Plastics by Thermal and Catalytic Processes: A Review." Ind. Eng. Chem. Res. **47**(21): 7982-7992.

Aguado, J., D. P. Serrano, J. M. Escola and L. Briones (2013). "Deactivation and regeneration of a Ni supported hierarchical Beta zeolite catalyst used in the hydroreforming of the oil produced by LDPE thermal cracking." Fuel 109: 679-686.

Aguado, J., D. P. Serrano, G. S. Miguel, J. M. Escola and J. M. Rodríguez (2007). "Catalytic activity of zeolitic and mesostructured catalysts in the cracking of pure and waste polyolefins." J. Anal. Appl. Pyrolysis 78(1): 153-161.

Ahmed, M. H. M., N. Batalha, Z. A. Alothman, Y. Yamauchi, Y. V. Kaneti and M. Konarova (2022). "Transforming red mud into an efficient Acid-Base catalyst by hybridization with mesoporous ZSM-5 for Co-pyrolysis of biomass and plastics." Chemical Engineering Journal 430.

Akah, A., J. Hernandez-Martinez, C. Rallan and A. A. Garforth (2015). Enhanced Feedstock Recycling of Post-Consumer Plastic Waste. Icheap12: 12th International Conference on Chemical & Process Engineering. S. Pierucci and J. J. Klemes. Milano, Aidic Servizi Srl. 43: 2395-2400.

Akahira, T. and T. Sunose (1971). "Method of determining activation deterioration constant of electrical insulating materials." Res Rep Chiba Inst Technol (Sci Technol) 16(1971): 22-31.

Akubo, K., M. A. Nahil and P. T. Williams (2019). "Aromatic fuel oils produced from the pyrolysis-catalysis of polyethylene plastic with metal-impregnated zeolite catalysts." J. Energy Inst. 92(1): 195-202.

Al-Fatesh, A. S., N. Y. A. Al-Garadi, A. I. Osman, F. S. Al-Mubaddel, A. A. Ibrahim, W. U. Khan, Y. M. Alanazi, M. M. Alrashed and O. Y. Alothman (2023). "From plastic waste pyrolysis to Fuel: Impact of process parameters and material selection on hydrogen production." Fuel 344: 128107.

Al-Salem, S. M., S. R. Chandrasekaran, A. Dutta and B. K. Sharma (2021). "Study of the fuel properties of extracted oils obtained from low and linear low density polyethylene pyrolysis." Fuel 304: 121396.

Ali, S. S., T. Elsamahy, E. Koutra, M. Kornaros, M. El-Sheekh, E. A. Abdelkarim, D. Zhu and J. Sun (2021). "Degradation of conventional plastic wastes in the environment: A review on current status of knowledge and future perspectives of disposal." Science of The Total Environment 771: 144719.

Almeida, D. and M. d. F. Marques (2016). "Thermal and catalytic pyrolysis of plastic waste." Polímeros 26: 44-51.

Alsaleh, A. and M. L. Sattler (2014). "Waste Tire Pyrolysis: Influential Parameters and Product Properties." Current Sustainable/Renewable Energy Reports 1(4): 129-135.

Alsayegh, M. F., R. Abdul Rahman and S. Homayoun (2020). "Corporate economic, environmental, and social sustainability performance transformation through ESG disclosure." Sustainability 12(9): 3910.

Aminu, I., M. A. Nahil and P. T. Williams (2020). "Hydrogen from Waste Plastics by Two-Stage Pyrolysis/Low-Temperature Plasma Catalytic Processing." Energy & Fuels 34(9): 11679-11689.

Antonakou, E. and D. Achilias (2013). "Recent advances in polycarbonate recycling: A review of degradation methods and their mechanisms." Waste and Biomass Valorization 4: 9-21.

Arabiourrutia, M., M. Olazar, R. Aguado, G. López, A. Barona and J. Bilbao (2008). "HZSM-5 and HY Zeolite Catalyst Performance in the Pyrolysis of Tires in a Conical Spouted Bed Reactor." Industrial & Engineering Chemistry Research 47(20): 7600-7609.

Araiza Aguilar, J. A., J. C. Chavez Moreno and J. A. Moreno Pérez (2017). "QUANTIFICATION OF MUNICIPAL SOLID WASTE IN BERRIOZABAL, CHIAPAS, MEXICO." Revista internacional de contaminación ambiental **33**(4): 691-699.

Areeprasert, C., J. Asingsamanunt, S. Srisawat, J. Kaharn, B. Inseemeesak, P. Phasee, C. Khaobang, W. Siwakosit and C. Chiemchaisri (2017). "Municipal plastic waste composition study at transfer station of Bangkok and possibility of its energy recovery by pyrolysis." Energy Procedia **107**: 222-226.

Areeprasert, C. and C. Khaobang (2018). "Pyrolysis and catalytic reforming of ABS/PC and PCB using biochar and e-waste char as alternative green catalysts for oil and metal recovery." Fuel Process. Technol. **182**: 26-36.

Arora, J. S. (2012). Chapter 13 - More on Numerical Methods for Constrained Optimum Design. Introduction to Optimum Design (Third Edition). J. S. Arora. Boston, Academic Press**:** 533-573.

Arora, S. and R. Prasad (2016). "An overview on dry reforming of methane: strategies to reduce carbonaceous deactivation of catalysts." RSC advances **6**(110): 108668-108688.

Arslan, H. M., I. Khan, M. I. Latif, B. Komal and S. Chen (2022). "Understanding the dynamics of natural resources rents, environmental sustainability, and sustainable economic growth: new insights from China." Environmental Science and Pollution Research **29**(39): 58746-58761.

Arturi, K. R., H. U. Sokoli, E. G. Søgaard, F. Vogel and S. Bjelić (2018). "Recovery of value-added chemicals by solvolysis of unsaturated polyester resin." J. Cleaner Prod. **170**: 131-136.

Awasthi, A. K., M. Shivashankar and S. Majumder (2017). Plastic solid waste utilization technologies: A Review. IOP conference series: Materials science and engineering, IOP Publishing.

Awayssa, O., N. Al-Yassir, A. Aitani and S. Al-Khattaf (2014). "Modified HZSM-5 as FCC additive for enhancing light olefins yield from catalytic cracking of VGO." Applied Catalysis A: General **477**: 172-183.

AZO Materials. "Walnut Shells (Versatile Soft Abrasive Media) Applications and Uses." Retrieved December 2023, from https://www.azom.com/article.aspx?ArticleID=10430.

Bai, B., H. Jin, S. Zhu, P. Wu, C. Fan and J. Sun (2019). "Experimental investigation on in-situ hydrogenation induced gasification characteristics of acrylonitrile butadiene styrene (ABS) microplastics in supercritical water." Fuel Processing Technology **192**: 170-178.

Bai, B., Y. Liu, Q. Wang, J. Zou, H. Zhang, H. Jin and X. Li (2019). "Experimental investigation on gasification characteristics of plastic wastes in supercritical water." Renew. Energy **135**: 32-40.

Bai, B., W. Wang and H. Jin (2020). "Experimental study on gasification performance of polypropylene (PP) plastics in supercritical water." Energy **191**: 116527.

Bai, B. J., Hui; Fan, Chao; Cao, Changqing; Wei, Wenwen; Cao, Wen (2019). "Experimental investigation on liquefaction of plastic waste to oil in supercritical water." Waste Manage. **89**: 247-253.

Ballout, W., N. Sallem-Idrissi, M. Sclavons, C. Doneux, C. Bailly, T. Pardoen and P. Van Velthem (2022). "High performance recycled CFRP composites based on reused carbon fabrics through sustainable mild solvolysis route." Scientific Reports **12**(1): 5928.

Barbarias, I., M. Artetxe, G. Lopez, A. Arregi, L. Santamaria, J. Bilbao and M. Olazar (2019). "Catalyst Performance in the HDPE Pyrolysis-Reforming under Reaction-Regeneration Cycles." Catalysts **9**(5): 414.

Bartholomew, C. H. and R. J. Farrauto (1976). "Chemistry of nickel-alumina catalysts." Journal of Catalysis **45**(1): 41-53.

Bauman, H. C. (1964). Fundamentals of cost engineering in the chemical industry, Reinhold Publishing Corporation.

Beccarello, M. and G. Di Foggia (2018). "Moving towards a circular economy: economic impacts of higher material recycling targets." Materials Today: Proceedings **5**(1, Part 1): 531-543.

Bender, M. L. (1960). "Mechanisms of catalysis of nucleophilic reactions of carboxylic acid derivatives." Chemical Reviews **60**(1): 53-113.

Benguerba, Y., L. Dehimi, M. Virginie, C. Dumas and B. Ernst (2015). "Modelling of methane dry reforming over Ni/Al2O3 catalyst in a fixed-bed catalytic reactor." Reaction Kinetics, Mechanisms and Catalysis **114**(1): 109-119.

Bennett, J. A., K. Wilson and A. F. Lee (2016). "Catalytic applications of waste derived materials." Journal of materials chemistry A **4**(10): 3617-3637.

Berčič, G., P. Djinović and A. Pintar (2019). "Simplified approach to modelling the catalytic degradation of low-density polyethylene (LDPE) by applying catalyst-free LDPE-TG profiles and the Friedman method." Journal of Thermal Analysis and Calorimetry **136**(3): 1011-1020.

Bergman, R. G. (2007). "C–H activation." Nature **446**(7134): 391-393.

Bhaskar, T. K., Jun; Muto, Akinori; Sakata, Yusaku; Jakab, Emma; Matsui, Toshiki; Uddin, Md Azhar (2004). "Pyrolysis studies of PP/PE/PS/PVC/HIPS-Br plastics mixed with PET and dehalogenation (Br, Cl) of the liquid products." J. Anal. Appl. Pyrolysis **72**(1): 27-33.

Bioplastics News. "Chemical Recycling Consortiums, Partnerships & Joint Ventures." Retrieved May 2023, from https://bioplasticsnews.com/chemical-recycling-consortiums-partnerships-joint-ventures/.

Blanco, I. and V. Siracusa (2013). "Kinetic study of the thermal and thermo-oxidative degradations of polylactide-modified films for food packaging." Journal of Thermal Analysis and Calorimetry **112**(3): 1171-1177.

Boeren, E. G., R. B. van Henegouwen, I. Bos and T. H. Gerner (1985). "Naphtha analysis: The advantages of a specific olefin trap." Journal of Chromatography A **349**(2): 377-384.

Bohre, A., P. R. Jadhao, K. Tripathi, K. K. Pant, B. Likozar and B. Saha "Chemical recycling processes of waste polyethylene terephthalate using solid catalysts." ChemSusChem: e202300142.

Bouckaert, S., A. F. Pales, C. McGlade, U. Remme, B. Wanner, L. Varro, D. D'Ambrosio and T. Spencer (2021). "Net zero by 2050: A roadmap for the global energy sector."

Brhane, Y. and T. Gabriel (2016). "Production, purification and functionalization of carbon nanotubes for medical applications." Int Res J Pharm **7**(7): 19-27.

British Plastics Federation. (2019). "Oil Consumption." Retrieved 24 Sep 2021, from https://www.bpf.co.uk/press/Oil_Consumption.

Buchwalter, S. L. (2001). Semiconductor Chip Underfill Materials. Encyclopedia of Materials: Science and Technology. K. H. J. Buschow, R. W. Cahn, M. C. Flemings et al. Oxford, Elsevier: 8332-8335.

Budrugeac, P., A. Cucos, R. Dascălu, I. Atkinson and P. Osiceanu (2022). "Application of model-free and multivariate nonlinear regression methods for evaluation of the kinetic scheme and

kinetic parameters of thermal decomposition of low density polyethylene." Thermochimica Acta 708: 179138.

Burgess, M., H. Holmes, M. Sharmina and M. P. Shaver (2021). "The future of UK plastics recycling: One Bin to Rule Them All." Resources, Conservation and Recycling 164: 105191.

Burnham, A. (2000). "Application of the Šesták-Berggren equation to organic and inorganic materials of practical interest." Journal of thermal analysis and calorimetry 60(3): 895-908.

Byrn, S., G. Zografi and X. Chen (2017). "Differential scanning calorimetry and thermogravimetric analysis." Solid State Properties of Pharmaceutical Materials, Willy online Library.

Carlson, E. C. (1996). "Don't gamble with physical properties for simulations." Chemical engineering progress 92(10): 35-46.

Castello, D., T. H. Pedersen and L. A. Rosendahl (2018). "Continuous Hydrothermal Liquefaction of Biomass: A Critical Review." Energies 11(11): 35.

Castello, D. and L. Rosendahl (2018). 9 - Coprocessing of pyrolysis oil in refineries. Direct Thermochemical Liquefaction for Energy Applications. L. Rosendahl, Woodhead Publishing: 293-317.

Ceamanos, J., J. F. Mastral, A. Millera and M. E. Aldea (2002). "Kinetics of pyrolysis of high density polyethylene. Comparison of isothermal and dynamic experiments." Journal of Analytical and Applied Pyrolysis 65(2): 93-110.

Chaabani, C., E. Weiss-Hortala and Y. Soudais (2017). "Impact of Solvolysis Process on Both Depolymerization Kinetics of Nylon 6 and Recycling Carbon Fibers from Waste Composite." Waste and Biomass Valorization 8(8): 2853-2865.

Chamas, A., H. Moon, J. Zheng, Y. Qiu, T. Tabassum, J. H. Jang, M. Abu-Omar, S. L. Scott and S. Suh (2020). "Degradation Rates of Plastics in the Environment." ACS Sustainable Chemistry & Engineering 8(9): 3494-3511.

Chang, T., C. Li, F. Fan, H. Wu, C. Wang and F. Yin (2022). "Effects of temperature zones on pyrolysis products of mixed plastic waste." Journal of Material Cycles and Waste Management: 1-11.

Chari, S., A. Sebastiani, A. Paulillo and M. Materazzi (2023). "The Environmental Performance of Mixed Plastic Waste Gasification with Carbon Capture and Storage to Produce Hydrogen in the U.K." ACS Sustainable Chemistry & Engineering 11(8): 3248-3259.

Chaudhary, B. I., C. L. Liotta, J. M. Cogen and M. Gilbert (2016). Plasticized PVC. Reference Module in Materials Science and Materials Engineering, Elsevier.

Chen, F., L. Ma, D.-g. Cheng and X. Zhan (2012). "Synthesis of hierarchical porous zeolite and its performance in n-heptane cracking." Catal. Commun. 18: 110-114.

Chen, H. L., T. K. Nath, S. Chong, V. Foo, C. Gibbins and A. M. Lechner (2021). "The plastic waste problem in Malaysia: management, recycling and disposal of local and global plastic waste." Sn Applied Sciences 3(4): 15.

Chen, W.-T., K. Jin and N.-H. Linda Wang (2019). "Use of Supercritical Water for the Liquefaction of Polypropylene into Oil." ACS Sustainable Chemistry & Engineering 7(4): 3749-3758.

Chen, X., F. Xi, Y. Geng and T. Fujita (2011). "The potential environmental gains from recycling waste plastics: Simulation of transferring recycling and recovery technologies to Shenyang, China." Waste Management 31(1): 168-179.

Chesnokov, V. V. and A. S. Chichkan (2009). "Production of hydrogen by methane catalytic decomposition over Ni–Cu–Fe/Al2O3 catalyst." International Journal of Hydrogen Energy 34(7): 2979-2985.

Chhabra, V., S. Bhattacharya and Y. Shastri (2019). "Pyrolysis of mixed municipal solid waste: Characterisation, interaction effect and kinetic modelling using the thermogravimetric approach." Waste Management 90: 152-167.

Chowlu, A. C. K., P. K. Reddy and A. Ghoshal (2009). "Pyrolytic decomposition and model-free kinetics analysis of mixture of polypropylene (PP) and low-density polyethylene (LDPE)." Thermochimica acta 485(1-2): 20-25.

Civancik-Uslu, D., T. T. Nhu, B. Van Gorp, U. Kresovic, M. Larrain, P. Billen, K. Ragaert, S. De Meester, J. Dewulf and S. Huysveld (2021). "Moving from linear to circular household plastic packaging in Belgium: Prospective life cycle assessment of mechanical and thermochemical recycling." Resources, Conservation and Recycling 171: 105633.

Clark, J. H., J. A. Alonso, J. A. Villalba, J. Aguado, D. P. Serrano and D. Serrano (1999). Feedstock recycling of plastic wastes, Royal society of chemistry.

Colnik, M., P. Kotnik, Z. Knez and M. Skerget (2022). "Chemical Recycling of Polyolefins Waste Materials Using Supercritical Water." Polymers 14(20).

Corma, A. (1997). "From Microporous to Mesoporous Molecular Sieve Materials and Their Use in Catalysis." Chem. Rev. 97(6): 2373-2420.

Costa, P., F. Pinto, R. Mata, P. Marques, F. Paradela and L. Costa (2021). "Validation of the application of the pyrolysis process for the treatment and transformation of municipal plastic wastes." Chemical Engineering Transactions 86: 859-864.

Creese, R. C. (2018). Depreciation Terms, Methods, and Systems. Strategic Cost Fundamentals: for Designers, Engineers, Technologists, Estimators, Project Managers, and Financial Analysts, Springer: 145-165.

Cullis, C. F. and M. M. Hirschler (1981). The combustion of organic polymers, Oxford University Press, USA.

Dabros, T. M. H., M. Z. Stummann, M. Høj, P. A. Jensen, J.-D. Grunwaldt, J. Gabrielsen, P. M. Mortensen and A. D. Jensen (2018). "Transportation fuels from biomass fast pyrolysis, catalytic hydrodeoxygenation, and catalytic fast hydropyrolysis." Progress in Energy and Combustion Science 68: 268-309.

Dai, L., N. Zhou, Y. Lv, Y. Cheng, Y. Wang, Y. Liu, K. Cobb, P. Chen, H. Lei and R. Ruan (2022). "Pyrolysis technology for plastic waste recycling: A state-of-the-art review." Progress in Energy and Combustion Science 93: 101021.

Dai, Z., B. Hatano, J.-i. Kadokawa and H. Tagaya (2002). "Effect of diaminotoluene on the decomposition of polyurethane foam waste in superheated water." Polymer Degradation and Stability 76(2): 179-184.

Daligaux, V., R. Richard and M.-H. Manero (2021). "Deactivation and regeneration of zeolite catalysts used in pyrolysis of plastic wastes—a process and analytical review." Catalysts 11(7): 770.

Darzi, R., Y. Dubowski and R. Posmanik (2022). "Hydrothermal processing of polyethylene-terephthalate and nylon-6 mixture as a plastic waste upcycling treatment: A comprehensive multi-phase analysis." Waste Management 143: 223-231.

Dascomb, J., A. Krothapalli and R. Fakhrai (2013). "Thermal conversion efficiency of producing hydrogen enriched syngas from biomass steam gasification." International Journal of Hydrogen Energy 38(27): 11790-11798.

Davidson, M. G., R. A. Furlong and M. C. McManus (2021). "Developments in the life cycle assessment of chemical recycling of plastic waste – A review." Journal of Cleaner Production 293: 126163.

De Hoe, G. X., T. Şucu and M. P. Shaver (2022). "Sustainability and Polyesters: Beyond Metals and Monomers to Function and Fate." Accounts of Chemical Research 55(11): 1514-1523.

de Oliveira, D. C., E. E. S. Lora, O. J. Venturini, D. M. Y. Maya and M. Garcia-Pérez (2023). "Gas cleaning systems for integrating biomass gasification with Fischer-Tropsch synthesis - A review of impurity removal processes and their sequences." Renewable and Sustainable Energy Reviews 172: 113047.

Deanin, R. D. (1975). "Additives in plastics." Environmental Health Perspectives 11: 35-39.

Delva, L., S. Hubo, L. Cardon and K. Ragaert (2018). "On the role of flame retardants in mechanical recycling of solid plastic waste." Waste Management 82: 198-206.

Demirbas, A. (2004). "Pyrolysis of municipal plastic wastes for recovery of gasoline-range hydrocarbons." J. Anal. Appl. Pyrolysis 72(1): 97-102.

Diaz-Silvarrey, L. S., A. McMahon and A. N. Phan (2018). "Benzoic acid recovery via waste poly(ethylene terephthalate) (PET) catalytic pyrolysis using sulphated zirconia catalyst." J. Anal. Appl. Pyrolysis 134: 621-631.

Diaz-Silvarrey, L. S., K. Zhang and A. N. Phan (2018). "Monomer recovery through advanced pyrolysis of waste high density polyethylene (HDPE)." Green Chemistry 20(8): 1813-1823.

Diaz, J. F. T. (2016). "Do scarce precious metals equate to safe harbor investments? The case of platinum and palladium." Economics Research International 2016.

Diaz Silvarrey, L. S. (2019). Advanced pyrolysis of plastic waste for chemicals, fuel and materials, Newcastle University.

Diaz Silvarrey, L. S. and A. N. Phan (2016). "Kinetic study of municipal plastic waste." Int. J. Hydrogen Energy 41(37): 16352-16364.

Dicholkar, D. D., V. G. Gaikar, S. Kumar and R. Natarajan (2012). "Modeling and optimizing of steam pyrolysis of dimethyl formamide by using response surface methodology coupled with Box-Behnken design." Journal of Analytical and Applied Pyrolysis 96: 6-15.

Dimitriadis, A. B., Stella (2017). "Hydrothermal liquefaction of various biomass and waste feedstocks for biocrude production: A state of the art review." Renew. Sust. Energ. Rev. 68: 113-125.

Djandja, O. S., D. Chen, L.-X. Yin, Z.-C. Wang and P.-G. Duan (2022). Roadmap to Low-Cost Catalytic Pyrolysis of Plastic Wastes for Production of Liquid Fuels. Production of Biofuels and Chemicals from Sustainable Recycling of Organic Solid Waste, Springer: 75-100.

Dods, M. N., E. J. Kim, J. R. Long and S. C. Weston (2021). "Deep CCS: Moving Beyond 90% Carbon Dioxide Capture." Environmental Science & Technology 55(13): 8524-8534.

Dodson, B. and I. McNeill (1976). "Degradation of polymer mixtures. VI. Blends of poly (vinyl chloride) with polystyrene." Journal of Polymer Science: Polymer Chemistry Edition **14**(2): 353-364.

Dogu, O., M. Pelucchi, R. Van de Vijver, P. H. M. Van Steenberge, D. R. D'Hooge, A. Cuoci, M. Mehl, A. Frassoldati, T. Faravelli and K. M. Van Geem (2021). "The chemistry of chemical recycling of solid plastic waste via pyrolysis and gasification: State-of-the-art, challenges, and future directions." Progress in Energy and Combustion Science **84**: 100901.

Dong, Q., C. Gao, Y. Ding, F. Wang, B. Wen, S. Zhang, T. Wang and M. Yang (2012). "A polycarbonate/magnesium oxide nanocomposite with high flame retardancy." Journal of applied polymer science **123**(2): 1085-1093.

Dong, Y., F. J. Keil, O. Korup, F. Rosowski and R. Horn (2016). "Effect of the catalyst pore structure on fixed-bed reactor performance of partial oxidation of n-butane: A simulation study." Chemical Engineering Science **142**: 299-309.

dos Passos, J. S., M. Glasius and P. Biller (2020). "Screening of common synthetic polymers for depolymerization by subcritical hydrothermal liquefaction." Process Safety and Environmental Protection **139**: 371-379.

Du, S., J. A. Valla, R. S. Parnas and G. M. Bollas (2016). "Conversion of polyethylene terephthalate based waste carpet to benzene-rich oils through thermal, catalytic, and catalytic steam pyrolysis." ACS Sustainable Chemistry & Engineering **4**(5): 2852-2860.

Duan, Y., P. Yuan, S. Huang, L. Wang, J. Deng, S. Yu, Q. Xie and Y. Nie (2023). "Experimental study on reactor scale-up for microwave-assisted pyrolysis of methyl ricinoleate." Chemical Engineering and Processing - Process Intensification **184**: 109293.

Dubdub, I. and M. Al-Yaari (2020). "Pyrolysis of Low Density Polyethylene: Kinetic Study Using TGA Data and ANN Prediction." Polymers **12**(4).

Eimontas, J., N. Striūgas, M. A. Abdelnaby and S. Yousef (2021). "Catalytic Pyrolysis Kinetic Behavior and TG-FTIR-GC–MS Analysis of Metallized Food Packaging Plastics with Different Concentrations of ZSM-5 Zeolite Catalyst." Polymers **13**(5): 702.

Ellis, L. D., N. A. Rorrer, K. P. Sullivan, M. Otto, J. E. McGeehan, Y. Román-Leshkov, N. Wierckx and G. T. Beckham (2021). "Chemical and biological catalysis for plastics recycling and upcycling." Nature Catalysis **4**(7): 539-556.

Elordi, G., M. Olazar, G. Lopez, P. Castaño and J. Bilbao (2011). "Role of pore structure in the deactivation of zeolites (HZSM-5, Hβ and HY) by coke in the pyrolysis of polyethylene in a conical spouted bed reactor." Appl. Catal., B **102**(1): 224-231.

Encinar, J. M. and J. F. González (2008). "Pyrolysis of synthetic polymers and plastic wastes. Kinetic study." Fuel Processing Technology **89**(7): 678-686.

Er-Rbib, H., C. Bouallou and F. Werkoff (2012). "Dry reforming of methane–review of feasibility studies." Chemical Engineering **29**.

Escola, J. M., J. Aguado, D. P. Serrano, L. Briones, J. L. Díaz de Tuesta, R. Calvo and E. Fernandez (2012). "Conversion of Polyethylene into Transportation Fuels by the Combination of Thermal Cracking and Catalytic Hydroreforming over Ni-Supported Hierarchical Beta Zeolite." Energy Fuels **26**(6): 3187-3195.

Escola, J. M., J. Aguado, D. P. Serrano, A. García, A. Peral, L. Briones, R. Calvo and E. Fernandez (2011). "Catalytic hydroreforming of the polyethylene thermal cracking oil over Ni supported hierarchical zeolites and mesostructured aluminosilicates." Appl. Catal., B **106**(3): 405-415.

Esquer, R. and J. J. García (2019). "Metal-catalysed Poly(Ethylene) terephthalate and polyurethane degradations by glycolysis." J. Organomet. Chem. **902**: 120972.

European Central Bank. (2023). "Economic Bulletin, Issue 2." Retrieved May 6, 2023, from https://www.ecb.europa.eu/pub/economic-bulletin/html/eb202302.en.html#:~:text=ECB%20staff%20now%20see%20inflation,underlying%20price%20pressures%20remain%20strong.

Exchange Rates UK. (2011). (2023). "USD to GBP Spot Exchange Rates History [Online]." Retrieved 9 May 2023, from https://www.exchangerates.org.uk/USD-GBP-spot-exchange-rates-history-2011.html#:~:text=Average%20exchange%20rate%20in%202011%3A%200.6236%20GBP.

Fakirov, S. (2019). "Condensation Polymers: Their Chemical Peculiarities Offer Great Opportunities." Progress in Polymer Science **89**: 1-18.

FAO, U. F. A. S. (2023). "Walnut production worldwide in 2022/23, by country (in 1,000 metric tons)*." Retrieved December 2023, from https://www.statista.com/statistics/675974/walnut-production-worldwide-by-country/.

Feng, R., P. Zhou, B. Liu, X. Yan, X. Hu and M. Zhou (2022). "Direct synthesis of HZSM-5 zeolites with enhanced catalytic performance in the methanol-to-propylene reaction." Catalysis Today **405**: 299-308.

Fivga, A. and I. Dimitriou (2018). "Pyrolysis of plastic waste for production of heavy fuel substitute: A techno-economic assessment." Energy **149**: 865-874.

Flynn, J. H. and L. A. Wall (1966). "General treatment of the thermogravimetry of polymers." Journal of research of the National Bureau of Standards. Section A, Physics and chemistry **70**(6): 487.

Freel, J. and A. K. Galwey (1968). "Hydrocarbon cracking reactions on nickel." Journal of Catalysis **10**(3): 277-289.

Friedman, H. L. (1964). Kinetics of thermal degradation of char-forming plastics from thermogravimetry. Application to a phenolic plastic. Journal of polymer science part C: polymer symposia, Wiley Online Library.

Fuentes-Ordóñez, E. G., J. A. Salbidegoitia, M. P. González-Marcos and J. R. González-Velasco (2016). "Mechanism and kinetics in catalytic hydrocracking of polystyrene in solution." Polym. Degrad. Stab. **124**: 51-59.

Gaide, I., V. Makareviciene, E. Sendzikiene and K. Kazancev (2021). "Natural rocks–heterogeneous catalysts for oil transesterification in biodiesel synthesis." Catalysts **11**(3): 384.

Gallo, A. (2014). "A refresher on net present value." Harvard Business Review **19**: 1-6.

Gao, G. and Y. Li (2016). "Mechanical properties of woven glass fiber-reinforced polymer composites." Emerging Materials Research **5**(2): 201-208.

Gao, W., S. Liang, R. Wang, Q. Jiang, Y. Zhang, Q. Zheng, B. Xie, C. Y. Toe, X. Zhu and J. Wang (2020). "Industrial carbon dioxide capture and utilization: state of the art and future challenges." Chemical Society Reviews **49**(23): 8584-8686.

Garforth, A. A., S. Ali, J. Hernández-Martínez and A. Akah (2004). "Feedstock recycling of polymer wastes." Current Opinion in Solid State and Materials Science **8**(6): 419-425.

Ge, Z., S. Guo, L. Guo, C. Cao, X. Su and H. Jin (2013). "Hydrogen production by non-catalytic partial oxidation of coal in supercritical water: explore the way to complete gasification of lignite and bituminous coal." International journal of hydrogen energy **38**(29): 12786-12794.

Genuino, H. C., M. P. Ruiz, H. J. Heeres and S. R. Kersten (2023). "Pyrolysis of mixed plastic waste: Predicting the product yields." Waste Management **156**: 208-215.

Gerö, L. (2004). "Bond Energies of Hydrocarbons." The Journal of Chemical Physics **16**(11): 1011-1013.

Geyer, R., J. R. Jambeck and K. L. Law (2017). "Production, use, and fate of all plastics ever made." Science Advances **3**(7): 5.

Ghavami, N., K. Özdenkçi, G. Salierno, M. Björklund-Sänkiaho and C. De Blasio (2021). "Analysis of operational issues in hydrothermal liquefaction and supercritical water gasification processes: a review." Biomass Conversion and Biorefinery.

Gholami, Z., F. Gholami, Z. Tišler, J. Hubáček, M. Tomas, M. Bačiak and M. Vakili (2022). "Production of light olefins via Fischer-Tropsch process using iron-based catalysts: A review." Catalysts **12**(2): 174.

Gilbert, P., C. Ryu, V. Sharifi and J. Swithenbank (2009). "Tar reduction in pyrolysis vapours from biomass over a hot char bed." Bioresource Technology **100**(23): 6045-6051.

Gioia, F. and F. Murena (1998). "Simultaneous catalytic hydroprocessing of chlorine-, nitrogen-, and sulphur-containing aromatic compounds." Journal of Hazardous Materials **57**(1): 177-192.

Giovannoni, E. and G. Fabietti (2013). "What is sustainability? A review of the concept and its applications." Integrated reporting: Concepts and cases that redefine corporate accountability: 21-40.

Glas, D., J. Hulsbosch, P. Dubois, K. Binnemans and D. E. De Vos (2014). "End-of-Life Treatment of Poly(Vinyl Chloride) and Chlorinated Polyethylene by Dehydrochlorination in Ionic Liquids." ChemSusChem **7**(2): 610-617.

Glendinning, R. (1988). "The concept of value for money." International Journal of Public Sector Management **1**(1): 42-50.

Gong, J., X. Chen and T. Tang (2019). "Recent progress in controlled carbonization of (waste) polymers." Progress in Polymer Science **94**: 1-32.

Gosselin, R., D. Rodrigue and C. Duchesne (2011). "A hyperspectral imaging sensor for on-line quality control of extruded polymer composite products." Computers & Chemical Engineering **35**(2): 296-306.

Goyal, H., T.-Y. Chen, W. Chen and D. G. Vlachos (2022). "A review of microwave-assisted process intensified multiphase reactors." Chemical Engineering Journal **430**: 133183.

Grafström, J. and S. Aasma (2021). "Breaking circular economy barriers." Journal of Cleaner Production **292**: 126002.

Grause, G., S. Matsumoto, T. Kameda and T. Yoshioka (2011). "Pyrolysis of Mixed Plastics in a Fluidized Bed of Hard Burnt Lime." Ind. Eng. Chem. Res. **50**(9): 5459-5466.

Griffiths, D. F. and D. J. Higham (2010). Euler's Method. Numerical Methods for Ordinary Differential Equations: Initial Value Problems. D. F. Griffiths and D. J. Higham. London, Springer London: 19-31.

Gunasee, S. D., M. Carrier, J. F. Gorgens and R. Mohee (2016). "Pyrolysis and combustion of municipal solid wastes: Evaluation of synergistic effects using TGA-MS." Journal of Analytical and Applied Pyrolysis **121**: 50-61.

Gupta, N., S. M. Gupta and S. Sharma (2019). "Carbon nanotubes: Synthesis, properties and engineering applications." Carbon Letters **29**: 419-447.

Haar, L. (1984). NBS/NRC steam tables, CRC Press.

Hahladakis, J. N., C. A. Velis, R. Weber, E. Iacovidou and P. Purnell (2018). "An overview of chemical additives present in plastics: Migration, release, fate and environmental impact during their use, disposal and recycling." Journal of hazardous materials **344**: 179-199.

Harden, C. J. (2014). Discount rate development in oil and gas valuation. SPE Hydrocarbon Economics and Evaluation Symposium, OnePetro.

Hargreaves, J. S. (2018). "Catalysts derived from waste materials."

Harris, J., A. N. Phan and K. Zhang (2018). "Cold plasma catalysis as a novel approach for valorisation of untreated waste glycerol." Green Chemistry **20**(11): 2578-2587.

Haynes, W. M. (2016). CRC handbook of chemistry and physics, CRC press.

He, P., Z. Hu, Z. Dai, H. Bai, Z. Fan, R. Niu, J. Gong, Q. Zhao and T. Tang (2023). "Mechanochemistry milling of waste poly (Ethylene terephthalate) into metal–organic frameworks." ChemSusChem **16**(2): e202201935.

He, Z., J.-L. Maurice, A. Gohier, C. S. Lee, D. Pribat and C. S. Cojocaru (2011). "Iron Catalysts for the Growth of Carbon Nanofibers: Fe, Fe3C or Both?" Chemistry of Materials **23**(24): 5379-5387.

Hesse, N. D. and R. L. White (2004). "Polyethylene catalytic hydrocracking by PtHZSM-5, PtHY, and PtHMCM-41." Journal of Applied Polymer Science **92**(2): 1293-1301.

Hijazi, A., H. Ala'a, S. Aouad, M. N. Ahmad and J. Zeaiter (2019). "Pyrolysis of waste rubber tires with palladium doped zeolite." Journal of Environmental Chemical Engineering **7**(6): 103451.

HM Revenue and Customs (2022). Plastic packaging tax. UK Government.

Holba, P. (2017). "Temperature dependence of activation energy of endothermic processes and related imperfections of non-isothermal kinetic evaluations." Journal of Thermal Analysis and Calorimetry **129**(1): 609-614.

Holland, B. J. and J. N. Hay (2002). "The thermal degradation of PET and analogous polyesters measured by thermal analysis–Fourier transform infrared spectroscopy." Polymer **43**(6): 1835-1847.

Hongthong, S., H. S. Leese and C. J. Chuck (2020). "Valorizing Plastic-Contaminated Waste Streams through the Catalytic Hydrothermal Processing of Polypropylene with Lignocellulose." Acs Omega **5**(32): 20586-20598.

Hu, Y. C., Y. Wang, X. Z. Zhang, J. Qian, X. Q. Xing and X. H. Wang (2020). "Synthesis of poly(ethylene terephthalate) based on glycolysis of waste PET fiber." Journal of Macromolecular Science Part a-Pure and Applied Chemistry **57**(6): 430-438.

Huang, J., A. Veksha, W. P. Chan, A. Giannis and G. Lisak (2022). "Chemical recycling of plastic waste for sustainable material management: A prospective review on catalysts and processes." Renewable and Sustainable Energy Reviews **154**: 111866.

Huang, P., J. Pitcher, A. Mushing, F. Lourenço and M. P. Shaver (2023). "Chemical recycling of multi-materials from glycol-modified poly(ethylene terephthalate)." Resources, Conservation and Recycling **190**: 106854.

Huang, W.-C., M.-S. Huang, C.-F. Huang, C.-C. Chen and K.-L. Ou (2010). "Thermochemical conversion of polymer wastes into hydrocarbon fuels over various fluidizing cracking catalysts." Fuel **89**(9): 2305-2316.

Hujuri, U., A. K. Ghoshal and S. Gumma (2008). "Modeling pyrolysis kinetics of plastic mixtures." Polymer Degradation and Stability **93**(10): 1832-1837.

Ikeda, A., K. Katoh and H. Tagaya (2008). "Monomer recovery of waste plastics by liquid phase decomposition and polymer synthesis." Journal of Materials Science **43**(7): 2437-2441.

Inc., C. M. C. "Walnut Shell Media." from https://compomat.com/walnut-shell-blasting-media/.

Inderthal, H., S. L. Tai and S. T. L. Harrison (2021). "Non-Hydrolyzable Plastics – An Interdisciplinary Look at Plastic Bio-Oxidation." Trends in Biotechnology **39**(1): 12-23.

Internal Revenue Service. (2022). "Publication 946: How to Depreciate Property." Retrieved May 9, 2023, from https://www.irs.gov/pub/irs-pdf/p946.pdf.

Isa, A., N. Nosbi, M. Che Ismail, H. Md Akil, W. F. F. Wan Ali and M. F. Omar (2022). "A review on recycling of carbon fibres: methods to reinforce and expected fibre composite degradations." Materials **15**(14): 4991.

Iwaya, T., M. Sasaki and M. Goto (2006). "Kinetic analysis for hydrothermal depolymerization of nylon 6." Polymer degradation and stability **91**(9): 1989-1995.

Jentoft, F. C. and B. C. Gates (1997). "Solid-acid-catalyzed alkane cracking mechanisms: evidence from reactions of small probe molecules." Topics in Catalysis **4**(1): 1-13.

Jerdy, A. C., T. Pham, M. Á. González-Borja, P. Atallah, D. Soules, R. Abbott, L. Lobban and S. Crossley (2023). "Impact of the presence of common polymer additives in thermal and catalytic polyethylene decomposition." Applied Catalysis B: Environmental **325**: 122348.

Jeswani, H., C. Krüger, M. Russ, M. Horlacher, F. Antony, S. Hann and A. Azapagic (2021). "Life cycle environmental impacts of chemical recycling via pyrolysis of mixed plastic waste in comparison with mechanical recycling and energy recovery." Science of The Total Environment **769**: 144483.

Jia, L., X. Sun, X. Ye, C. Zou, H. Gu, Y. Huang, G. Niu and D. Zhao (2013). "Core–shell composites of USY@Mesosilica: Synthesis and application in cracking heavy molecules with high liquid yield." Microporous and Mesoporous Materials **176**: 16-24.

Jiang, J., K. Shi, X. Zhang, K. Yu, H. Zhang, J. He, Y. Ju and J. Liu (2022). "From plastic waste to wealth using chemical recycling: A review." Journal of Environmental Chemical Engineering **10**(1): 106867.

Jin, K., P. Vozka, G. Kilaz, W. T. Chen and N. Wang (2020). "Conversion of polyethylene waste into clean fuels and waxes via hydrothermal processing (HTP)." Fuel **273**: 11.

Job, S. (2013). "Recycling glass fibre reinforced composites – history and progress." Reinforced Plastics **57**(5): 19-23.

Johar, P., E. L. Rylott, C. R. McElroy, A. S. Matharu and J. H. Clark (2023). "Biologically bound nickel accelerated de-polymerization of polyethylene to high value hydrocarbons and hydrogen." RSC Sustainability.

Karuppannan Gopalraj, S. and T. Kärki (2020). "A review on the recycling of waste carbon fibre/glass fibre-reinforced composites: Fibre recovery, properties and life-cycle analysis." SN Applied Sciences **2**(3): 433.

Kassouf, A., J. Maalouly, D. N. Rutledge, H. Chebib and V. Ducruet (2014). "Rapid discrimination of plastic packaging materials using MIR spectroscopy coupled with independent components analysis (ICA)." Waste Management **34**(11): 2131-2138.

Kawai, K. and T. Tasaki (2016). "Revisiting estimates of municipal solid waste generation per capita and their reliability." Journal of Material Cycles and Waste Management **18**: 1-13.

Khan, I. and F. Hou (2021). "The impact of socio-economic and environmental sustainability on CO 2 emissions: a novel framework for thirty IEA countries." Social Indicators Research **155**: 1045-1076.

Khedri, S. and S. Elyasi (2016). "Kinetic analysis for thermal cracking of HDPE: A new isoconversional approach." Polymer Degradation and Stability **129**: 306-318.

Khoja, A. H., M. Tahir and N. A. S. Amin (2019). "Recent developments in non-thermal catalytic DBD plasma reactor for dry reforming of methane." Energy Conversion and Management **183**: 529-560.

Kijo-Kleczkowska, A. and A. Gnatowski (2022). "Recycling of plastic waste, with particular emphasis on thermal methods." Energies **15**(6): 2114.

Kim, S., W. Ko, S. Youn, R. Gao, Y. Chung and S. Bang (2016). "Advanced Depreciation Cost Analysis for a Commercial Pyroprocess Facility in Korea." Nuclear Engineering and Technology **48**(3): 733-743.

Klaimy, S., C. Ciotonea, J. Dhainaut, S. Royer, M. Casetta, S. Duquesne, G. Tricot and J. F. Lamonier (2020). "Flash catalytic pyrolysis of polyethylene over (alumino) silicate materials." ChemCatChem **12**(4): 1109-1116.

Klinghoffer, N. B., M. J. Castaldi and A. Nzihou (2012). "Catalyst Properties and Catalytic Performance of Char from Biomass Gasification." Industrial & Engineering Chemistry Research **51**(40): 13113-13122.

Knorr, D., J. Lukas and P. Schoen (2013). Production of Advanced Biofuels via Liquefaction-Hydrothermal Liquefaction Reactor Design: April 5, 2013, National Renewable Energy Lab.(NREL), Golden, CO (United States).

Koga, N. (2018). Chapter 6 - Physico-Geometric Approach to the Kinetics of Overlapping Solid-State Reactions. Handbook of Thermal Analysis and Calorimetry. S. Vyazovkin, N. Koga and C. Schick, Elsevier Science B.V. **6:** 213-251.

Kohansal, K., K. Sharma, M. S. Haider, S. S. Toor, D. Castello, L. A. Rosendahl, J. Zimmermann and T. H. Pedersen (2022). "Hydrotreating of bio-crude obtained from hydrothermal liquefaction of biopulp: effects of aqueous phase recirculation on the hydrotreated oil." Sustainable Energy & Fuels **6**(11): 2805-2822.

Kooduvalli, K., J. Unser, S. Ozcan and U. K. Vaidya (2022). "Embodied Energy in Pyrolysis and Solvolysis Approaches to Recycling for Carbon Fiber-Epoxy Reinforced Composite Waste Streams." Recycling **7**(1): 6.

Krungsri Research. (2022). "Monthly price of naphtha worldwide from January 2020 to June 2022 (in U.S. dollars per metric ton)." May 06, 2023, from https://www.statista.com/statistics/1318098/monthly-price-naphtha-worldwide/.

Kumagai, S., J. Nakatani, Y. Saito, Y. Fukushima and T. Yoshioka (2020). "Latest Trends and Challenges in Feedstock Recycling of Polyolefinic Plastics." Journal of the Japan Petroleum Institute **63**(6): 345-364.

Kunwar, B., H. Cheng, S. R. Chandrashekaran and B. K. Sharma (2016). "Plastics to fuel: a review." Renewable and Sustainable Energy Reviews **54**: 421-428.

Kusenberg, M., A. Eschenbacher, L. Delva, S. De Meester, E. Delikonstantis, G. D. Stefanidis, K. Ragaert and K. M. Van Geem (2022). "Towards high-quality petrochemical feedstocks from mixed plastic packaging waste via advanced recycling: The past, present and future." Fuel Processing Technology **238**: 107474.

Kusenberg, M., A. Eschenbacher, M. Djokic, A. Zayoud, K. Ragaert, S. De Meester and K. Van Geem (2021). Challenges and opportunities for plastic waste pyrolysis oils as steam cracking feedstock. 33rd Ethylene Producers' Conference (EPC).

Kusenberg, M., A. Eschenbacher, M. R. Djokic, A. Zayoud, K. Ragaert, S. De Meester and K. M. Van Geem (2022). "Opportunities and challenges for the application of post-consumer plastic waste pyrolysis oils as steam cracker feedstocks: To decontaminate or not to decontaminate?" Waste Management **138**: 83-115.

Kusenberg, M., M. Roosen, A. Doktor, L. Casado, A. Jamil Abdulrahman, B. Parvizi, A. Eschenbacher, E. Biadi, N. Laudou, D. Jänsch, S. De Meester and K. M. Van Geem (2023). "Contaminant removal from plastic waste pyrolysis oil via depth filtration and the impact on chemical recycling: A simple solution with significant impact." Chemical Engineering Journal **473**: 145259.

Kusenberg, M., M. Roosen, A. Zayoud, M. R. Djokic, H. D. Thi, S. De Meester, K. Ragaert, U. Kresovic and K. M. Van Geem (2022). "Assessing the feasibility of chemical recycling via steam cracking of untreated plastic waste pyrolysis oils: Feedstock impurities, product yields and coke formation." Waste Management **141**: 104-114.

Kwon, E. E., S. Kim and J. Lee (2019). "Pyrolysis of waste feedstocks in CO2 for effective energy recovery and waste treatment." Journal of Co2 Utilization **31**: 173-180.

Lampman, S. (2003). Characterization and failure analysis of plastics, Asm International.

Laredo, G. C., J. Reza and E. Meneses Ruiz (2023). "Hydrothermal liquefaction processes for plastics recycling: A review." Cleaner Chemical Engineering **5**: 100094.

Lase, I. S., A. Bashirgonbadi, F. van Rhijn, J. Dewulf, K. Ragaert, L. Delva, M. Roosen, M. Brandsma, M. Langen and S. De Meester (2022). "Material flow analysis and recycling performance of an improved mechanical recycling process for post-consumer flexible plastics." Waste Management **153**: 249-263.

Lase, I. S., D. Tonini, D. Caro, P. F. Albizzati, J. Cristóbal, M. Roosen, M. Kusenberg, K. Ragaert, K. M. Van Geem, J. Dewulf and S. De Meester (2023). "How much can chemical recycling contribute to plastic waste recycling in Europe? An assessment using material flow analysis modeling." Resources, Conservation and Recycling **192**: 106916.

Le Minh, C., A. K. Alanazi, D. J. Miron and T. C. Brown (2012). "Carbon–Carbon Bond Cleavage and Dehydrogenation of Isobutane Over HZSM-5 at Low Pressures and Temperatures." Catalysis letters **142**: 1470-1473.

Leal Filho, W., A. L. Salvia, A. Paço, C. Dias-Ferreira, S. Neiva, I. S. Rampasso, R. Anholon, C. R. P. de Vasconcelos, J. H. P. P. Eustachio and C. J. C. Jabbour (2022). "Assessing the Connections between COVID-19 and Waste Management in Brazil." Sustainability **14**(13): 8083.

Lebreton, L. and A. Andrady (2019). "Future scenarios of global plastic waste generation and disposal." Palgrave Communications **5**(1): 6.

LECO Corporation. "CHN628 Series: Determination of Carbon, Hydrogen, and Nitrogen in Biomass." Retrieved May 2023, from https://eu.leco.com/images/Analytical-Application-Library/CHN628_BIOMASS_203-821-510.pdf.

Lee, K.-H. (2007). "Pyrolysis of municipal plastic wastes separated by difference of specific gravity." Journal of Analytical and Applied pyrolysis **79**(1-2): 362-367.

Lee, K.-H. (2012). "Effects of the types of zeolites on catalytic upgrading of pyrolysis wax oil." Journal of Analytical and Applied Pyrolysis **94**: 209-214.

Lee, K.-H., N.-S. Noh, D.-H. Shin and Y. Seo (2002). "Comparison of plastic types for catalytic degradation of waste plastics into liquid product with spent FCC catalyst." Polymer Degradation and Stability **78**(3): 539-544.

Li, C., C. Zhang, M. Gholizadeh and X. Hu (2020). "Different reaction behaviours of light or heavy density polyethylene during the pyrolysis with biochar as the catalyst." Journal of Hazardous Materials **399**: 123075.

Li, K. and Z. Xu (2019). "A review of current progress of supercritical fluid technologies for e-waste treatment." Journal of Cleaner Production **227**: 794-809.

Li, L., J. Chen, Q. Zhang, Z. Yang, Y. Sun and G. Zou (2020). "Methane dry reforming over activated carbon supported Ni-catalysts prepared by solid phase synthesis." Journal of Cleaner Production **274**: 122256.

Lim, J., Y. Ahn, H. Cho and J. Kim (2022). "Optimal strategy to sort plastic waste considering economic feasibility to increase recycling efficiency." Process Safety and Environmental Protection **165**: 420-430.

Lin, X., H. Lei, C. Wang, M. Qian, W. Mateo, X. Chen, Y. Guo and E. Huo (2023). "The effects of pore structures and functional groups on the catalytic performance of activated carbon catalysts for the co-pyrolysis of biomass and plastic into aromatics and hydrogen-rich syngas." Renewable Energy **202**: 855-864.

Lin, Y.-H. and M.-H. Yang (2007). "Catalytic conversion of commingled polymer waste into chemicals and fuels over spent FCC commercial catalyst in a fluidised-bed reactor." Applied Catalysis B: Environmental **69**(3-4): 145-153.

Lin, Y.-H., M.-H. Yang, T.-F. Yeh and M.-D. Ger (2004). "Catalytic degradation of high density polyethylene over mesoporous and microporous catalysts in a fluidised-bed reactor." Polymer Degradation and Stability **86**(1): 121-128.

Lindfors, C., D. C. Elliott, W. Prins, A. Oasmaa and J. Lehtonen (2023). "Co-processing of Biocrudes in Oil Refineries." Energy & Fuels **37**(2): 799-804.

Ling, J. S. J., Y. H. Tan, N. M. Mubarak, J. Kansedo, A. Saptoro and C. Nolasco-Hipolito (2019). "A review of heterogeneous calcium oxide based catalyst from waste for biodiesel synthesis." SN Applied Sciences 1(8): 810.

Liu, K., F. Xing, Y. Xiao, N. Yan, K.-i. Shimizu and S. Furukawa (2023). "Development of a Highly Stable Ternary Alloy Catalyst for Dry Reforming of Methane." ACS Catalysis 13: 3541-3548.

Liu, W.-W., A. Aziz, S.-P. Chai, A. R. Mohamed and U. Hashim (2013). "Synthesis of single-walled carbon nanotubes: Effects of active metals, catalyst supports, and metal loading percentage." Journal of Nanomaterials 2013: 63-63.

Liu, X., Y. Zhang, M. A. Nahil, P. T. Williams and C. Wu (2017). "Development of Ni- and Fe-based catalysts with different metal particle sizes for the production of carbon nanotubes and hydrogen from thermo-chemical conversion of waste plastics." Journal of Analytical and Applied Pyrolysis 125: 32-39.

Lobo, H. and J. V. Bonilla (2003). Handbook of plastics analysis, Crc Press.

Lopez-Urionabarrenechea, A., I. De Marco, B. Caballero, M. Laresgoiti and A. Adrados (2012). "Catalytic stepwise pyrolysis of packaging plastic waste." Journal of analytical and applied pyrolysis 96: 54-62.

López, A., I. De Marco, B. Caballero, M. Laresgoiti and A. Adrados (2011). "Dechlorination of fuels in pyrolysis of PVC containing plastic wastes." Fuel Processing Technology 92(2): 253-260.

López, A., I. de Marco, B. M. Caballero, A. Adrados and M. F. Laresgoiti (2011). "Deactivation and regeneration of ZSM-5 zeolite in catalytic pyrolysis of plastic wastes." Waste Management 31(8): 1852-1858.

López, A., I. de Marco, B. M. Caballero, M. F. Laresgoiti and A. Adrados (2010). "Pyrolysis of municipal plastic wastes: Influence of raw material composition." Waste Management 30(4): 620-627.

López, A., I. de Marco, B. M. Caballero, M. F. Laresgoiti and A. Adrados (2011). "Influence of time and temperature on pyrolysis of plastic wastes in a semi-batch reactor." Chemical Engineering Journal 173(1): 62-71.

López, A., I. de Marco, B. M. Caballero, M. F. Laresgoiti, A. Adrados and A. Aranzabal (2011). "Catalytic pyrolysis of plastic wastes with two different types of catalysts: ZSM-5 zeolite and Red Mud." Applied Catalysis B: Environmental 104(3): 211-219.

Lopez, G., M. Artetxe, M. Amutio, J. Alvarez, J. Bilbao and M. Olazar (2018). "Recent advances in the gasification of waste plastics. A critical overview." Renewable and Sustainable Energy Reviews 82: 576-596.

Lopez, G., M. Artetxe, M. Amutio, J. Bilbao and M. Olazar (2017). "Thermochemical routes for the valorization of waste polyolefinic plastics to produce fuels and chemicals. A review." Renewable and Sustainable Energy Reviews 73: 346-368.

Lu, P., Q. Huang, Y. Chi, F. Wang and J. Yan (2019). "Catalytic cracking of tar derived from the pyrolysis of municipal solid waste fractions over biochar." Proceedings of the Combustion Institute 37(3): 2673-2680.

Lu, P., Q. Huang, Y. Chi and J. Yan (2017). "Coking and regeneration of nickel catalyst for the cracking of toluene as a tar model compound." Energy & Fuels 31(8): 8283-8290.

Ma, C., J. Yu, B. Wang, Z. Song, J. Xiang, S. Hu, S. Su and L. Sun (2017). "Catalytic pyrolysis of flame retarded high impact polystyrene over various solid acid catalysts." Fuel Processing Technology 155: 32-41.

MacKenzie, K. J., O. M. Dunens and A. T. Harris (2010). "An updated review of synthesis parameters and growth mechanisms for carbon nanotubes in fluidized beds." Industrial & Engineering Chemistry Research 49(11): 5323-5338.

Mankiw, N. G. (2020). Principles of economics, Cengage Learning.

Maqsood, T., J. Dai, Y. Zhang, M. Guang and B. Li (2021). "Pyrolysis of plastic species: A review of resources and products." Journal of Analytical and Applied Pyrolysis 159: 105295.

Martínez-Narro, G., P. Prasertcharoensuk, L. S. Diaz-Silvarrey, L. Dixon and A. N. Phan (2022). "Chemical recycling of mixed plastic waste via catalytic pyrolysis." Journal of Environmental Chemical Engineering 10(5): 108494.

Martínez-Narro, G., N. J. Royston, K. L. Billsborough and A. N. Phan (2023). "Kinetic modelling of mixed plastic waste pyrolysis." Chemical Thermodynamics and Thermal Analysis 9: 100105.

Martínez-Narro, G. and A. N. Phan (2021). "Co-Liquefaction of Biomass to Biofuels." Liquid Biofuels: Fundamentals, Characterization, and Applications: 145-182.

McKee, D. W. (1962). "The Kinetics of Propane Cracking on Nickel." Journal of the American Chemical Society 84(23): 4427-4431.

Meegoda, J. N., H. Hettiarachchi and P. Hettiaratchi (2016). "Landfill design and operation." Sustainable Solid Waste Management: 577-604.

Miandad, R., M. A. Barakat, A. S. Aburiazaiza, M. Rehan and A. S. Nizami (2016). "Catalytic pyrolysis of plastic waste: A review." Process Safety and Environmental Protection 102: 822-838.

Miandad, R., M. Rehan, M. A. Barakat, A. S. Aburiazaiza, H. Khan, I. M. Ismail, J. Dhavamani, J. Gardy, A. Hassanpour and A.-S. Nizami (2019). "Catalytic pyrolysis of plastic waste: moving toward pyrolysis based biorefineries." Frontiers in energy research 7: 27.

Miceli, M., P. Frontera, A. Macario and A. Malara (2021). "Recovery/reuse of heterogeneous supported spent catalysts." Catalysts 11(5): 591.

Mickey, C. D. (1980). "Chemical kinetics: Reaction rates." Journal of Chemical Education 57(9): 659.

Miranda, R., J. Yang, C. Roy and C. Vasile (2001). "Vacuum pyrolysis of commingled plastics containing PVC I. Kinetic study." Polymer Degradation and Stability 72(3): 469-491.

Miskolczi, N., L. Bartha, G. Deák and B. Jóver (2004). "Thermal degradation of municipal plastic waste for production of fuel-like hydrocarbons." Polymer Degradation and Stability 86(2): 357-366.

Miskolczi, N., T. Juzsakova and J. Sója (2019). "Preparation and application of metal loaded ZSM-5 and y-zeolite catalysts for thermo-catalytic pyrolysis of real end of life vehicle plastics waste." Journal of the Energy Institute 92(1): 118-127.

Miskolczi, N. and R. Nagy (2012). "Hydrocarbons obtained by waste plastic pyrolysis: comparative analysis of decomposition described by different kinetic models." Fuel processing technology 104: 96-104.

Moorthy Rajendran, K., V. Chintala, A. Sharma, S. Pal, J. K. Pandey and P. Ghodke (2020). "Review of catalyst materials in achieving the liquid hydrocarbon fuels from municipal mixed plastic waste (MMPW)." Materials Today Communications **24**: 100982.

Moraes, V. T. d., L. A. Jermolovicius, J. A. S. Tenório, S. M. G. Lebrão and G. W. Lebrão (2020). "Microwave-assisted recycling process to recover fiber from fiberglass polyester composites." Materials Research **22**.

Mordi, R. C., R. Fields and J. Dwyer (1994). "Thermolysis of low density polyethylene catalysed by zeolites." Journal of Analytical and Applied Pyrolysis **29**(1): 45-55.

Moreno, M., C. De los Rios, Z. Rowe and F. Charnley (2016). "A conceptual framework for circular design." Sustainability **8**(9): 937.

Morin, C., A. Loppinet-Serani, F. Cansell and C. Aymonier (2012). "Near- and supercritical solvolysis of carbon fibre reinforced polymers (CFRPs) for recycling carbon fibers as a valuable resource: State of the art." The Journal of Supercritical Fluids **66**: 232-240.

Moriya, T. and H. Enomoto (1999). "Characteristics of polyethylene cracking in supercritical water compared to thermal cracking." Polymer Degradation and Stability **65**(3): 373-386.

Mosio-Mosiewski, J., M. Warzala, I. Morawski and T. Dobrzanski (2007). "High-pressure catalytic and thermal cracking of polyethylene." Fuel processing technology **88**(4): 359-364.

Mota, B., M. I. Gomes, A. Carvalho and A. P. Barbosa-Povoa (2015). "Towards supply chain sustainability: economic, environmental and social design and planning." Journal of cleaner production **105**: 14-27.

Muller, B. (2011). Colorants for thermoplastic polymers. Applied plastics engineering handbook, Elsevier**:** 435-440.

Munir, D., M. F. Irfan and M. R. Usman (2018). "Hydrocracking of virgin and waste plastics: A detailed review." Renewable and Sustainable Energy Reviews **90**: 490-515.

Murata, K. and M. Akimoto (1979). "Thermal degradation of mixed polymer (**混合ポリマーの熱分解**)." Nippon Kagaku Kaishi(6): 774-781.

Muravyev, N. V., A. N. Pivkina and N. Koga (2019). "Critical appraisal of kinetic calculation methods applied to overlapping multistep reactions." Molecules **24**(12): 2298.

Murena, F. and F. Gioia (1998). "Catalytic hydroprocessing of chlorobenzene–pyridine mixtures." Journal of Hazardous Materials **60**(3): 271-285.

Naseeb, A., A. Ramadan and S. M. Al-Salem (2022). "Economic feasibility study of a carbon capture and storage (CCS) integration project in an oil-driven economy: the case of the state of Kuwait." International Journal of Environmental Research and Public Health **19**(11): 6490.

Neste. (2021). "Neste and Ravago plan to set up a joint venture to focus on chemical recycling of waste plastic." Retrieved May 2023, from https://www.neste.com/releases-and-news/circular-economy/neste-and-ravago-plan-set-joint-venture-focus-chemical-recycling-waste-plastic.

Nielsen, T. D., J. Hasselbalch, K. Holmberg and J. Stripple (2020). "Politics and the plastic crisis: A review throughout the plastic life cycle." Wiley Interdisciplinary Reviews-Energy and Environment **9**(1): 18.

Nikiema, J. and Z. Asiedu (2022). "A review of the cost and effectiveness of solutions to address plastic pollution." Environmental Science and Pollution Research **29**(17): 24547-24573.

Noritake, A., M. Hori, M. Shigematsu and M. Tanahashi (2008). "Recycling of polyethylene terephthalate using high-pressure steam treatment." Polymer journal 40(6): 498-502.

Obalı, Z., N. A. Sezgi and T. Doğu (2012). "Catalytic degradation of polypropylene over alumina loaded mesoporous catalysts." Chemical engineering journal 207: 421-425.

Oliveira, C. and T. Van Dril (2021). Decarbonisation options for large volume organic chemicals production, Sabic geleen, PBL/TNO (MIDDEN).

Onwudili, J. A., C. Muhammad and P. T. Williams (2019). "Influence of catalyst bed temperature and properties of zeolite catalysts on pyrolysis-catalysis of a simulated mixed plastics sample for the production of upgraded fuels and chemicals." Journal of the Energy Institute 92(5): 1337-1347.

Onwudili, J. A. and P. T. Williams (2016). "Catalytic supercritical water gasification of plastics with supported RuO2: A potential solution to hydrocarbons–water pollution problem." Process Safety and Environmental Protection 102: 140-149.

Opfermann, J. (2000). "Kinetic Analysis Using Multivariate Non-linear Regression. I. Basic concepts." Journal of Thermal Analysis and Calorimetry 60(2): 641-658.

Oster, K., A. Tedstone, A. J. Greer, N. Budgen, A. Garforth and C. Hardacre (2020). "Dehydrochlorination of PVC in multi-layered blisterpacks using ionic liquids." Green Chemistry 22(15): 5132-5142.

Pal, S., A. Kumar, A. K. Sharma, P. K. Ghodke, S. Pandey and A. Patel (2022). "Recent Advances in Catalytic Pyrolysis of Municipal Plastic Waste for the Production of Hydrocarbon Fuels." Processes 10(8): 1497.

Pala, L. P. R., Q. Wang, G. Kolb and V. Hessel (2017). "Steam gasification of biomass with subsequent syngas adjustment using shift reaction for syngas production: An Aspen Plus model." Renewable Energy 101: 484-492.

Pandey, A., T. Bhaskar, M. Stöcker and R. Sukumaran (2015). "Recent advances in thermochemical conversion of biomass."

Pandey, P., M. Dhiman, P. Chopra and A. Adlakha (2022). "Investigating the Role of Tourists and Impact of Knowledge, Behaviour, and Attitude Towards Plastic Waste Generation." Circular Economy and Sustainability: 1-15.

Pandey, U., J. A. Stormyr, A. Hassani, R. Jaiswal, H. H. Haugen and B. M. E. Moldestad (2020). "Pyrolysis of plastic waste to environmentally friendly products." Energy Produc Manage in the 21st century IV: The Quest for Sustain Energy 246: 61-74.

Papuga, S., M. Djurdjevic, A. Ciccioli and S. Vecchio Ciprioti (2022). "Catalytic Pyrolysis of Plastic Waste and Molecular Symmetry Effects: A Review." Symmetry 15(1): 38.

Park, S., J. Jae, A. Farooq, E. E. Kwon, E. D. Park, J.-M. Ha, S.-C. Jung and Y.-K. Park (2019). "Continuous pyrolysis of organosolv lignin and application of biochar on gasification of high density polyethylene." Applied Energy 255: 113801.

Parku, G. K., F.-X. Collard and J. F. Görgens (2020). "Pyrolysis of waste polypropylene plastics for energy recovery: Influence of heating rate and vacuum conditions on composition of fuel product." Fuel Processing Technology 209: 106522.

Parvin, F. and S. M. Tareq (2021). "Impact of landfill leachate contamination on surface and groundwater of Bangladesh: a systematic review and possible public health risks assessment." Applied water science 11(6): 100.

Pawelczyk, E., I. Wysocka and J. Gebicki (2022). "Pyrolysis Combined with the Dry Reforming of Waste Plastics as a Potential Method for Resource Recovery-A Review of Process Parameters and Catalysts." Catalysts **12**(4).

Pedersen, T. H. and F. Conti (2017). "Improving the circular economy via hydrothermal processing of high-density waste plastics." Waste management **68**: 24-31.

Perejón, A., P. E. Sánchez-Jiménez, J. M. Criado and L. A. Pérez-Maqueda (2011). "Kinetic Analysis of Complex Solid-State Reactions. A New Deconvolution Procedure." The Journal of Physical Chemistry B **115**(8): 1780-1791.

Perez-Maqueda, L., J. Criado and P. Sanchez-Jimenez (2006). "Combined kinetic analysis of solid-state reactions: a powerful tool for the simultaneous determination of kinetic parameters and the kinetic model without previous assumptions on the reaction mechanism." The Journal of Physical Chemistry A **110**(45): 12456-12462.

Phan, H. H. (2021). Biomass-derived carbon as a precursor for bipolar plate in vanadium redox flow battery, Newcastle University.

PlasticsEurope. (2019). "Plastics–the Facts 2019." Retrieved March, 2020, from https://plasticseurope.org/knowledge-hub/plastics-the-facts-2019/.

PlasticsEurope. (2020). "Plastics–the Facts 2020." Retrieved March, 2021, from https://www.plasticseurope.org/en/resources/publications/4312-plastics-facts-2020.

PlasticsEurope. (2022). "Plastics–the Facts 2022." Retrieved March, 2023, from https://plasticseurope.org/knowledge-hub/plastics-the-facts-2022/.

Prabhansu, M. K. Karmakar, P. Chandra and P. K. Chatterjee (2015). "A review on the fuel gas cleaning technologies in gasification process." Journal of Environmental Chemical Engineering **3**(2): 689-702.

Praveenkumar, T., P. Velusamy and D. Balamoorthy (2022). "Pyrolysis oil for diesel engines from plastic solid waste: a performance, combustion and emission study." International Journal of Ambient Energy **43**(1): 3223-3227.

Prinçaud, M., C. Aymonier, A. Loppinet-Serani, N. Perry and G. Sonnemann (2014). "Environmental Feasibility of the Recycling of Carbon Fibers from CFRPs by Solvolysis Using Supercritical Water." ACS Sustainable Chemistry & Engineering **2**(6): 1498-1502.

Pritchard, G. (2012). Plastics additives: an AZ reference, Springer Science & Business Media.

Protsenko, A. and V. Petrov (2022). "Recycling of fiberglass fillers obtained from polymer composites based on an epoxy vinyl ester binder." Mechanics of Composite Materials **58**(4): 537-544.

Ptáček, P., F. Šoukal and T. Opravil (2018). "Introduction to the transition state theory." Introducing the Effective Mass of Activated Complex and the Discussion on the Wave Function of this Instanton **27**.

Ragaert, K., L. Delva and K. Van Geem (2017). "Mechanical and chemical recycling of solid plastic waste." Waste Management **69**: 24-58.

Raheem, A. B., Z. Z. Noor, A. Hassan, M. K. Abd Hamid, S. A. Samsudin and A. H. Sabeen (2019). "Current developments in chemical recycling of post-consumer polyethylene terephthalate wastes for new materials production: A review." Journal of Cleaner Production **225**: 1052-1064.

Rasi, R. Z., H. Ismail, M. S. Shahbaz and V. P. K. Sundram (2023). "Interdisciplinary challenges in the circular supply chains: A systematic literature review." Heliyon.

Ratnasari, D. K., M. A. Nahil and P. T. Williams (2017). "Catalytic pyrolysis of waste plastics using staged catalysis for production of gasoline range hydrocarbon oils." Journal of Analytical and Applied Pyrolysis **124**: 631-637.

Recycled UK Limited. (2023). "Current Plastic Recycling Prices." Retrieved 6 May 2023, from https://blog.recycleduklimited.com/current-plastic-recycling-prices.

Ritchie, H., M. Roser and P. Rosado (2020). Energy. Published online at OurWorldInData. org.

Rosi, L., M. Bartoli and M. Frediani (2018). "Microwave assisted pyrolysis of halogenated plastics recovered from waste computers." Waste Management **73**: 511-522.

Rouf, S. A., Z. Usman, H. T. Masood, A. M. Majeed, M. Sarwar and W. Abbas (2021). Synthesis and Purification of Carbon Nanotubes. Carbon nanotubes-redefining the world of electronics, IntechOpen London.

Rouquerol, J., D. Avnir, C. Fairbridge, D. Everett, J. Haynes, N. Pernicone, J. Ramsay, K. Sing and K. Unger (1994). "Recommendations for the characterization of porous solids (Technical Report)." Pure and applied chemistry **66**(8): 1739-1758.

Roussi, A. T., E. C. Vouvoudi and D. S. Achilias (2020). "Pyrolytic degradation kinetics of HIPS, ABS, PC and their blends with PP and PVC." Thermochimica Acta **690**: 178705.

Saad, J. M., M. A. Nahil and P. T. Williams (2015). "Influence of process conditions on syngas production from the thermal processing of waste high density polyethylene." Journal of Analytical and Applied Pyrolysis **113**: 35-40.

Saad, J. M., M. A. Nahil, C. Wu and P. T. Williams (2015). "Influence of nickel-based catalysts on syngas production from carbon dioxide reforming of waste high density polyethylene." Fuel Processing Technology **138**: 156-163.

Saad, J. M. and P. T. Williams (2016). "Catalytic dry reforming of waste plastics from different waste treatment plants for production of synthesis gases." Waste Management **58**: 214-220.

Saad, J. M. and P. T. Williams (2016). "Pyrolysis-Catalytic-Dry Reforming of Waste Plastics and Mixed Waste Plastics for Syngas Production." Energy & Fuels **30**(4): 3198-3204.

Saad, J. M. and P. T. Williams (2017). "Manipulating the H2/CO ratio from dry reforming of simulated mixed waste plastics by the addition of steam." Fuel Processing Technology **156**: 331-338.

Saad, J. M. and P. T. Williams (2017). "Pyrolysis-catalytic dry (CO2) reforming of waste plastics for syngas production: Influence of process parameters." Fuel **193**: 7-14.

Saad, J. M., P. T. Williams, Y. S. Zhang, D. Yao, H. Yang and H. Zhou (2021). "Comparison of waste plastics pyrolysis under nitrogen and carbon dioxide atmospheres: A thermogravimetric and kinetic study." Journal of Analytical and Applied Pyrolysis **156**: 105135.

Saha, B. and A. Ghoshal (2007). "Model-free kinetics analysis of decomposition of polypropylene over Al-MCM-41." Thermochimica acta **460**(1-2): 77-84.

Saha, B. and A. Ghoshal (2007). "Model-free kinetics analysis of ZSM-5 catalyzed pyrolysis of waste LDPE." Thermochimica acta **453**(2): 120-127.

Sakhuja, D., H. Ghai, R. K. Bhatia and A. K. Bhatt (2022). "Management of E-waste: technological challenges and opportunities." Handbook of Solid Waste Management: Sustainability through Circular Economy: 1523-1557.

Santamaria, L., G. Lopez, E. Fernandez, M. Cortazar, A. Arregi, M. Olazar and J. Bilbao (2021). "Progress on Catalyst Development for the Steam Reforming of Biomass and Waste Plastics Pyrolysis Volatiles: A Review." Energy & Fuels **35**(21): 17051-17084.

Santos, B. P. S., D. Almeida, V. M. Maria de Fatima and C. A. Henriques (2018). "Petrochemical feedstock from pyrolysis of waste polyethylene and polypropylene using different catalysts." Fuel **215**: 515-521.

Schwarz, A. E., T. N. Ligthart, D. Godoi Bizarro, P. De Wild, B. Vreugdenhil and T. van Harmelen (2021). "Plastic recycling in a circular economy; determining environmental performance through an LCA matrix model approach." Waste Management **121**: 331-342.

Schyns, Z. O. and M. P. Shaver (2021). "Mechanical recycling of packaging plastics: A review." Macromolecular rapid communications **42**(3): 2000415.

Sengodan, S., R. Lan, J. Humphreys, D. Du, W. Xu, H. Wang and S. Tao (2018). "Advances in reforming and partial oxidation of hydrocarbons for hydrogen production and fuel cell applications." Renewable and Sustainable Energy Reviews **82**: 761-780.

Serra, A. C. S., J. V. Milato, J. G. Faillace and M. R. C. M. Calderari (2022). "Reviewing the use of zeolites and clay based catalysts for pyrolysis of plastics and oil fractions." Brazilian Journal of Chemical Engineering.

Serrano, D. P., J. Aguado and J. M. Escola (2012). "Developing Advanced Catalysts for the Conversion of Polyolefinic Waste Plastics into Fuels and Chemicals." ACS Catalysis **2**(9): 1924-1941.

Serrano, D. P., J. Aguado, J. M. Escola, J. M. Rodríguez and Á. Peral (2006). "Hierarchical Zeolites with Enhanced Textural and Catalytic Properties Synthesized from Organofunctionalized Seeds." Chemistry of Materials **18**(10): 2462-2464.

Seshasayee, M. S. and P. E. Savage (2020). "Oil from plastic via hydrothermal liquefaction: Production and characterization." Applied Energy **278**: 115673.

Šesták, J. and G. Berggren (1971). "Study of the kinetics of the mechanism of solid-state reactions at increasing temperatures." Thermochimica Acta **3**(1): 1-12.

Shangdiar, S., Y. C. Lin, P. C. Cheng, F. C. Chou and W. D. Wu (2021). "Development of biochar from the refuse derived fuel (RDF) through organic / inorganic sludge mixed with rice straw and coconut shell." Energy **215**: 9.

Sharma, M., D. S. Pilkhwal, P. K. Vijayan, D. Saha and R. K. Sinha (2010). "Steady state and linear stability analysis of a supercritical water natural circulation loop." Nuclear Engineering and Design **240**(3): 588-597.

Sharuddin, S., F. Abnisa, W. Daud and M. Aroua (2018). Pyrolysis of plastic waste for liquid fuel production as prospective energy resource. IOP Conference Series: Materials Science and Engineering, IOP Publishing.

Shell. (2021). "Shell invests in plastic waste-to-chemicals technology company BlueAlp." Retrieved May 2023, from https://www.shell.com/business-customers/chemicals/media-releases/2021-media-releases/shell-invests-in-plastic-waste-to-chemicals-technology-company-bluealp.html.

Shen, X., Z. Zhao, H. Li, X. Gao and X. Fan (2022). "Microwave-assisted pyrolysis of plastics with iron-based catalysts for hydrogen and carbon nanotubes production." Materials Today Chemistry **26**: 101166.

Shin, S.-K., N. Um, Y.-J. Kim, N.-H. Cho and T.-W. Jeon (2020). "New policy framework with plastic waste control plan for effective plastic waste management." Sustainability **12**(15): 6049.

Show, P. L., P. Pal, H. Y. Leong, J. C. Juan and T. C. Ling (2019). "A review on the advanced leachate treatment technologies and their performance comparison: an opportunity to keep the environment safe." Environmental Monitoring and Assessment **191**(4): 227.

Sietsma, J. R. A., A. Jos van Dillen, P. E. de Jongh and K. P. de Jong (2006). Application of ordered mesoporous materials as model supports to study catalyst preparation by impregnation and drying. Studies in Surface Science and Catalysis. E. M. Gaigneaux, M. Devillers, D. E. De Vos et al., Elsevier. **162:** 95-102.

Singh, R. K. and B. Ruj (2016). "Time and temperature depended fuel gas generation from pyrolysis of real world municipal plastic waste." Fuel **174**: 164-171.

Sinnott, R. K. (2005). Coulson & Richardson's chemical engineering. Vol. 6, Chemical engineering design. Oxford, Oxford : Elsevier Butterworth-Heinemann.

Snowden-Swan, L. J., Y. Zhu, M. D. Bearden, T. E. Seiple, S. B. Jones, A. J. Schmidt, J. M. Billing, R. T. Hallen, T. R. Hart and J. Liu (2017). Conceptual Biorefinery Design and Research Targeted for 2022: Hydrothermal Liquefacation Processing of Wet Waste to Fuels, Pacific Northwest National Lab.(PNNL), Richland, WA (United States).

Sokoli, H. U., M. E. Simonsen, R. P. Nielsen, K. R. Arturi and E. G. Søgaard (2016). "Conversion of the matrix in glass fiber reinforced composites into a high heating value oil and other valuable feedstocks." Fuel Processing Technology **149**: 29-39.

Song, C. and W. Pan (2004). "Tri-reforming of methane: a novel concept for catalytic production of industrially useful synthesis gas with desired H2/CO ratios." Catalysis Today **98**(4): 463-484.

Soni, V. K., G. Singh, B. K. Vijayan, A. Chopra, G. S. Kapur and S. S. V. Ramakumar (2021). "Thermochemical Recycling of Waste Plastics by Pyrolysis: A Review." Energy & Fuels **35**(16): 12763-12808.

Sørum, L., M. G. Grønli and J. E. Hustad (2001). "Pyrolysis characteristics and kinetics of municipal solid wastes." Fuel **80**(9): 1217-1227.

Stivala, S., J. Kimura and S. Gabbay (1983). "In Degradation and Stabilization of Polyolefins; Allen, NS, Ed." Appl. Sci. Publ.: London.

Sumter, D., J. de Koning, C. Bakker and R. Balkenende (2020). "Circular economy competencies for design." Sustainability **12**(4): 1561.

Sun, K., Q. Huang, Y. Chi and J. Yan (2018). "Effect of ZnCl2-activated biochar on catalytic pyrolysis of mixed waste plastics for producing aromatic-enriched oil." Waste Management **81**: 128-137.

Sun, K., Q. X. Huang, M. Ali, Y. Chi and J. H. Yan (2018). "Producing Aromatic-Enriched Oil from Mixed Plastics Using Activated Biochar as Catalyst." Energy & Fuels **32**(4): 5471-5479.

Sun, K., N. J. Themelis, A. C. Bourtsalas and Q. X. Huang (2020). "Selective production of aromatics from waste plastic pyrolysis by using sewage sludge derived char catalyst." Journal of Cleaner Production **268**: 13.

Syamsiro, M., H. Saptoadi, T. Norsujianto, P. Noviasri, S. Cheng, Z. Alimuddin and K. Yoshikawa (2014). "Fuel oil production from municipal plastic wastes in sequential pyrolysis and catalytic reforming reactors." Energy Procedia **47**: 180-188.

Tagaya, H. K., Kazuya; Kadokawa, Jun-ichi; Chiba, Koji (1999). "Decomposition of polycarbonate in subcritical and supercritical water." Polymer Degradation and Stability **64**(2): 289-292.

Trading Economics. "Naphtha." Retrieved May 10, 2023, from https://tradingeconomics.com/commodity/naphtha.

Trombetta, M., A. d. G. Alejandre, J. R. Solis and G. Busca (2000). "An FT-IR study of the reactivity of hydrocarbons on the acid sites of HZSM5 zeolite." Applied Catalysis A: General **198**(1-2): 81-93.

Tsakona, M. and I. Rucevska (2020). Plastic waste background report, Basel convention.

Tuffi, R., S. D'Abramo, L. M. Cafiero, E. Trinca and S. V. Ciprioti (2018). "Thermal behavior and pyrolytic degradation kinetics of polymeric mixtures from waste packaging plastics." Express Polymer Letters **12**(1): 82-99.

Uddin, M. A., T. Bhaskar, J. Kaneko, A. Muto, Y. Sakata and T. Matsui (2002). "Dehydrohalogenation during pyrolysis of brominated flame retardant containing high impact polystyrene (HIPS-Br) mixed with polyvinylchloride (PVC)." Fuel **81**(14): 1819-1825.

Valerio, O., R. Muthuraj and A. Codou (2020). "Strategies for polymer to polymer recycling from waste: Current trends and opportunities for improving the circular economy of polymers in South America." Current Opinion in Green and Sustainable Chemistry **25**: 100381.

van Deelen, T. W., C. Hernández Mejía and K. P. de Jong (2019). "Control of metal-support interactions in heterogeneous catalysts to enhance activity and selectivity." Nature Catalysis **2**(11): 955-970.

Venderbosch, R. and H. Heeres (2011). "Pyrolysis oil stabilisation by catalytic hydrotreatment." Biofuel's engineering process technology: 385-410.

Victory, M. (2021). "Mixed plastic waste price volatility rising as mechanical recycling economics shift and chemical recyclers enter chain." Sustainable Plastics, from https://www.sustainableplastics.com/news/mixed-plastic-waste-price-volatility-rising-mechanical-recycling-economics-shift-and-chemical#:~:text=With%20sharp%20increases%20in%20single,input%20has%20become%20economically%20viable.

Voisin, T., A. Erriguible, D. Ballenghien, D. Mateos, A. Kunegel, F. Cansell and C. Aymonier (2017). "Solubility of inorganic salts in sub- and supercritical hydrothermal environment: Application to SCWO processes." The Journal of Supercritical Fluids **120**: 18-31.

Vollmer, I., M. J. F. Jenks, M. C. P. Roelands, R. J. White, T. van Harmelen, P. de Wild, G. P. van der Laan, F. Meirer, J. T. F. Keurentjes and B. M. Weckhuysen (2020). "Beyond Mechanical Recycling: Giving New Life to Plastic Waste." Angewandte Chemie-International Edition **59**(36): 15402-15423.

Vrandečić, N. S., M. Erceg, M. Jakić and I. Klarić (2010). "Kinetic analysis of thermal degradation of poly(ethylene glycol) and poly(ethylene oxide)s of different molecular weight." Thermochimica Acta **498**(1): 71-80.

Vyazovkin, S. (2015). Isoconversional kinetics of thermally stimulated processes, Springer.

Vyazovkin, S. (2018). Chapter 4 - Modern Isoconversional Kinetics: From Misconceptions to Advances. Handbook of Thermal Analysis and Calorimetry. S. Vyazovkin, N. Koga and C. Schick, Elsevier Science B.V. 6: 131-172.

Vyazovkin, S., A. K. Burnham, J. M. Criado, L. A. Pérez-Maqueda, C. Popescu and N. Sbirrazzuoli (2011). "ICTAC Kinetics Committee recommendations for performing kinetic computations on thermal analysis data." Thermochimica Acta 520(1): 1-19.

Vyazovkin, S., A. K. Burnham, L. Favergeon, N. Koga, E. Moukhina, L. A. Pérez-Maqueda and N. Sbirrazzuoli (2020). "ICTAC Kinetics Committee recommendations for analysis of multi-step kinetics." Thermochimica Acta 689: 178597.

Vyazovkin, S. and N. Sbirrazzuoli (2006). "Isoconversional kinetic analysis of thermally stimulated processes in polymers." Macromolecular Rapid Communications 27(18): 1515-1532.

Walendziewski, J. and M. Steininger (2001). "Thermal and catalytic conversion of waste polyolefines." Catalysis Today 65(2): 323-330.

Wang, C., H. Lei, X. Kong, R. Zou, M. Qian, Y. Zhao and W. Mateo (2021). "Catalytic upcycling of waste plastics over nanocellulose derived biochar catalyst for the coupling harvest of hydrogen and liquid fuels." Science of The Total Environment 779: 146463.

Wang, C. X., H. W. Lei, M. R. O. Qian, E. G. Huo, Y. F. Zhao, Q. F. Zhang, W. Mateo, X. N. Lin, X. Kong, R. G. Zou and R. Ruan (2020). "Application of highly stable biochar catalysts for efficient pyrolysis of plastics: a readily accessible potential solution to a global waste crisis." Sustainable Energy & Fuels 4(9): 4614-4624.

Wang, F. J., S. Zhang, Z. D. Chen, C. Liu and Y. G. Wang (2014). "Tar reforming using char as catalyst during pyrolysis and gasification of Shengli brown coal." Journal of Analytical and Applied Pyrolysis 105: 269-275.

Wang, S., S. A. Nabavi and P. T. Clough (2023). "A review on bi/polymetallic catalysts for steam methane reforming." International Journal of Hydrogen Energy 48(42): 15879-15893.

Wang, W. M., Linghui; Yu, Jiali; Xie, Fei; Huang, Yudong (2017). "Enhanced hydrothermal conversion of caprolactam from waste monomer casting polyamide over H-Beta zeolite and its mechanism." Journal of Analytical and Applied Pyrolysis 125: 218-226.

Wang, Z., R. Wei, X. Ning, T. Xie and J. Wang (2019). "Thermal degradation properties of LDPE insulation for new and aged fine wires." Journal of Thermal Analysis and Calorimetry 137(2): 461-471.

Watanabe, M., H. Hirakoso, S. Sawamoto, A. Tadafumi and K. Arai (1998). "Polyethylene conversion in supercritical water." The Journal of Supercritical Fluids 13(1): 247-252.

Weiland, F., L. Lundin, M. Celebi, K. van der Vlist and F. Moradian (2021). "Aspects of chemical recycling of complex plastic waste via the gasification route." Waste Management 126: 65-77.

Weitkamp, J. (2012). "Catalytic hydrocracking—mechanisms and versatility of the process." ChemCatChem 4(3): 292-306.

Westerhout, R., J. Waanders, J. Kuipers and W. P. M. van Swaaij (1997). "Kinetics of the low-temperature pyrolysis of polyethene, polypropene, and polystyrene modeling, experimental determination, and comparison with literature models and data." Industrial & Engineering Chemistry Research 36(6): 1955-1964.

Wilberforce, T., A. G. Olabi, E. T. Sayed, K. Elsaid and M. A. Abdelkareem (2021). "Progress in carbon capture technologies." Science of The Total Environment 761: 143203.

Williams, E. A. and P. T. Williams (1997). "Analysis of products derived from the fast pyrolysis of plastic waste." Journal of Analytical and Applied Pyrolysis 40-41: 347-363.

Williams, P. T. and E. A. Williams (1999). "Interaction of Plastics in Mixed-Plastics Pyrolysis." Energy & Fuels 13(1): 188-196.

Wong, S. L., S. Armenise, B. B. Nyakuma, A. Bogush, S. Towers, C. H. Lee, K. Y. Wong, T. H. Lee, E. Rebrov and M. Muñoz (2023). "Plastic pyrolysis over HZSM-5 zeolite and fluid catalytic cracking catalyst under ultra-fast heating." Journal of Analytical and Applied Pyrolysis 169: 105793.

World Economic Forum, Ellen MacArthur Foundation and McKinsey & Company (2016). The New Plastics Economy — Rethinking the future of plastics.

Wu, J. and J. M. Prausnitz (1998). "Phase Equilibria for Systems Containing Hydrocarbons, Water, and Salt: An Extended Peng–Robinson Equation of State." Industrial & Engineering Chemistry Research 37(5): 1634-1643.

Wu, L. M., C. H. Zhou, D. S. Tong and W. H. Yu (2014). Catalytic thermochemical processes for biomass conversion to biofuels and chemicals. Bioenergy Research: Advances and Applications, Elsevier: 243-254.

Wu, S.-L., J.-H. Kuo and M.-Y. Wey (2019). "Thermal degradation of waste plastics in a two-stage pyrolysis-catalysis reactor over core-shell type catalyst." Journal of Analytical and Applied Pyrolysis 142: 104641.

Xin, J., Q. Zhang, J. Huang, R. Huang, Q. Z. Jaffery, D. Yan, Q. Zhou, J. Xu and X. Lu (2021). "Progress in the catalytic glycolysis of polyethylene terephthalate." Journal of Environmental Management 296: 113267.

Xu, F., B. Wang, D. Yang, J. Hao, Y. Qiao and Y. Tian (2018). "Thermal degradation of typical plastics under high heating rate conditions by TG-FTIR: Pyrolysis behaviors and kinetic analysis." Energy Conversion and Management 171: 1106-1115.

Xu, R., C. Yan, Q. Liu, E. Liu, H. Zhang, X. Zhang, X. Yuan, L. Han, H. Lei, R. Ruan and X. Zhang (2022). "Development of metal-doping mesoporous biochar catalyst for co-valorizing biomass and plastic waste into valuable hydrocarbons, syngas, and carbons." Fuel Processing Technology 227: 107127.

Xu, Y. M., G. N. Xie, K. Bei, L. Wang, J. L. Wang, I. M. Chou and Z. Y. Pan (2020). "Recycling of phenol from poly (1,4-cyclohexylene dimethylene terephthalate) using subcritical water from 260 to 340 degrees C." Journal of Material Cycles and Waste Management 22(5): 1639-1647.

Xue, Y., P. Johnston and X. Bai (2017). "Effect of catalyst contact mode and gas atmosphere during catalytic pyrolysis of waste plastics." Energy Conversion and Management 142: 441-451.

Yadav, G., A. Singh, A. Dutta, T. Uekert, J. S. DesVeaux, S. R. Nicholson, E. C. Tan, C. Mukarakate, J. A. Schaidle and C. J. Wrasman (2023). "Techno-economic analysis and life cycle assessment for catalytic fast pyrolysis of mixed plastic waste." Energy & Environmental Science.

Yahyazadeh, A., A. K. Dalai, W. Ma and L. Zhang (2021). "Fischer–Tropsch synthesis for light olefins from syngas: a review of catalyst development." Reactions 2(3): 227-257.

Yang, J. H., Quan; Yang, Linxi (2019). "A review on hydrothermal co-liquefaction of biomass." Appl. Energy 250: 926-945.

Yang, R.-X., K.-H. Chuang and M.-Y. Wey (2015). "Effects of Nickel Species on Ni/Al2O3 Catalysts in Carbon Nanotube and Hydrogen Production by Waste Plastic Gasification: Bench- and Pilot-Scale Tests." Energy & Fuels **29**(12): 8178-8187.

Ye, X., J. Zhang, Z. Chen, J. Xiang, Y. Jiang, F. Xie and X. Ma (2021). "Microwave absorption properties of Ni/C@ SiC composites prepared by precursor impregnation and pyrolysis processes." Defence Technology.

Yoshioka, T., T. Handa, G. Grause, Z. Lei, H. Inomata and T. Mizoguchi (2005). "Effects of metal oxides on the pyrolysis of poly(ethylene terephthalate)." Journal of Analytical and Applied Pyrolysis **73**(1): 139-144.

You, S., Y. S. Ok, D. C. Tsang, E. E. Kwon and C.-H. Wang (2018). "Towards practical application of gasification: a critical review from syngas and biochar perspectives." Critical Reviews in Environmental Science and Technology **48**(22-24): 1165-1213.

Younis, A., C. Gennequin, E. A. Aad, J. Estephane and S. Aouad (2021). Valorization of plastics in the presence of Ru-Ni/Al2O3 catalysts to produce syngas. 2021 12th International Renewable Energy Congress (IREC).

Yu, H., C. Wang, T. Lin, Y. An, Y. Wang, Q. Chang, F. Yu, Y. Wei, F. Sun and Z. Jiang (2022). "Direct production of olefins from syngas with ultrahigh carbon efficiency." Nature Communications **13**(1): 5987.

Yu, J., L. Sun, C. Ma, Y. Qiao and H. Yao (2016). "Thermal degradation of PVC: A review." Waste management **48**: 300-314.

Zhang, K., G. Zhang, X. Liu, A. N. Phan and K. Luo (2017). "A study on CO2 decomposition to CO and O2 by the combination of catalysis and dielectric-barrier discharges at low temperatures and ambient pressure." Industrial & Engineering Chemistry Research **56**(12): 3204-3216.

Zhang, S., K. Jiang and S. Yao (2018). Economic Evaluation of a Full Value Chain CO2-ECBM Project in China. 14th Greenhouse Gas Control Technologies Conference Melbourne.

Zhang, W., F. W. Starr, K. L. Beers and J. F. Douglas (2022). "Reactive molecular dynamics simulations of the depolymerization of polyethylene using graphene-oxide-supported platinum nanoparticles." The Journal of Physical Chemistry A **126**(20): 3167-3173.

Zhang, X., D.-g. Cheng, F. Chen and X. Zhan (2017). "n-Heptane catalytic cracking on hierarchical ZSM-5 zeolite: The effect of mesopores." Chemical Engineering Science **168**: 352-359.

Zhang, X., D. G. Cheng, F. Chen and X. Zhan (2018). "The Role of External Acidity of Hierarchical ZSM-5 Zeolites in n-Heptane Catalytic Cracking." ChemCatChem **10**(12): 2655-2663.

Zhang, Y., D. Duan, H. Lei, E. Villota and R. Ruan (2019). "Jet fuel production from waste plastics via catalytic pyrolysis with activated carbons." Applied Energy **251**: 113337.

Zhang, Y., M. A. Nahil, C. Wu and P. T. Williams (2017). "Pyrolysis–catalysis of waste plastic using a nickel–stainless-steel mesh catalyst for high-value carbon products." Environmental technology **38**(22): 2889-2897.

Zhang, Y. L., W. G. Wu, S. H. Zhao, Y. F. Long and Y. H. Luo (2015). "Experimental study on pyrolysis tar removal over rice straw char and inner pore structure evolution of char." Fuel Processing Technology **134**: 333-344.

Zhao, P. T., Z. L. Yuan, J. Zhang, X. P. Song, C. P. Wang, Q. J. Guo and A. J. Ragauskas (2021). "Supercritical water co-liquefaction of LLDPE and PP into oil: properties and synergy." Sustainable Energy & Fuels **5**(2): 575-583.

Zhao, T., Q. Zhou, X. L. He, S. D. Wei, L. Wang, J. M. N. van Kasteren and Y. Z. Wang (2010). "A highly efficient approach for dehydrochlorinating polyvinyl chloride: catalysis by 1-butyl-3-methylimidazolium chloride." Green Chemistry **12**(6): 1062-1065.

Zhao, X., Y. Xia, L. Zhan, B. Xie, B. Gao and J. Wang (2019). "Hydrothermal Treatment of E-Waste Plastics for Tertiary Recycling: Product Slate and Decomposition Mechanisms." ACS Sustain. Chem. Eng. **7**(1): 1464-1473.

Zhao, X. Z., Lu; Xie, Bing; Gao, Bin (2018). "Products derived from waste plastics (PC, HIPS, ABS, PP and PA6) via hydrothermal treatment: Characterization and potential applications." Chemosphere **207**: 742-752.

Zheng, Y., J. Bai, J. Xu, X. Li and Y. Zhang (2018). "A discrimination model in waste plastics sorting using NIR hyperspectral imaging system." Waste Management **72**: 87-98.

Zhou, H., J. M. Saad, Q. Li and Y. Xu (2020). "Steam reforming of polystyrene at a low temperature for high H2/CO gas with bimetallic Ni-Fe/ZrO2 catalyst." Waste Management **104**: 42-50.

Zhou, J. B., J. P. Zhao, J. L. Zhang, T. Zhang, M. Ye and Z. M. Liu (2020). "Regeneration of catalysts deactivated by coke deposition: A review." Chinese Journal of Catalysis **41**(7): 1048-1061.

Zhou, N., L. Dai, Y. Lv, H. Li, W. Deng, F. Guo, P. Chen, H. Lei and R. Ruan (2021). "Catalytic pyrolysis of plastic wastes in a continuous microwave assisted pyrolysis system for fuel production." Chemical Engineering Journal **418**: 129412.

Zia, K. M., H. N. Bhatti and I. Ahmad Bhatti (2007). "Methods for polyurethane and polyurethane composites, recycling and recovery: A review." Reactive and Functional Polymers **67**(8): 675-692.

BS 1016 : Part 3 : October 1973
UDC [662.66+662.74]:543+662.66:543.71

Methods for

The analysis and testing of coal and coke

Part 3 Proximate analysis of coal

Amendments issued since publication

Amd. No.	Date of issue	Text affected

British Standards Institution · 2 Park Street · London W1A 2BS
Telephone 01-629 9000
Telex 266933

BS 1016 : Part 3 : 1973

Contents

Foreword

This publication is Part 3 of a series of sixteen Parts issued under the same number, BS 1016, dealing with methods for the analysis and testing of coal and coke. The methods given in BS 1016 are specified for the analysis of coal or of coke or, in some instances, for the analysis of both coal and coke. Experience has shown that, in general, the methods may also be used for the analysis of manufactured smokeless fuels other than coke made by a conventional process. However, as no systematic survey has been made of their applicability to all such fuels, it is not possible to state whether the methods for coal or those for coke will be more appropriate for a particular fuel; usually the former are likely to be satisfactory for fuels prepared at temperatures below 800 °C.

The revision of Part 3 has been undertaken in order to introduce metric units throughout and to adopt a uniform presentation. No mandatory technical changes have been made from the 1965 edition. It deals with the determination of moisture, volatile matter and ash in the analysis sample of coal. The methods are such that it is sometimes convenient to analyse a number of different samples simultaneously. When multiple determinations are possible, any additional apparatus required has been specified. However, for simplicity, all procedures have been written for a single sample. When a system of multiple determination is adopted, duplicates on the same sample are carried out at separate times or in separate apparatus.

For the determination of moisture the direct gravimetric method has been retained and, apart from editorial differences, it is equivalent to that specified in ISO/R 331, 'Determination of moisture in the analysis sample of coal by the direct gravimetric method.' Two indirect methods are also described, one using the minimum-free-space oven and the other using evacuated retort tubes.

The methods for the determination of volatile matter and of ash described here are technically equivalent to those specified respectively in ISO/R 562, 'Determination of the volatile matter of hard coal and of coke', and ISO/R 1171, 'Determination of ash of solid mineral fuels'. In the latter, however, no reference is made to the method for the determination of ash using two furnaces, given here in **6.3**.

During the course of the present revision a method was submitted by the N.C.B. by means of which large numbers of routine ash determinations could be made. The sample is placed in a dish on a chain conveyor passing through a muffle furnace*. The temperature distribution within the furnace and the rate of travel of the grate are arranged so that ashing is complete and the dish cool enough to handle at the end of the conveyor. The precision of the results reported was, however, insufficient to meet the requirements of Clause **8.**

*Suitable apparatus may be obtained from Hedin Ltd., Ilford, Essex or from United Analysts Ltd., East Bolden, Co. Durham.

British Standard Methods for

The analysis and testing of coal and coke

Part 3 Proximate analysis of coal

1. Scope

This British Standard describes the determinations to be made on the analysis sample of coal in order to obtain its proximate analysis, namely, moisture, volatile matter and ash; fixed carbon is obtained by difference.

2. Definitions

For the purposes of this British Standard, the following definitions apply:

(1) *Proximate analysis.* The analysis of coal expressed in terms of moisture in the analysis sample, volatile matter, ash and fixed carbon.

(2) *Moisture in the analysis sample.* The moisture in the analysis sample of coal after it has attained approximate equilibrium with the laboratory atmosphere to which it has been exposed.

(3) *Volatile matter.* The loss in mass, less that due to moisture, that occurs when the coal is heated out of contact with air under standardized conditions.

(4) *Ash.* The inorganic matter remaining after the coal has been incinerated to constant mass under standardized conditions.

(5) *Fixed carbon.* A calculated figure obtained by subtracting the sum of the percentages of moisture in the analysis sample, volatile matter and ash from 100.

(6) *Repeatability*.* The maximum acceptable difference between duplicate determinations carried out at different times in the same laboratory on the same analysis sample by the same operator using the same apparatus.

(7) *Reproducibility*.* The maximum acceptable difference between the mean of duplicate determinations carried out in one laboratory and the mean of duplicate determinations carried out in any other laboratory on representative samples taken from the same bulk sample after the last stage of the reduction process.

3. Coal sample

The coal used for proximate analysis is the analysis sample of 50 g to 150 g having a top size not greater than 0.2 mm (ground to pass a 212 μm test sieve to BS 410), taken and prepared according to BS 1017 : Part 1.

The sample received in the laboratory shall be brought into approximate equilibrium with the laboratory atmosphere by exposure in a thin layer on a tray. The exposure time shall be kept to the minimum necessary, particularly with coals liable to oxidation. The sample shall be thoroughly mixed, preferably by mechanical means†, immediately before analysis. Portions for duplicate determinations shall be weighed out consecutively, although the determinations shall not be made in the same apparatus at the same time.

*See BS 1016 : Part 16.
†A mixer of a type similar to that described in BS 1017 : Part 2, is suitable.

4. Moisture in the analysis sample

4.1 General. The moisture in the analysis sample, while having little significance in itself, is required for calculating other results to any desired basis. Moisture determinations shall therefore be made at the same time as those for volatile matter and ash.

Any of three methods may be used for the determination:

Direct gravimetric determination (see **4.2**);

Drying in nitrogen (see **4.3**);

Drying in vacuo (see **4.4**).

In the direct method (see **4.2**), the moisture is obtained from the mass of water evolved, whereas the methods in **4.3** and **4.4** are indirect and the moisture is calculated from the loss of mass of the coal on drying. Although the direct and indirect methods have been found to give substantially the same results, occasionally the indirect methods may give slightly lower values.

4.2 Direct gravimetric determination

4.2.1 *Principle.* A known mass of the sample is heated in a current of nitrogen at 105 °C to 110 °C and the water driven off is collected in an absorption tube. The moisture in the sample is calculated from the increase in mass of the absorption tube.

4.2.2 *Special reagents.* The following reagents are required:

(1) *Nitrogen*, containing less than 10 p.p.m. of oxygen.

(2) *Magnesium perchlorate**, 0.9 mm to 1.2 mm.

4.2.3 *Special apparatus.* The apparatus required is shown diagrammatically in Fig. 1. It consists of the following components:

(1) *Oven.* An oven, preferably of the block type, capable of accommodating a glass retort tube and of maintaining a temperature within the range 105 °C to 110 °C in the tube. The oven may be designed to accommodate a number of these tubes.

(2) *Retort tube.* A glass retort tube, 275 mm long and having a 15 mm internal diameter, with a depression 170 mm from the sealed end, fitted with a flexible, heat resistant stopper through which pass two glass tubes. One of these, the inlet tube,is connected to the flowmeter and terminates just inside the stopper. The other, the outlet tube, is connected to the absorption tube and passes down the retort tube almost to the sealed end (see Fig. 2). The connection between the flowmeter and the inlet tube is made with polyvinyl chloride tubing. The connection between the outlet tube and the absorption tube is made with a short length of rubber tubing.

(3) *Drying tower.* A drying tower, 250 ml capacity, packed with magnesium perchlorate for drying the nitrogen.

(4) *Flowmeter.* A flowmeter capable of measuring a flow rate of 100 ml per minute. If the flowmeter contains a liquid this shall be a non-volatile oil.

(5) *Absorption tube.* An absorption tube which shall be either a U-tube, fitted with glass stoppers and filled with magnesium perchlorate retained by plugs of glass wool, or a Riley tube, the centre column of which is filled with magnesium perchlorate retained by plugs of glass wool.

If multiple determinations are made, the following will also be required:

(6) *Manifold.* A manifold made so that the branches are in line with the corresponding flowmeters.

(7) *Control valves.* A needle valve or screw clip, placed between each flowmeter and the manifold, for controlling the nitrogen flow rate.

4.2.4 *Procedure.* Adjust the rate of flow of the nitrogen passing through the flowmeter to 100 ml/min. Connect an empty retort tube to a closed absorption tube and to the nitrogen stream from the flowmeter. Check for leaks in the system. Open the tap(s) of the absorption tube and re-adjust the flow rate to 100 ml/min.

Insert the retort tube into the oven heated to 105 °C to 110 °C. After 15 min (see Note 1) close the tap(s) of the absorption tube, disconnect, wipe with a clean dry cloth free from loose fibres and allow the absorption tube to stand for 20 min in the balance room. Open the tap(s) of the absorption tube momentarily to equalize the pressure and then weigh to the nearest 0.1 mg. While the absorption tube is standing prior to weighing, remove the retort tube from the oven and allow to cool with a stream of dry nitrogen passing through it. When the retort tube is cool remove it, with the stopper and tubes still in it, to the balance room.

*This is the quality of reagent referred to as 'magnesium perchlorate (dried)', sometimes known as 'Anhydrone'.

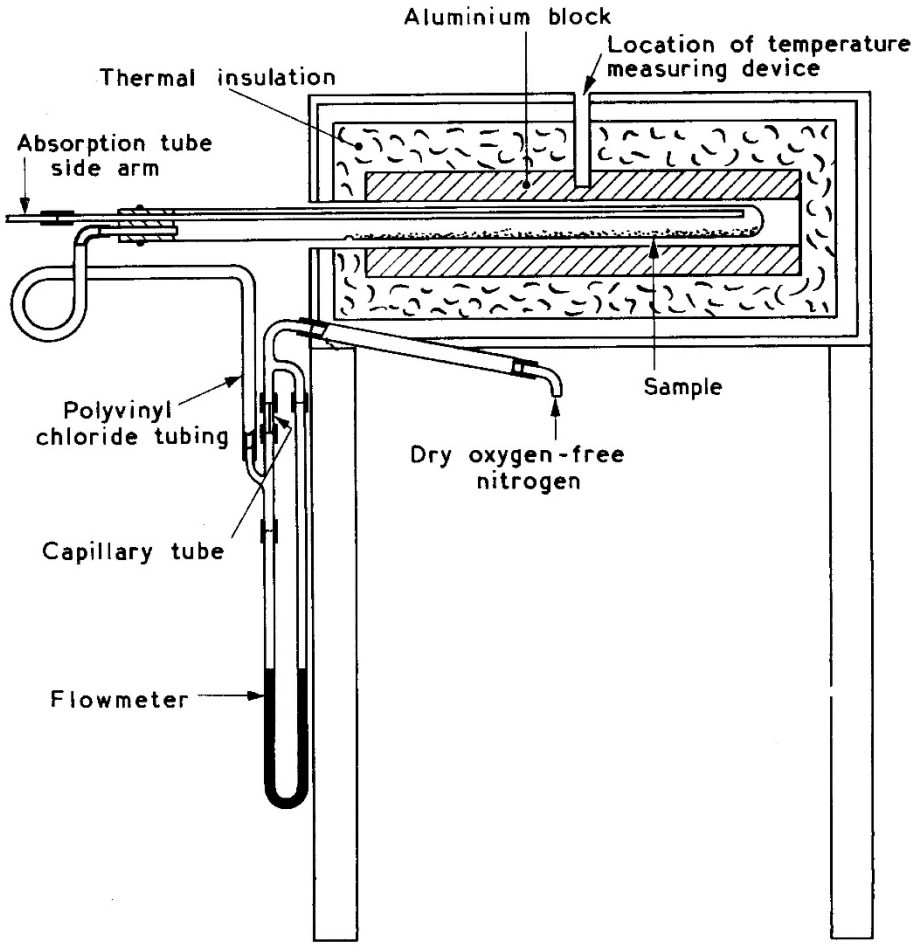

Fig. 1. Apparatus for the direct determination of moisture

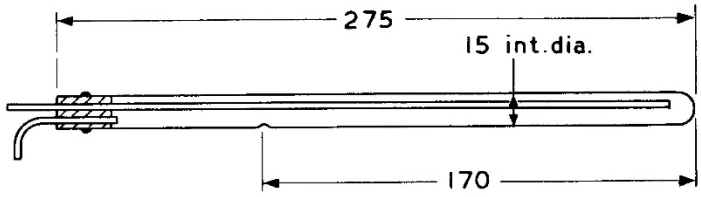

Dimensions in millimetres.

Fig. 2. Retort tube

Weigh about 1 g of the coal sample to the nearest 0.1 mg on a scoop and transfer the coal to the retort tube, removing the stopper and tubes just prior to the introduction of the sample. Spread the coal in an even layer between the sealed end and the depression in the retort tube. Replace the stopper and tubes, reassemble the apparatus and check for leaks as before (see Note 2). Resume the passage of nitrogen at 100 ml/min.

Insert the charged retort tube into the oven. After 60 min close the tap(s) of the absorption tube, disconnect, condition and weigh the absorption tube as described above.

Carry out a blank determination using the same procedure as for the moisture determination but omitting the coal sample (see Note 3). The increase in mass of the absorption tube should not be more than 1 mg.

4.2.5 *Calculation of result.* The result shall be calculated as follows:

If m_1 = mass of coal used (g)

m_2 = mass of absorption tube before the determination (g)

m_3 = mass of absorption tube after the determination (g)

m_4 = mass of absorption tube before the blank determination (g)

m_5 = mass of absorption tube after the blank determination (g)

M_{ad} = percentage of moisture in the analysis sample.

then

$$M_{ad} = \frac{(m_3 - m_2) - (m_5 - m_4)}{m_1} \times 100$$

4.3 Drying in nitrogen

4.3.1 *Principle.* A known mass of the sample is heated to constant mass in a current of nitrogen, in an oven maintained at 105 °C to 110 °C and the percentage moisture is calculated from the loss in mass.

4.3.2 *Special reagents.* The following reagents are required:

(1) *Nitrogen.* Dry and containing less than 10 p.p.m. of oxygen; this is commercially available in cylinders.

(2) *Desiccant.* Self-indicating activated alumina or silica gel, or magnesium perchlorate*.

4.3.3 *Special apparatus.* The following apparatus is required:

(1) *Oven.* A minimum-free-space oven capable of maintaining a temperature within the range 105 °C to 110 °C and with provision for the nitrogen to pass through it at about 15 oven volumes per hour. A suitable oven is illustrated in Fig. 3. Arrangements should be made for measuring the flow of nitrogen through the oven.

(2) *Weighing vessels.* Shallow vessels, of glass with ground-on covers or of corrosion-resistant metal with well-fitting covers, of such a size that the loading of the coal layer does not exceed 0.15 g/cm^2.

4.3.4 *Procedure.* Raise the oven to its working temperature while passing nitrogen through it at the specified rate. Weigh a clean dry empty weighing vessel with its cover to the nearest 0.1 mg. Spread into it in an even layer about 1 g of the coal sample, cover and reweigh to determine the mass of sample taken. Place the cover on a metal plate in a desiccator and heat the uncovered vessel in the oven until constant in mass (see Note 4). Remove the vessel and dry sample from the oven, replace the cover and allow to cool on a metal plate for not longer than 5 min; transfer to the metal plate in the desiccator and weigh when cold.

4.3.5 *Calculation of result.* The result shall be calculated as follows:

If m_1 = mass of vessel plus cover (g)

m_2 = mass of vessel plus cover plus sample, before heating (g)

m_3 = mass of vessel plus cover plus sample, after heating (g)

M_{ad} = percentage of moisture in the analysis sample,

then

$$M_{ad} = \frac{m_2 - m_3}{m_2 - m_1} \times 100$$

*This is the quality of reagent referred to as 'magnesium perchlorate (dried)', sometimes known as 'Anhydrone'.

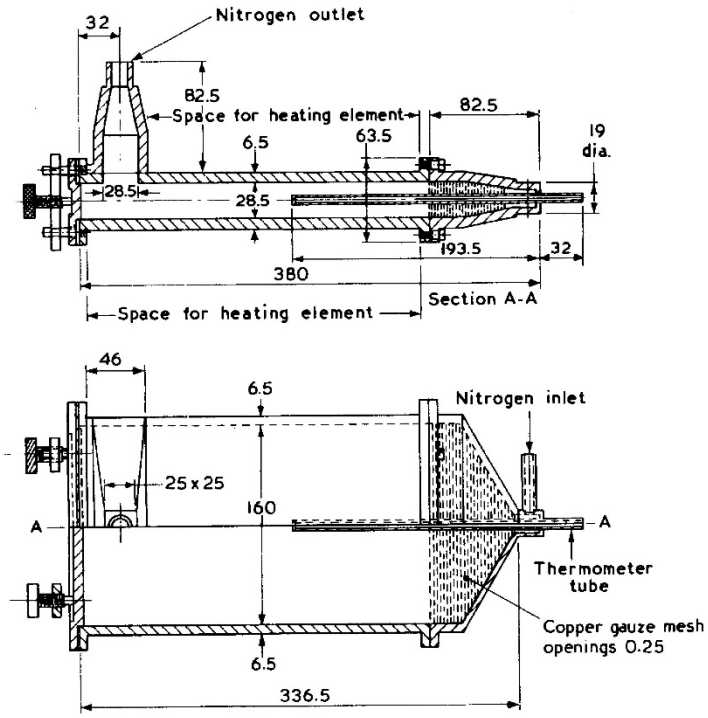

Dimensions in millimetres.

Fig. 3. Suitable nitrogen oven

4.4 Drying in vacuo

4.4.1 *Principle.* A known mass of the sample is heated in vacuo at 105 °C to 110 °C and the percentage moisture is calculated from the loss in mass. The weighing vessel containing the coal is evacuated while being maintained at 105 °C to 110 °C in an oven.

4.4.2 *Special reagent.* The following reagent is required:
*Magnesium perchlorate**, 0.7 mm to 1.2 mm.

4.4.3 *Special apparatus.* The following apparatus, shown assembled in Fig. 4, is required:

(1) *Oven.* An oven capable of accommodating the weighing vessel and of maintaining a temperature within the range 105 °C to 110 °C in the vessel. The oven may be designed to accommodate a number of vessels.

(2) *Weighing vessel.* A glass weighing vessel, 130 mm long by 15 mm internal diameter, closed at one end and fitted at the other with a flexible heat resistant stopper (see Note 5) carrying a microfilter of porosity grade No. 3 to BS 1752 (see Fig. 5).

(3) *Absorption tube.* A drying tube, straight, with bulb, to the dimensions given in Fig. 5, filled with magnesium perchlorate retained by plugs of glass wool.

(4) *Vacuum pump.* A vacuum pump capable of maintaining an absolute pressure of less than 7 mbar† in the weighing vessel.

(5) *Vacuum gauge.*

(6) *Manifold.* If more than one vessel is used, a manifold of copper or brass tubing, made so that the branches are in line with the corresponding holes in the oven, is required.

*This is the quality of reagent referred to as 'magnesium perchlorate (dried)', sometimes known as 'Anhydrone'.
† 1 mbar = 10 N/m^2.

4.4.4 *Procedure.* Raise the oven to its working temperature. Attach an absorption tube to a clean dry empty weighing vessel, connect to the vacuum pump and reduce the pressure to less than 7 mbar. Insert the vessel into the oven for 15 min. Withdraw the vessel from the oven, allow to cool slightly, re-admit air slowly, disconnect from the absorption tube and place a rubber cap over the stem of the microfilter to act as a seal. Cool in a desiccator charged with magnesium perchlorate and weigh to the nearest 0.1 mg after removing the cap (see Note 6). Introduce about 1 g of the sample into the vessel and reweigh to determine the mass of sample taken. Spread the coal in a thin even layer by rotating the vessel, attach the absorption tube, connect to the vacuum pump as before and evacuate the system. Insert vessel into the oven and heat for 40 min. Remove the vessel, condition and weigh as described above.

4.4.5 *Calculation of result.* The result shall be calculated as follows:

If m_1 = mass of weighing vessel plus stopper and microfilter (g),

m_2 = mass of weighing vessel plus stopper and microfilter plus sample before heating (g)

m_3 = mass of weighing vessel plus stopper and microfilter plus sample after heating (g)

M_{ad} = percentage of moisture in the analysis sample,

then

$$M_{ad} = \frac{m_2 - m_3}{m_2 - m_1} \times 100$$

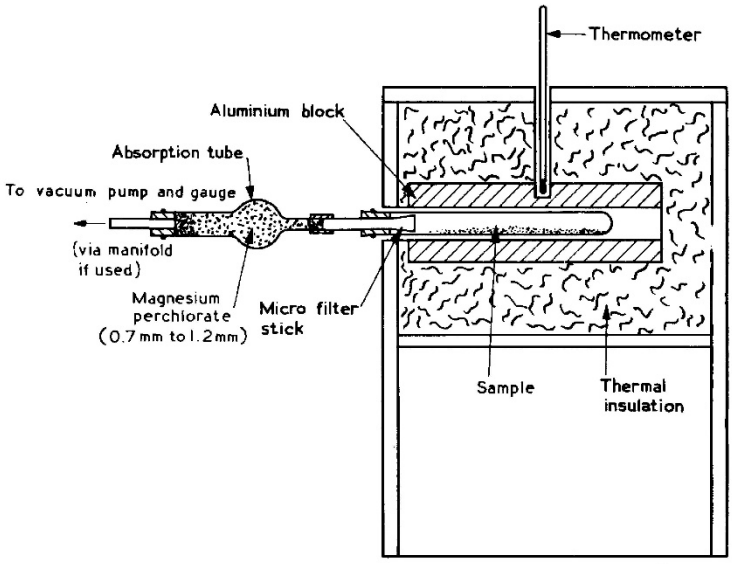

Fig. 4. Apparatus for the determination of moisture (vacuum method)

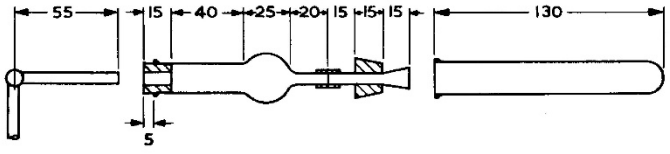

Fig. 5. Absorption tube and weighing vessel

Dimensions in millimetres

5. Volatile matter

5.1 General. The determination of volatile matter is empirical and hence the value obtained will depend on the conditions specified, e.g. the type of crucible stand, the temperature and the time of heating. These having been fixed, it is essential to adhere rigidly to the specified conditions in order to ensure reproducible results. It is also essential to exclude air from the coal during heating to prevent oxidation and therefore the fit of the lid of the crucible is critical.

The apparatus and procedure are so specified that one or more determinations may be carried out simultaneously in the muffle furnace. The moisture of the coal shall be determined at the same time as the volatile matter.

5.2 Principle. A known mass of the sample is heated at 900 °C out of contact with air for 7 min. The volatile matter is calculated from the loss in mass of the sample; a deduction is made for the loss in mass due to moisture.

5.3 Special reagent. The following reagent is required:

Desiccant. Self-indicating activated alumina or silica gel, or magnesium perchlorate*.

5.4 Special apparatus. The following apparatus is required:

(1) *Muffle furnace*†. A gas-heated or electrically-heated muffle furnace in which an adequate zone can be maintained at a uniform temperature of 900 ± 5 °C. A muffle with internal dimensions approximately 250 mm long by 100 mm wide by 65 mm high is suitable. It may be of the type closed at one end or fitted at the back with a flue not larger than 25 mm in diameter by 150 mm tall. It shall be provided at the front with a well-fitting, readily manipulated door. Its heat capacity shall be such that with an initial temperature of 900 °C a minimum temperature of 885 °C is regained within 3 min of the insertion of a cold stand and its crucible(s), both temperatures being measured with an unsheathed thermocouple as described below. If the furnace is electrically-heated, a rating of about 1750 W is satisfactory and it is preferable for the temperature to be controlled automatically.

A position for the crucible stand shall be chosen within the zone of uniform temperature and this position shall be used in all determinations.

(2) *Thermocouples.* Two thermocouples are required, one sheathed and permanently in position, one unsheathed and inserted periodically for checking the temperature at the base of the crucibles (see Note 7).

The temperature of the uniform zone of the muffle furnace shall be checked periodically by means of an unsheathed thermocouple of wire not thicker than 1 mm. The thermojunction shall be inserted midway between the base of the crucible in its stand and the floor of the muffle furnace and its reading related to that of the sheathed thermocouple, whose position shall be as shown in Fig. 6. If a multiple stand is used then the thermojunction of the sheathed thermocouple shall be at the mid-point of the centres of the four crucibles. The thermojunction of the unsheathed thermocouple shall be inserted under each crucible in turn and the mean temperature related to that of the sheathed thermocouple. The temperature in the four positions shall be within 900 ± 5 °C.

The sheathed thermocouple also serves to locate the stand in the zone of uniform temperature.

(3) *Crucible and lid.* A cylindrical crucible with capsule type lid, both of translucent silica, having dimensions approximating to those in Fig. 7.

The crucible and lid shall be matched by the operator so that the combined mass is between 10 g and 14 g. The fit of the lid is critical and the lid for a particular crucible shall be selected so that when placed in position the maximum horizontal clearance around the lip of the crucible is 0.5 mm. After selection each crucible and lid shall be ground together to give smooth surfaces and then identified with a distinguishing number or mark.

(4) *Stand.* A stand constructed from heat resistant steel wire‡. Stands for single and for multiple determinations are shown in Fig. 8; in order to facilitate handling with tongs, the upper and lower surfaces of the handle of the single crucible stand are ground flat.

(5) *Asbestos discs.* Asbestos discs, 25 mm in diameter and 1 mm thick.

*This is the quality of reagent referred to as 'magnesium perchlorate (dried)', sometimes known as 'Anhydrone'.
†A muffle furnace with flue, as described by C. W. G. Ockelford (*Fuel*, London, 1945, **24**, 3), is suitable for single and probably also for multiple determinations. Some existing furnaces may not have an adequate zone of uniform temperature or a sufficiently rapid rate of temperature recovery to meet the requirements for multiple determinations and all furnaces should be checked before they are used for this purpose.
‡Steel filler rod to BS 1453, Type A8, is suitable.

5.5 Procedure. The following description applies to a single determination; when carrying out multiple determinations each crucible is dealt with consecutively with the minimum of delay.

Heat, at 900 °C for 7 min, the crucible and lid supported on two asbestos discs in the stand. Remove the crucible from the furnace and cool, first on a metal slab for not longer than 5 min and finally in a desiccator beside the balance.

As soon as it is cold, weigh the empty crucible and lid to the nearest 0.1 mg and introduce into it 1 ± 0.01 g of the coal sample. Weigh the covered crucible and contents to determine the mass of sample taken. Tap the crucible on a clean hard surface until the coal forms a layer of even thickness on the bottom of the crucible.

Adjust the temperature of the muffle furnace, containing a stand and empty crucible, to 900 °C as indicated by the correctly located unsheathed thermocouple, or to the equivalent temperature as indicated by the sheathed thermocouple. Remove the empty crucible and stand and close the door of the furnace to restore steady conditions.

Place the covered crucible containing the sample in a cold stand, fitted with two asbestos discs (see Note 8). Transfer the stand and crucible to the muffle furnace and heat for exactly 7 min from the time of insertion. Remove, cool and weigh the crucible in the same manner as described for the empty crucible (see Note 9).

5.6 Calculation of result

If m_1 = mass of crucible plus lid (g),

m_2 = mass of crucible plus lid plus sample, before heating (g),

m_3 = mass of crucible plus lid plus sample, after heating (g),

M_{ad} = percentage of moisture in the analysis sample,

V = percentage of volatile matter in the analysis sample,

then

$$V = \frac{m_2 - m_3}{m_2 - m_1} \times 100 - M_{ad}$$

6. Ash

6.1 General. During the incineration of coal the associated mineral matter undergoes chemical changes and the ash remaining is generally less than the mineral matter originally present in the coal. These changes include the loss of water of constitution from shaly matter, the loss of carbon dioxide from carbonates, the oxidation of pyrites to iron oxide and the fixation of oxides of sulphur. The determination of ash is empirical because the conditions of incineration control the extent to which these reactions occur and it is essential, therefore, to adhere strictly to the procedures specified in either of the alternative methods (but see also the Foreword, paragraph 5).

Two methods are described for the determination of ash:

Single furnace method (see **6.2**)

Two furnace method (see **6.3**).

The two furnace method is particularly useful in laboratories where large numbers of ash determinations are required. In both methods the ventilation of the muffle is such as to minimize fixation of extraneous oxides of sulphur by any highly basic coal ash.

6.2 Single furnace method

6.2.1 *Principle.* A known mass of the sample is heated in air to 500 °C in 30 min, from 500 °C to 815 °C in 60 to 90 min and is then kept at 815 °C until constant in mass. The percentage of ash is calculated from the mass of the residue remaining after incineration.

6.2.2 *Special apparatus.* The following apparatus is required:

(1) *Muffle furnace**. A muffle furnace capable of giving an adequate zone at a uniform temperature of 500 ± 10 °C in 30 min from cold, of being raised to 815 ± 10 °C in a further 60 to 90 min and of maintaining this latter temperature at the end of the run-up period. The ventilation shall be such as to give at least four atmosphere changes per minute at 815 °C (see Note 10).

(2) *Dish.* A silica dish, 10 mm to 15 mm deep, with cover, of such a size that the loading of the coal layer does not exceed 0.15 g/cm².

*The high temperature muffle furnace described by C. W. G. Ockelford (*Fuel*, London, 1945, **24**, 151) is suitable.

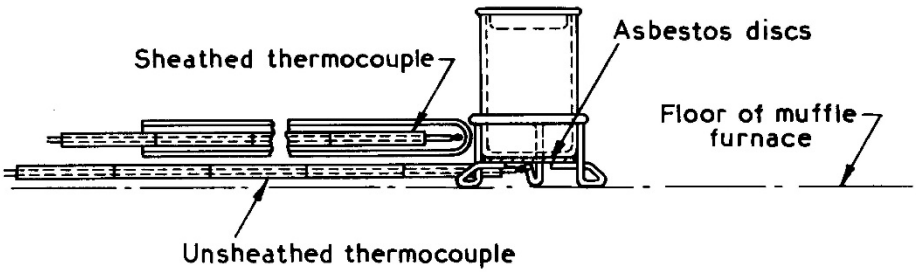

Fig. 6. Determination of volatile matter: location of thermocouples for single crucible stands

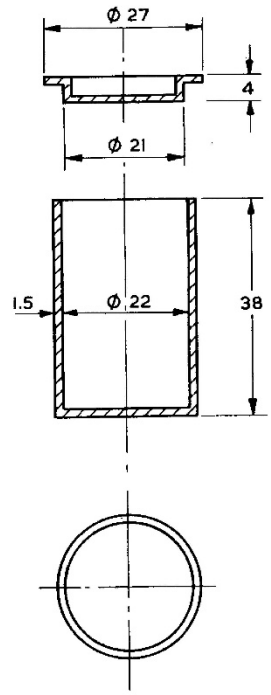

Dimensions in millimetres.

Fig. 7. Silica crucible and lid

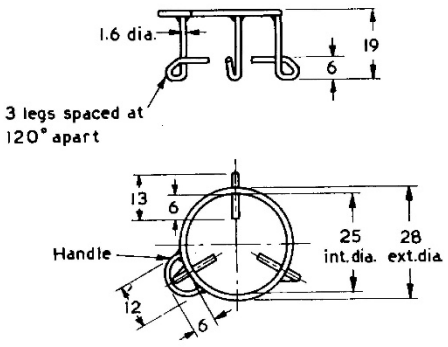

Fig. 8*a*. Single type

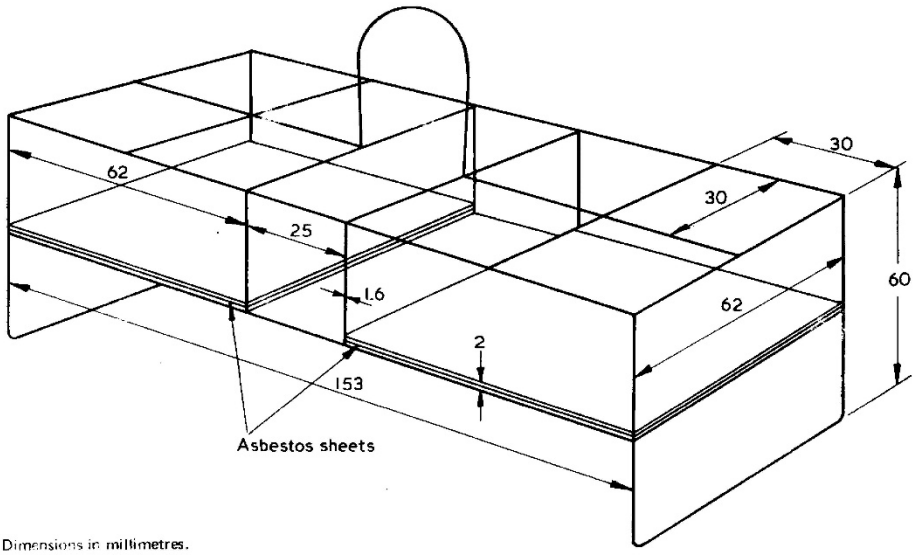

Dimensions in millimetres.

Fig. 8*b*. Multiple type

Fig. 8. Crucible stands

6.2.3 *Procedure.* Weigh a clean dry empty dish with its cover to the nearest 0.1 mg. Spread into it in an even layer either about 1 g or about 2 g of the coal sample, according to the size of dish, and replace the cover. Reweigh to determine the mass of sample taken.

Place the cover in a desiccator and insert the uncovered dish into the muffle furnace at room temperature. Raise the temperature to 500 °C in 30 min and to 815 °C in a further 60 to 90 min and maintain at this temperature until constant in mass (see Note 11). When incineration is complete, remove the dish from the furnace, replace the cover (see Note 12) and allow to cool, first on a thick metal plate for 10 min and finally in a desiccator for a further 15 min. Weigh the covered dish, brush out the ash completely and reweigh the empty dish and cover. Obtain the mass of the ash by calculating the difference.

6.3 Two furnace method

6.3.1 *Principle.* A known mass of the sample is heated in air to 500 °C in 30 min, maintained at this temperature for 30 min, and then heated at 815 °C until constant in mass. The percentage of ash is calculated from the mass of the residue remaining after incineration.

6.3.2 *Special apparatus.* The following apparatus is required:

(1) *Muffle furnaces**.

A muffle furnace (A) capable of giving an adequate zone at a uniform temperature of 500 ± 10 °C in 30 min from cold and of being maintained at this temperature. The ventilation shall be such as to give 10 to 12 atmosphere changes per minute at 500 °C (see Note 10).

A muffle furnace (B) capable of maintaining a temperature of 815 ± 10 °C. The ventilation shall be such as to give at least 4 atmosphere changes per minute at 815 °C (see Note 10).

(2) *Dish.* A silica dish, 10 mm to 15 mm deep, with cover, of such a size that the loading of the coal layer does not exceed 0.15 g/cm^2.

6.3.3 *Procedure.* Weigh a clean dry empty dish with its cover to the nearest 0.1 mg. Spread into it in an even layer either about 1 g or about 2 g of the coal sample, according to the size of the dish, and replace the cover. Reweigh to determine the mass of sample taken.

Place the cover in a desiccator and insert the uncovered dish into the muffle furnace (A), raise the temperature to 500 °C in 30 min and maintain at this temperature for 30 min.

Replace the cover on the dish and transfer it to the muffle furnace (B), previously heated to 815 °C. Remove the cover and complete the incineration and subsequent weighing as in 6.2.3.

6.4 Calculation of result (for both methods)

If m_1 = mass of dish plus cover (g),

m_2 = mass of dish plus cover plus sample (g),

m_3 = mass of dish plus cover plus ash (g),

m_4 = mass of dish plus cover after ash has been brushed out (g),

A = percentage of ash in the analysis sample,

then

$$A = \frac{m_3 - m_4}{m_2 - m_1} \times 100$$

7. Reporting of results

The results (preferably the means of duplicate determinations) of the moisture, volatile matter and ash determinations shall each be reported to the nearest 0.1 %. The difference between the sum of the three results and 100 shall be reported as 'fixed carbon'.

For the calculation of results to bases other than 'as analysed', see BS 1016 : Part 16.

* Muffle furnaces described by C. W. G. Ockelford (*Fuel*, London, 1945, **24**, 151) are suitable.

8. Precision of the determinations

	Repeatability, % absolute	Reproducibility, % absolute
Moisture:		
less than 5 %	0.10	–
5 % and above	0.15	–
Volatile matter:		
less than 10 %	0.20	0.5
10 % and above	0.30	1.0
Ash:		
less than 10 %	0.15	0.3
10 % to 20 %	0.20	0.4
more than 20 %	0.25	0.5

8.1 When the methods described in this Part are operated satisfactorily, the numerical values for repeatability and reproducibility (see Clause 2 for definitions) should not exceed those given above; otherwise, reference should be made to **4.4**, Part 16.

8.2 As moisture in the analysis sample varies with laboratory atmospheric conditions, it is not possible to quote values for the reproducibility of the results.

8.3 For the same reason, comparison of volatile matter or ash values to determine their reproducibilities should be made only after calculation to a common moisture basis.

9. Notes

NOTE 1. The conditioning of the retort tube is necessary only before the first determination of the day. In subsequent determinations the retort tube is emptied and recharged immediately with the next sample. Care should be taken to ensure that no moisture enters the tube during emptying.

NOTE 2. Alternatively, the coal may be weighed into a clean dry boat about 150 mm long. The boat may be inserted into a cold retort tube, which then does not need to have the depression in its wall.

NOTE 3. A blank determination is carried out each day.

NOTE 4. Under the conditions described, drying should be complete in 1½ h to 3 h. Constancy in mass (± 0.3 mg) should be established by reheating for a further period of 30 min, followed by cooling and weighing as described above.

NOTE 5. Because new stoppers often lose mass when first heated, they shall be fitted to weighing vessels and heated in the oven for 2 h before use.

NOTE 6. If successive determinations are made using the same weighing vessel, conditioning is necessary only before the first determination so long as there is no possibility of introducing moisture whilst cleaning the vessel after a determination.

NOTE 7. This method of checking at the base of the crucible is used because the sheathed thermocouple cannot be inserted under the crucible and a thermocouple with a bare junction constantly exposed under the specified conditions may change its characteristics.

NOTE 8. If the rate of recovery of the furnace is adjusted for multiple determinations, fill any vacant places in the multiple stand with empty crucibles.

NOTE 9. Precisely similar treatment of the crucible before and after the determination minimizes the effect of sorption of moisture by the crucible.

NOTE 10. The atmosphere changes per minute can be determined by measurement of the air flow in the flue by means of a pitot-static tube and sensitive manometer*.

NOTE 11. Heating at 815 °C for one hour is sufficient in most cases. If incomplete combustion is suspected, e.g. with high ash coals, do not brush out the ash after the first weighing but re-ignite at 815 °C for further periods of 15 min until constant in mass (± 0.3 mg); then brush out and reweigh the empty dish. The brushing out procedure eliminates errors due to the hygroscopicity of the silica dish.

NOTE 12. If the ash is light and fluffy, place the cover on the dish before removal from the muffle.

*E. Owen, *Measurement of Air Flow*, Third Edn. Revised, p. 88 (Chapman & Hall).

Appendix B – Pyrolysis condenser and baffles

Figure B.1. Pyrolysis system showing reactor, heating elements, and condensers (insulation not shown).

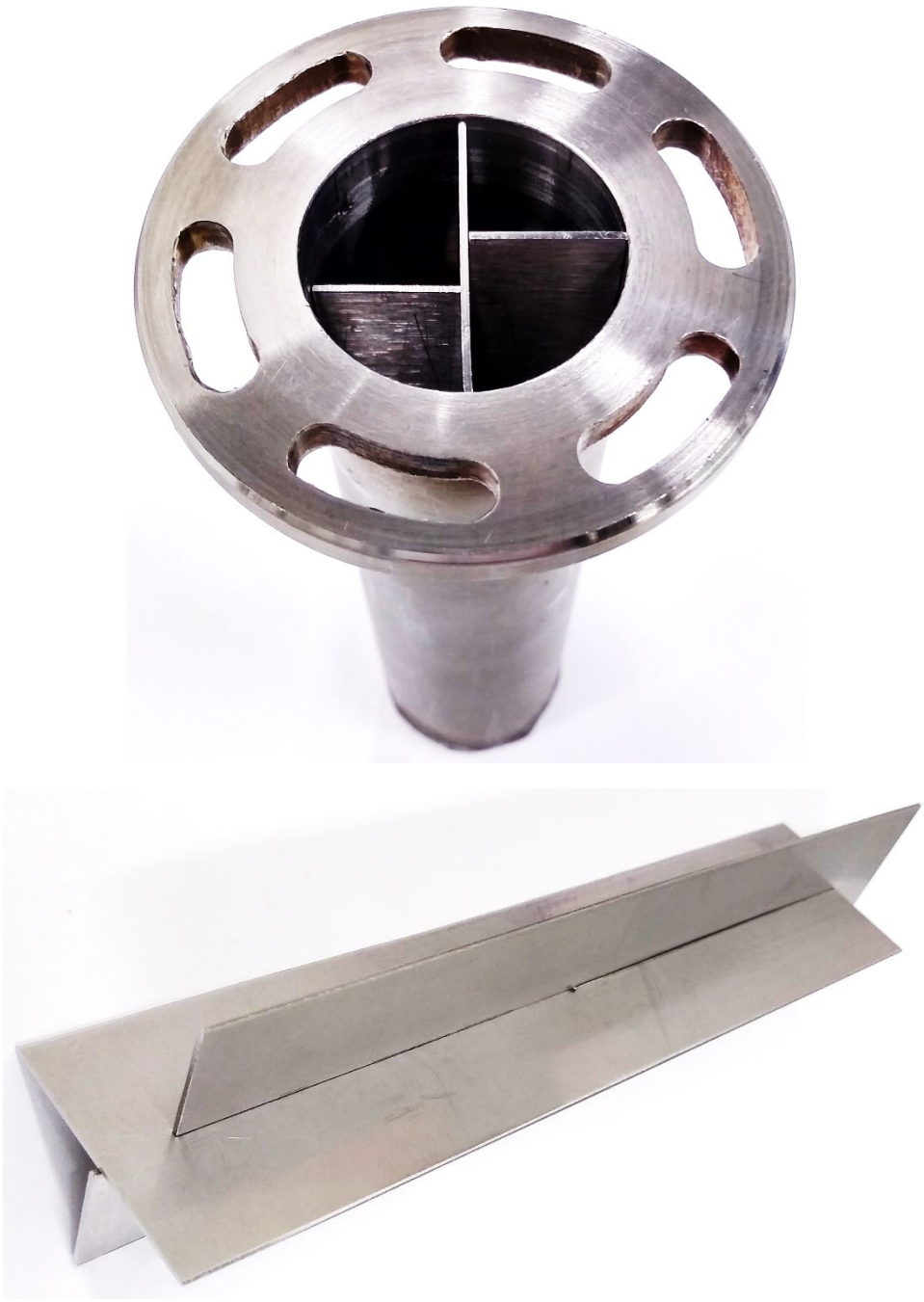

Figure B.2. Condenser design (upper), and internal baffles (lower).

The two condensers used for pyrolysis, made of stainless steel, were specifically designed to allow four longitudinal passes on each, with baffles magnifying the heat transfer area for improved condensation capability.

Appendix C – Reactor temperature profile

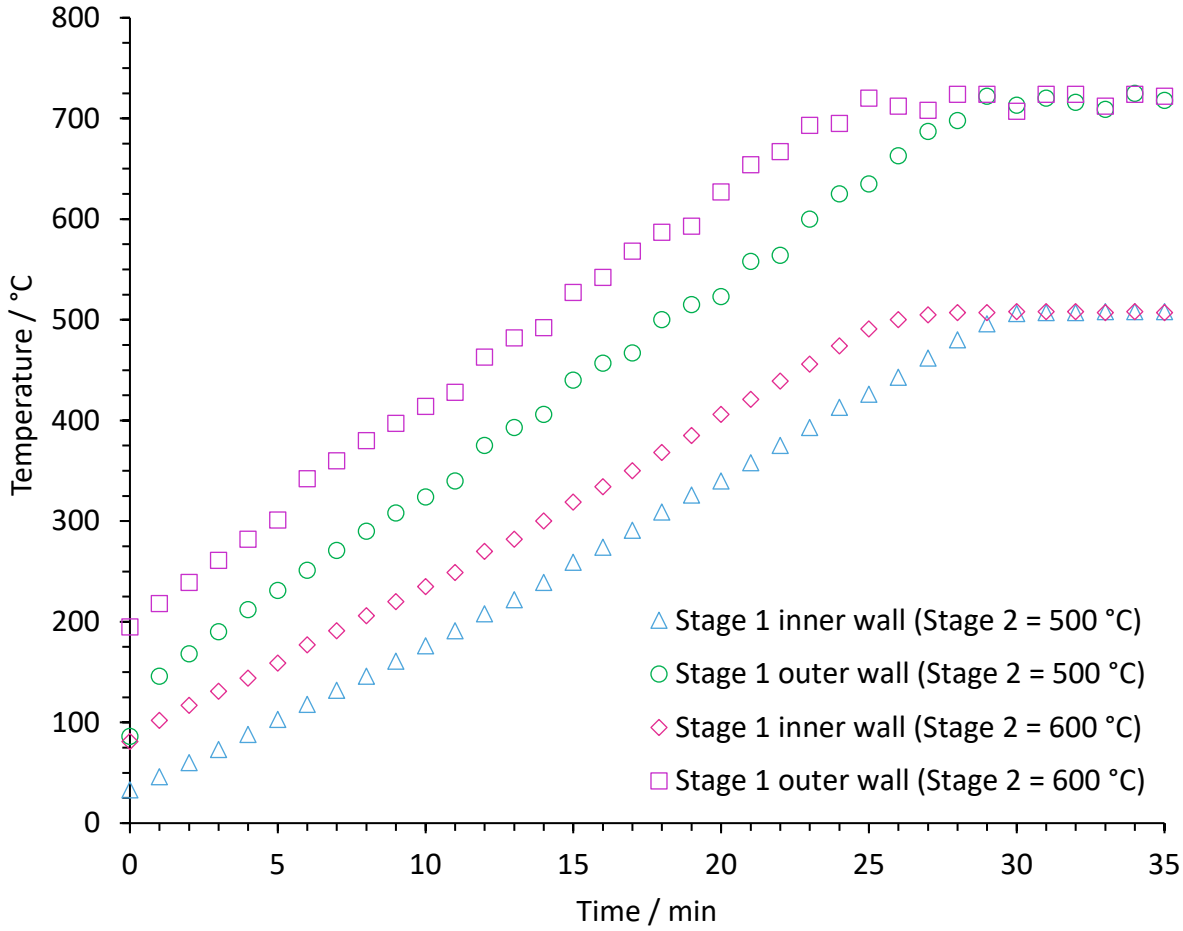

Figure C.1. Reactor's inner and outer wall temperatures in the first stage (pyrolysis), at different Set Point (SP) temperatures of the second stage (catalysis).

In the pyrolysis experiments, the second stage was heated first to the desired set point. As shown in Figure C.1, this does not affect the pyrolysis zone. The only observed difference is that the first stage's temperature (500 °C) is attained approximately 5 min earlier when the temperature of the second stage is 100 °C higher. After both set points are reached, the system maintains a stable temperature.

Appendix D

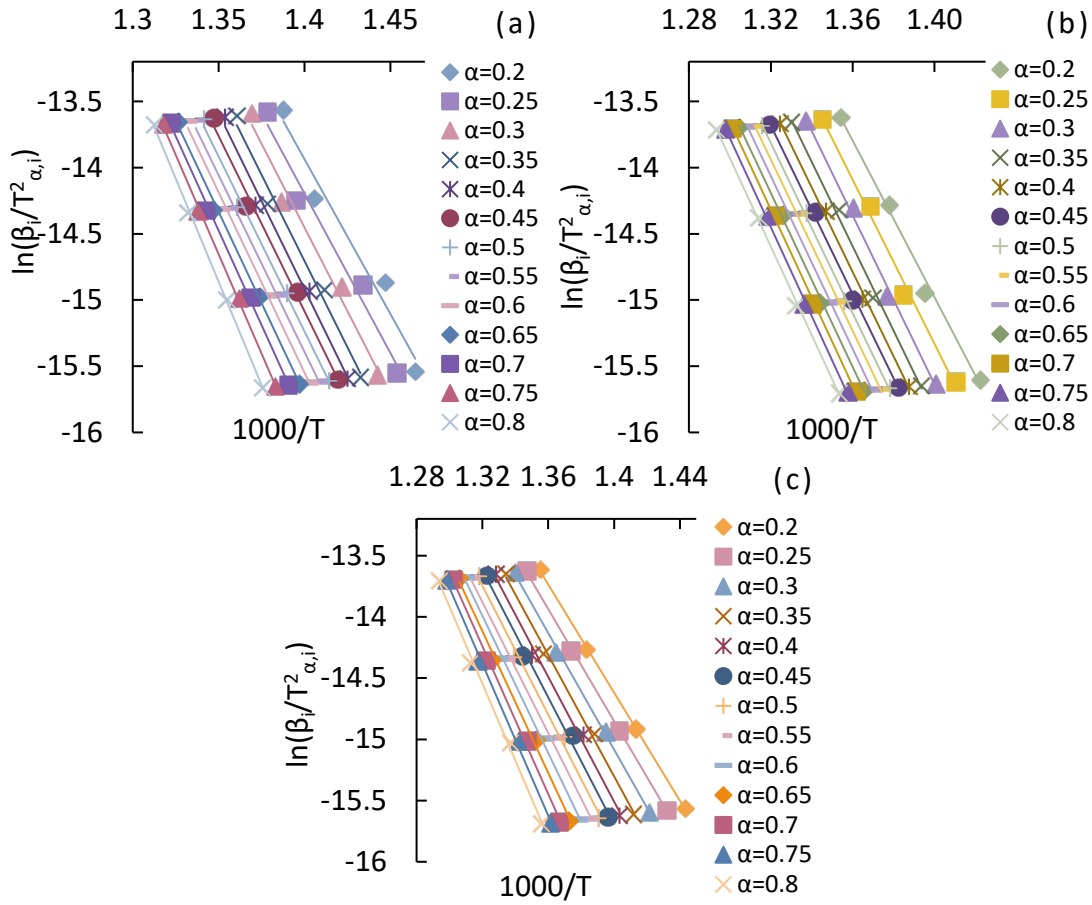

Figure D.1. KAS isoconversional plots of EU (a), TH (b), and MX (c) plastic mixtures.

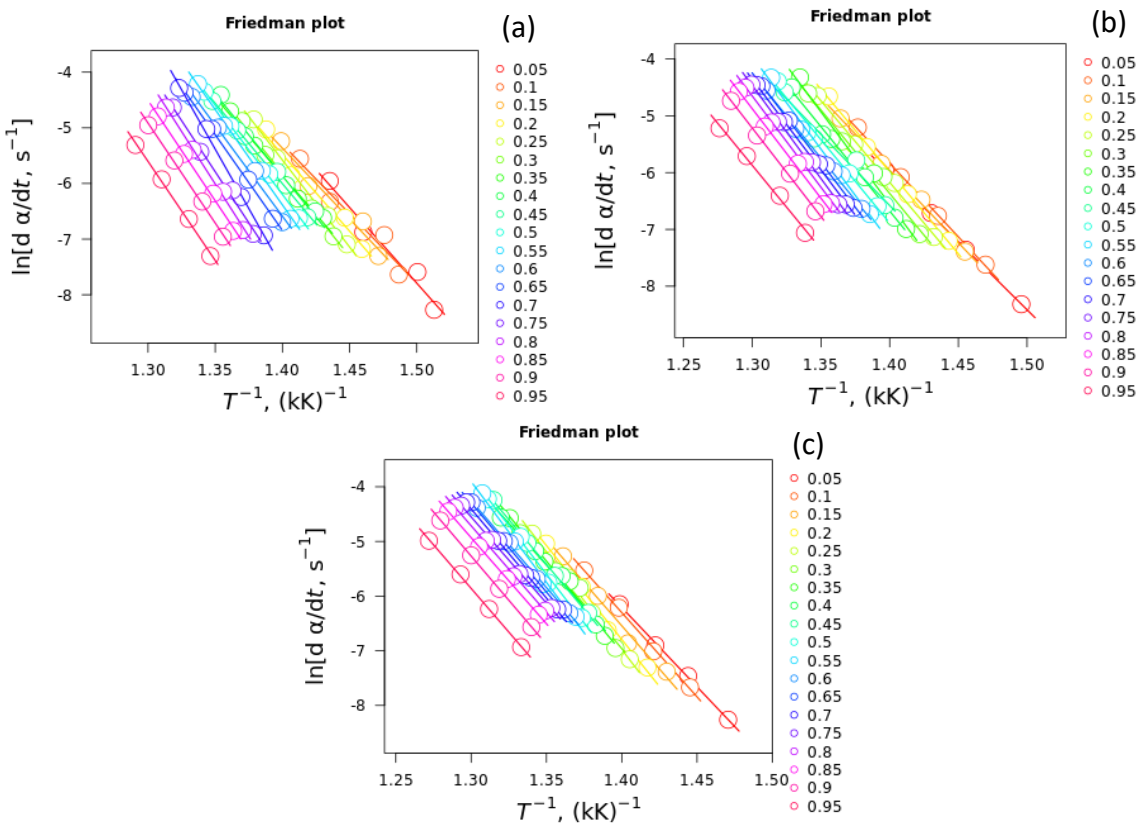

Figure D.2. Friedman isoconversional plots of EU (a), MX (b), and TH (c) plastic mixtures.

Appendix E – Mathematical deconvolution analysis

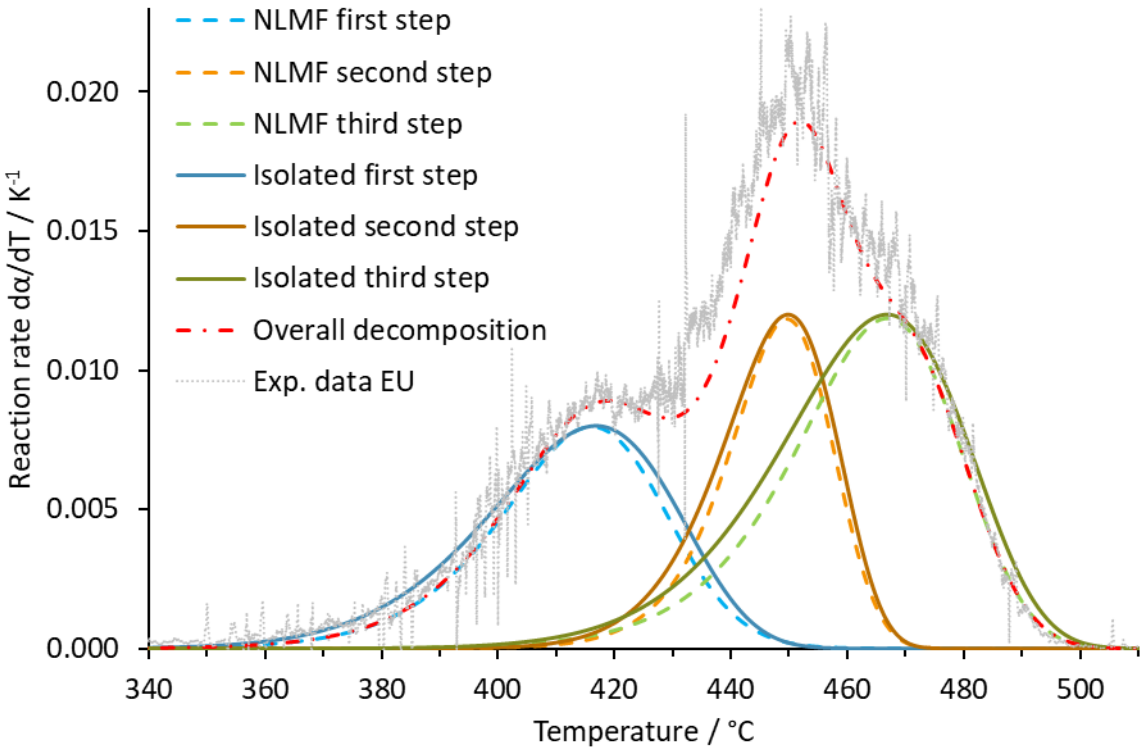

Figure E.1. Isolated reaction steps by mathematical deconvolution analysis (MDA), fitted by nonlinear model fitting (NLMF).

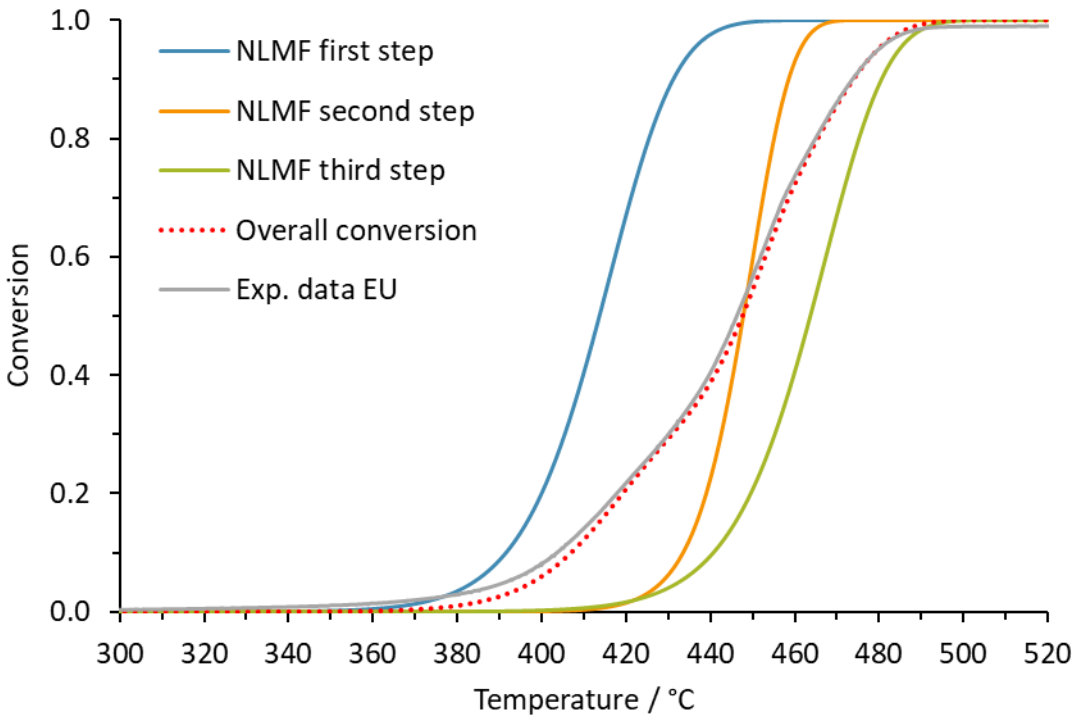

Figure E.2. Conversion of isolated reaction steps by mathematical deconvolution analysis, fitted by nonlinear model fitting (NLMF).

Appendix F – Failed HTL experiment

Figure F.1. Plastic mixture after HTL processing at 330 °C.

During the HTL process, the plastic mixture (HDPE,LDPE, PP, and PS) melted and fused together with no conversion, finally solidifying into the cluster shown in Figure F.1.

Appendix G – Pyrolysis process mass and energy balance

Table F.1. Material and energy balance from pyrolysis process streams simulated in ASPEN Plus.

	Units	AIR	CHAR	FLUE	GAS	GAS-RCY	LIGHT	ME-DIUM	N2	OIL	PLAS-TIC	S1	S2	S3	S4	S5	S6	S7	VENT	WAX
From			CYC-LONE	CND-100	Sep-03	SPLIT	Sep-03	Sep-02		MIX		REACT OR	B8	CND-200	Sep-01	CND-100	Sep-02	CND-20	SPLIT	Sep-01
To		BURN ER	BURN ER		SPLIT	CND-100	MIX	MIX	REAC TOR		REAC-TOR	Sep-01	CND-200	Sep-01	CND-100	Sep-02	CND-20	Sep-03		CND-100
Phase		Vap.	Solid	Vap.	Vap.	Vap.	Liq.	Liq.	Vap.	Liq.	Solid	Vap.	Vap.	Vap.	Vap.	Vap.	Vap.	Mixed	Vap.	Liq.
Tempera ture	°C	20	500	500	10	10	10	100	20	48	20	507	500	200	200	100	100	10	10	200
Pressure	atm	1	1	1	1	1	1	1	1	1	1	1	1	1	1	1	1	1	1	1
Vap. Frac.		1.0	0.0	1.0	1.0	1.0	0.0	0.0	1.0	0.0	0.0	1.0	1.0	1.0	1.0	1.0	1.0	0.9	1.0	0.0
Liq. Frac.		0.0	0.0	0.0	0.0	0.0	1.0	1.0	0.0	1.0	1.0	0.0	0.0	0.0	0.0	0.0	0.0	0.1	0.0	1.0
Solid Frac.		0.0	1.0	0.0	0.0	0.0	0.0	0.0	0.0	0.0	0.0	0.0	0.0	0.0	0.0	0.0	0.0	0.0	0.0	0.0
Enthalpy	kJ/kg	-5.4	643.4	-1400.5	-274.2	-274.2	-2184	-1808	-5.5	-2027.7	-1662.1	214.7	198.6	-252.2	-214.1	-355.8	-281.4	-410.9	-274.2	-1485
Entropy	J/kg-K	122.0	1194	1128	-370.9	-370.9	-7564	-6894	-18.5	-7243.8	-6900.0	130.5	103.5	-632.4	-457.8	-795.3	-482.8	-885.8	-370.9	-6286
Density	kg/cu m	1.2	2250.0	0.5	1.3	1.3	676.3	604.2	1.2	555.2	25.4	0.5	0.5	0.9	0.8	1.1	1.0	1.4	1.3	560.8
Enthalpy Flow	kJ/hr	-123337.3	510520.8	-43993604.4	-15477043.2	-2089400.8	-9502299.7	-5633812.3	-274203.4	-15136112.0	-27701652.2	14315531.5	13080288.8	-16611543.2	-13680450.3	-22737981.8	-17104169.5	-24979343.0	-13387642.4	-2931092.8
Av.MW		28.8	12.0	29.3	29.3	29.3	119.9	236.0	28.0	150.8	395.6	32.6	33.3	33.3	32.4	32.4	31.0	31.0	29.3	381.5
Mole Flows	kmol/hr	799.6	66.1	1071.9	1924.4	259.8	36.3	13.2	1784.9	49.5	42.1	2045.1	1979.1	1979.1	1973.9	1973.9	1960.7	1960.7	1664.6	5.2
Mass Flows	tonne/day	552.000	19.042	753.892	1354.446	182.850	104.404	74.752	1200.000	179.156	400.000	1600.000	1580.958	1580.958	1533.602	1533.602	1458.850	1458.850	1171.596	47.356
ETHANE	tonne/day	0.000	0.000	0.000	3.861	0.521	0.003	0.000	0.000	0.003	0.000	3.864	3.864	3.864	3.864	3.864	3.864	3.864	3.340	0.000
N-C8	tonne/day	0.000	0.000	0.000	40.891	5.520	91.991	1.897	0.000	93.888	0.000	134.853	134.853	134.853	134.779	134.779	132.882	132.882	35.370	0.075
N-C16	tonne/day	0.000	0.000	0.000	0.001	0.000	11.771	60.829	0.000	72.600	0.000	74.407	74.407	74.407	72.601	72.601	11.772	11.772	0.000	1.807
N-C28	tonne/day	0.000	0.000	0.000	0.000	0.000	0.001	11.982	0.000	11.983	0.000	57.446	57.446	57.446	11.983	11.983	0.001	0.001	0.000	45.463

C70	tonne /day	0.000	0.000	0.000	0.000	0.000	0.000	0.000	0.000	0.000	380.000	0.000	0.000	0.000	0.000	0.000	0.000	0.000	0.000	0.000
CH4	tonne /day	0.000	0.000	0.000	3.480	0.470	0.000	0.000	0.000	0.000	0.000	3.480	3.480	3.480	3.480	3.480	3.480	3.480	3.010	0.000
PROPANE	tonne /day	0.000	0.000	0.000	7.880	1.064	0.026	0.002	0.000	0.028	0.000	7.909	7.909	7.909	7.908	7.908	7.907	7.907	6.817	0.000
N-BUTANE	tonne /day	0.000	0.000	0.000	11.648	1.572	0.154	0.007	0.000	0.160	0.000	11.809	11.809	11.809	11.808	11.808	11.802	11.802	10.075	0.001
1-BUTENE	tonne /day	0.000	0.000	0.000	27.251	3.679	0.288	0.014	0.000	0.302	0.000	27.555	27.555	27.555	27.553	27.553	27.539	27.539	23.572	0.002
PROPYLEN	tonne /day	0.000	0.000	0.000	18.399	2.484	0.050	0.004	0.000	0.054	0.000	18.454	18.454	18.454	18.453	18.453	18.449	18.449	15.915	0.001
ETHYLENE	tonne /day	0.000	0.000	0.000	9.011	1.217	0.005	0.001	0.000	0.005	0.000	9.017	9.017	9.017	9.017	9.017	9.016	9.016	7.795	0.000
CO	tonne /day	0.000	0.000	0.000	11.200	1.512	0.000	0.000	0.000	0.001	0.000	11.201	11.201	11.201	11.201	11.201	11.201	11.201	9.688	0.000
CO2	tonne /day	0.000	0.000	125.862	20.628	2.785	0.012	0.001	0.000	0.014	0.000	20.642	20.642	20.642	20.642	20.642	20.640	20.640	17.843	0.000
H2	tonne /day	0.000	0.000	0.000	0.320	0.043	0.000	0.000	0.000	0.000	0.000	0.320	0.320	0.320	0.320	0.320	0.320	0.320	0.277	0.000
CARBON	tonne /day	0.000	19.042	0.000	0.000	0.000	0.000	0.000	0.000	0.000	0.000	19.042	0.000	0.000	0.000	0.000	0.000	0.000	0.000	0.000
O2	tonne /day	115.920	0.000	6.100	0.000	0.000	0.000	0.000	0.000	0.000	20.000	0.000	0.000	0.000	0.000	0.000	0.000	0.000	0.000	0.000
N2	tonne /day	436.080	0.000	598.063	1199.875	161.983	0.102	0.016	1200.000	0.118	0.000	1200.000	1200.000	1200.000	1199.993	1199.993	1199.977	1199.977	1037.892	0.007
WATER	tonne /day	0.000	0.000	23.866	0.000	0.000	0.000	0.000	0.000	0.000	0.000	0.000	0.000	0.000	0.000	0.000	0.000	0.000	0.000	0.000
Mass Fractions																				
ETHANE		0.000	0.000	0.0000	0.0029	0.0029	0.0000	0.0000	0.000	0.0000	0.0000	0.0024	0.0024	0.0024	0.0025	0.0025	0.0026	0.0026	0.0029	0.0000
N-C8		0.000	0.000	0.0000	0.0302	0.0302	0.8811	0.0254	0.000	0.5241	0.0000	0.0843	0.0853	0.0853	0.0879	0.0879	0.0911	0.0911	0.0302	0.0016
N-C16		0.000	0.000	0.0000	0.0000	0.0000	0.1127	0.8137	0.000	0.4052	0.0000	0.0465	0.0471	0.0471	0.0473	0.0473	0.0081	0.0081	0.0000	0.0382
N-C28		0.000	0.000	0.0000	0.0000	0.0000	0.0000	0.1603	0.000	0.0669	0.0000	0.0359	0.0363	0.0363	0.0078	0.0078	0.0000	0.0000	0.0000	0.9600
C70		0.000	0.000	0.0000	0.0000	0.0000	0.0000	0.0000	0.000	0.0000	0.9500	0.0000	0.0000	0.0000	0.0000	0.0000	0.0000	0.0000	0.0000	0.0000
CH4		0.000	0.000	0.0000	0.0026	0.0026	0.0000	0.0000	0.000	0.0000	0.0000	0.0022	0.0022	0.0022	0.0023	0.0023	0.0024	0.0024	0.0026	0.0000
PROPANE		0.000	0.000	0.0000	0.0058	0.0058	0.0003	0.0000	0.000	0.0002	0.0000	0.0049	0.0050	0.0050	0.0052	0.0052	0.0054	0.0054	0.0058	0.0000
BUTANE		0.000	0.000	0.0000	0.0086	0.0086	0.0015	0.0001	0.000	0.0009	0.0000	0.0074	0.0075	0.0075	0.0077	0.0077	0.0081	0.0081	0.0086	0.0000
BUTENE		0.000	0.000	0.0000	0.0201	0.0201	0.0028	0.0002	0.000	0.0017	0.0000	0.0172	0.0174	0.0174	0.0180	0.0180	0.0189	0.0189	0.0201	0.0000

PROPYLENE		0.0000	0.0000	0.0000	0.0136	0.0136	0.0005	0.0001	0.0000	0.0003	0.0000	0.0115	0.0117	0.0117	0.0120	0.0120	0.0126	0.0126	0.0136	0.0000
ETHYLENE		0.0000	0.0000	0.0000	0.0067	0.0067	0.0000	0.0000	0.0000	0.0000	0.0000	0.0056	0.0057	0.0057	0.0059	0.0059	0.0062	0.0062	0.0067	0.0000
CO		0.0000	0.0000	0.0000	0.0083	0.0083	0.0000	0.0000	0.0000	0.0000	0.0000	0.0070	0.0071	0.0071	0.0073	0.0073	0.0077	0.0077	0.0083	0.0000
CO2		0.0000	0.0000	0.1669	0.0152	0.0152	0.0001	0.0000	0.0000	0.0001	0.0000	0.0129	0.0131	0.0131	0.0135	0.0135	0.0141	0.0141	0.0152	0.0000
H2		0.0000	0.0000	0.0000	0.0002	0.0002	0.0000	0.0000	0.0000	0.0000	0.0000	0.0002	0.0002	0.0002	0.0002	0.0002	0.0002	0.0002	0.0002	0.0000
CARBON		0.0000	1.0000	0.0000	0.0000	0.0000	0.0000	0.0000	0.0000	0.0000	0.0000	0.0119	0.0000	0.0000	0.0000	0.0000	0.0000	0.0000	0.0000	0.0000
O2		0.2100	0.0000	0.0081	0.0000	0.0000	0.0000	0.0000	0.0000	0.0000	0.0500	0.0000	0.0000	0.0000	0.0000	0.0000	0.0000	0.0000	0.0000	0.0000
N2		0.7900	0.0000	0.7933	0.8859	0.8859	0.0010	0.0002	1.0000	0.0007	0.0000	0.7500	0.7590	0.7590	0.7825	0.7825	0.8226	0.8226	0.8859	0.0001
WATER		0.0000	0.0000	0.0317	0.0000	0.0000	0.0000	0.0000	0.0000	0.0000	0.0000	0.0000	0.0000	0.0000	0.0000	0.0000	0.0000	0.0000	0.0000	0.0000
Volume Flow	cum/hr	19224.7	0.4	68022.0	44667.0	6030.0	6.4	5.2	42919.8	13.4	657.3	126710.0	125607.3	76651.4	76647.9	60023.1	60018.0	44673.4	38636.9	3.5